Synthesis and Spectroscopy of Ruthenium-Modified Nucleic Acids

Thesis by

Elizabeth Stratford Krider

In Partial Fulfillment of the Requirements

for the Degree of

Doctor of Philosophy

California Institute of Technology

Pasadena, California

(Submitted 12 September 2000)

Acknowledgments

I am extremely grateful to the many individuals who have contributed to my personal and professional growth during these years at Caltech.

I thank Harry Gray for his support and encouragement during the good and bad times of my research project. He never failed to lift my spirits regarding my work – I always left his office feeling better than when I went in! It was pleasure to finally share spectroscopic results with him after so many group meetings filled with synthesis and more synthesis. I consider his praise of my fielding ability on the softball field to be a true compliment.

I thank Tom Meade for the opportunity to tackle such a difficult research project and for his unending enthusiasm toward the work. Of the many lessons I learned while in his lab, the importance of pressing forward in spite of disappointing results is the one I will remember the most. I have truly learned to endure to the end through this project.

I have been privileged to work with several outstanding post-doctoral researchers. These associations have added an invaluable dimension to my experience at Caltech. I am grateful to Jeff Rack for his insight, patience, and willingness to help me understand inorganic chemistry and various spectroscopic techniques. His attitude toward solving complex research problems has been and will continue to be an inspiration to me. I thank Natia Frank, Tom Welch, Phil Dawson, and Andrea Staubli for additional guidance through the course of my research. Collecting data in the very cold sub-basement, eating lunch at Baja and "The Spamlet," and spending lots of time in the lab together are highlights I will remember about my grad school days with the post-docs.

I thank Jay Winkler and Gary Hathaway for the exceptional assistance I received from them. I am indebted to Peter Green, Nathan Dalleska, Jay Zhou, and Felicia Rusnak for mass spectral analysis of my ruthenium-modified samples.

The folks in the Gray and Meade groups have added great memories to my life. My fellow classmates – Ivan Dmochowski, Akif Tezcan, Mike Machzynski, and Lila Guterman – have been true inspirations to me personally. Because of their examples, I am motivated to learn as much chemistry as I can. I thank Angie Louie for introducing me to mountain biking in the San Gabriels and aerobics classes at the Caltech gym,

pointing me to all the great bakeries in town, and daring me to try out for the Krypton Factor. My experiences here would not have been as meaningful if it weren't for friends like Don Low, Toshi Takeuchi, Kevin Hoke, Jeff Regan, Xenia Amashukeli, Martina Huber, Jason Telford, Jennifer Lee, Angelo Di Bilio, William Wehbi, Adrian Ponce, Randy Villahermosa, Jon Wilker, Brian Crane, Alex Dunn, Michele McGuirl, and Tim Hubin. Thanks for the trips to Buster's, good plays on the softball field, adventures at conferences, research suggestions, computer room chats, technical assistance, and all those great Cake Days.

My life has been brightened by my lunches with Aileen Chang, Deanna Zubris, and Claudine Chen. I'll never find another group of gals who are so generous and kind.

I have made many friends outside the lab but inside Caltech that have made my time here more enjoyable. Thanks to Felicia Rusnak, Susan Conner, Andres Ductoc, Bob, Catherine May, Mary Flowers, Virginia Russell, and Dian DeSha.

I especially want to thank my family for their constant support during my years at Caltech. I owe a great deal to the unfailing support of my mom, Charlene Stratford. As for my siblings – Alysia, Rich, Rene, Charles, and Virginia – I appreciate their patience, phone calls, letters, tasty meals, free lawn-mowings, cat duty, and overall moral support throughout this experience. I also want to thank my in-laws, Jesse and Sharon Krider, for being so supportive of my interests, especially when these interests have delayed the arrival of more Krider grandchildren.

I could not have embarked on this personal journey without the endless support and encouragement from my husband, Dave. His patience and faith in my raw talent kept me going when I was ready to give up. My feeling of overwhelming gratitude toward him for supporting me through this experience is indescribable.

Dedication

This work is dedicated to my Dad for teaching me how to work hard, to keep my chin up, and to charge! I regret that I was never able to share this great experience with him so he could see for himself what it's like to work at the interface of an exciting research problem. I think he would have liked seeing how a rotavap works.

In memory of Richard C. Stratford

Abstract

Redox-active probes are designed and prepared for use in DNA-mediated electron transfer studies. These probes consist of ruthenium(II) complexes bound to nucleosides that possess metal-binding ligands. Low- and high-potential oxidants are synthesized from these modified nucleosides and display reversible one-electron electrochemical behavior. The ruthenium-modified nucleosides exhibit distinct charge-transfer transitions in the visible region that resemble those of appropriate model complexes. Resonance Raman and time-resolved emission spectroscopy are used to characterize the nature of these transitions.

The site-specific incorporation of these redox-active probes into oligonucleotides is explored using post-synthetic modification and solid-phase synthetic methods. The preparation of the metal-binding nucleosides, their incorporation into oligonucleotides, and characterization of the resulting oligonucleotides is described. Because the insertion of these probes into modified oligonucleotides using post-synthetic modification is unsuccessful, solid-phase synthetic methods are explored. These efforts lead to the first report of 3′-metallated oligonucleotides prepared completely by automated solid-phase synthesis. Preliminary efforts to prepare a bis-metallated oligonucleotide by automated synthesis are described.

The electrochemical, absorption, and emissive features of the ruthenium-modified oligonucleotides are unchanged from those of the precursor metallonucleoside. The absence of any change in these properties upon incorporation into oligonucleotides and subsequent hybridization suggests that the incorporated ruthenium(II) complex is a valuable probe for DNA-mediated electron transfer studies.

Table of Contents

Chapter 1: Ruthenium Modification of Nucleic Acids 1

I. Introduction 2

II. Designing Donors and Acceptors for DNA-Electron Transfer Reactions 3

III. Methods for Modifying DNA with Ruthenium Complexes 9

A. Post-Synthetic Modification 12

B. On-Column Derivatization 22

C. Solid-Phase Synthesis 28

IV. Characterization of Ruthenium-Modified Oligonucleotides 35

A. Effect of Ruthenium Complexes on Duplex Stability 35

B. Absorption of Ruthenium-Modified Oligonucleotides 39

C. Emission of Ruthenium-Modified Oligonucleotides 42

D. Summary 48

V. Scope of Thesis 52

VI. References 53

Chapter 2: 2′-Modified Nucleosides for Site-Specific Labeling of Oligonucleotides 61

I. Introduction 62

II. Results 65

A. Synthesis of 2′-Modified Nucleosides 65

B. Oligonucleotide Synthesis 70

C. Thermal Denaturation Studies 70

III. Discussion 83

A. Synthetic Strategy 83

B. Synthesis of 2′-Modified Nucleosides 86

C. Oligonucleotide Synthesis with 2′-Modified Nucleosides 87

D. Effect of 2′-Modified Nucleosides on Duplex Stability 88

IV. Conclusion 89

V. Experimental Procedure 90

VI. References and Notes 127

Chapter 3: Post-Synthetic Modification of Oligonucleotides with Ruthenium(II) Reagents 132

I. Introduction 133

II. Results 138

A. Metallation Reactions with $[Ru(bpy)_2CO_3]$ 138

B. Experimental Procedure 152

C. Metallation Reactions with $[Ru(NH_3)_5(OH_2)]^{2+}$ 154

1. Modified Oligonucleotides 154

2. Model Complexes 154

3. G-containing Oligonucleotides 165

D. Experimental Procedure 170

E. Metallation Reactions with Ruthenium(II) Acetylacetonate Reagents 173

1. Model Complexes 173

2. Modified Oligonucleotides 176

F. Experimental Procedure 176

III. Discussion 186

A. Metallation Reactions with $[Ru(bpy)_2CO_3]$ 186

B. Metallation Reactions with $[Ru(NH_3)_5(OH_2)]^{2+}$ 187

C. Metallation Reactions with Ruthenium(II) Acetylacetonate Reagents 189

IV. Conclusion 189

V. References and Notes 191

Chapter 4: Automated Synthesis of 3′-Metallated Oligonucleotides 193

I. Introduction 194

II. Results 198

A. Synthesis of Ruthenium-Containing Solid Support 198

B. Oligonucleotides Synthesis with **5** 198

C. Absorption 201

D. Therman Denaturation Studies 201

E. Electrochemistry 213

F. Emission 218
III. Discussion 222
A. Incorporation Strategy 222
B. Effect of Metal Complexes on Duplex Stability 223
C. Absorption 224
D. Emission 225
E. Guanine Oxidation 228
IV. Conclusion 228
V. Experimental Section 229
VI. References and Notes 243

Chapter 5: Spectroscopy of Ruthenium-Modified Nucleic Acids 248
I. Introduction 249
II. Results 250
A. Electrochemistry 250
B. Absorption 255
C. Resonance Raman 262
D. Emission 279
III. Discussion 279
A. Electrochemistry 279
B. Absorption of **1,** $[Ru(acac)_2(impy')]$ 280
C. Resonance Raman of **1,** $[Ru(acac)_2(impy')]$ 284
D. Absorption and Resonance Raman of **2**, $[Ru(bpy)_2(impy')]^{2+}$ 285
E. Emission of **2**, $[Ru(bpy)_2(impy')]^{2+}$ 287
IV. Conclusion 287
V. Experimental Section 288
VI. References and Notes 297

Appendix A: Additional Nucleoside Synthesis 301
I. Synthesis of 2′-Modified Nucleoside, **3a** 302
II. Deprotection of 2′-Modified Nucleoside, **3b** 308

III. Synthesis of Modified Oligonucleotides 309

Appendix B: Synthesis of Ruthenium Model Complexes 311

I. Summary 312

II. Experimental Section 312

III. Results and Discussion 319

A. Acid Treatment of $[Ru(acac)_2(impy)]$ and $[Ru(acac)_2(impy')]$ 324

B. Synthesis of $[Ru(bpy)_2(U_{impy})]^{2+}$ 325

C. Synthesis of $[Re(CO)_3(phen)(U_a)]^{+}$ 325

IV. Conclusion 326

V. References 326

Appendix C: Fluorescence Quenching Experiments with Ruthenium-Modified Nucleic Acids 328

I. Introduction 329

II. Results 332

III. Discussion and Conclusion 346

IV. References 348

Appendix D: Automated Synthesis of an Oligonucleotide Containing Ruthenium(II) Complexes at 3′ and 5′ Ends 349

Appendix E: HPLC Columns and Solvent Systems 357

List of Figures

Figure 1.1	Three-dimensional structures of (a) the metalloprotein azurin surface-labeled with $Ru(bpy)_2(im)^{2+}$ at histidine 83, and (b) an unmodified B-form DNA duplex.	4
Figure 1.2	Solid-phase oligonucleotide synthesis by the phosphite-triester method.	10
Figure 1.3	Scheme outlining the steps involved in Post-Synthetic Modification.	13
Figure 1.4	Reaction scheme outlining the coupling of $[Ru(bphen)_2(bphen')]^{2+}$ to an amine-bearing oligonucleotide.	15
Figure 1.5	Examples of ruthenium-modified oligonucleotides prepared by the Post-Synthetic Modification method.	18
Figure 1.6	Scheme outlining the steps involved in On-Column Derivatization.	24
Figure 1.7	Examples of ruthenium-modified oligonucleotides prepared by the On-Column Derivatization method.	26
Figure 1.8	Structures of ruthenium-modified phosphonate (red) and phosphoramidite (blue) monomers, and examples of oligonucleotides prepared by Solid-Phase Synthesis.	30
Figure 1.9	Structures of an octahedral Ru(II) polypyridyl model complex, corresponding monomer complex possessing a substituted polypyridyl ligand (B), and the oligonucleotides containing the monomer complexes (C).	40
Figure 1.10	Schematic structure of DNA assembly containing spectroscopically unique, non-intercalating ruthenium complexes.	50
Figure 2.1	Structures of nucleosides modified at the 2′ ribose position with metal-binding ligands.	63
Figure 2.2	Synthesis of nucleosides containing bidentate ligands at the 2′ ribose position.	66
Figure 2.3	Synthesis of 2′-modified nucleosides as solid-support-bound and phosphoramidite derivatives.	68
Figure 2.4	Steps in the automated synthesis of oligonucleotide **14**.	72
Figure 2.5	Products of enzymatic digestion of **11** as analyzed by reverse-phase HPLC.	74

Figure 2.6	Products of enzymatic digestion of **12** as analyzed by reverse-phase HPLC.	76
Figure 2.7	Products of enzymatic digestion of **13** as analyzed by reverse-phase HPLC.	78
Figure 2.8	Products of enzymatic digestion of **14** as analyzed by reverse-phase HPLC.	80
Figure 2.9	Thermal denaturation curves for duplex **17:18** (□) and duplex **14:18** (♦).	84
Figure 2.10	^{1}H NMR spectrum of **2a** in $CDCl_3$ (500 MHz).	92
Figure 2.11	ESI mass spectrum of **2a** conducted in positive ionization mode.	94
Figure 2.12	^{1}H NMR spectrum of **2b** in $CDCl_3$ (300 MHz).	97
Figure 2.13	ESI mass spectrum of **2b** conducted in positive ionization mode.	99
Figure 2.14	^{1}H NMR spectrum of **3a** in $CDCl_3$ (300 MHz).	101
Figure 2.15	ESI mass spectrum of **3a** conducted in positive ionization mode.	103
Figure 2.16	^{1}H NMR spectrum of **3b** in $CDCl_3$ (500 MHz).	106
Figure 2.17	ESI mass spectrum of **3b** conducted in positive ionization mode.	108
Figure 2.18	ESI mass spectrum of **5** conducted in negative ionization mode.	111
Figure 2.19	ESI mass spectrum of **6** conducted in negative ionization mode.	113
Figure 2.20	MALDI-TOF mass spectrum of **11** conducted in negative ionization mode.	118
Figure 2.21	MALDI-TOF mass spectrum of **12** conducted in negative ionization mode.	120
Figure 2.22	MALDI-TOF mass spectrum of **13** conducted in negative ionization mode.	122
Figure 2.23	MALDI-TOF mass spectrum of **14** conducted in negative ionization mode.	124

Figure 3.1	Reaction scheme for preparing metal-containing oligonucleotides using post-synthetic modification method.	134
Figure 3.2	Structures of 2′-modified nucleosides and their positions in 11-mer oligonucleotides.	136
Figure 3.3	Structures of nucleoside model complexes.	140
Figure 3.4	Oligonucleotide sequences used in metallation reactions with $[Ru(bpy)_2CO_3]$.	142
Figure 3.5	Reaction scheme for metallation of duplexed $_a$**UU**$_a$ with $[Ru(bpy)_2CO_3]$.	144
Figure 3.6	HPLC trace of metallation reaction involving $_a$**UU**$_a$ and $[Ru(bpy)_2CO_3]$.	148
Figure 3.7	HPLC trace of metallation reaction involving $_a$**UT** and $[Ru(bpy)_2CO_3]$.	150
Figure 3.8	Oligonucleotides used in metallation reactions with $[Ru(NH_3)_5(OH_2)]^{2+}$.	155
Figure 3.9	Reaction scheme for metallation reactions with $[Ru(NH_3)_5(OH_2)]^{2+}$.	157
Figure 3.10	Absorption spectrum of purified oligonucleotide **11B** following metallation with $[Ru(NH_3)_5(OH_2)]^{2+}$.	159
Figure 3.11	Reaction scheme for the synthesis of $[Ru(NH_3)_4(impy)]^{2+}$.	161
Figure 3.12	Absorption spectra of (a) $[Ru(NH_3)_4(ampy')]^{2+}$ (solid line) and (b) $[Ru(NH_3)_4(impy')]^{2+}$ (dashed line) in 50 mM Tris, pH 7.2.	163
Figure 3.13	Scheme showing the mechanism of oxidative dehydrogenation of amines coordinated to Ru(II) bis(bipyridine).	166
Figure 3.14	Reaction scheme for metallation of duplexes containing an overhanging guanine base at the 5′ end.	168
Figure 3.15	HPLC trace of metallation reaction involving duplexed **9G** and $[Ru(NH_3)_5(OH_2)]^{2+}$.	171
Figure 3.16	Reaction scheme for the synthesis of $[Ru(acac)_2(impy')]$.	174
Figure 3.17	HPLC trace of metallation reaction involving $_a$**UU**$_b$ and $[Ru(acac)_2(CH_3CN)_2]$.	178
Figure 3.18	HPLC trace of metallation reaction involving duplexed **11B** and $[Ru(acac)_2(CH_3CN)_2]$.	180

Figure 3.19	MALDI-TOF mass spectrum of fractions collected after HPLC purification of reaction involving $_{a}\mathbf{UU}_{b}$ and $[Ru(acac)_2(CH_3CN)_2]$.	182
Figure 3.20	MALDI-TOF mass spectrum of fractions collected after HPLC purification of reaction involving duplexed **11B** and $[Ru(acac)_2(CH_3CN)_2]$.	184
Figure 4.1	Synthesis of metallonucleosides and metal-containing solid support.	195
Figure 4.2	Oligonucleotide synthesis with the metal-containing solid support.	199
Figure 4.3	Ion-exchange HPLC trace of the crude mixture following synthesis, cleavage, and deprotection of oligonucleotide **7**.	202
Figure 4.4	MALDI-TOF mass spectra for ruthenium-containing oligonucleotides, **6** (top) and **7** (bottom).	204
Figure 4.5	Products of enzymatic digestion of **6** as analyzed by reverse-phase HPLC.	206
Figure 4.6	Products of enzymatic digestion of **7** as analyzed by reverse-phase HPLC.	208
Figure 4.7	Absorption spectra of **3** (top; methanol) and **7** (bottom; 0.05 M sodium phosphate, pH 7.0, 0.5 M sodium chloride).	210
Figure 4.8	Thermal denaturation curves for duplex **8·9** (□) and metal-containing duplex **7·9** (♦).	214
Figure 4.9	Square-wave voltammogram of oligonucleotide **7** in 50 mM sodium phosphate (pH 7.0) containing 500 mM sodium chloride.	216
Figure 4.10	Steady-state emission spectrum of **3** in aerated methanol (λ_{exc} = 480 nm, λ_{max} = 730 nm).	219
Figure 4.11	500 MHz NMR spectrum of **3** in CD_3CN.	233
Figure 4.12	ESI mass spectra of **3** obtained in positive ionization mode.	236
Figure 4.13	Analytical HPLC trace of **3**.	238
Figure 4.14	ESI mass spectra of **4** obtained in positive ionization mode.	240
Figure 5.1	Structure and sequence of ruthenium-modified nucleic acids.	251

Figure 5.2	Differential pulse voltammograms showing ligand centered reductions of **3** (solid) and $[Ru(bpy)_3]^{2+}$ (dashed) in acetonitrile containing 0.1 M TBAH.	256
Figure 5.3	Absorption spectra of **2** (dotted line) and **3** (solid line) in ethanol and methanol, respectively.	258
Figure 5.4	Resonance Raman spectrum of **1** in dichloromethane (441.6 nm excitation).	260
Figure 5.5	Resonance Raman spectrum of **1** in dichloromethane (457.9 nm excitation).	263
Figure 5.6	Resonance Raman spectrum of **1** in dichloromethane (514.5 nm excitation).	265
Figure 5.7	Resonance Raman spectrum of **2** in deuterated methanol (441.6 nm excitation).	267
Figure 5.8	Resonance Raman spectrum obtained with 441.6 nm excitation of $[Ru(bpy)_3]^{2+}$ (top) and **3** (bottom) in water.	269
Figure 5.9	Resonance Raman spectrum of **2** in deuterated methanol (457.9 nm excitation).	271
Figure 5.10	Resonance Raman spectrum of **2** in deuterated methanol (488.0 nm excitation).	273
Figure 5.11	Resonance Raman spectrum of **2** in deuterated methanol at three excitation wavelengths: 441.6 (bottom), 457.9 (middle), and 488.0 nm (top).	275
Figure 5.12	Steady-state emission spectrum of **2** in aerated methanol (480.0 nm excitation).	277
Figure 5.13	Latimer diagrams for $[Ru(bpy)_2(impy')]^{2+}$ (top) and $[Ru(bpy)_3]^{2+}$ (bottom).	281
Figure 5.14	^1H NMR spectrum of **1** in $CDCl_3$ (500 MHz).	290
Figure 5.15	ESI mass spectrum of **1** in positive ionization mode (top) and MALDI-TOF mass spectrum of **1** showing isotopic distribution (bottom).	292
Figure 5.16	ESI mass spectrum of $[Ru(acac)_2(impy)]$ in positive ionization mode.	295
Figure A.1	ESI mass spectrum of crude **1** conducted in negative ionization mode.	304

Figure A.2	ESI mass spectrum of crude **1** conducted in positive ionization mode.	306
Figure B.1	Emission decay of a solution containing $Re(CO)_3(phen)(OH_2)^+$ and $Re(CO)_3(phen)$(2′-amino-2′-deoxyuridine)$^+$ (50 mM HEPES, pH 8.5; λ_{exc} = 396 nm; λ_{obs} = 575 nm).	317
Figure B.2	Scheme showing the synthetic route to various Ru(II) acetylacetonate complexes.	320
Figure B.3	Synthesis of $Ru(acac)_2(impy)$.	322
Figure C.1	Scheme outlining the bimolecular quenching cycle designed for studying electron transfer reactions in biological systems.	330
Figure C.2	Scheme for Stern-Volmer analysis of quenching reactions.	333
Figure C.3	Structure of ruthenium-containing nucleoside **3** and sequences of oligonucleotides **6**, **7**, and **9**.	335
Figure C.4	Scheme showing oxidative and reductive quenchers employed in quenching studies.	337
Figure C.5	A sample Stern-Volmer plot derived from quenching experiments involving photoexcited **7:9** (35 μM) in the presence of $[Ru(NH_3)_6]^{3+}$ (12-52 mM).	339
Figure C.6	Plot of excited-state lifetime of **7:9** (35 μM) in the presence of $[Ru(NH_3)_6]^{3+}$ (0, 30, and 52 mM).	342
Figure C.7	Transient absorption difference spectrum constructed for oligonucleotide **6** (35 μM) following irradiation at 480 nm.	344
Figure D.1	Sequence of target 11-mer oligonucleotide prepared by solid-phase methods using the metal-containing monomers indicated.	351
Figure D.2	HPLC trace of the crude mixture from the synthesis of 5′-^{Ru}TCTCCTACACU$_{Ru}$ achieved by solid-phase methods.	353

List of Tables

Table 1.1	Electrochemical and Absorption Data for Donor-Acceptor Candidate Complexes.	8
Table 1.2	Transition Melting Temperatures for Duplexes Modified with Ru(II) Complexes.	37
Table 1.3	Absorption and Emission Data for Ru(II) Polypyridyl Complexes Incorporated into Oligonucleotides.	43
Table 2.1	Oligonucleotide Sequences.	71
Table 2.2	Thermal Denaturation Temperatures for Oligonucleotides containing 2′-Substituted Nucleosides.	82
Table 3.1	Electrochemical and Absorption Data for Model Complexes.	139
Table 3.2	Summary of Conditions for Metallations with $[Ru(bpy)_2(CO_3]$.	146
Table 3.3	Conditions for Metallation Reactions involving Ruthenium(II) Acetylacetonate Reagents.	177
Table 4.1	Thermal Denaturation Temperatures for Metallated and Modified Oligonucleotides.	212
Table 4.2	Absorption and Emission Data for $Ru(bpy)_2(impy)^{2+}$ Derivatives at Room Temperature.	221
Table 4.3	Absorption and Emission Data for Ru(II) Polypyridyl Complexes Incorporated into Oligonucleotides.	226
Table 5.1	Reduction Potentials and Absorption Data for Ru(II) Acetylacetonate Complexes.	253
Table 5.2	Ground and Excited State Properties in Acetonitrile at Room Temperature.	254

List of Abbreviations and Symbols

ε	extinction coefficient (M^{-1} cm^{-1})
A	adenine
A	electron acceptor
acac	acetylacetonate
AEPy or aepy	aminoethylpyridine
aepy′	5′-deprotected form of **3b**
AMPy or ampy	aminomethylpyridine
ampy′	*N*-(isopropyl)-aminomethylpyridine
BOP	benzotriazol-1-yloxytris(dimethylamino)phosphonium hexafluorophosphate
bphen	bathophenanthroline
bpy	2,2′-bipyridine
C	cytidine
D	electron donor
DBU	1,8-Diazabicyclo[5.4.0]undec-7-ene (1,5-5)
DCC	dicyclohexylcarbodiimide
DIEA	diisopropylethanolamine
DMAP	dimethylaminopyridine
DMF	dimethylformamide
DMT	4,4′-dimethoxytrityl
DNA	deoxyribonucleic acid
dppz	dipyrido[3,2:*a*-2′,3′:*c*]phenazine
ESI-MS	electrospray ionization mass spectrometry
ET	electron transfer
EtOAC	ethyl acetate
G	guanine
HOBT	hydroxybenzotriazole
HOMO	highest occupied molecular orbital
HPLC	high performance liguid chromatography
im	imidazole
IMPy or impy	iminomethylpyridine
impy′	5'-O-(4,4'-dimethoxytrityl)-2'-iminomethylpyridyl-2'-deoxyuridine
LLCT	ligand-to-ligand charge-transfer
MALDI-TOF	matrix-assisted laser desorption/ionization time-of-flight
Me_2-dppz	7,8-dimethyldipyridophenazine
MLCT	metal-to-ligand charge-transfer
N^7	N^7 of guanine
NHE	normal hydrogen electrode
NMR	nuclear magnetic resonance
phen	1,10-phenanthroline
phen′	5-(glutaric acid monoamide)-1,10-phenanthroline
phi	9,10-phenanthrene quinone diimine
pp	polypyridine
pyr	pyridine

RP	reverse-phase
SCE	saturated calomel electrode
T	thymine
tap	1,4,5,8-tetraazaphenanthrene
TBAH	n-tetrabutylammonium hexafluorophosphate
TEA	triethylamine
THF	tetrahydrofuran
TLC	thin-layer chromatography
tmen	tetramethylethylenediamine
U_a	2′-amino-2′-deoxyuridine
U_b	$N^{2'}$-(2-pyridylmethyl)-2′-amino-2′-deoxyuridine
U_{impy}	2'-iminomethylpyridyl-2'-deoxyuridine

Chapter 1

Introduction

Introduction

The interaction between ruthenium and nucleic acids is of on-going interest, due to the importance of developing agents that inhibit DNA synthesis and tumor growth.[1] Various Ru^{II} and Ru^{III} complexes exhibiting high binding affinities for nucleic acids have been investigated for potential antitumor activity.[2] Several studies have established that Ru(II) and Ru(III) ammine complexes bind DNA at N^7 of guanine bases, in addition to adenine and cytidine bases.[3,4] This propensity to bind nucleic acids is consistent with the observation that many ruthenium complexes inhibit DNA replication, display mutagenic activity, and retard RNA synthesis.[2,5-7]

A second motivation for investigating the interaction between ruthenium and nucleic acids is to assess the ability of DNA to mediate energy- and electron-transfer reactions.[8,9] Experiments involving ruthenium-modified duplexes have shown that DNA can mediate energy transfer.[10-13] Considerably more attention has centered on electron transfer (ET) processes in ruthenium-modified DNA assemblies.[14-17] ET reactions employing DNA as the intervening medium[16-22] have generated intense interest due to implications regarding the electronic properties of nucleic acids and the role ET plays in DNA damage and repair mechanisms.[23-29] Debate over the mechanism and distance dependence of radical cation migration in DNA underscores the need for DNA assemblies modified in specific locations with redox-active probes.[30-33] The design, synthesis, and subsequent incorporation of such probes into oligonucleotides pose major challenges in this area.[34]

Designing Donors and Acceptors for DNA-ET Reactions

Helpful lessons for designing redox-active probes for DNA-ET experiments can be derived from studies evaluating proteins as bridging media for ET reactions.[35-38] These studies employ electron donors (D) and acceptors (A) whose orbitals mix relatively weakly with those of the surrounding protein; the D and A do not possess redox potentials sufficient enough to allow reactions with the bridging medium. As a result, the effectiveness of the protein structure in coupling a D/A pair is directly assessed. The judicious choice of a D/A pair that is energetically well-separated from the bridging medium facilitates a clear evaluation of the parameters governing ET rates in biological settings.

Understanding the distinctions between protein and nucleic acid structures guides the design of D/A pairs suitable for DNA-ET studies (Figure 1.1). For the metalloproteins used in ET experiments, either D or A is a redox-active chromophore native to the protein; the other probe is incorporated via site-selective surface labeling. Since DNA does not contain naturally occurring chromophores nor unique ligands suitable for labeling, *two* redox-active chromophores must be prepared and incorporated into the DNA assembly. Unlike proteins, nucleic acids are highly negatively charged, and this characteristic strongly influences the association between cationic metal complexes and DNA. These considerations present significant obstacles to the design and preparation of D/A pairs.

Ideal donor and acceptor complexes possess several important characteristics, which are numbered here. (1) Each complex displays distinct absorption spectra so that the formation of the ET products may be monitored by time-resolved absorption

Figure 1.1: Three-dimensional structures of (a) the metalloprotein azurin surface-labeled with $Ru(bpy)_2(im)^{2+}$ at His 83, and (b) an unmodified B-form DNA duplex. Both structures are rendered from crystallographic datasets using Insight.

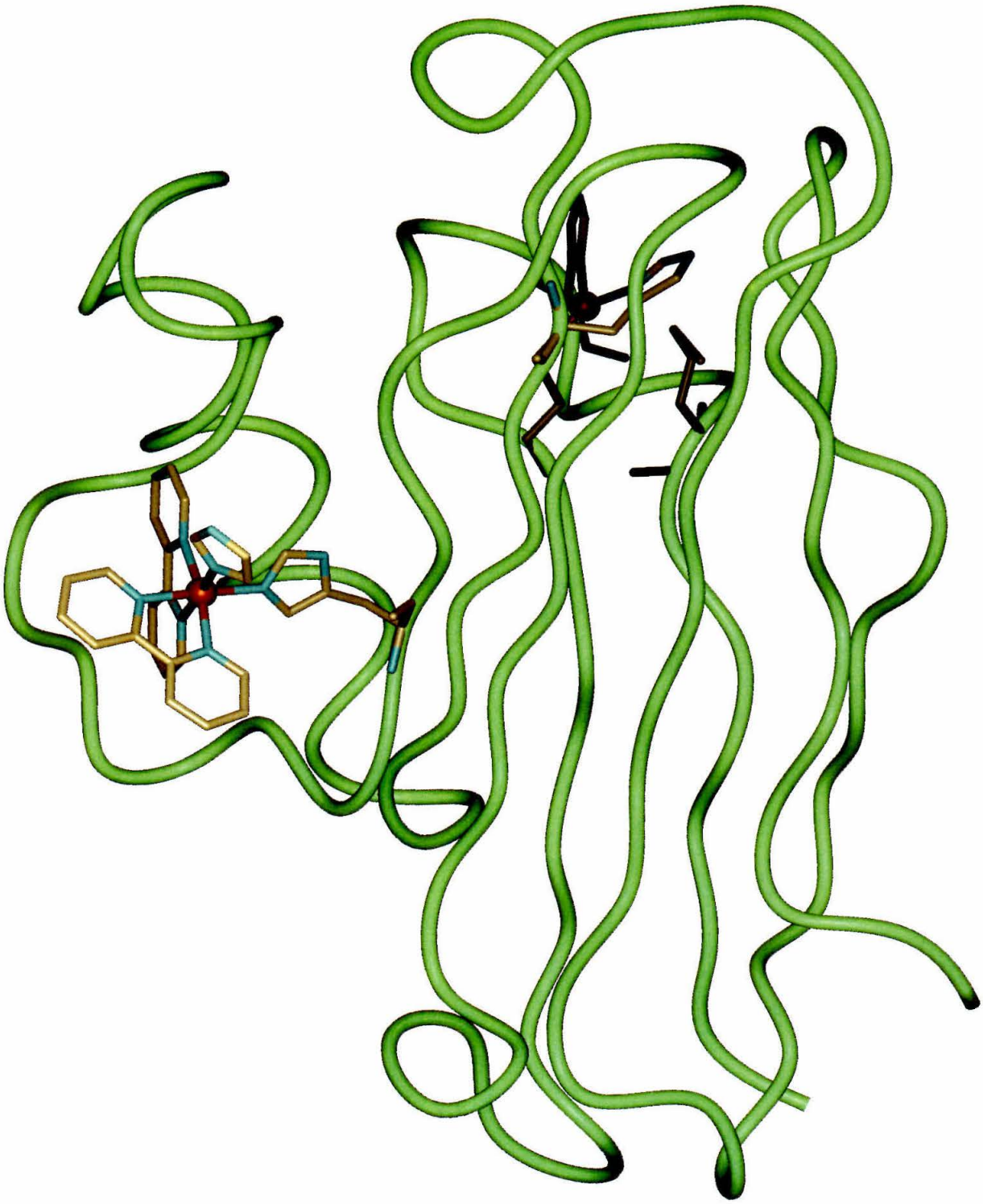

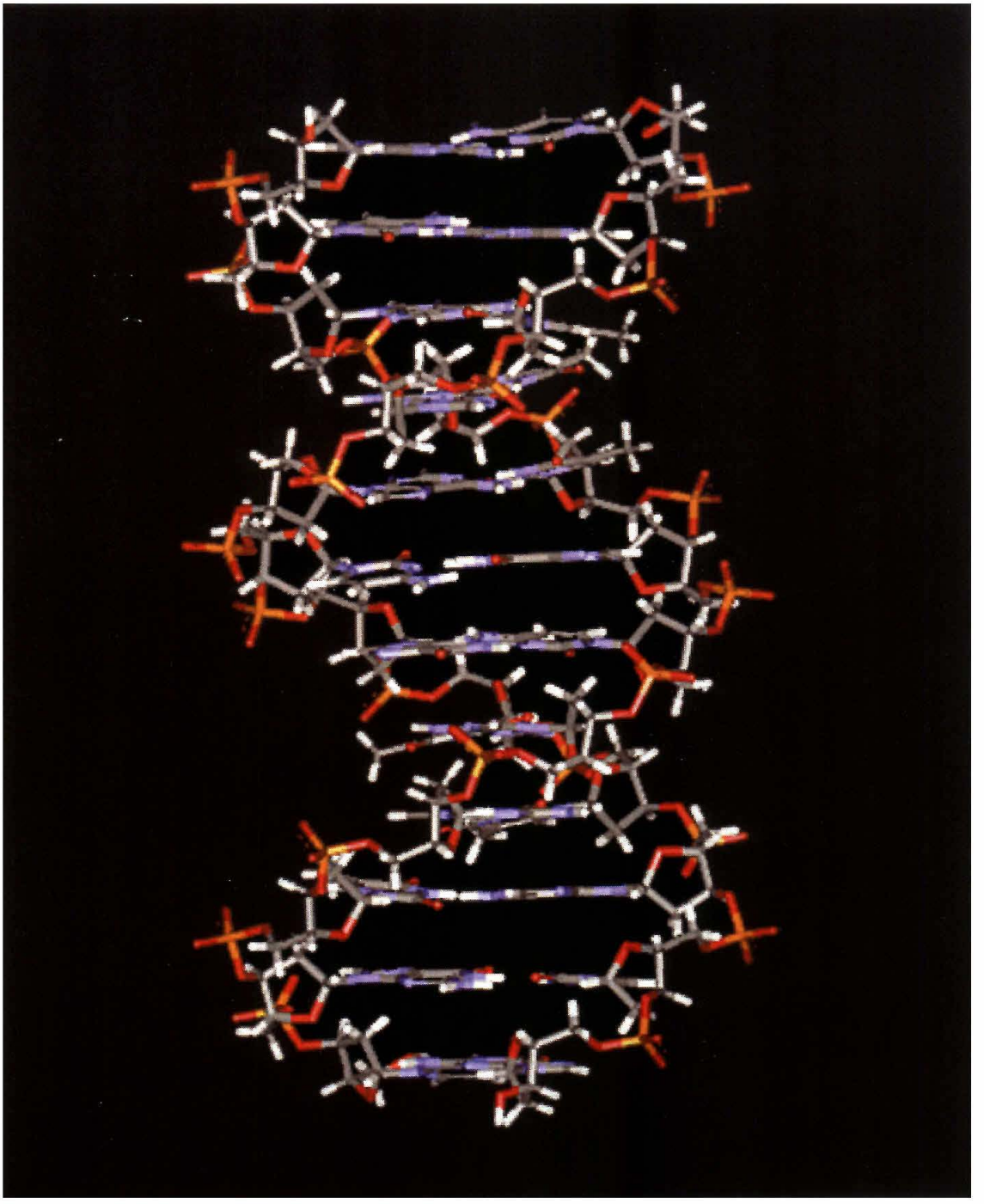

spectroscopy. In such experiments, wavelengths coinciding with the regions of MLCT absorption are monitored as the oxidation state of each metal complex changes in the course of the electron transfer reaction. Kinetic data are derived from the time-resolved changes in these bands. Extraction of the ET rate constant is aided by the use of metal complexes that display non-overlapping absorption bands. (2) Each complex exhibits reversible, one-electron redox chemistry so that the samples may be studied over several cycles without decomposition. The difference in the ground-state reduction potentials of the D/A pair provides sufficient thermodynamic driving force for the ET step. The complexes contain tunable ligands so that the dependence of ET rates on this value can be addressed. However, these probes do not possess reduction potentials strong enough to oxidize the DNA bases. (3) Additionally, the donor-acceptor complexes are incorporated at fixed locations within the DNA assembly so as to minimize the uncertainty in the distance separating these probes, as well as the number of conformations the metallated species can adopt.

With these design considerations in mind, we investigated several ruthenium complexes for their suitability as D/A complexes (Table 1.1). This series consists of ruthenium(II) complexes that exhibit metal-to-ligand charge-transfer (MLCT) transitions that may be easily tracked during transient absorption experiments. These D/A candidates possess reversible one-electron reduction potentials. Differences in the reduction potentials for this series are large, amounting to substantial thermodynamic driving force for ground-state ET reactions. By design, some of these complexes are emissive so that the envisioned DNA-ET experiments can employ the bimolecular quenching method developed for studying protein-ET.[39] While a limited number of

Table 1.1. Electrochemical and Absorption Data for Donor-Acceptor Candidate Complexes.[a]

Complex	$E_{1/2}$, V[b] vs. NHE	λ_{max}, nm[b] ($\varepsilon \times 10^{-3}$, M^{-1} cm^{-1})	Ref.
$[Ru(bpy)_2(im)(NH_2R)]^{2+}$	~1.2[c]	480 (11.0)[c]	40
$[Ru(bpy)_2(impy)]^{2+}$	1.51[c]	470 (13.0)	41
$[Ru(NH_3)_5(pyr)]^{2+}$	0.35	407 (7.7)	42
$[Ru(NH_3)_4(ampy)]^{2+}$	0.30	414 (6.3)	42
$[Ru(NH_3)_4(impy)]^{2+}$	0.56	520 (6.1) 378 (4.4)	42
$[Ru(acac)_2(impy)]$	0.23[c]	576 (4.6) 402 (4.6)	43
$[Ru(NH_3)_5(N^7(G))]^{2+}$	0.15	565 (0.44)	44

[a] Complexes in bold are emissive at room temperature. [b] Ru(III/II) potentials measured in aqueous solution (unless otherwise noted). [c] Measured in CH_3CN.
[d] Measured in EtOH.

ruthenium complexes meet the criteria prescribed above for ideal D/A complexes, we predicted that the few listed in Table 1.1 could be site-specifically incorporated into oligonucleotides. This assessment is based on the available literature for incorporating metal complexes into oligonucleotides.

Methods for Modifying DNA with Ruthenium Complexes

Incorporating D/A complexes at specific locations within single- and double-stranded oligonucleotides is a daunting challenge. The preparation of metal-containing oligonucleotides is achieved using the following methods: (a) post-synthetic modification,[17,45-59] (b) on-column derivatization,[27,60-63] and (c) solid-phase synthesis.[13,43,64-72] Of the metal complexes that have been introduced into DNA, ruthenium is the most widely used. The ruthenium complexes typically contain two types of ligands: an unmodified polypyridine ligand (pp) and a substituted polypyridine ligand containing a linker required for oligonucleotide attachment (pp′). While each method has specific requirements and advantages, the applicability of these methods is limited by the substitution chemistry of the individual metal center and stability of the metal complex to the conditions required by the method. Examples of the types of ruthenium-modified oligonucleotides prepared by each method, as well as an analysis of each method, are given below. To provide a clear understanding of how these methods rely on automated oligonucleotide synthesis, a description of the procedure is given first.

Oligonucleotide synthesis proceeds step-wise in a 3′→5′ direction, beginning with the nucleoside pre-derivatized to a solid support (Figure 1.2).[73-75] Treatment with mild acid removes the DMT group protecting the 5′ hydroxyl group on the ribose ring. Subsequent activation and coupling of the newly introduced phosphoramidite monomer

Figure 1.2: Solid-phase oligonucleotide synthesis by the phosphite-triester method.[73]

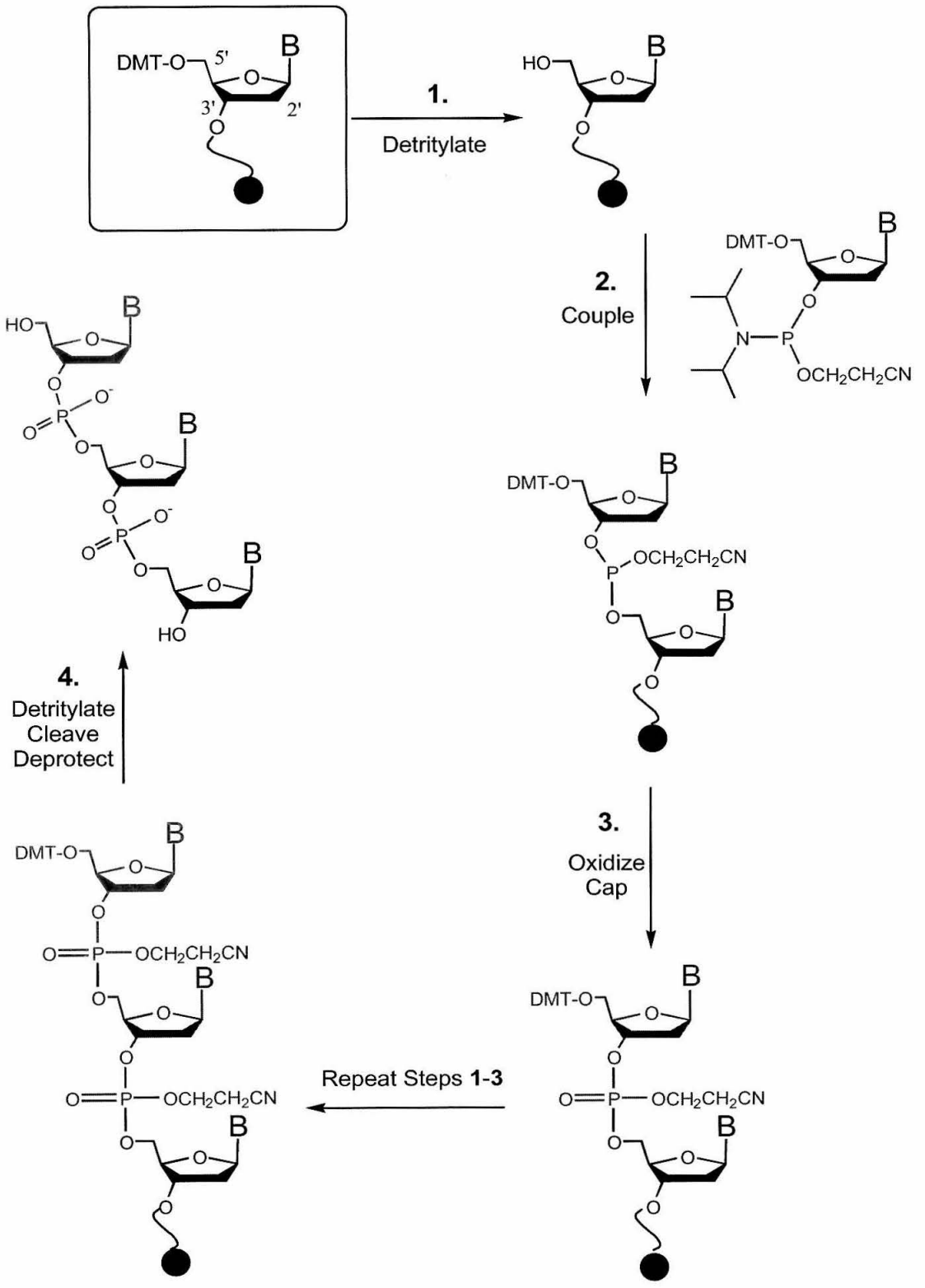
DMT-O
5'
3'
2'
B
O
1.
Detritylate
HO
2.
Couple
DMT-O
N
P
OCH2CH2CN
3.
Oxidize
Cap
Repeat Steps 1-3
4.
Detritylate
Cleave
Deprotect

yields a dinucleotide derivatized to the solid support. The phosphorus moiety is oxidized to form a stable P^V intermediate, and the synthesis cycle repeats until the sequence has been completed. The efficiency of each coupling is monitored by the release of the DMT cation after the introduction of each monomer. At the end of the cycle, the DMT group on the 5′ end is removed, and the oligonucleotide is cleaved from the solid support with concentrated aqueous ammonia. Prolonged incubation in this solution removes the protecting groups on the phosphorus and base moieties, producing the crude oligonucleotide in yields determined by the individual step-wise coupling reactions.

Post-Synthetic Modification. The post-synthetic modification method involves the (a) synthesis of nucleosides that possess reactive functional groups or metal-binding ligands, (b) incorporation of these modified nucleosides into oligonucleotides by solid-phase DNA synthesis, and (c) subsequent labeling of the reactive functional groups with the desired metal complex (Figure 1.3). This method is attractive because it enables the preparation of various metal-containing oligonucleotides from the same precursor strand.

There are two classes of oligonucleotides used in this method. The first class consists of oligonucleotides possessing a reactive functional group to which a metal complex can be coupled via an amide bond.[46,48,49,51] An example by Bannwarth illustrates how this class of oligonucleotides is used for ruthenium complex incorporation (Figure 1.4).[46] A single primary amine group is introduced at the 5′ termini of several oligonucleotides using amine-bearing phosphoramidites, with an overall incorporation yield of >60%. The ruthenium complexes are prepared in the form of activated *N*-succinimidyl esters in good yields (65-100%). Coupling of the ruthenium complexes to the amine-bearing oligonucleotides uses 25-fold excess metal reagent in a

Figure 1.3: Scheme outlining the steps involved in Post-Synthetic Modification. A nucleoside containing a reactive functional group is introduced into a growing oligonucleotide using standard phosphoramidite techniques. Upon completion of the synthesis, the oligonucleotide is cleaved from the solid support. Incubation of the crude mixture in concentrated aqueous ammonia removes the protecting groups on the base and phosphate moieties. The oligonucleotide is purified, and subsequently reacted with the desired metal complex, leading to the metal-modified oligonucleotide.

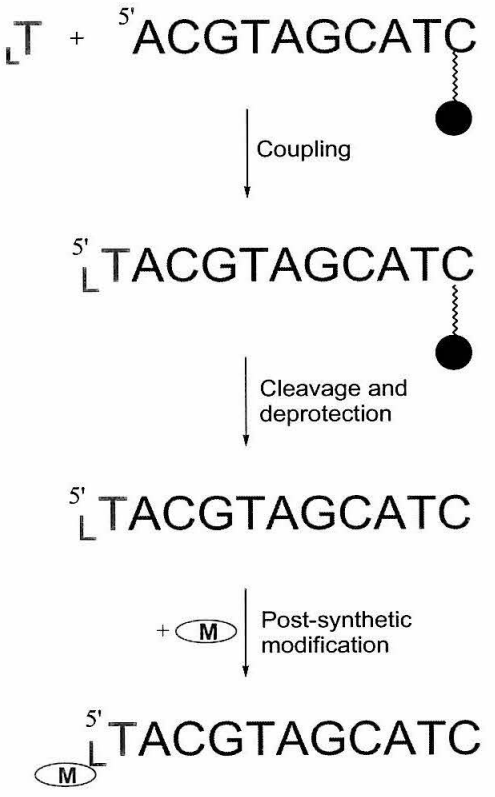
L T + 5' ACGTAGCATC
Coupling
5' L TACGTAGCATC
Cleavage and deprotection
5' L TACGTAGCATC
+ M
Post-synthetic modification
5' L TACGTAGCATC
M
L = Reactive functional group
= Alkylamine linker
= Solid support
M = Metal complex

Figure 1.4: Reaction scheme outlining the coupling of $[Ru(bphen)_2(bphen')]^{2+}$ to an amine-bearing oligonucleotide.

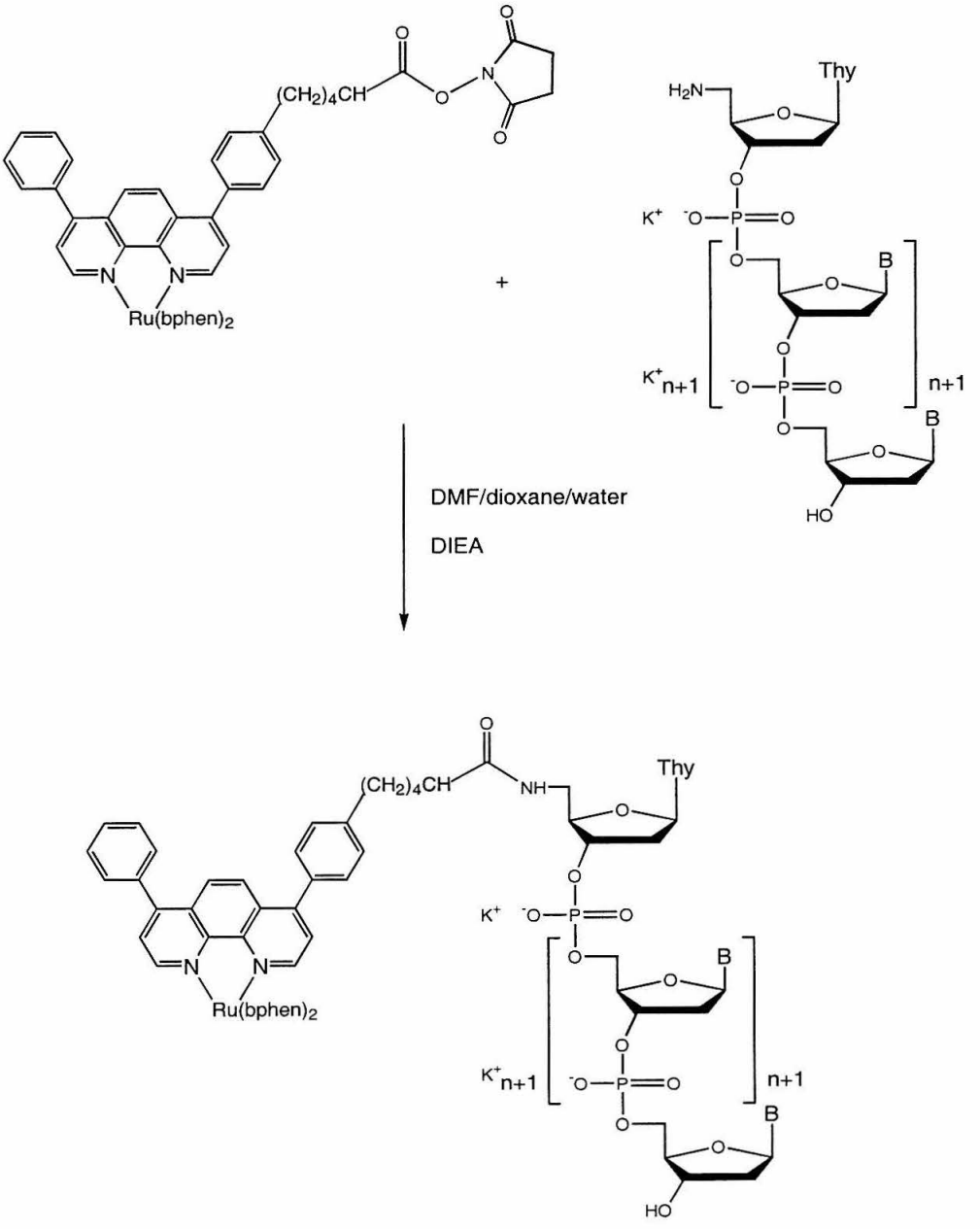
Ru(bphen)2
+
DMF/dioxane/water
DIEA
Thy
B
HO
n+1

dioxane/DMF/water mixture, producing 5′-modified ruthenated oligonucleotides in moderate yields (Figure 1.5:A).

Other examples using this class of oligonucleotides offer minor modifications to the above procedure. Barton and coworkers employ oligonucleotides modified with a hexylamine linker at the 5′ terminal phosphate group.[48,49] The ruthenium complexes contain a pp′ ligand bearing a glutaric acid arm that is subsequently coupled to the 5′ amine groups of the modified oligonucleotides. The coupling reaction takes place in the presence of DCC in a DMF/dioxane slurry, giving 5′-modified ruthenated oligonucleotides in very low yields (<1%) (Figure 1.5:B). Work by Kirsch-De Mesmaeker utilizes a method analogous to that described by Bannwarth, with the exception that the ruthenium complex is coupled to an amine-bearing nucleoside placed in the middle of the oligonucleotide sequence.[51] The amine group is tethered to the base of uracil, and the modified nucleoside is introduced into the oligonucleotide by standard phosphoramidite coupling chemistry. Following activation, a 150-fold excess of ruthenium complex is added to the amino-oligonucleotide, leading to ruthenium-modified oligonucleotides in yields of 20% (Figure 1.5:C).

The second class of oligonucleotides employed in post-synthetic modification methods possess metal-binding ligands at either the 5′ end or in the middle of the strand.[17,47,58] The metal-binding ligands (primary amine or bipyridine groups) are introduced into the oligonucleotide via modified nucleosides. Metal complexation occurs upon addition of the free metal reagent to the ligand-bearing oligonucleotide. Hybridization of the modified oligonucleotide prior to metal complexation reduces the number of undesired side-products.[17]

Figure 1.5: Examples of ruthenium-modified oligonucleotides prepared by the Post-Synthetic Modification method. References for each example: A[46], B[48], C[51], D[47], E[17], F[58]. "Ru" represents Ru(II) unless otherwise noted.

A

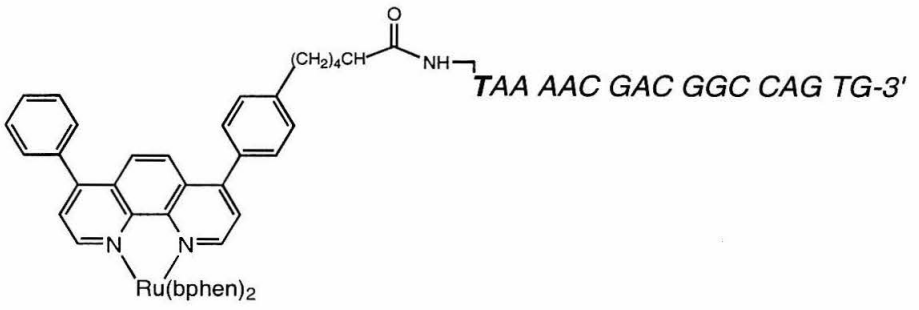
(CH2)4CH
O
NH
TAA AAC GAC GGC CAG TG-3'
N
N
Ru(bphen)2

B

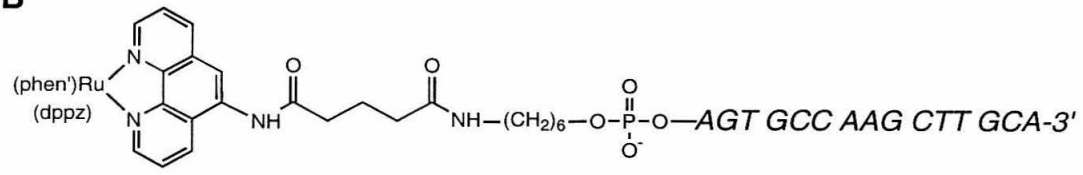
(phen')Ru
(dppz)
N
N
NH
O
O
NH—(CH2)6—O—P—O—AGT GCC AAG CTT GCA-3'
O
O-

C

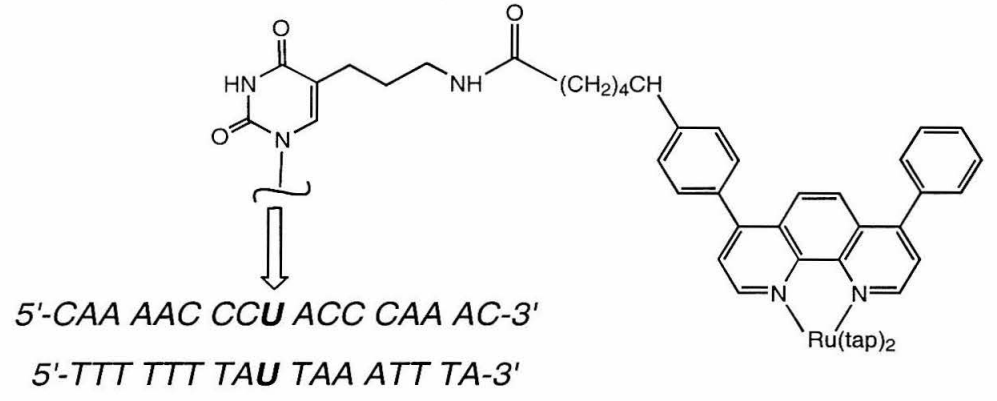
HN
O
O
N
NH
O
(CH2)4CH
N
N
Ru(tap)2
5'-CAA AAC CCU ACC CAA AC-3'
5'-TTT TTT TAU TAA ATT TA-3'

D

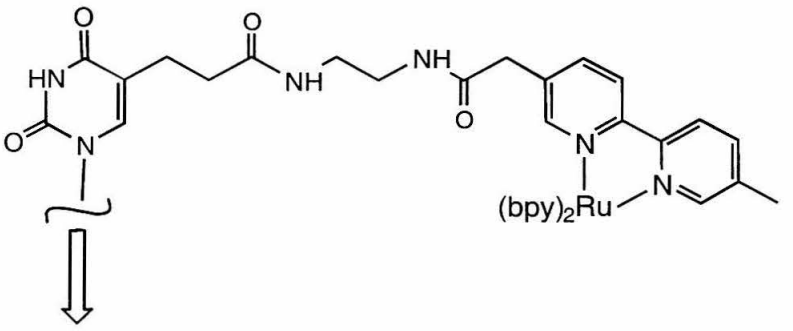

5'-GCA C**T**C AG-3'

E

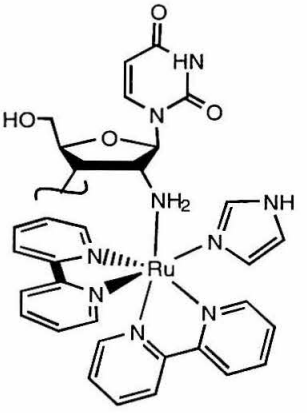

5'-**U**GCATCGA-3'

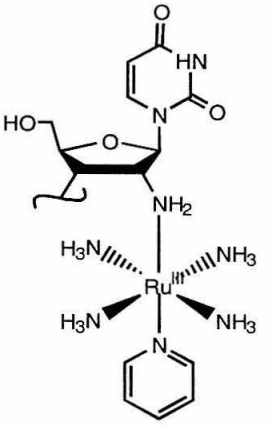

5'-**U**CGATGCA-3'

F

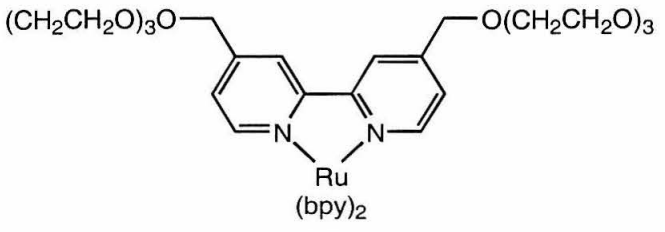

5'-TTT TTT TT-**L**-TTT TTT TT3'

Netzel and coworkers utilize nucleosides modified at the base with an amine-bearing linker.[47,76] The modified nucleoside is introduced into oligonucleotides using standard phosphoramidite techniques; a DMF solution of activated bipyridine ligand is added in 100-200-fold excess to the amine-bearing oligonucleotide in a borate buffer solution. The yield of bipyridine-containing oligonucleotides produced from this coupling reaction is between 40-60%. Complexation of ruthenium reagents with these modified oligonucleotides takes place in aqueous ethanol and gives ruthenium-modified oligonucleotides in 5-10% yields (Figure 1.5:D).

Meade employs a multi-step synthetic route to prepare 2′-amino-modified nucleosides that are subsequently introduced into oligonucleotides using standard phosphoramidite techniques.[17] The modified oligonucleotides are hybridized to complementary strands, and the ruthenium reagents are added in 10-fold excess to the resulting amine-containing duplexes in buffered aqueous solution. The yield of ruthenium-modified oligonucleotides obtained by this method ranges from 25-50% (Figure 1.5:E).

McLaughlin incorporates a non-nucleosidic bipyridine linker into the backbone of several oligonucleotides using standard phosphoramidite techniques.[58] The ruthenium reagent is added in slight excess to the bipyridine-containing oligonucleotides in refluxing aqueous ethanol. While the yield of ruthenium-modified oligonucleotides was not specified, analytical measurements suggest a nearly quantitative complexation reaction (Figure 1.5:F).

Analysis. The types of ruthenium-oligonucleotide conjugates prepared using this method include base-, ribose-, and phosphate-modified oligonucleotides (Figure 1.5).

The preparation of the first class of oligonucleotides takes advantage of commercially available reagents that bear the desired amine group. The ruthenium complexes are easily synthesized as activated ester derivatives. However, the coupling reactions involve large amounts of ruthenium reagents and lengthy reaction times; the overall yields of ruthenium-modified oligonucleotides are poor-to-moderate. The second class of oligonucleotides requires multi-step syntheses to obtain the nucleosides containing metal-binding ligands. Excess unreacted ruthenium reagents likewise complicate isolation of the products, since multiple chromatographic separations are necessary for best isolation. While these efforts are rewarded in part by the moderate overall yields of ruthenium-modified oligonucleotides, this method is not an efficient means of incorporating ruthenium into DNA relative to the other two methods described below.

On-Column Derivatization. The method of on-column derivatization exploits the step-wise nature of solid-phase DNA synthesis by introducing non-phosphitylated ruthenium reagents to the oligonucleotide during or after automated synthesis.[27,60-63] The ruthenium complex is coupled to a reactive functional group positioned in the oligonucleotide at 5′-terminal or internal locations of the sequence. This reaction takes place prior to cleavage of the oligonucleotide from the solid support. The resulting ruthenium-modified oligonucleotide is liberated, deprotected, and isolated. Delivering ruthenium reagents in this manner takes advantage of the fact that all of the bases are protected; this both eliminates a purification step and minimizes the number of side-products. A few examples illustrate the utility of this method.

Recent work by Grinstaff involves the preparation of an iodo-substituted nucleoside that is incorporated via phosphoramidite coupling techniques into an

oligonucleotide (Figure 1.6).[61,62] This modified nucleoside is used in Pd(0) cross-coupling reactions with an alkynyl-derivatized ruthenium complex. Following incorporation of the modified nucleoside into the oligonucleotide, the column is removed from the synthesizer and subjected to the cross-coupling reagents. The excess reagents are washed away, the column is returned to the DNA synthesizer, and the oligonucleotide synthesis is resumed. Subsequent cleavage and deprotection of the ruthenium-containing oligonucleotide produces the desired product in 75-92% yields (Figure 1.7:A).

Barton and coworkers prepare an unmodified oligonucleotide using standard solid-phase DNA methodology, introduce an amine-bearing linker to the 5′ hydroxyl group of the oligonucleotide, and couple the ruthenium complex to the amino-terminated strand in organic solvents.[60] Treatment of the ruthenium-modified oligonucleotide with concentrated aqueous ammonia cleaves the product from the solid support, and subsequent purification gives the desired oligonucleotide (Figure 1.7:B). While this method has been used extensively by the Barton group, the overall yield of ruthenium-modified oligonucleotides has not been reported.[15]

Additional work by this group demonstrates the incorporation of two metal complexes at the 5′ and 3′ ends of an oligonucleotide.[63] This work is analogous to the on-column derivatization chemistry for the 5′-end modifications just described. The method uses a commercially available solid support that contains a hydroxy aminoalkane masked with Fmoc and DMT protecting groups. Oligonucleotide synthesis proceeds from the deprotected DMT hydroxy group. At the conclusion of the oligonucleotide synthesis, an osmium complex is coupled to the 5′ end as described above. At the opposite end, the Fmoc group is removed and a rhodium complex is coupled as an

Figure 1.6: Scheme outlining the steps involved in On-Column Derivatization: (a) removal of the DMT protecting group followed by introduction of a modified nucleoside in phosphoramidite form; (b) removal of reaction column from synthesizer and subsequent cross-coupling of alkynyl-derivatized ruthenium complex to the iodo-substituted nucleoside; (c) return of reaction column to synthesizer and resumption of oligonucleotide synthesis; (d) cleavage of the product oligonucleotide from the solid support and deprotection of the base- and phosphate-protecting groups.[61]

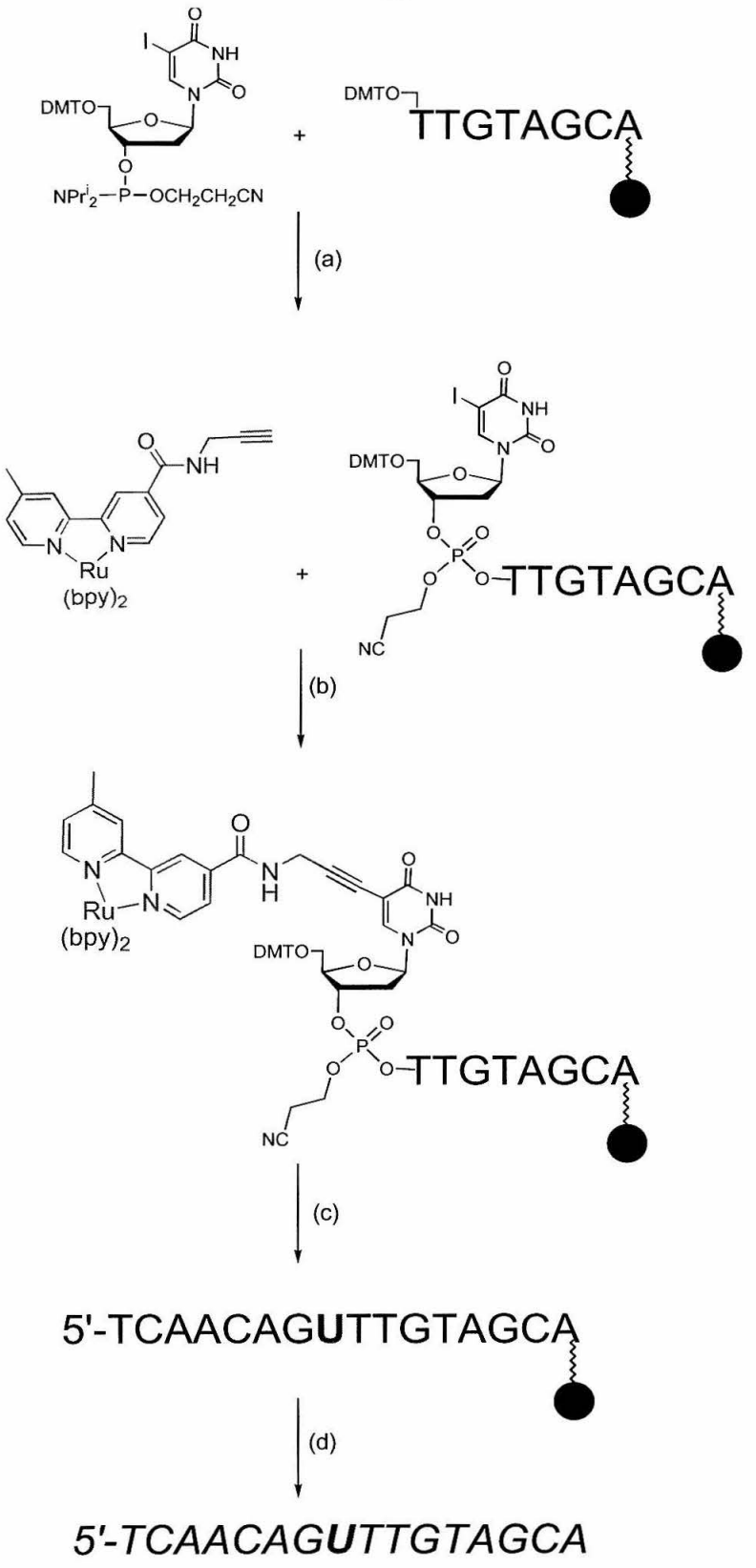
DMTO
TTGTAGCA
(a)
(bpy)2
(b)
(c)
5'-TCAACAGUTTGTAGCA
(d)
5'-TCAACAGUTTGTAGCA

Figure 1.7: Examples of ruthenium-modified oligonucleotides prepared by the On-Column Derivatization method. References for each example: A[61], B[60], C[63].

A

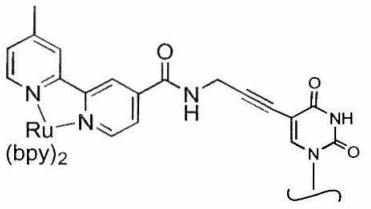

5'-TCAACAG**U**TTGTAGCA

B

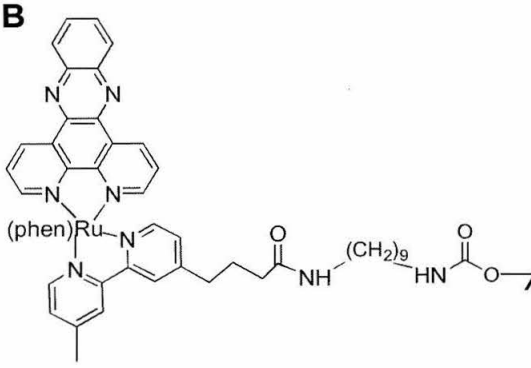

AGT CTC AGA CGC ACC GAT CA-3'

C

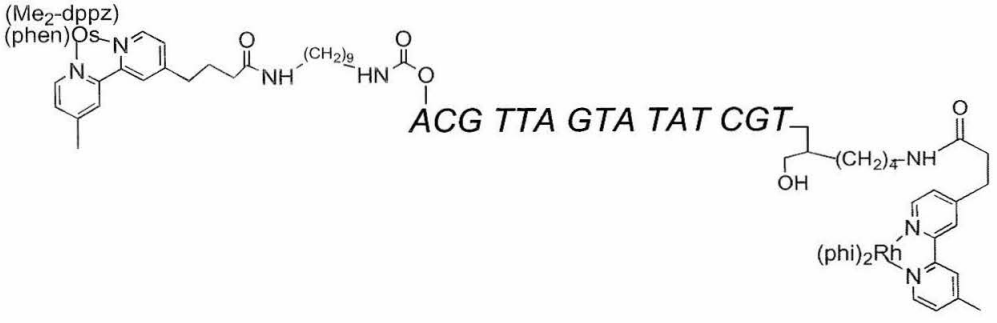

ACG TTA GTA TAT CGT

activated ester to the newly deprotected amine group. The bis-metallated oligonucleotide is cleaved and deprotected completely to give an oligonucleotide bearing an osmium complex at the 5′ end and a rhodium complex at the 3′ end (yield not given) (Figure 1.7:C). Although this chemistry is performed with rhodium and osmium complexes, it could easily be extended to similarly substituted ruthenium complexes.

Analysis. Base-modified and 5′ end-labeled oligonucleotides can be prepared using the on-column derivatization method. This method relies on the coupling chemistry developed for the first class of oligonucleotides described above in the section on post-synthetic modification. Introducing the metal reagents during or following oligonucleotide synthesis reduces the number of synthetic steps needed to prepare the desired metal-modified oligonucleotide, although the reaction times are lengthy. Incorporation yields appear to be higher than those reported for post-synthetic modification, although the yield data are incomplete. The absence of side-products greatly aids isolation of the product. While this method represents an improvement upon the Post-Synthetic Modification method, it is limited by the reliance upon coupling chemistries compatible with the conditions of automated oligonucleotide synthesis. Additional synthetic constraints are imposed by the requirement that the ruthenium complexes be converted into activated esters or alkynyl derivatives to bring about coupling.

Solid-Phase Synthesis. The last method discussed in this section involves the preparation of metal-containing monomers that can be incorporated during solid-phase DNA synthesis using standard phosphoramidite coupling techniques.[13,43,64,68-72] Advantages of this method include: rapid preparation of metal-containing

oligonucleotides, high yields of metal incorporation, and routine product isolation. However, the success of this method depends on the construction of individual metallated monomers that are compatible with automated DNA synthesis techniques.

Ruthenium complexes can be introduced during automated synthesis as either metallated phosphoramidite or phosphonate monomers (Figure 1.8). Bannwarth describes the preparation of $[Ru(bphen)_2(bphen')]^{2+}$, where bphen′ is a substituted bathophenanthroline ligand bearing a hydroxyl group that is phosphitylated to form the ruthenated phosphoramidite monomer (Figure 1.8A).[64] Because isolating this monomer results in moderate yields, it is generated *in situ* and coupled directly to the growing oligonucleotide chain; this procedure leads to a high coupling yield (value not reported). Work by Giese provides an example of incorporating ruthenium complexes as phosphonate monomers (Figure 1.8B).[68] A tris-heteroleptic Ru(II) complex is prepared wherein one ligand containing a hydroxyl group is converted to a phosphonate. Again the crude monomer is used directly in the coupling reaction, resulting in a high incorporation yield (value not reported).

Additional work by the Tor and Grinstaff groups illustrates the routine nature of preparing and incorporating metallated monomers. Tor applies a versatile Pd(0)-mediated cross-coupling method that enables the selective functionalization of mixed-chelate complexes.[13] This approach allows the preparation of base-modified nucleosides in high yields after a few steps; likewise, high yields are observed for the synthesis of the corresponding phosphoramidites of $[Ru(bpy)_2(phen')]^{2+}$ (80%) (Figure 1.8D). Manual coupling of the ruthenated monomers results in coupling yields that are greater than 90%. Work by Grinstaff follows similar synthetic procedures for preparing base-modified

Figure 1.8: Structures of ruthenium-modified phosphonate (red) and phosphoramidite (blue) monomers, and examples of oligonucleotides prepared by Solid-Phase Synthesis. References for each example: A[64], B[68], C[70], D[13], E[62,69,77], F[71], G[78].

A

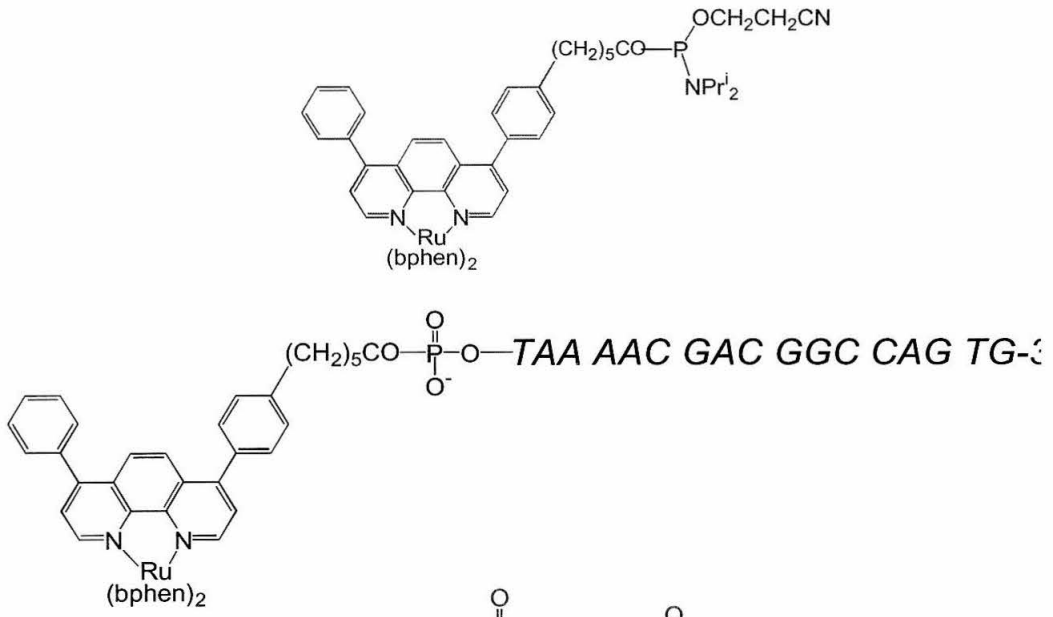
OCH2CH2CN
(CH2)5CO—P
NPri2
N
Ru
N
(bphen)2
(CH2)5CO—P—O—TAA AAC GAC GGC CAG TG-3
O
O-
(bphen)2

B

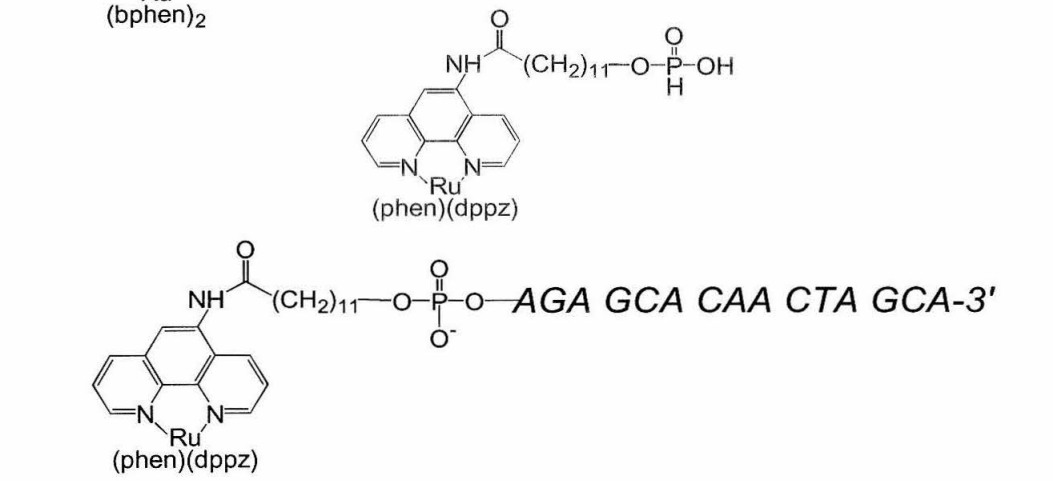
NH
(CH2)11—O—P—OH
O
H
(phen)(dppz)
NH
(CH2)11—O—P—O—AGA GCA CAA CTA GCA-3'
O-
(phen)(dppz)

C

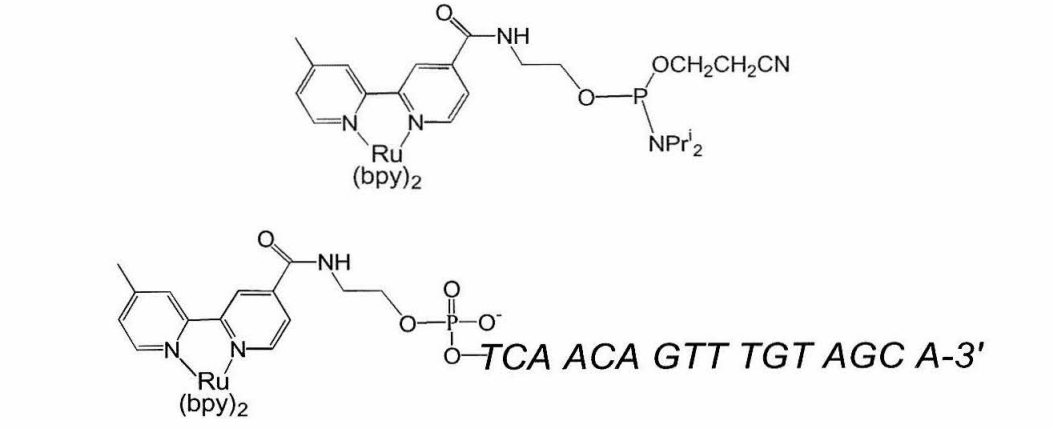
NH
OCH2CH2CN
O—P
NPri2
Ru
(bpy)2
NH
O—P—O-
O—TCA ACA GTT TGT AGC A-3'
(bpy)2

D

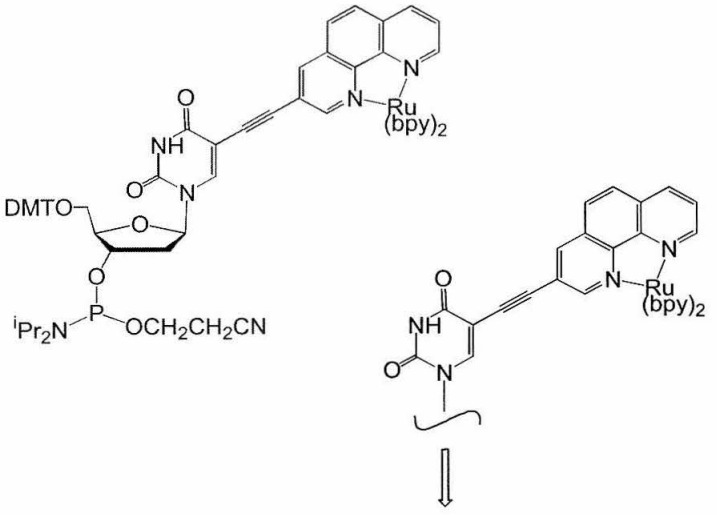

*5'-**U**CG GCG CGA ATT CGC GTG CC-3*

*5' TCG GCG CGA A**U**T CGC GTG CC-3'*

E

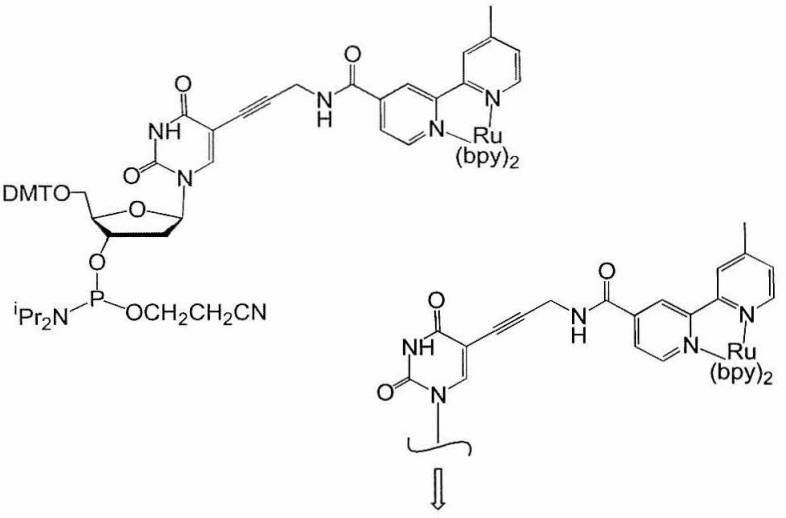

*5'-**U**CA ACA GTT TGT AGC A-3'*

*5'-TCA ACA G**U**T TGT AGC A-3'*

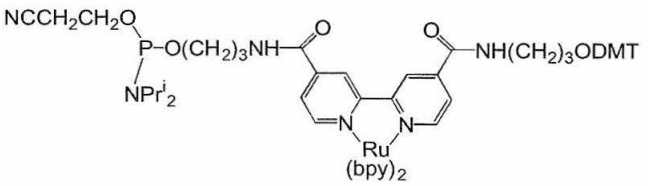

F

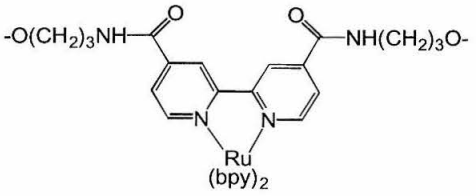

⇩

*5′ TTT T-**L**-A AAA-3′*

*5′ GGG-**L**-CCC 3′*

*5′ GCA ATT GC-**L**-GCA ATT GC-3′*

G

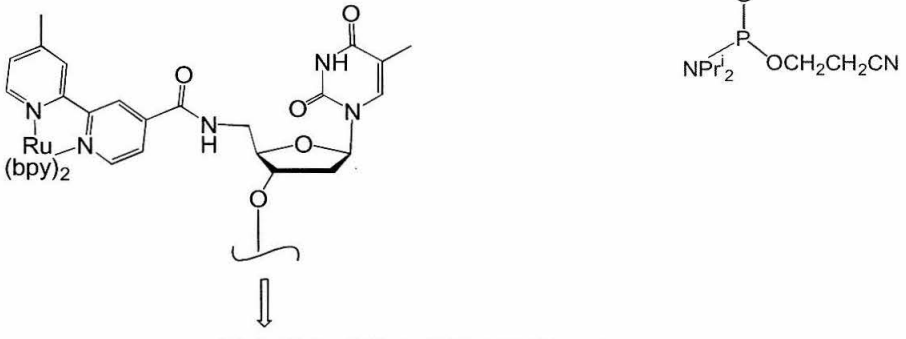

⇩

*5′-**T**CA ACA GTT TGT AGC A-3′*

*5′-**T**TC AAC AGT TTG T-3′*

phosphoramidites of the form $[Ru(bpy)_2(bpy')]^{2+}$, for which comparable coupling yields are observed (Figure 1.8E).[69,77] Other phosphoramidite derivatives can be prepared in high yields by the methods employed above (Figure 1.8C,F,G).[70,71,78] Coupling yields for the non-nucleosidic derivative in Figure 1.8F are > 95%, whereas the overall yield of ruthenium-modified oligonucleotides is 3-5% after purification. The metallated monomers in Figure 1.8F and Figure 1.8G give ruthenium-modified oligonucleotides in 50-75% yield.

An attractive approach to introducing metallated monomers during automated oligonucleotide synthesis involves the preparation of customized solid supports. Oligonucleotide synthesis can be initiated with a DMT-protected nucleoside that is derivatized to a silica- or polymer-based solid support. In principle, the solid support may contain a metallonucleoside that is stable under the extreme conditions required for automated synthesis. Synthesis begins with the metal-containing solid support and yields an oligonucleotide modified at the 3′ terminus with a metal complex. This approach is demonstrated for the first time using a ruthenium(II) polypyridine complex.[43] Details of this work are described in Chapter 4.

Analysis. This method is a successful way to prepare several oligonucleotides modified with ruthenium(II) polypyridine complexes at the 5′ terminus and intervening positions. While this method was first demonstrated by Bannwarth in 1989, several years elapsed before it was further explored as a general method. Recent advances in nucleoside chemistry have facilitated the preparation of several metallated monomers. Synthesizing these monomers typically requires several steps and produces metallated phosphoramidites that are highly moisture sensitive. Additionally, the extreme

conditions routinely encountered during automated synthesis—mild acid and strong base—preclude the widespread application of solid-phase synthetic methods to a host of ruthenium complexes. However, high coupling yields are observed for the metallated monomers; the judicious placement of the ruthenium complex away from the 3′ position is responsible for this observation in many cases. Additionally, the overall yields of ruthenium-containing oligonucleotides are far greater than those achieved via the post-synthetic modification and on-column derivatization methods, due to the ease of both oligonucleotide synthesis and product isolation.

Characterization of Ruthenium-Modified Oligonucleotides

Two consequences arise from the incorporation of mixed-chelate ruthenium(II) complexes into oligonucleotides. First, the presence of the ruthenium complex influences the duplex stability; the extent of structural destabilization caused by the incorporated ruthenium complex is evaluated with thermal denaturation studies. Second, the oligonucleotide environment alters the properties of the ruthenium complex. Analysis of the absorption and emission properties of the ruthenium-modified oligonucleotides assesses the impact of oligonucleotide incorporation upon the ruthenium center. Changes in these properties are ascribed to (a) the presence of substituted ligands containing linkers needed for oligonucleotide attachment (pp′), and (b) the environment typical of a DNA duplex. A summary of these consequences is given for the ruthenium-modified oligonucleotides presented in the previous section.

Effect of Ruthenium Complexes on Duplex Stability. Thermal denaturation studies serve as a limited evaluation of how the incorporated metal influences the duplex stability. In the case of ruthenium-containing duplexes, it is difficult to ascertain from the

transition melting temperatures (T_m) if the cationic nature of the ruthenium complex partially offsets the destabilization caused by the modification. For example, the T_m values for duplexes labeled with nonintercalating ruthenium complexes are similar to the T_m values for the unmodified duplexes. Slight changes in the T_m values are dependent on the specific placement of the ruthenium complex within the duplex, as well as the nature of attachment to the duplex (i.e., base- or phosphate-derivatized). The presence of sodium ions has a large stabilizing effect on these duplexes. Examples of these trends are summarized below. (The reader is referred to Figures 1.5-1.8 for the structures of the metal-containing oligonucleotides. Specific T_m values are not quoted in the discussion, but rather the specific entry in Table 1.2 is cited in italics so that the reader can consult the table for all relevant data.)

Duplexes end-labeled with nonintercalating ruthenium complexes typically display T_m values that are essentially unchanged from the values reported for unmodified duplexes. For example, a 20-mer duplex containing $[Ru(bpy)_2(phen')]^{2+}$ attached to the base of the 5′-terminal nucleoside exhibits a T_m only one degree higher than that of the unmodified duplex (Table 1.2:*1a*; Figure 1.8D).[13] The T_m values for a 16-mer duplex containing $[Ru(bpy)_2(bpy')]^{2+}$ attached to the base of the 5′-terminal nucleoside and the corresponding unmodified duplex are identical (Table 1.2:*2a*; Figure 1.8E).[62] When the same metallonucleosides in these two examples are placed mid-way in the duplex sequence, the T_m values decrease slightly (Table 1.2:*1b-2b*; Figure 1.8D,E). Interestingly, a dramatic dependence on $[Na^+]$ is revealed in the T_m values for one of these modified duplexes (Table 1.2:*2b-c*; Figure 1.8E).

Table 1.2. Transition Melting Temperatures for Duplexes Modified with Ru(II) Complexes.[a]

Entry #		Complex/Sequence	T_m Ru DNA	T_m control	NaP_i (mM)	NaCl (mM)	Ref.
1	a	$Ru(bpy)_2(phen')^{2+}$ 5′-**X**CGGCGCGAATTCGCGTGCC-3′	79	78	10	100	13
	b	$Ru(bpy)_2(phen')^{2+}$ 5′-TCGGCGCGAA**X**TCGCGTGCC-3′	75	78	10	100	13
2	a	$Ru(bpy)_2(bpy')^{2+}$ 5′-**X**CAACAGTTTGTAGCA-3′	49	49	5	50	62
	b	$Ru(bpy)_2(bpy')^{2+}$ 5′-TCAACAG**X**TTGTAGCA-3′	48	49	5	50	62
	c	$Ru(bpy)_2(bpy')^{2+}$ 5′-TCAACAG**X**TTGTAGCA-3′	51	60	150	-	77
3	a	$Ru(bpy)_2(bpy')^{2+}$ 5′- **X**TCAACAGTTTGT-3′	39	42	5	50	78
	b	$Ru(bpy)_2(bpy')^{2+}$ 5′- **X**TCAACAGTTTGTAGCA-3′	51	53	5	50	78
	c	$Ru(bpy)_2(im)(NRH_2)^{2+}$ [b] 5′-**X**GCATCGA-3′/5′-**X**CGATGCA-3′	36-42	45	100	900	17
4	a	$Ru(bpy)_2(bpy')^{2+}$ 5′-GCAC^{X}TCAG-3′	35	-	10	1000	47
	b	$Ru(bpy)_2(bpy')^{2+}$ 5′-^{X}TCAACAGTTTGTAGCA-3′	42	60	5	150	70
5	a	$Ru(bpy)_2(bpy')^{2+}$ 5′-TTTT-**X**-AAAA-3′	<20	49	-	1000	71
	b	$Ru(bpy)_2(bpy')^{2+}$ 5′-GGG-**X**-CCC-3′	50	>80	-	1000	71
	c	$Ru(bpy)_2(bpy')^{2+}$ 5′-GCAATTGC-**X**-GCAATTGC-3′	50	-	-	1000	71
6	a	$Ru(phen)(phen')(dppz)^{2+}$ 5′-^{X}AGAGCACAACTAGCA-3′	59	52	10	50	68
	b	$Ru(tap)_2(dip)^{2+}$ 5′-CAAAACCC**X**ACCCAAAC-3′	62	60	10	50	51
	c	$Ru(tap)_2(dip)^{2+}$ 5′-TTTTTTTA**X**TAAATTTA-3′	40	40	10	50	51

[a] Values are reported for solutions containing sodium phosphate and sodium chloride at pH 7.0 (°C) unless otherwise noted. Duplexes are formed with the ruthenium-modified oligonucleotide listed and the corresponding unmodified complementary strand (not shown), except where noted. **X** denotes metal attachment to oligonucleotide via linker to nucleoside base, ribose, or phosphate. Please see Figure 1.8 for details of metal attachment for each system. [b] Complementary strand contains $[Ru(NH_3)_4(pyr)]^{3+}$ attached to a 5′ aminoribose.

Further changes are observed when similar ruthenium complexes are attached directly to the 5′ ribose position, as opposed to the base of a terminal nucleoside (Table 1.2:*3a-b*; Figure 1.8G). An 8-mer duplex that is labeled with two ruthenium complexes at both 5′ termini, displays a broad helix-to-coil transition, with a T_m value in the range of 36-42 °C (Table 1.2:*3c*; Figure 1.5E). Comparing this value to that obtained for the unmodified duplex suggests that the short duplex is reasonably stable in spite of the presence of two ruthenium complexes.

Attaching non-intercalating ruthenium complexes to duplexes via extended linkers leads to mixed results. For example, linking $[Ru(bpy)_2(bpy')]^{2+}$ to a nucleobase using a long tether does not cause large changes in the T_m values of metallated vs. unmodified duplexes, provided that the metallonucleoside is incorporated into the middle of the duplex (Table 1.2:*4a*; Figure 1.5D).[47] However, when $[Ru(bpy)_2(bpy')]^{2+}$ is tethered to the 5′-terminal phosphate group, the difference in the T_m values is dramatic (Table 1.2:*4b*; Figure 1.8C).[70] This result suggest that attaching a cationic ruthenium complex with a short ethylene spacer to the 5′ terminal phosphate has a large destabilizing effect on the duplex. The absence of a nucleoside that imparts rigidity to the oligonucleotide terminus may be responsible for the lower T_m value.

For the ruthenium-modified oligonucleotides designed to form hairpins under high ionic strength, the T_m values indicate that two 8-mer strands do not adopt well-defined structures (Table 1.2:*5a-c*; Figure 1.8F).[71] The T_m value for the 16-mer oligonucleotide suggests that a stable hairpin is formed in the presence of 1.0 M sodium chloride.

For intercalating complexes covalently tethered to duplexes, the T_m values are higher compared to those for unmodified duplexes. As a result, the extent of destabilization appears to be compensated by the insertion of a π-stacking ligand into the duplex. However, dramatic structural changes are imposed on the duplex to accommodate the inserted ligand. Therefore, thermal denaturation studies of duplexes modified with intercalating complexes provide only a preliminary assessment of how the incorporated ruthenium influences the duplex stability. For example, a substantial increase in the T_m value is observed for a duplex end-labeled with an intercalator (Table 1.2:*6a*; Figure 1.8B).[68] This increase of 7 °C is attributed to the presence of the intercalating ruthenium complex. However, the T_m values for duplexes containing an intercalator conjugated to the middle of the sequence are identical or only slightly increased relative to the T_m values of unmodified duplexes (Table 1.2:*6b-c*; Figure 1.5C).[51] In these two examples, tethering the intercalator to the end has a large effect on the T_m value.

Absorption of Ruthenium-Modified Oligonucleotides. The oligonucleotides containing non-intercalating ruthenium complexes display electronic spectra that are similar to those of the appropriate model complexes. Changes in the absorption maximum occur when the model complex is modified to accommodate linkers needed for oligonucleotide attachment (Figure 1.9). The resulting monomer complex (i.e., $[Ru(bpy)_2(bpy')]^{2+}$, where bpy′ denotes a substituted bipyridine ligand containing the linker) exhibits an absorption maximum that is unchanged or slightly red-shifted from λ_{max} for $[Ru(bpy)_3^{2+}]$.[40] Typically, incorporation of the monomer complex into an

Figure 1.9: Structures of an octahedral Ru(II) polypyridyl model complex (A), its corresponding monomer complex possessing a substituted polypyridyl ligand needed for oligonucleotide attachment (B), and the oligonucleotides containing the monomer complexes (C).

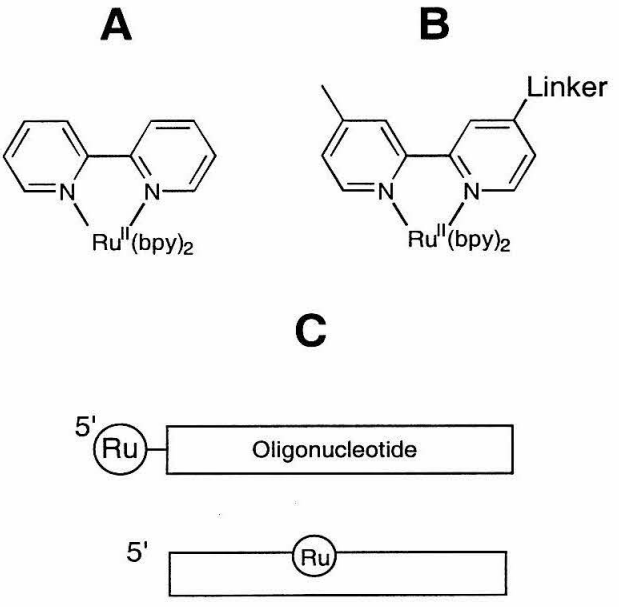
A
B
Linker
N
N
Ru^{II}(bpy)$_2$
C
5'
Ru
Oligonucleotide
5'
Ru

oligonucleotide does not alter the position of λ_{max} for the ruthenium-containing oligonucleotides (Table 1.3).

Emission of Ruthenium-Modified Oligonucleotides. Comparison of the emissive properties of the ruthenium-containing monomers and oligonucleotides with those of reference complexes helps in understanding the observed changes in λ(em) summarized in Table 1.3. For example, monomer complexes based on $[Ru(bpy)_3]^{2+}$ display emission maxima that are shifted from 628 nm to lower energy (660-675 nm). When these monomer complexes are incorporated into oligonucleotides, the emission maxima are unchanged or shifted to lower energy. An exception to this trend is a 16-mer oligonucleotide containing a complex attached to the base of a nucleoside located mid-strand; λ(em) is centered at 660 nm, blue-shifted from the corresponding value of the monomer complex (675 nm).[62,69]

The excited-state lifetimes of the single-stranded ruthenated oligonucleotides are dramatically different from those of the monomer complexes (Table 1.3). This suggests that the ruthenium complex is situated in an environment that has different solvation characteristics after incorporation into an oligonucleotide. Likewise, hybridization to unmodified complementary strands in some cases leads to further alterations in the excited-state lifetimes. For example, Grinstaff and coworkers report an increase in the lifetime values upon both incorporation and hybridization of three separate $[Ru(bpy)_2(bpy')]^{2+}$ derivatives, regardless of the attachment linkage or placement of the metal complex within the duplex (Figure 1.7A, 1.8C,E,G).[62,70,72] Conversely, Lewis and coworkers observe a decrease in the lifetime of single-stranded oligonucleotides containing a $[Ru(bpy)_2(bpy')]^{2+}$ label (Figure 1.8F).[71] The lifetimes of two short strands

Table 1.3. Absorption and Emission Data for Ru(II) Polypyridyl Complexes Incorporated into Oligonucleotides.[a]

	compd	λ_{max} (abs)	λ_{max} (em)	τ (μsec)	Ref.
	$Ru(bpy)_3^{2+}$	452	628	0.65	40
	$Ru(phen)_3^{2+}$	447	603	0.96	40
	$Ru(bphen)_3^{2+}$	460	610	4.68	40
	$Ru(bpy)_2(phen)^{2+}$	450	601[b]	0.301	40
	$Ru(tap)_2(dip)^{2+}$	418	652	0.58	51
Grinstaff	$Ru(bpy)_2(bpy')^{2+}$	460	670	0.407	70
	5′-^{X}TCAACAGTTTGTAGCA	465	670	0.616	
	Duplex			0.629	
Grinstaff	$Ru(bpy)_2(bpy')^{2+}$	454	675	0.485	62,69
	5′-TCAACAG**X**TTGTAGCA	450	660	0.544	
	Duplex	450	660	0.594	
Grinstaff	$Ru(bpy)_2(bpy')^{2+}$	450	666	0.430	78
	5′-**X**TCAACAGTTTGT	450	677	0.572	
	Duplex	450	677	0.586	
Lewis	$Ru(bpy)_2(bpy')^{2+}$ [c]	468	665	0.850	71
	5′-TTTT-**X**-AAAA	468	665	0.815	
	5′-GGG-**X**-CCC	468	665	0.790	
	5′-GCAATTGC-**X**-GCAATTGC	468	665	0.608	
Netzel	$Ru(bpy)_2(bpy')^{2+}$	460	660	-	47
	5′-GCAC^{X}TCAG	460	660	-	
	Duplex	460	-	-	
Meade	$Ru(bpy)_2(im)(NRH_2)^{2+}$	480	-	-	17
	5′-**X**GCATCGA	480	-	-	
	Duplex	480	-	-	
Tor	$Ru(bpy)_2(phen')^{2+}$ [d]	450	629	-	13
	5′-TCGGCGCGAA**X**TCGCGTGCC	456	630	-	
	Duplex	456		-	
Bannwarth	$Ru(bphen)_2(bphen')^{2+}$	464	616	-	46
	5′-^{X}TAAAACGACGGCCAGTG	464	616	2.0	

[a] Values measured in buffered aqueous solution (pH 7.0) at room temperature unless otherwise noted. **X** denotes metal attachment to oligonucleotide via linker to nucleoside base, ribose, or phosphate. Please see Figure 1.5-1.8 for details of metal attachment for each system. [b] Measured in unbuffered aqueous solution. [c] Monomer complex values measured in acetonitrile.

Table 1.3. (continued)

	compd	λ_{max} (abs)	λ_{max} (em)	τ (μsec)	Ref.
	$Ru(tap)_2(dip)^{2+}$	418	652	0.58	51
	$Ru(phen)_2(dppz)^{2+}$		619	0.18	79
K. DeMesmaeker	$Ru(tap)_2(dip')^{2+}$	418	652	0.580	51
	5′-CAAAACCC**X**ACCCAAAC-3′	420	652	0.315 (16%)	
				0.707 (84%)	
	duplex	420	652	0.046 (71%)	
				0.229 (21%)	
				0.659 (8%)	
	5′-TTTTTTTA**X**TAAATTTA-3′	420	654	0.721 (58%)	
				1.268 (42%)	
	duplex	420	654	0.632 (28%)	
				1.176 (72%)	
Giese	$Ru(phen)(phen')(dppz)^{2+}$	447	-	-	68
	5′-^{X}AGAGCACAACTAGCA-3′	437	-	-	
Barton	$Ru(phen')(phen'')(dppz)^{2+}$	482	598	-	48
	5′-**X**AGTGCCAAGCTTGCA-3′	482	598	-	
	Duplex	482	598	0.500 (60%)	
				0.110 (40%)	

[a] Values measured in buffered aqueous solution (pH 7.0) at room temperature unless otherwise noted. **X** denotes metal attachment to oligonucleotide via linker to nucleoside base, ribose, or phosphate. Please see individual references for details of metal attachment for each system. [b] Measured in dichloromethane. [c] Measured in unbuffered aqueous solution. [d] Monomer complex values measured in acetonitrile.

are within 10% of the value for the monomer complex; a third strand forms a hairpin structure at high ionic strength and exhibits a lifetime that is 30% shorter compared to the lifetime of the monomer complex.

A rationale for the contrasting changes in the excited-state lifetime values of the metal-containing oligonucleotides summarized in Table 1.3 is unclear. The decrease in excited-state lifetime reported by Lewis for the single-stranded vs. hairpin oligonucleotides could be attributed to structural differences between the conformations available to the strands. The two 8-mer strands do not form well-defined hairpin structures at high ionic strength; therefore, the emission lifetimes for these oligonucleotides are expected to resemble that of the monomer complex.[71] The 16-mer oligonucleotide forms a stable hairpin structure, and this structural difference may cause the observed decrease in the excited-state lifetime.[80] However, the increase in lifetime values upon both incorporation and hybridization reported by Grinstaff must be due to interactions between the metal complex and the duplex not operative in Lewis' hairpin assembly. Subtle factors involving duplex conformation and ionic strength may be responsible for these trends.

An example of how the compositon of the buffer solution impacts the emissive properties of a ruthenium-modified oligonucleotide is provided here. Modulations in the excited-state lifetime are observed by Bannwarth for the ruthenium-modified oligonucleotide shown in Figure 1.5A.[46] The addition of detergents, salts, and reducing agents to the solution containing the single strand prolongs the lifetime from 2.0 μsec to 7.5 μsec. This dramatic enhancement illustrates how the surrounding environment influences the emissive properties of the metal complex.

The most striking alteration in the excited-state lifetime observed upon incorporation of a monomer complex occurs for oligonucleotides containing intercalating ruthenium complexes. Kirsch-De Mesmaeker and coworkers report that the emission of two single-stranded oligonucleotides containing $[Ru(tap)_2(dip)]^{2+}$ is characterized by a bi-exponential decay. This observation is in sharp contrast to the monoexponential behavior exhibited by the model complex (Figure 1.5C).[51] It appears from close inspection of Table 1.3 that the base composition of the two 17-mer oligonucleotides may influence the excited-state behavior of the tethered complexes by dictating the structural conformations that the single strands can adopt. Hybridization of $[Ru(tap)_2(dip)]^{2+}$-containing oligonucleotides introduces further complexity into the emission decay, as multi-exponential behavior is observed for the duplexes.

This unusual excited-state behavior may be a direct manifestation of subtle conformational differences between the oligonucleotides. The biexponential decay behavior persists for the 17-mer single-stranded oligonucleotides, despite the fact these strands do not support intercalation of the tethered ruthenium complex. The contrasting lifetime values observed for these strands ($\tau_1 = 0.315$, $\tau_2 = 0.707$ vs. $\tau_1' = 0.721$, $\tau_2' = 1.268$ μs) can be attributed to the different conformations dictated by the respective oligonucleotide sequence. The extended linker (joining the metal complex to the base of an intervening nucleoside) amplifies the number of conformations adopted by the oligonucleotides, leading to multiple components for the excited-state lifetime.[51] Additionally, the excited-state behavior is more complicated for the duplex containing a GC-rich strand vs. an AT-rich strand. The presence of a guanine-rich strand may cause quenching of the luminescent MLCT state based on the following: (1) guanine is the

most facile electron donor of the DNA bases ($E^{+\bullet/0}$ = 1.3 V vs. NHE, pH 7),[81] and (2) photoexcited $[Ru(tap)_2(dip)]^{2+}$ is a powerful oxidant (1.3 V NHE, CH_3CN).[82] Taken together, these results suggest that excited-state lifetimes are diagnostic of different conformational states that are populated on the timescale of the emission decay.

Barton and coworkers likewise report biexponential decay for the emission of $[Ru(phen')_2(dppz)]^{2+}$ covalently bound to 15-mer duplexes.[48] In this setting the tethered intercalator displays lifetime values of 500 (60%) and 110 (40%) nsec, whereas minimal emission is observed when the ruthenium-containing oligonucleotide is unhybridized. When $[Ru(phen)_2(dppz)]^{2+}$ is bound noncovalently to DNA duplexes, it also displays biexponential decay behavior (τ_1 = 420 (35%), τ_2 = 90 (65%) nsec).[48,83] Complicating a thorough understanding of how the emission decay of the metal complex is influenced by the presence of DNA is the fact that the model complex possesses a very short emission lifetime. The authors propose that intercalation protects the phenazine ring from interactions with the surrounding solvent that are responsible for quenching the excited state of the ruthenium complex. If the interpretation given above for the Kirsch-De Mesmaeker assemblies is applied here, it would appear that the biexponential emission decay is suggestive of at least two distinct conformations of the ruthenium-modified duplex. Whether these conformations are dictated by the multiple binding modes available to the intercalator or by the oligonucleotide sequence remains to be established for the *covalently tethered* ruthenium-oligonucleotide conjugates.

Additional work involving $[Ru(phen)_2(dppz)]^{2+}$ bound noncovalently to DNA duplexes has provided insight into this issue. Barton and coworkers have conducted several experiments investigating the possible binding modes adopted by

$[Ru(phen)_2(dppz)]^{2+}$ in the presence of duplex DNA.[79,84,85] These studies provide evidence for two different binding interactions between $[Ru(phen)_2(dppz)]^{2+}$ and DNA. However, results from linear dichroism studies by Norden suggest that one binding mode dominates.[86,87] Additional studies probing the emission behavior exhibited by the Λ and Δ enantiomers of $[Ru(phen)_2(dppz)]^{2+}$ reveal an enantiospecificity of the lifetimes. That is, each enantiomer displays two distinct lifetimes when bound to DNA; one of these values increases as the concentration of the enantiomer increases. The authors speculate that the prolonged lifetime is the direct consequence of the enhanced protection from solvent that the clustered intercalators afford one another. Regardless of the validity of the models proposed by Barton and by Norden for the interaction between $[Ru(phen)_2(dppz)]^{2+}$ and duplex DNA, these studies showcase the complexity of interpreting emission decay kinetics for intercalating assemblies.

Summary. Analyzing the methods developed for inserting ruthenium complexes into oligonucleotides highlights the importance of selecting ligands that facilitate routine incorporation. Likewise, a review of the resulting ruthenium-modified oligonucleotides shows how the different ligands used for the purposes of incorporation influence the spectroscopic properties of the incorporated metal complex. It is clear from the preceding discussion that non-intercalating ruthenium complexes offer distinct advantages over intercalating ruthenium complexes since the emissive properties of the former are not substantially altered by the presence of oligonucleotides.

Inspection of the various ruthenium-modified oligonucleotides described above reveals that nearly all of these complexes are based on $[Ru(bpy)_3]^{2+}$. This is to be expected since $[Ru(bpy)_3]^{2+}$ has been widely used as a photosensitizer in many different

studies.[40,88] However, the preceding review uncovers the absence of low-potential complexes that can be incorporated into DNA. In an ET reaction scheme, both an electron donor and an acceptor are needed; the difference in the reduction potentials of these complexes constitutes the overall driving force for the ET reactio. Low-potential complexes that are spectroscopically distinct from high-potential complexes are needed to facilitate a systematic evaluation DNA-mediated ET processes. The design of a low-potential complex exhibiting reversible electrochemistry and displaying unique absorption bands thus becomes an important endeavor.

To this end, Meade and coworkers designed a DNA assembly modified with non-intercalating ruthenium complexes that possess the features discussed above regarding ideal D/A complexes (Figure 1.10).[17] The high-potential complex $[Ru(bpy)_2(im)(NRH_2)]^{2+}$ (where NRH_2 represents an amine-bearing oligonucleotide) is amenable to the bimolecular quenching method. The low-potential complex $[Ru(NH_3)_4(pyr)(NH_2R)]^{2+}$ displays an absorption maximum at 410 nm that is distinct from that of the high-potential complex (480 nm). The powerful combination of these two complexes allows the unambiguous detection of the products formed upon ground-state electron transfer. The preparation of additional low-potential complexes, suitable for both incorporation into oligonucleotides and use in ET studies, will augment these results.

A second hallmark of the Meade assembly is the use of 2′-modified nucleosides to facilitate ruthenium incorporation. The 2′ position of the ribose ring is selected as the metal attachment point since metal complexes in this location do not directly interfere with the hydrogen bonding of the DNA bases. Additionally, metal attachment to the

Figure 1.10: Schematic structure of DNA assembly containing spectroscopically unique, non-intercalating ruthenium complexes. The ruthenium complexes are covalently attached to the 2′ positions of the 5′ terminal ribose rings of complementary oligonucleotides.

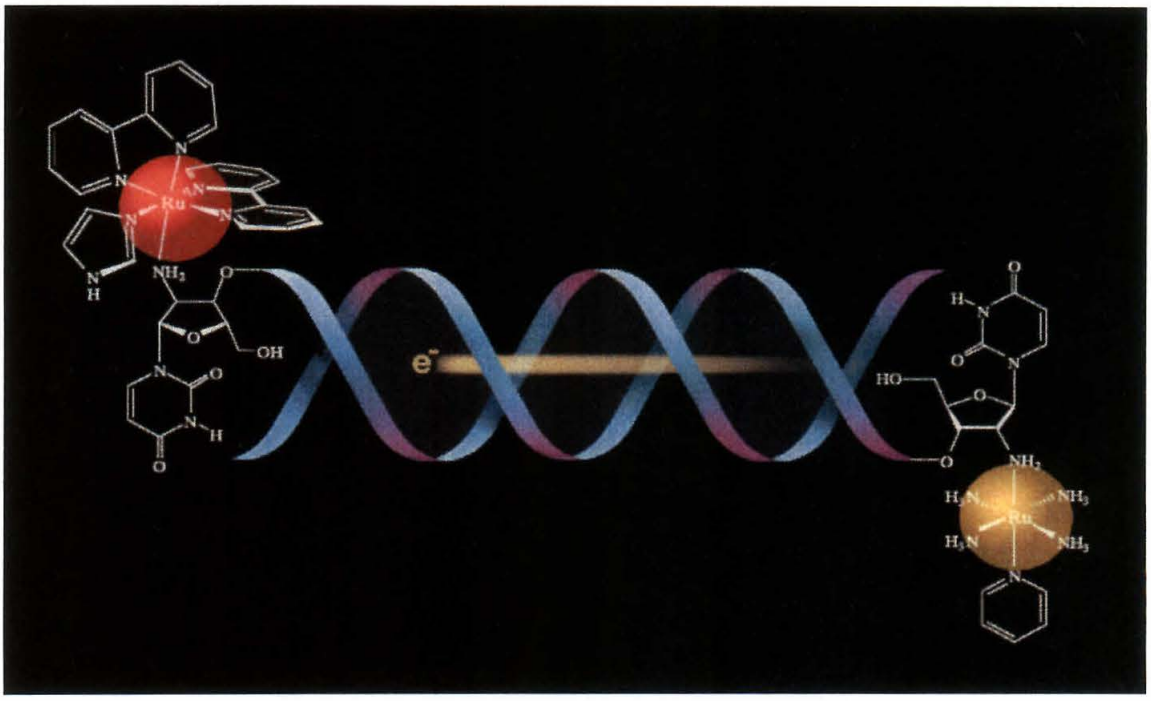
e⁻

ribose ring may afford an efficient pathway to the stacked array of π bonds present in the secondary structure of a duplex. This stacked array may prove ideal for enhancing the electronic coupling of a donor-acceptor pair.[34]

Scope of Thesis

The design and subsequent oligonucleotide incorporation of redox-active probes is the focus of this thesis. These two activities form an iterative cycle, in that results obtained from initial incorporation attempts refine the design of the candidate ruthenium complexes. Likewise, newly designed ruthenium complexes become avenues to incorporation methods unavailable with other D/A candidates. Ultimately, the successful incorporation of a ruthenium complex elevates this candidate to further evaluation as a suitable probe.

Site-specific incorporation of the candidate complexes is initially explored using post-synthetic modification. This method requires the preparation of nucleosides containing a metal-binding substituent. The synthesis of such nucleosides, their incorporation into oligonucleotides, and characterization of the resulting oligonucleotides is presented (Chapter 2). Because the insertion of the candidate complexes into the modified oligonucleotides using the post-synthetic modification method is unsuccessful (Chapter 3), an alternative method is explored. These efforts result in the first report of 3′-metallated oligonucleotides prepared completely by automated solid-phase synthesis (Chapter 4). The electrochemical, absorption, and emissive features of the ruthenium-modified oligonucleotides are unchanged from those of the precursor metallonucleoside (Chapter 4). The absence of any change in these properties upon incorporation into oligonucleotides and subsequent hybridization suggests that the incorporated

ruthenium(II) complex is a valuable probe for DNA-ET studies. Additional spectroscopic characterization of the ruthenium-modified nucleic acids prepared in this work documents the influence of the ligands that facilitate oligonucleotide attachment (Chapter 5).

Work that is supplementary to the objectives of designing and incorporating redox-active probes into oligonucleotides represent avenues to future directions for this project: alternative nucleosides synthesis (Appendix A), model complex syntheses (Appendix B), oxidative and reductive quenching experiments with high-potential ruthenium-modified nucleic acids (Appendix C), and solid-phase synthesis of a bis-metallated oligonucleotide (Appendix D). Relevant HPLC information is summarized (Appendix E).

References

(1) Clarke, M. J.; Stubbs, M. In *Metal Ions in Biological Systems, Vol 32*, 1996; Vol. 32.

(2) Clarke, M. J. In *Electron Transfer Reactions*, 1997; Vol. 253.

(3) Clarke, M. J.; Jansen, B.; Marx, K. A.; Kruger, R. *Inorg. Chim. Acta-Bioinorg. Chem.* **1986**, *124*, 13-28.

(4) McNamara, M. A.; Clarke, M. J. *Inorg. Chim. Acta* **1992**, *195*, 175-185.

(5) Zhao, M.; Clarke, M. J. *J. Biol. Inorg. Chem.* **1999**, *4*, 318-324.

(6) Zhao, M.; Clarke, M. J. *J. Biol. Inorg. Chem.* **1999**, *4*, 325-340.

(7) Clarke, M. J.; Zhu, F. C.; Frasca, D. R. *Chem. Rev.* **1999**, *99*, 2511-2533.

(8) Stemp, E. D. A.; Barton, J. K. In *Metal Ions in Biological Systems*; Sigel, A., Sigel, H., Eds., 1996; Vol. 33.

(9) Meade, T. J. In *Metal Ions in Biological Systems*; Sigel, H., Sigel, A., Eds.; Marcel Dekker: New York, 1995; Vol. 32.

(10) Bannwarth, W.; Pfleiderer, W.; Muller, F. *Helv. Chim. Acta* **1991**, *74*, 1991-1999.

(11) Bannwarth, W.; Muller, F. *Helv. Chim. Acta* **1991**, *74*, 2000-2008.

(12) Fu, P. K. L.; Turro, C. *J. Am. Chem. Soc.* **1999**, *121*, 1-7.

(13) Hurley, D. J.; Tor, Y. *J. Am. Chem. Soc.* **1998**, *120*, 2194-2195.

(14) Tierney, M. T.; Sykora, M.; Khan, S. I.; Grinstaff, M. W. *J. Phys. Chem. B* **2000**, *104*, 7574-7576.

(15) Holmlin, R. E.; Dandliker, P. J.; Barton, J. K. *Angew. Chem. Int. Ed.* **1997**, *36*, 2715-2730.

(16) Arkin, M. A.; Stemp, E. D.; Holmlin, R. E.; Barton, J. K.; Hormann, A.; Olson, E. J.; Barbara, P. F. *Science* **1996**, *273*, 475.

(17) Meade, T. J.; Kayyem, J. F. *Angew. Chem. Int. Ed. Engl.* **1995**, *34*, 352-353.

(18) Lewis, F. D.; Wu, T. F.; Liu, X. Y.; Letsinger, R. L.; Greenfield, S. R.; Miller, S. E.; Wasielewski, M. R. *J. Am. Chem. Soc.* **2000**, *122*, 2889-2902.

(19) Kelley, S. O.; Barton, J. K. *Science* **1999**, *283*, 375-381.

(20) Harriman, A. *Angew. Chem. Int. Ed.* **1999**, *38*, 945-949.

(21) Okahata, Y.; Kobayashi, T.; Tanaka, K.; Shimomura, M. *J. Am. Chem. Soc.* **1998**, *120*, 6165-6166.

(22) Fukui, K.; Tanaka, K. *Angew. Chem. Int. Ed.* **1998**, *37*, 158-161.

(23) Bixon, M.; Giese, B.; Wessely, S.; Langenbacher, T.; Michel-Beyerle, M. E.; Jortner, J. *Proc. Natl. Acad. Sci. U.S.A.* **1999**, *96*, 11713-11716.

(24) Giese, B.; Wessely, S.; Spormann, M.; Lindemann, U.; Meggers, E.; Michel-Beyerle, M. E. *Angew. Chem. Int. Ed.* **1999**, *38*, 996-998.

(25) Kan, Y. Z.; Schuster, G. B. *J. Am. Chem. Soc.* **1999**, *121*, 11607-11614.

(26) Kan, Y. Z.; Schuster, G. B. *J. Am. Chem. Soc.* **1999**, *121*, 10857-10864.

(27) Hall, D. B.; Holmlin, R. E.; Barton, J. K. *Nature* **1996**, *382*, 731-735.

(28) Dandliker, P. J.; Nunez, M. E.; Barton, J. K. *Biochem.* **1998**, *37*, 6491-6502.

(29) Dandliker, P. J.; Holmlin, R. E.; Barton, J. K. *Science* **1997**, *275*, 1465-1468.

(30) Jortner, J.; Bixon, M.; Langenbacher, T.; Michel-Beyerle, M. E. *Proc. Natl. Acad. Sci. U.S.A.* **1998**, *95*, 12759-12765.

(31) Ratner, M. *Nature* **1999**, *397*, 480-481.

(32) Henderson, P. T.; Jones, D.; Hampikian, G.; Kan, Y. Z.; Schuster, G. B. *Proc. Natl. Acad. Sci. U.S.A.* **1999**, *96*, 8353-8358.

(33) Beratan, D. N.; Priyadarshy, S.; Risser, S. M. *Chem. & Bio.* **1997**, *4*, 3-8.

(34) Krider, E. S.; Meade, T. J. *J. Biol. Inorg. Chem.* **1998**, *3*, 222-225.

(35) Gray, H. B.; Winkler, J. R. *Annu. Rev. Biochem.* **1996**, *65*, 537-561.

(36) DiBilio, A. J.; Hill, M. G.; Bonander, N.; Karlsson, B. G.; Villahermosa, R. M.; Malmstrom, B. G.; Winkler, J. R.; Gray, H. B. *J. Am. Chem. Soc.* **1997**, *119*, 9921-9922.

(37) Skov, L. K.; Pascher, T.; Winkler, J. R.; Gray, H. B. *J. Am. Chem. Soc.* **1998**, *120*, 1102-1103.

(38) Beratan, D. N.; Skourtis, S. S. *Curr. Op. in Chem. Biol.* **1998**, *2*, 235-243.

(39) Chang, I.-J.; Winkler, J. R.; Gray, H. B. *J. Am. Chem. Soc.* **1991**, *113*, 7056-7057.

(40) Juris, A.; Balzani, V.; Barigelletti, F.; Campagna, S.; Belser, P.; Vonzelewsky, A. *Coord. Chem. Rev.* **1988**, *84*, 85-277.

(41) Brown, G. M.; Weaver, T. R.; Keene, F. R.; Meyer, T. J. *Inorg. Chem.* **1976**, *15*, 190-196.

(42) Alvarez, V. E.; Allen, R. J.; Matsubara, T.; Ford, P. C. *J. Am. Chem. Soc.* **1974**, *96*, 7686-7692.

(43) Rack, J. J.; Krider, E. S.; Meade, T. J. *J. Am. Chem. Soc.* **2000**, *122*, 6287-6288.

(44) Clarke, M. J.; Taube, H. *J. Am. Chem. Soc.* **1974**, *96*, 5413-5419.

(45) Ledoan, T.; Perrouault, L.; Chassignol, M.; Thuong, N. T.; Helene, C. *Nucleic Acids Res.* **1987**, *15*, 8643-8659.

(46) Bannwarth, W.; Schmidt, D.; Stallard, R. L.; Hornung, C.; Knorr, R.; Muller, F. *Helv. Chim. Acta* **1988**, *71*, 2085-2099.

(47) Telser, J.; Cruickshank, K. A.; Schanze, K. S.; Netzel, T. L. *J. Am. Chem. Soc.* **1989**, *111*, 7221-7226.

(48) Jenkins, Y.; Barton, J. K. *J. Am. Chem. Soc.* **1992**, *114*, 8736-8738.

(49) Murphy, C. J.; Arkin, M. A.; Jenkins, Y.; Ghatlia, N. D.; Bossman, S. H.; Turro, N. J.; Barton, J. K. *Science* **1993**, *262*, 1025-1029.

(50) Magda, D.; Miller, R. A.; Sessler, J. L.; Iverson, B. L. *J. Am. Chem. Soc.* **1994**, *116*, 7439-7440.

(51) Ortmans, I.; Content, S.; Boutonnet, N.; Kirsch-De Mesmaeker, A.; Bannwarth, W.; Constant, J. F.; Defrancq, E.; Lhomme, J. *Chem. Eur. J.* **1999**, *5*, 2712-2721.

(52) Dreyer, G. B.; Dervan, P. B. *Proc. Natl. Acad. Sci. U.S.A.* **1985**, *82*, 968-972.

(53) Chen, C. H. B.; Sigman, D. S. *J. Am. Chem. Soc.* **1988**, *110*, 6570-6572.

(54) Modak, A. S.; Gard, J. K.; Merriman, M. C.; Winkeler, K. A.; Bashkin, J. K.; Stern, M. K. *J. Am. Chem. Soc.* **1991**, *113*, 283-291.

(55) Bashkin, J. K.; Frolova, E. I.; Sampath, U. S. *J. Am. Chem. Soc.* **1994**, *116*, 5981-5982.

(56) Bergstrom, D. E.; Gerry, N. P. *J. Am. Chem. Soc.* **1994**, *116*, 12067-12068.

(57) Matsumura, K.; Endo, M.; Komiyama, M. *J. Chem. Soc.-Chem. Commun.* **1994**, 2019-2020.

(58) Wiederholt, K.; McLaughlin, L. W. *Nucleic Acids Res.* **1999**, *27*, 2487-2493.

(59) Inoue, H.; Furukawa, T.; Shimizu, R.; Tamura, T.; Matsui, M. N.; Ohtsuka, E. *Chem. Commun.* **1999**, 45-46.

(60) Arkin, M. R.; Stemp, E. D. A.; Pulver, S. C.; Barton, J. K. *Chem. & Biol.* **1997**, *4*, 389-400.

(61) Khan, S. I.; Grinstaff, M. W. *J. Am. Chem. Soc.* **1999**, *121*, 4704-4705.

(62) Khan, S. I.; Beilstein, A. E.; Tierney, M. T.; Sykora, M.; Grinstaff, M. W. *Inorg. Chem.* **1999**, *38*, 5999-6002.

(63) Holmlin, R. E.; Dandliker, P. J.; Barton, J. K. *Bioconj. Chem.* **1999**, *10*, 1122-1130.

(64) Bannwarth, W.; Schmidt, D. *Tet. Lett.* **1989**, *30*, 1513-1516.

(65) Manchanda, R.; Dunham, S. U.; Lippard, S. J. *J. Am. Chem. Soc.* **1996**, *118*, 5144-5145.

(66) Schliepe, J.; Berghoff, U.; Lippert, B.; Cech, D. *Angew. Chem. Int. Ed.* **1996**, *35*, 646-648.

(67) Magda, D.; Crofts, S.; Lin, A.; Miles, D.; Wright, M.; Sessler, J. L. *J. Am. Chem. Soc.* **1997**, *119*, 2293-2294.

(68) Meggers, E.; Kusch, D.; Giese, B. *Helv. Chim. Acta* **1997**, *80*, 640-652.

(69) Khan, S. I.; Beilstein, A. E.; Smith, G. D.; Sykora, M.; Grinstaff, M. W. *Inorg. Chem.* **1999**, *38*, 2411-2415.

(70) Khan, S. I.; Beilstein, A. E.; Sykora, M.; Smith, G. D.; Hu, X.; Grinstaff, M. W. *Inorg. Chem.* **1999**, *38*, 3922-3925.

(71) Lewis, F. D.; Helvoigt, S. A.; Letsinger, R. L. *Chem. Commun.* **1999**, 327-328.

(72) Hu, X.; Smith, G. D.; Sykora, M.; Lee, S. J.; Grinstaff, M. W. *Inorg. Chem.* **2000**, *39*, 2500-2504.

(73) *Oligonucleotide Synthesis: A Practical Approach*; Gait, M., Ed.; Oxford Univ. Press: Oxford, 1984.

(74) Goodchild, J. *Bioconj. Chem.* **1990**, *1*, 165-191.

(75) *Oligonucleotides and Analogues: A Practical Approach*; Eckstein, F., Ed.; Oxford Univ. Press: Oxford, 1991.

(76) Telser, J.; Cruickshank, K. A.; Morrison, L. E.; Netzel, T. L.; Chan, C. K. *J. Am. Chem. Soc.* **1989**, *111*, 7226-7232.

(77) Khan, S. I.; Beilstein, A. E.; Grinstaff, M. W. *Inorg. Chem.* **1999**, *38*, 418-419.

(78) Hu, X.; Smith, G. D.; Sykora, M.; Lee, S. J.; Grinstaff, M. W. *Inorg. Chem.* **2000**, *39*, 2500-2504.

(79) Jenkins, Y.; Friedman, A. E.; Turro, N. J.; Barton, J. K. *Biochem.* **1992**, *31*, 10809-10816.

(80) An estimate of the excited-state reduction potential of $[Ru(bpy)_2(bpy')]^{2+}$, based on data collected for $[Ru(bpy)_3]^{2+}$, suggests that guanine oxidation from the excited-state is not likely (Ref. 40).

(81) Steenken, S.; Jovanovic, S. V. *J. Am. Chem. Soc.* **1997**, *119*, 617-618.

(82) Ortmans, I.; Moucheron, C.; Kirsch-De Mesmaeker, A. *Coord. Chem. Rev.* **1998**, *168*, 233-271.

(83) Jacquet, L.; Kelly, J. M.; Kirsch-De Mesmaeker, A. *Inorg. Chem. Commun.* **1999**, *2*, 135-138.

(84) Friedman, A. E.; Chambron, J. C.; Sauvage, J. P.; Turro, N. J.; Barton, J. K. *J. Am. Chem. Soc.* **1990**, *112*, 4960-4962.

(85) Dupureur, C. M.; Barton, J. K. *J. Am. Chem. Soc.* **1994**, *116*, 10286-10287.

(86) Hiort, C.; Lincoln, P.; Norden, B. *J. Am. Chem. Soc.* **1993**, *115*, 3448-3454.

(87) Tuite, E.; Lincoln, P.; Norden, B. *J. Am. Chem. Soc.* **1997**, *119*, 239-240.

(88) Meyer, T. J. *Acc. of Chem. Res.* **1989**, *22*, 163-170.

Chapter 2

2′-Modified Nucleosides for Site-Specific Labeling of Oligonucleotides

Introduction

Nucleosides containing modifications in place of a hydroxyl group at the 2′ ribose position are important structural and mechanistic probes of nuclease resistance and ribozyme catalysis.[1-3] These nucleosides are used in the development of anti-sense therapeutics[2] and in the rapid screening of oligonucleotide sequences displaying high affinity toward protein targets.[4,5] Nucleosides containing a primary amine group at the 2′ position also facilitate the incorporation of several reporter molecules or labels into oligonucleotides.[6,7] This is achieved by (a) introducing the amine-containing nucleoside into an oligonucleotide using standard automated DNA synthesis, (b) purifying the resulting oligonucleotide, and (c) reacting the reporter group with the amine-containing oligonucleotide and isolating the conjugate (Chapter 1). Labels such as fluorescent dyes,[6,8] aromatic and aliphatic isocyanates,[7,9] and transition metal complexes[10] have been successfully incorporated into oligonucleotides using this method.

Our approach is to develop new methods of incorporating labels, namely transition metal complexes, into DNA site-specifically.[11] To this end we have designed nucleosides containing bidentate amine groups at the 2′ ribose position to which transition metal complexes are chelated (Figure 2.1). The 2′ position of the ribose ring is selected so that both solid support-bound and phosphoramidite forms of the nucleosides can be prepared. The solid support-bound nucleoside is used as the starting material in oligonucleotide synthesis, whereas the phosphoramidite monomer can be introduced at any later position in the oligonucleotide sequence. As a result, labels can be incorporated at the 3′, intervening, or 5′ locations of an oligonucleotides. Herein we report the

Figure 2.1: Structures of nucleosides modified at the 2′ ribose position with metal-binding ligands. The synthesis of nucleosides **a-c** is described in this chapter; the preparation of **d** is given in Chapter 4.

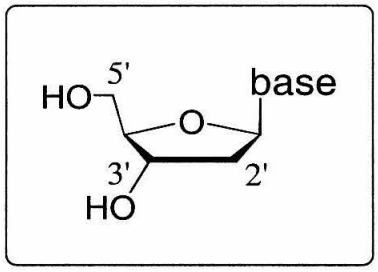
5'
HO
base
O
3'
2'
HO

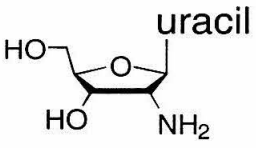
uracil
HO
O
HO
NH2

a

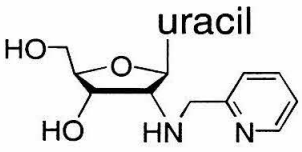
uracil
HO
O
HO
HN
N

b

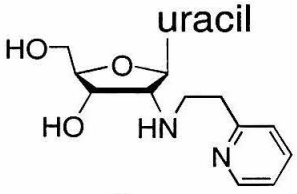
uracil
HO
O
HO
HN
N

c

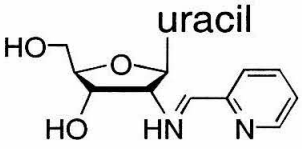
uracil
HO
O
HO
HN
N

d

synthesis of 2′-modified nucleosides as both solid support-bound and phosphoramidite derivatives, and their incorporation into oligonucleotides via solid-phase methods. The characterization and thermal stability of the resulting oligonucleotides are discussed.

Results

Synthesis of 2′-Modified Nucleosides. Nucleosides with bidentate amine groups such as aminomethylpyridine (AMPy)[12] and aminoethylpyridine (AEPy) at the 2′ ribose position were prepared as shown in Figure 2.2. This approach was based on methods developed recently for incorporating 2′-N-alkylamino substituents into nucleosides.[13,14] Nucleoside **1** was converted to the 3′ N-alkyl carbamate upon prolonged treatment with carbonyl diimidazole in pyridine; this was followed by the addition of AMPy or AEPy in the presence of DIEA and dichloromethane. Subsequent cyclization in THF using the cyclization agent DBU produced either **2a** or **2b** in yields of 20% and 10%, respectively. Prolonged heating of **2a** and **2b** in a basic dioxane-methanol solution caused deprotection at the 2′,3′-positions, giving **3a** and **3b** in high yield (92% and 88%, respectively).

Derivatization of solid supports with 2′-modified nucleosides was achieved according to Figure 2.3. Nucleoside **4** was prepared according to previously published procedures.[6,15,16] Both **3a** and **4** were treated with succinic anhydride to give the corresponding hemisuccinates **5** and **6** in yields of 60% and 74%, respectively.[17,18] Solid supports such as controlled pore glass (CPG) containing long-chain alkyl amine groups were derivatized with **6** using *p*-nitrophenol and DCC. This method resulted in solid supports with low nucleoside loading. Subsequent attempts to prepare the nucleoside-modified solid supports employed the coupling agent BOP in the presence of HOBT and

Figure 2.2: Synthesis of nucleosides containing bidentate ligands at the 2′ ribose position: (a) $(imid)_2CO$, pyridine, rt, 30 h; (b) NH_2R (R = $-CH_2pyr$, $-CH_2CH_2pyr$), DIEA, CH_2Cl_2, rt, 60 h; (c) DBU, THF, reflux, 46 h; (d) 6 N NaOH, dioxane, CH_3OH, 50 °C, 36 h. Abbreviation: R = 4,4′-dimethoxytrityl.

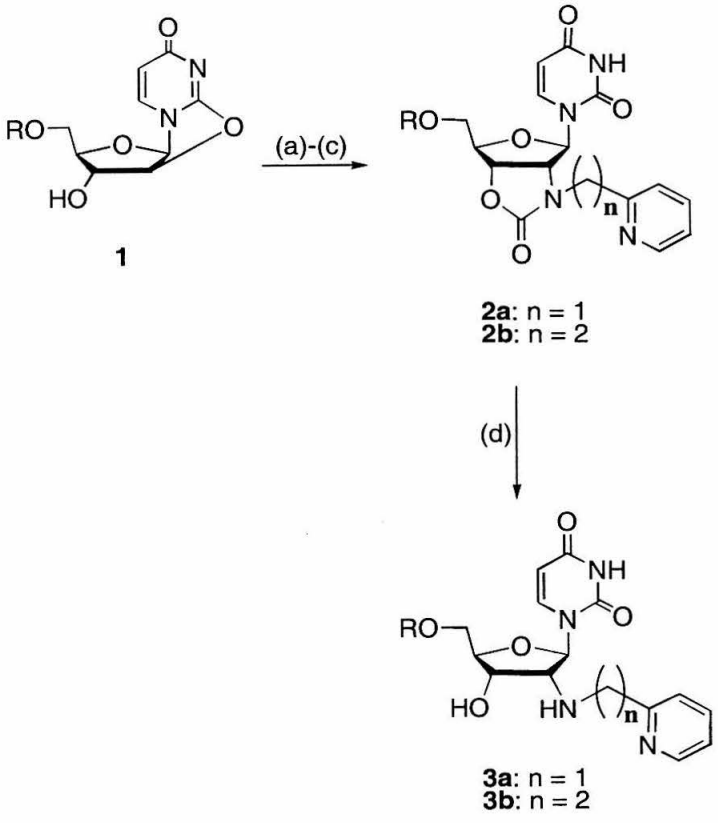

1

2a: n = 1
2b: n = 2

3a: n = 1
3b: n = 2

Figure 2.3: Synthesis of 2′-modified nucleosides as solid-support-bound and phosphoramidite derivatives: (a) succinic anhydride, pyridine, DMAP, rt, 16 h; (b) solid support, TEA, HOBT, BOP, CH_2Cl_2, rt, 16 h; acetic anhydride, N-methylimidazole, pyridine, rt, 12 h; (c) amidite, DIEA, CH_2Cl_2, rt, 50 min. Abbreviation: R′ = 4,4′-dimethoxytrityl.

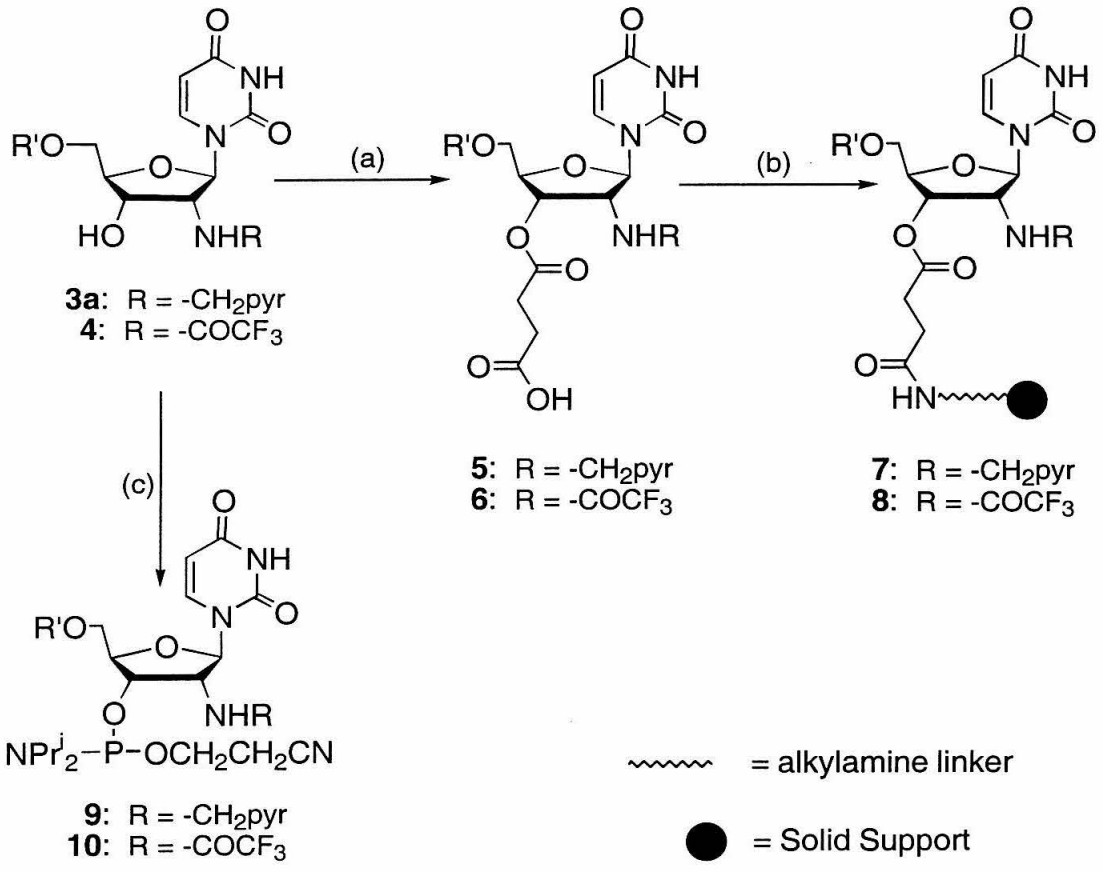

3a: R = -CH_2pyr
4: R = -$COCF_3$

5: R = -CH_2pyr
6: R = -$COCF_3$

7: R = -CH_2pyr
8: R = -$COCF_3$

9: R = -CH_2pyr
10: R = -$COCF_3$

TEA.[19] The unreacted amine groups were treated with acetic anhydride, and the nucleoside loadings of the solid supports **7** and **8** were determined by spectrophotometric assay (60 and 52 μmol/gram, respectively).[17]

The preparation of phosphoramidite derivatives of nucleosides **3a** and **4** relied on standard methods.[6,16,17] As shown in Figure 2.3, **3a** and **4** were treated with 2-chlorocyanoethyl N,N-diisopropylaminophosphoramidite in the presence of DIEA to give **9** and **10** in 57% and 65% yield, respectively.

Oligonucleotide Synthesis. A series of oligonucleotides (Table 2.1) were prepared from the support-bound and phosphoramidite nucleoside derivatives as outlined in Figure 2.4. To ensure maximum coupling, the reaction time for the first step was increased from 30 seconds to 2 minutes (yield > 95%). The reaction times for **9** and **10** were 15 minutes in length, leading to coupling yields > 90%.

All oligonucleotides were cleaved from the solid support with concentrated ammonia as a part of the automated synthesis routine, except in the case of **14**, which was manually cleaved. The yield of purified oligonucleotide for **11-14** ranged from 30-40%, which was comparable to those values observed for **15-18**. Results from matrix-assisted laser desorption-time of flight (MALDI-TOF) mass spectrometry on **11-14** were in excellent agreement with the calculated values. Further characterization of these oligonucleotides was achieved by enzymatic digestion.[20] Analysis of the digestion products showed the expected distribution of nucleosides determined for each oligonucleotide sequence (Figures 2.5-2.8).

Thermal Denaturation Studies. We investigated the thermal stability of duplexes containing 2′-modified nucleosides. Table 2.2 shows the transition melting

Table 2.1. Oligonucleotide Sequences.[a]

sequence	abbreviation
5′-$\mathbf{U_a}$CAGCTGTAGA	**11**
5′-$\mathbf{U_b}$CTACAGCTGA	**12**
5′-$\mathbf{U_a}$CTCCTACAC$\mathbf{U_a}$	**13**
5′-$\mathbf{U_a}$CTCCTACAC$\mathbf{U_b}$	**14**
5′- TCTACAGCTGA	**15**
5′- TCAGCTGTAGA	**16**
5′- TCTCCTACACT	**17**
5′- AGTGTAGGAGA	**18**

[a] The symbol $\mathbf{U_a}$ denotes 2′-amino-2′-deoxyuridine; $\mathbf{U_b}$ denotes $N^{2'}$-(2-pyridylmethyl)-2′-amino-2′-deoxyuridine.

Figure 2.4: Steps in the automated synthesis of oligonucleotide **14**: (a) detritylation of **7**; monomer coupling; normal synthesis cycle; (b) coupling of **10**; (c) cleavage and deprotection. R = -$COCF_3$, R′ = 4,4′-dimethoxytrityl.

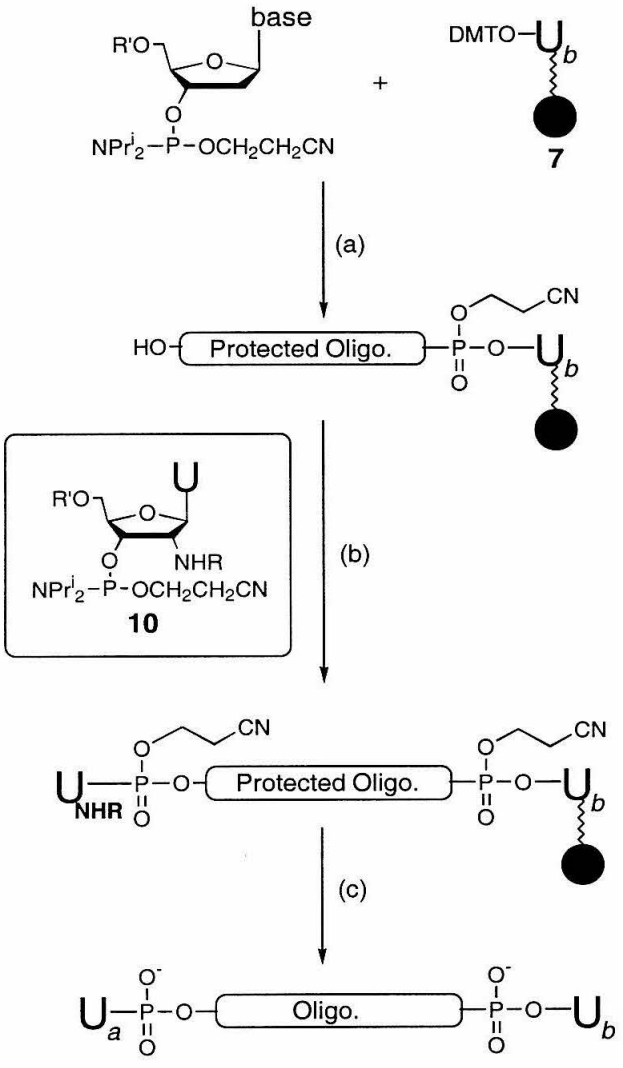

● = solid support

U$_b$ = $N^{2'}$-(2-pyridylmethyl)-2'-amino-2'-deoxyuridine

U$_a$ = 2'-amino-2'-deoxyuridine

Figure 2.5: Products of enzymatic digestion of **11** as analyzed by reverse-phase HPLC. Column: Prism C18. Gradient: 0-17% B over 15 minutes, then 17-75% B over 15 minutes. Solvent A = 0.1 M triethylamine acetate, pH 7.0, 2% acetonitrile; Solvent B = acetonitrile.

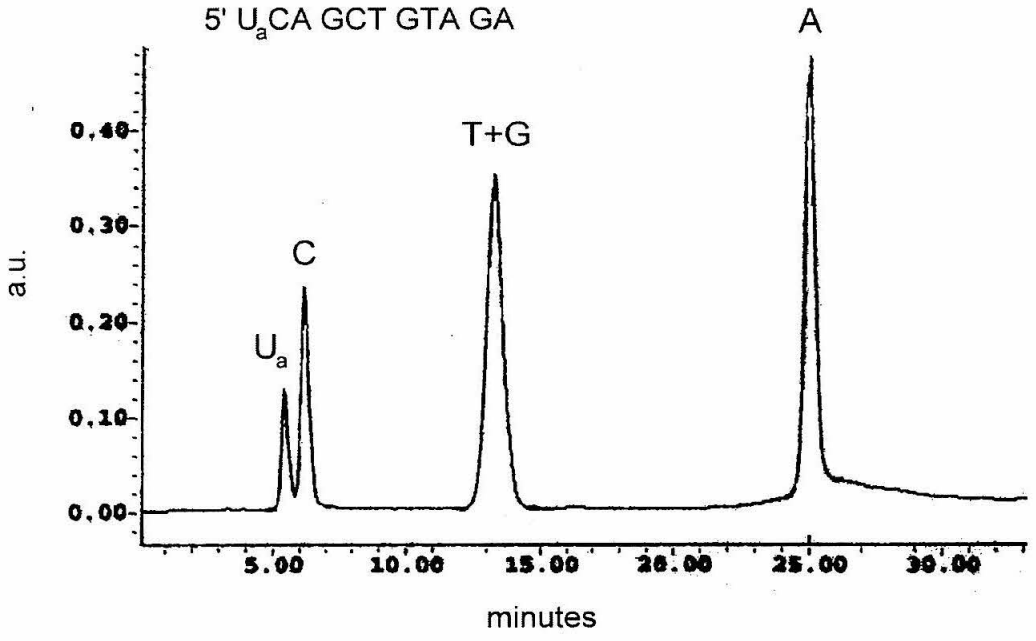
5' U$_a$CA GCT GTA GA
A
T+G
C
U$_a$
0,40
0,30
0,20
0,10
0,00
a.u.
5.00
10.00
15.00
20.00
25.00
30.00
minutes

Figure 2.6: Products of enzymatic digestion of **12** as analyzed by reverse-phase HPLC. Column: Prism C18. Gradient: 0-17% B over 15 minutes, then 17-75% B over 15 minutes. Solvent A = 0.1 M triethylamine acetate, pH 7.0, 2% acetonitrile; Solvent B = acetonitrile.

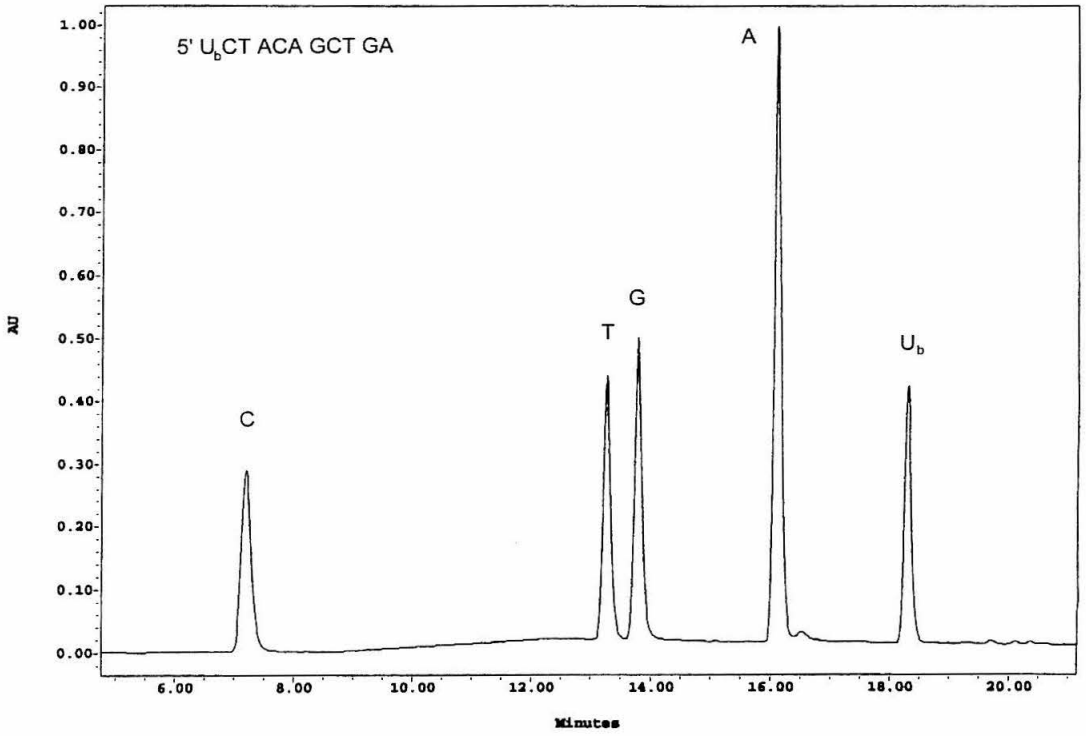
5' U$_b$CT ACA GCT GA
C
T
G
A
U$_b$
AU
1.00
0.90
0.80
0.70
0.60
0.50
0.40
0.30
0.20
0.10
0.00
6.00
8.00
10.00
12.00
14.00
16.00
18.00
20.00
Minutes

Figure 2.7: Products of enzymatic digestion of **13** as analyzed by reverse-phase HPLC. Column: Prism C18. Gradient: 0-17% B over 15 minutes, then 17-75% B over 15 minutes. Solvent A = 0.1 M triethylamine acetate, pH 7.0, 2% acetonitrile; Solvent B = acetonitrile.

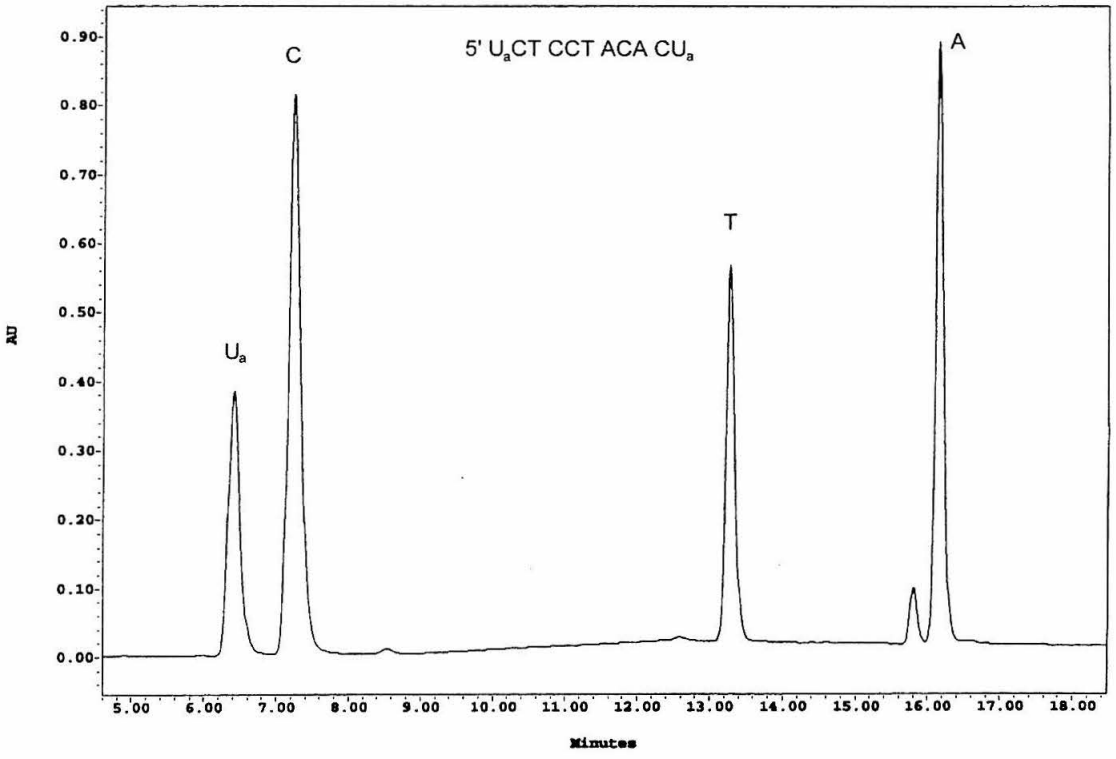
5' UaCT CCT ACA CUa
C
A
T
Ua
AU
0.90
0.80
0.70
0.60
0.50
0.40
0.30
0.20
0.10
0.00
5.00
6.00
7.00
8.00
9.00
10.00
11.00
12.00
13.00
14.00
15.00
16.00
17.00
18.00
Minutes

Figure 2.8: Products of enzymatic digestion of **14** as analyzed by reverse-phase HPLC. Column: Prism C18. Gradient: 0-17% B over 15 minutes, then 17-75% B over 15 minutes. Solvent A = 0.1 M triethylamine acetate, pH 7.0, 2% acetonitrile; Solvent B = acetonitrile.

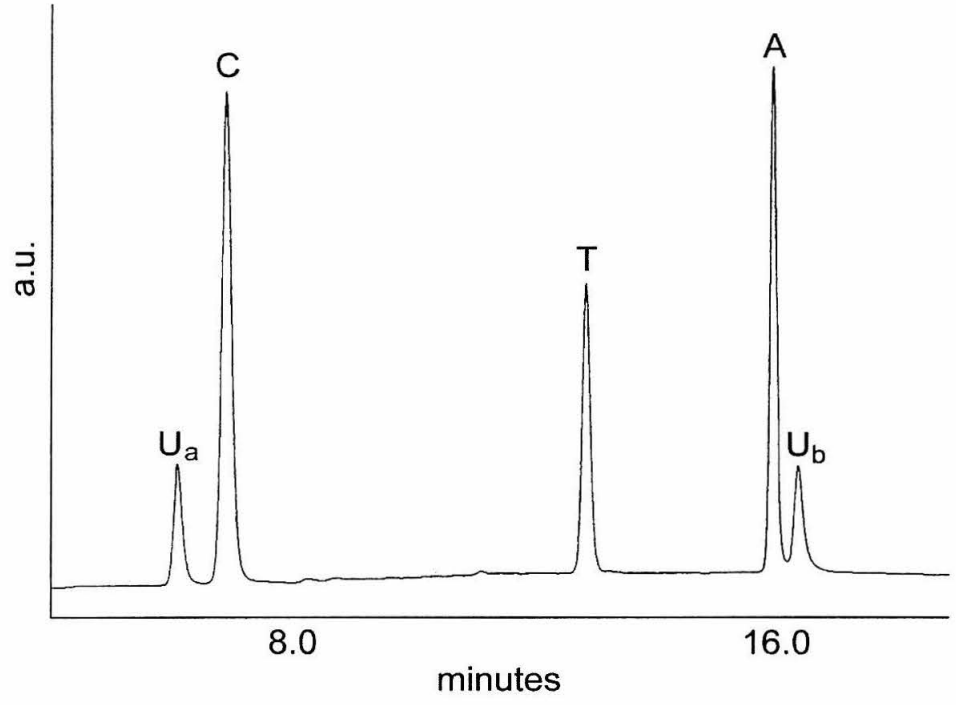
a.u.
C
A
T
U_a
U_b
8.0
16.0
minutes

Table 2.2. Thermal Denaturation Temperatures for Oligonucleotides containing 2′-Substituted Nucleosides.

Duplex	T_m [a] (°C)	Modification [b]
15:16	48.2 ± 0.5	none
11:15	46.6 ± 0.4	5′ $\mathbf{U_a}$
12:16	46.7 ± 0.4	5′ $\mathbf{U_b}$
11:12	45.0 ± 0.5	5′ $\mathbf{U_a}$, 5′ $\mathbf{U_b}$
17:18	47.6 ± 0.2	none
13:18	45.8 ± 0.5	5′ $\mathbf{U_a}$, 3′ $\mathbf{U_a}$
14:18	46.2 ± 0.5	5′ $\mathbf{U_a}$, 3′ $\mathbf{U_b}$

[a] Values determined in 50 mM NaP_i buffer (pH 7.0) containing 0.5 M NaCl. The concentration of each oligomer was 2.7 μM. [b] The symbol $\mathbf{U_a}$ denotes 2′-amino-2′-deoxyuridine; $\mathbf{U_b}$ denotes $N^{2'}$-(2-pyridylmethyl)-2′-amino-2′-deoxyuridine.

temperatures (T_m) for each duplex prepared in 50 mM sodium phosphate buffer (pH 7.0) containing 0.5 M sodium chloride. The T_m of the 11-mer duplex formed by the unmodified olignucleotides **15** and **16** was 48 °C. When one 5′-terminal nucleoside from this duplex was substituted with either 2′-amino-2′-deoxyuridine ($\mathbf{U_a}$) or $N^{2'}$-(2-pyridylmethyl)-2′-amino-2′-deoxyuridine ($\mathbf{U_b}$), the T_m value remained essentially unchanged (T_m = 47 °C for duplexes **11**:**15** and **12:16**). When both $\mathbf{U_a}$ and $\mathbf{U_b}$ were incorporated at the 5′ ends of the same duplex (**11:12**), the T_m value was decreased to 45 °C.

This small change in the melting profile was similar to the results obtained with duplexes of identical length, GC content, and type of nucleoside modification, but of different sequence. This second set of duplexes contained 2′-modified nucleosides at both the 3′ and 5′ ends of the same strand. Duplex **13:18** contained $\mathbf{U_a}$ nucleosides at the 5′ and 3′ termini, whereas duplex **14:18** contained $\mathbf{U_a}$ at the 5′ end and $\mathbf{U_b}$ at the 3′ end. The T_m values (46 °C) for duplexes **13:18** and **14:18** were decreased slightly in comparison to the value of the unmodified duplex **17:18** (T_m = 48 °C; Figure 2.9).

Discussion

Synthetic Strategy. This chapter describes the preparation of nucleosides containing 2′ ribose substituents designed for incorporating reporter molecules into oligonucleotides. Two general methods exist for preparing oligonucleotides containing these labels. The post-synthetic modification method involves (a) the synthesis of nucleosides that possess reactive functional groups (such as a primary amine), (b) incorporation of these modified nucleosides into oligonucleotides, and (c) subsequent

Figure 2.9: Thermal denaturation curves for duplex **17:18** (□) and duplex **14:18** (♦).

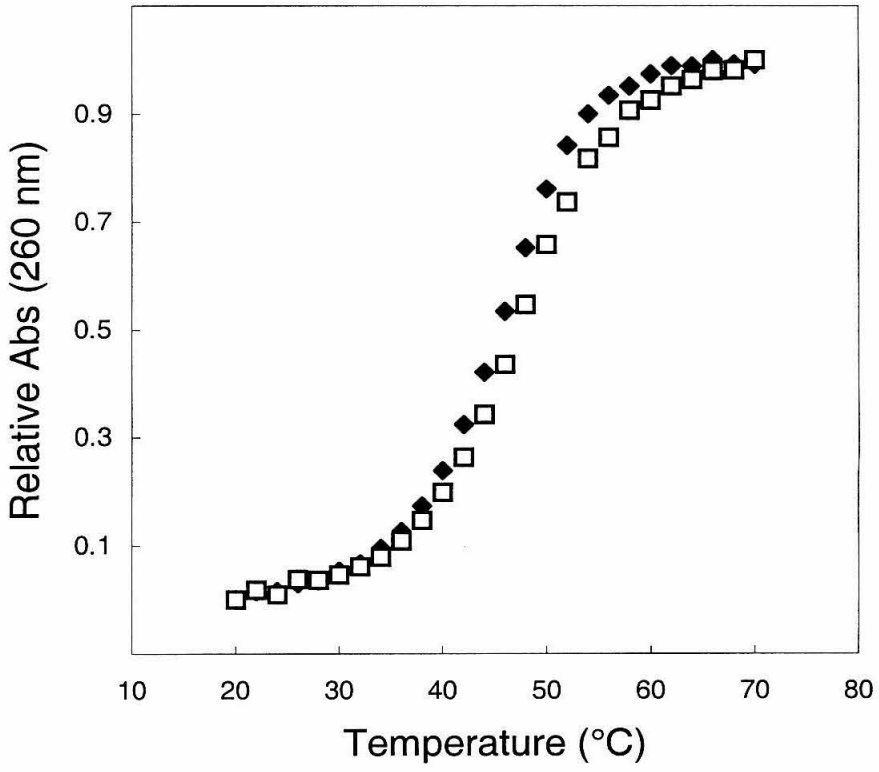
Relative Abs (260 nm)
0.9
0.7
0.5
0.3
0.1
10
20
30
40
50
60
70
80
Temperature (°C)

labeling of the reactive functional groups with desired reporter molecules. The solid-phase synthesis method entails the synthesis of label-containing nucleosides that are incorporated during solid-phase oligonucleotide synthesis. Both methods can be explored with the 2′-modified nucleosides described in this work.[10,11]

The choice of 2′-substituents developed here are based on ligands that will bind transition metal complexes (Figure 2.1). These nucleoside ligands include AMPy and AEPy, and are contained in a variety of metal complexes.[21,22] The first example of metalled 2′-modified nucleosides were prepared with a nucleoside containing a primary amine group at the 2′ position.[10]

The site-specific labeling of oligonucleotides with metal reagents is of considerable interest. Experiments involving ruthenium-modified duplexes have shown that DNA can mediate energy and electron transfer reactions.[10,23-29] Additional work has led to the use of metal-modified primers in dideoxy DNA sequencing techniques.[30] The introduction of nucleosides containing metal-binding ligands can expand the use of metal complexes as probes of nucleic acid structure and function.[10,11]

Synthesis of 2′-Modified Nucleosides. The synthesis of nucleosides containing 2′-N-alkylamino substituents is an extension of methods developed by Sebesta, McGee, and coworkers.[13,14] The yields of isolation determined for **2a** and **2b** are lower than those observed for nucleosides containing similarly bulky substituents, and may be attributed to the purification conditions required for DMT-protected vs. silyl-protected intermediates.[13] The products **3a** and **3b** are isolated in yields comparable to the yields reported by Sebesta for similar 2′-modified nucleosides.

The preparation of supports derivatized with 2′-modified nucleosides is complicated, due to the poor accessibility of the 3′ ribose site.[31] The steric bulk at the 2′ position hinders the reaction of the 3′ hydroxyl with succinic anhydride. Succination of **3a** and **4** proceeds in reasonable yields and demonstrates that both small and large functional groups at the 2′ position can be tolerated in succination step. High nucleoside loadings for **7** and **8** are achieved using the coupling agent BOP and an excess of nucleoside hemisuccinate in the derivatization step. While the solid support employed here is glass-based, the method is applicable to other solid supports containing a long-chain alkylamine linker.

Successful derivatization of supports with nucleosides like **3a** and **4** now affords the synthesis of 3′ oligonucleotide conjugates in which the label is incorporated on the ribose ring. Currently, the preparation of 3′ oligonucleotide conjugates is achieved with supports containing either nucleosides with base-tethered primary amine groups[32] or non-nucleosidic amine derivatives.[33-45] The ribose is an attractive attachment since labels introduced here may cause fewer perturbations to the secondary duplex structure than labels attached to the nucleoside base. The absence of a long linker between the attachment site and the incorporated label minimizes possible disruptions to the hydrogen bonding capacity of the oligonucleotide conjugate.

Oligonucleotide Synthesis with 2′-Modified Nucleosides. The successful large-scale synthesis of several 11-mer oligonucleotides validates the utility of 2′-modified nucleosides as support-bound and phosphoramidite derivatives (Table 2.1). Oligonucleotide synthesis beginning with **7** or **8** proceeds with minor modification to the

automated protocol. The coupling yields of phosphoramidites **9** and **10** are suitable for routine oligonucleotide preparation. The purification of the several 11-mer modified oligonucleotides is straightforward. The isolation yields for **11-14** are comparable to values determined for oligonucleotides **15-18** under identical synthetic and purification conditions, implying that the use of 2′-modified nucleosides does not compromise the overall yield.

Effect of 2′-Modified Nucleosides on Duplex Stability. The presence of nucleosides containing ribose substituents at the 2′ position causes slight destabilization to the modified duplexes, as assessed by thermal denaturation studies. Interestingly, analysis of the transition melting (T_m) temperatures listed in Table 2.2 suggests that the T_m values are influenced by the number of 2′-modified nucleosides present in a duplex, not the size of the 2′ substituent. For example, thermal denaturation of duplexes **11:15** and **12:16** produces identical T_m values, despite the difference in the size of the 2′ substituent (primary amine vs. AMPy). The T_m of **11:12** shows the effect of placing two 2′-modified nucleosides at the 5′ ends of the duplex. Similar results are obtained with a second set of duplexes identical in length, GC content, and type of nucleoside modification. The placement of two 2′-modified nucleosides at the 5′ and 3′ ends of the same strand results in duplexes destabilized by 1-2 °C (**13:18** and **14:18** vs. **17:18**). We conclude that the extent of duplex destabilization is the same when two 2′-modified nucleosides are introduced at either (1) the 5′ and 3′ ends of a one strand hybridized to its complement, or (2) the 5′ ends of complementary strands.

2′-Aminonucleosides favor the 2′-endo conformation to a higher degree than 2′-deoxynucleosides do.[46] This observation suggests that 2′-aminonucleosides should stabilize DNA/DNA duplexes. However, T_m data for a series of 9-mer duplexes containing a 2′-aminonucleoside in the middle of the sequence indicate that the presence of these modified nucleosides has a destabilizing effect.[6] Our work shows that placement of the 2′-modified nucleosides at the ends of the duplexes minimizes the destabilization imposed by the altered sugar conformation.

Conclusion

We report the synthesis of 2′-modified nucleosides designed specifically for incorporating reporter molecules into oligonucleotides. Because these nucleosides contain modifications to the ribose ring, as opposed to the nucleobase, they are important contributions to current library of nucleoside analogs. The introduction of metal-binding ligands at the 2′ position is achieved after two steps. Conversion of these nucleosides to solid support-bound and phosphoramidite derivatives proceeds in good yield. The powerful combination of these derivatives affords the preparation of an entirely new class of oligonucleotides—those which contain label attachment sites at 3′, intervening, and 5′ locations of a duplex.

Thermal denaturation studies indicate that the presence of 2′-modified nucleosides in 11-mer duplexes has a slight destabilizing effect on the duplex structure. This effect is limited by the selective placement of these nucleosides at the ends of the duplexes. Interestingly, the size of the metal-binding substituent does not influence the magnitude

of the destabilization. This characteristic makes these 2′-modified nucleosides attractive for use in the site-specific incorporation of reporter molecules into oligonucleotides.

The methodologies employed here can be extended to other modified nucleosides. Succination yields for nucleosides containing metal-binding ligands at locations other than the 2′ position are expected to be much higher, due to the absence of steric constraints. While the solid support is glass-based, the method is applicable to other solid supports containing any long-chain alkylamine linker. The library of solid supports containing modified nucleosides can be significantly expanded with the coupling conditions described here. These nucleoside reagents will enable the incorporation of labels that probe nucleic acid structure and function.

Experimental Procedure

General. ^{1}H were acquired using Varian 300 and 500 spectrometers. Chemical shifts are reported in parts per million and referenced to the proton chemical shifts of deuterated solvent or trimethylsilane. Reagents and starting materials were used as received from Aldrich. Flash chromatography was performed on EM Science/Merck silica gel 60 (230-400 mesh). Thin-layer chromatography (TLC) was performed on 0.25 mm Merck precoated silica plates (60 F_{254}). Combustion analysis was performed by Quantitative Technologies Inc. Enzymes were purchased from Pharmacia. Mass spectrometry was performed by the Caltech Peptide/Protein Microanalytical Laboratory.

5′-*O*-(4,4′-dimethoxytrityl)-2,2′-*O*-anhydro-1-(β-D-arabinofuranosyl)uracil, 1. This compound was prepared from reaction of 2,2′-*O*-anhydro-1-(*β*-D-arabinofuranosyl)uracil and 4,4′-dimethoxytrityl chloride as previously described.[15]

5′-*O*-(4,4′-dimethoxytrityl)-2′-*N*,3′-*O*-(2-oxooxazolidin)-2′-aminomethylpyridyl-2′-deoxyuridine, **2a**. To a solution of **1** (2.2 g, 4.2 mmol) in pyridine (40 mL) was added 1,1′-carbonyldiimidazole (1.01 g, 6.2 mmol). After 30 hours of stirring at ambient temperature, the solvent was removed and the residue was resuspended in dichloromethane (40 mL); DIEA (1.1 mL, 6.3 mmol) and AMPy (649 μL, 6.3 mmol) were delivered to the solution. After 60 hours of stirring at ambient temperature, the reaction was quenched with 5% citric acid, extracted with fresh dichloromethane, dried with Na_2SO_4, and concentrated to an oil. The residue was dissolved in tetrahydrofuran (25 mL), DBU (628 μL, 4.2 mmol) was added to the flask, and the solution was refluxed for 46 hours. The solvent was removed and the residue was purified on silica (using 22% EtOAc in dichloromethane containing 1% TEA and 3% methanol) to afford **2a** in 20% yield (548 mg, 828 μmol). ^{1}H NMR ($CDCl_3$, 500 MHz; Figure 2.10) δ 3.48-3.58 (m, 2H), 3.78 (s, 6H), 4.35-4.40 (m, 1H), 4.54 (d, 1H), 4.75 (dd, 2H), 5.14-5.17 (m, 1H), 5.41 (d, 1H), 6.06 (d, 1H), 6.82 (d, 4H), 7.21-7.30 (m, 9H), 7.33-7.37 (m, 2H), 7.53 (d, 1H), 7.69 (t, 1H), 8.51 (d, 1H), 8.84 (s, 1H). ESI-MS mass calculated for $C_{37}H_{35}N_4O_8$ $[M+H]^+$: 663.24. Found: 663.2 (Figure 2.11).

5′-*O*-(4,4′-dimethoxytrityl)-2′-*N*,3′-*O*-(2-oxooxazolidin)-2′-aminoethylpyridyl-2′-deoxyuridine, **2b**. To a solution of **1** (1.0 g, 1.9 mmol) in pyridine (30 mL) was added 1,1′-carbonyldiimidazole (0.460 g, 2.8 mmol). After 30 hours of stirring at ambient temperature, the solvent was removed by rotary evaporation and the residue was resuspended in dichloromethane (30 mL); DIEA (500 μL, 2.85 mmol) and AEPy (340 μL, 2.85 mmol) were delivered to the solution. After 60 hours of stirring at ambient

Figure 2.10: ^{1}H NMR spectrum of **2a** in $CDCl_3$ (500 MHz).

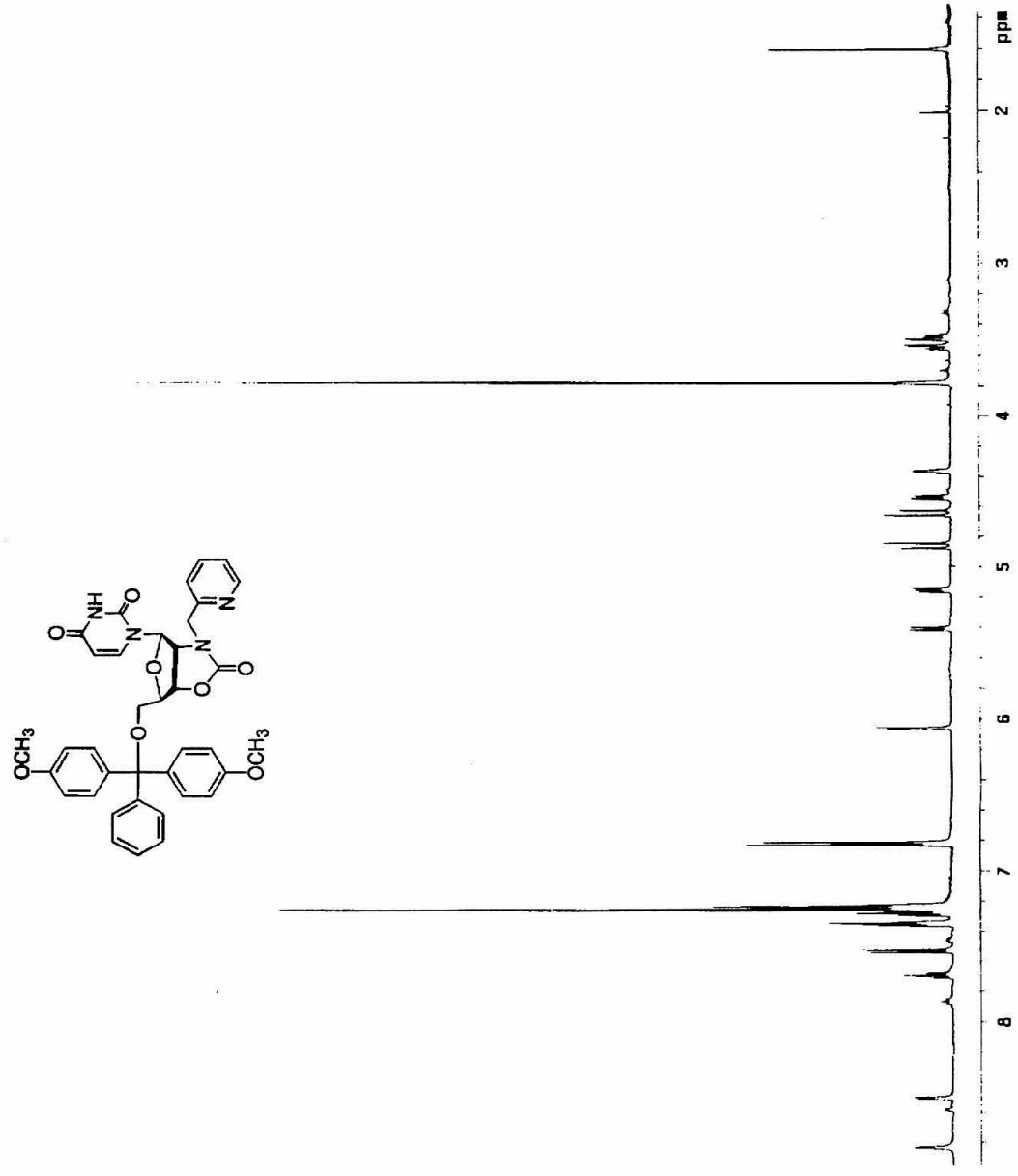
NH
O
O
N
N
O
O
O
N
O
OCH3
OCH3
8
7
6
5
4
3
2
ppm

Figure 2.11: ESI mass spectrum of **2a** conducted in positive ionization mode.

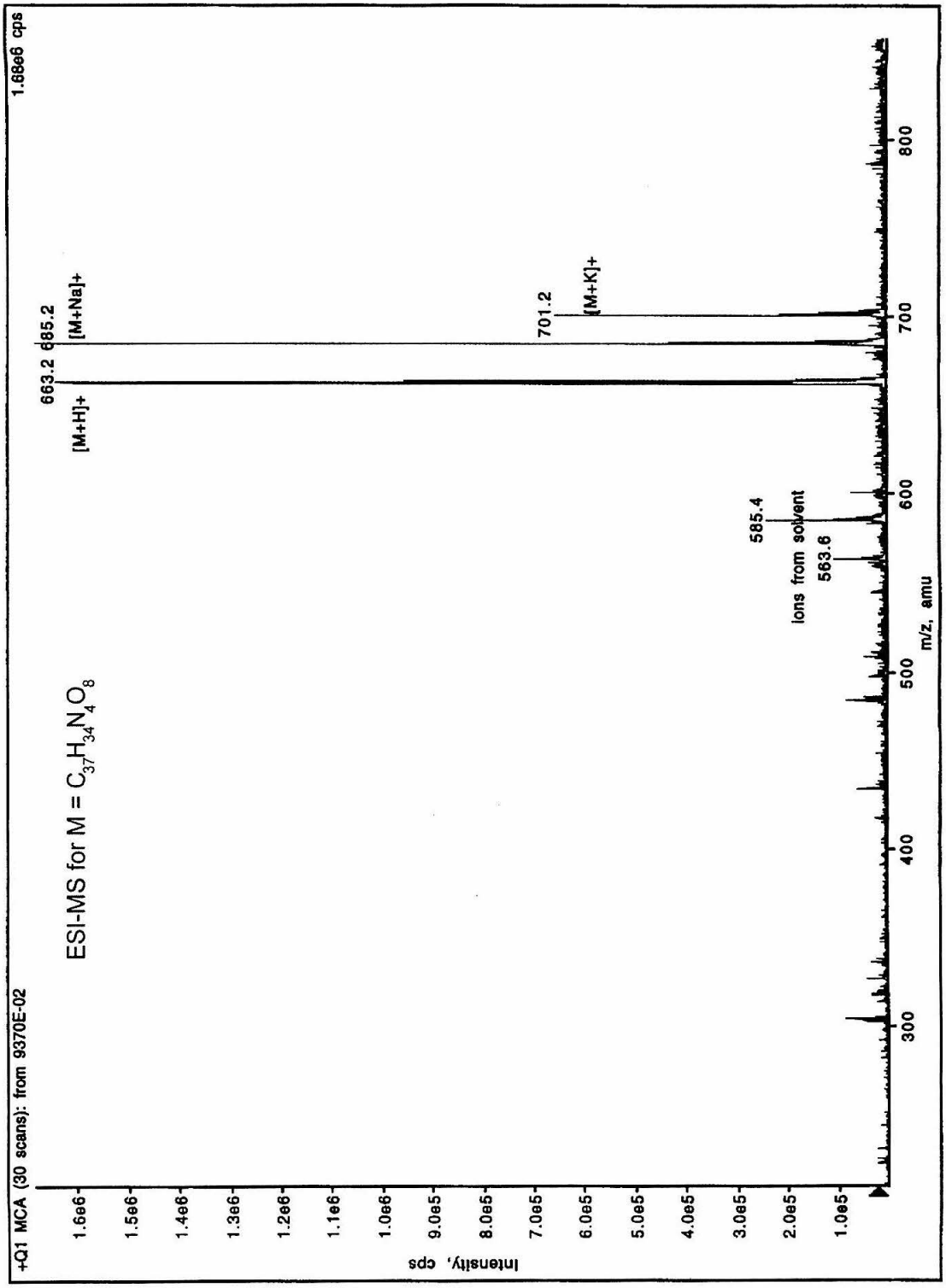
+Q1 MCA (30 scans): from 9370E-02
1.68e6 cps
ESI-MS for M = C37H34N4O8
663.2
[M+H]+
685.2
[M+Na]+
701.2
[M+K]+
585.4
Ions from solvent
563.6
Intensity, cps
m/z, amu
1.6e6
1.5e6
1.4e6
1.3e6
1.2e6
1.1e6
1.0e6
9.0e5
8.0e5
7.0e5
6.0e5
5.0e5
4.0e5
3.0e5
2.0e5
1.0e5
300
400
500
600
700
800

temperature, the reaction was worked up as described for **2a**. The residue was dissolved in THF (11 mL), DBU (284 μL, 1.9 mmol) was added to the flask, and the solution was refluxed for 46 hours. The solvent was removed by rotary evaporation and the residue was purified on silica (eluting with 5-15% methanol in EtOAc) to afford **2b** in 10% yield (127 mg, 188 μmol). ^{1}H NMR ($CDCl_3$, 300 MHz, Figure 2.12) δ 3.07-3.39 (m, 2H), 3.43-3.60 (m, 2H), 3.74-3.77 (m, 6H), 3.93-4.04 (m, 1H), 4.26-4.31 (m, 1H), 4.64 (dd, 2H), 5.09-5.14 (m, 1H), 5.35 (d, 1H), 6.09 (d, 1H), 6.84 (d, 4H), 7.15-7.39 (m, 11H), 7.59-7.69 (m, 2H), 8.57 (d, 1H). ESI-MS mass calculated for $C_{38}H_{37}N_4O_8$ $[M+H]^+$: 677.25. Found: 677.2 (Figure 2.13).

5′-*O*-(4,4′-dimethoxytrityl)-2′-aminomethylpyridyl-2′-deoxyuridine, 3a. Compound **2a** (242 mg, 0.36 mmol) was suspended in dioxane (6 mL), 4 M NaOH (4.7 mL), and methanol (4.7 mL), and the mixture was stirred at 50 °C for 36 hours. The solvents were removed by rotary evaporation and the residue was dissolved in dichloromethane (55 mL). The solution was extracted with brine, dried over sodium sulfate, and evaporated to dryness to give **3a** in 92% yield (216 mg, 0.34 mmol). ^{1}H NMR ($CDCl_3$, 300 MHz, Figure 2.14) δ 3.3 (s(br), 4H), 3.73-3.78 (m, 6H), 3.94-4.02 (m, 1H), 4.1 (d, 1H), 4.2 (s, 1H), 5.3 (d, 1H), 6.1 (d, 1H), 6.7 (dd, 4H), 7.1-7.3 (m, 11H), 7.5-7.6 (m, 2H), 8.4 (s, 1H). ESI-MS mass calculated for $C_{36}H_{37}N_4O_7$ $[M+H]^+$: 637.26. Found: 637.2 (Figure 2.15).

5′-*O*-(4,4′-dimethoxytrityl)-2′-aminomethylpyridyl-2′-deoxyuridine, 3b. Compound **2b** (1.7 g, 2.51 mmol) was suspended in dioxane (43 mL), 4 M NaOH (26 mL), and methanol (26 mL), and the mixture was stirred at room temperature for 20 hrs. The reaction was heated at 60 °C for an additional 2 hours, after which the solvents

Figure 2.12: ^{1}H NMR spectrum of **2b** in $CDCl_3$ (300 MHz).

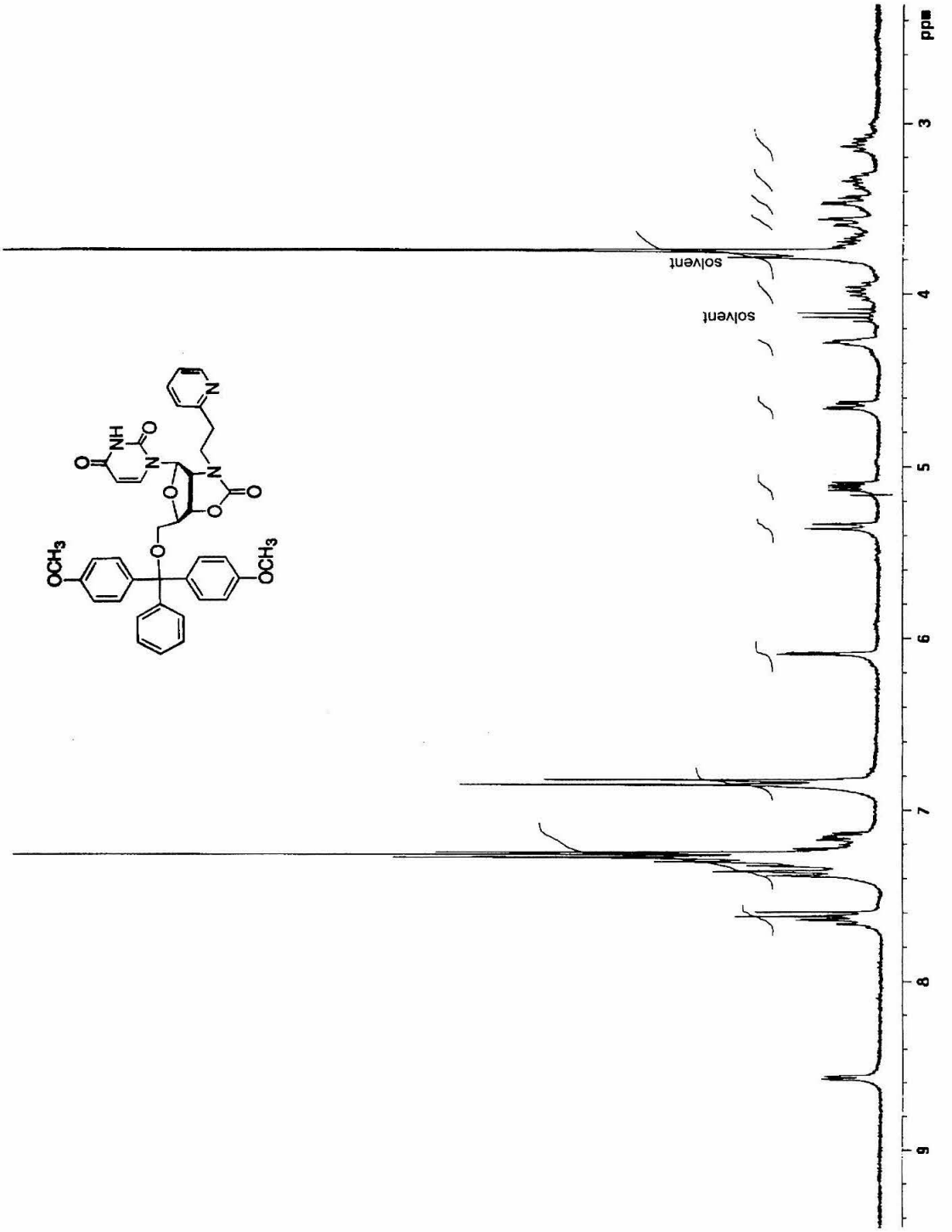
solvent
solvent
ppm
9
8
7
6
5
4
3
OCH3
OCH3
NH
O
N
O

Figure 2.13: ESI mass spectrum of **2b** conducted in positive ionization mode.

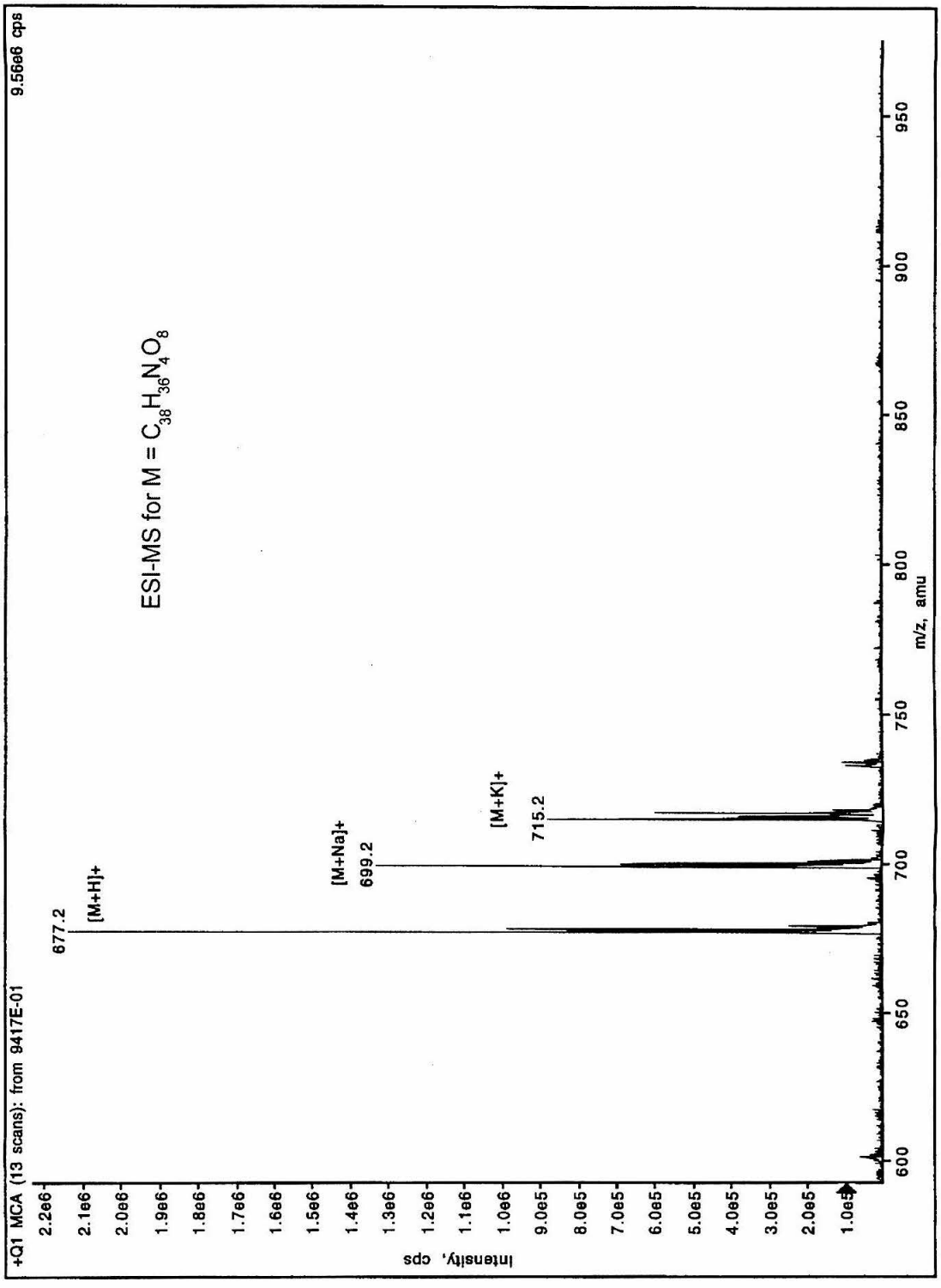
+Q1 MCA (13 scans): from 9417E-01
9.5666 cps
ESI-MS for M = C38H36N4O8
677.2
[M+H]+
699.2
[M+Na]+
715.2
[M+K]+
Intensity, cps
m/z, amu

Figure 2.14: ^{1}H NMR spectrum of **3a** in $CDCl_3$ (300 MHz).

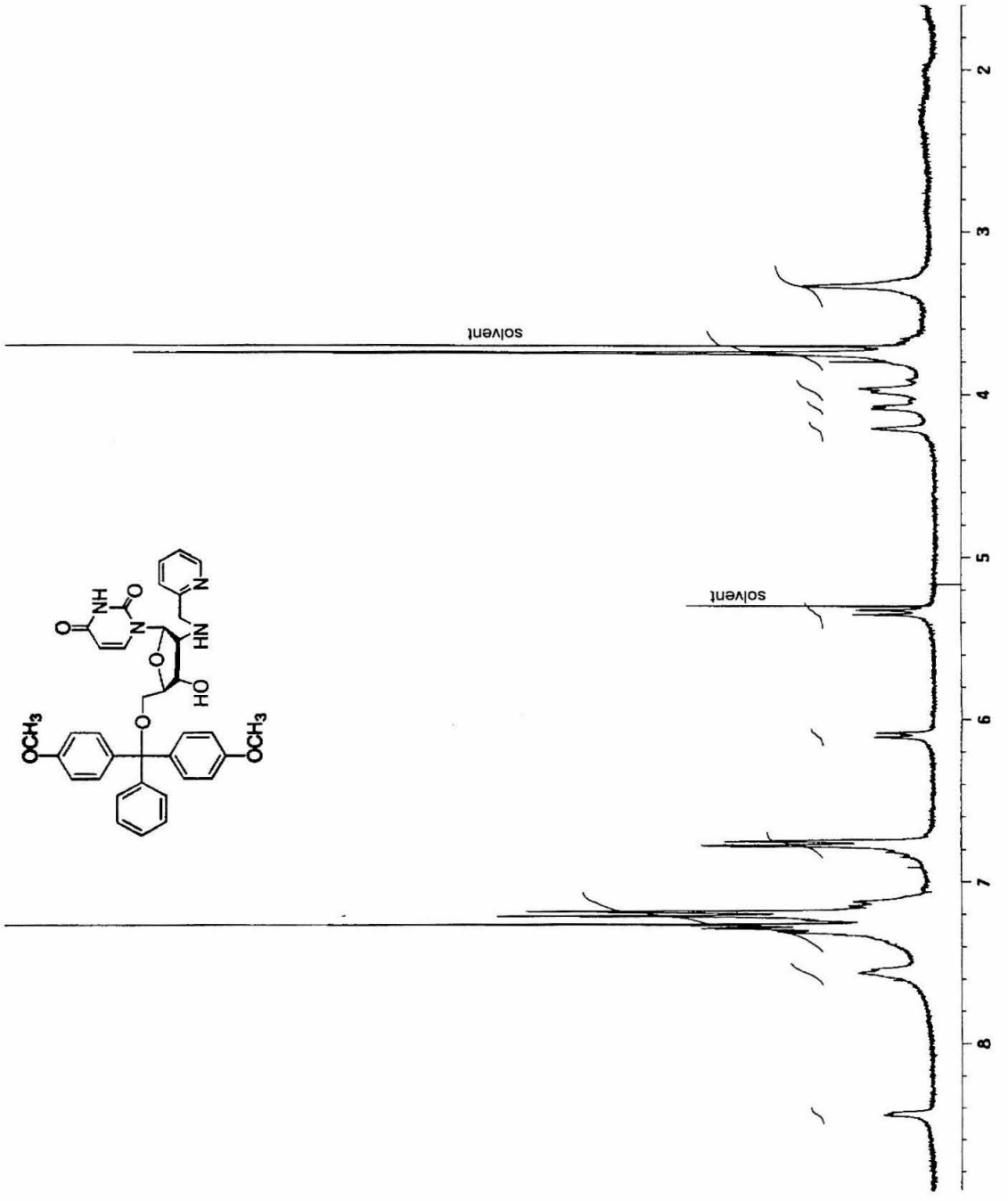
solvent
solvent
OCH3
OCH3
HO
HN
NH
O
N
2
3
4
5
6
7
8

Figure 2.15: ESI mass spectrum of **3a** conducted in positive ionization mode. (Peak at 303.2 represents the DMT ion.)

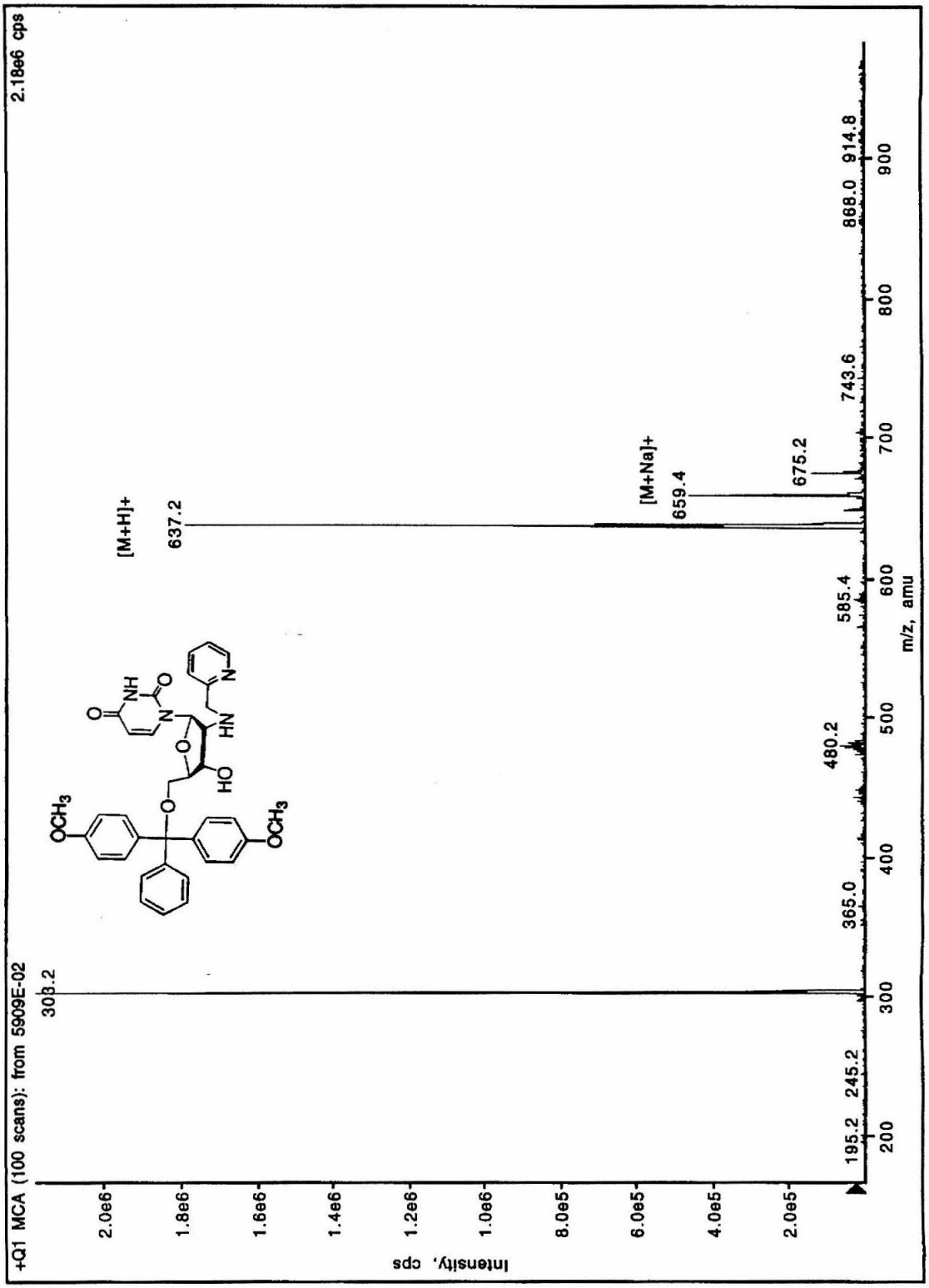
+Q1 MCA (100 scans): from 5909E-02
2.18e6 cps
Intensity, cps
m/z, amu
[M+H]+
637.2
[M+Na]+
659.4
303.2
365.0
480.2
585.4
675.2
743.6
868.0
914.8
195.2
245.2
OCH3
OCH3
HO
NH
HN
N
O

were removed by rotary evaporation. The residue dissolved in dichloromethane, extracted with brine, dried over sodium sulfate, and evaporated to dryness. The material was purified on silica (eluting with 23% ethyl acetate in dichloromethane containing 1% each of methanol and triethylamine) to give **3b** in 88% yield (1.44 g, 2.21 mmol). ^{1}H NMR ($CDCl_3$, 500 MHz, Figure 2.16) δ 3.03 (t, 2H), 3.12-3.25 (m, 2H), 3.43-3.53 (m, 3H), 3.80 (s, 6H), 4.29 (s, 1H), 4.49 (d, 1H), 5.37 (d, 1H), 5.94 (d, 1H), 6.14 (s(br), 1H), 6.85 (d, 4H), 7.18-7.33 (m, 10H), 7.40 (d, 1H), 7.67 (t, 1H), 7.74 (d, 1H), 8.49 (d, 1H). ESI-MS mass calculated for $C_{37}H_{39}N_4O_7$ $[M+H]^+$: 651.27. Found: 651.2 (Figure 2.17).

5'-*O*-(4,4'-dimethoxytrityl)-N$^{2'}$-trifluoroacetamido-2'-deoxyuridine, 4. This compound was prepared either from reaction of 2′-amino-5′-*O*-(4,4′-dimethoxytrityl)-2′-deoxyuridine and ethyl trifluoroacetate[15] or from reaction N$^{2'}$-trifluoroacetyl-2′-amino-2'-deoxyuridine and 4,4'-dimethoxytrityl chloride as previously described.[6]

5'-O-(4,4'-dimethoxytrityl)-2'-aminomethylpyridyl -2'-deoxyuridine-3'-O-succinate, 5. Compound **3a** (100 mg, 0.157 mmol), DMAP (9.4 mg, 0.5 eq), and succinic anhydride (17.3 mg, 1.1 eq) were suspended in dry pyridine (1 mL), and allowed to stir under argon for two hours, at which time an additional 0.2 equivalents of succinic anhydride were added. The reaction proceeded overnight at room temperature, after which the solvent was removed. The residue was dissolved in dichloromethane (20 mL) and stirred with an equal volume of 5% $NaHCO_3$ solution for two hours. The mixture was partitioned, and the organic phase was extracted with brine. Each phase was back-extracted with fresh solutions once. The combined organic phases were washed with cold 5% citric acid, and concentrated to a small volume (3-5 mL). The sample was precipitated in stirring hexanes, and the white solid **5** was collected by filtration in 60%

Figure 2.16: ^{1}H NMR spectrum of **3b** in $CDCl_3$ (500 MHz).

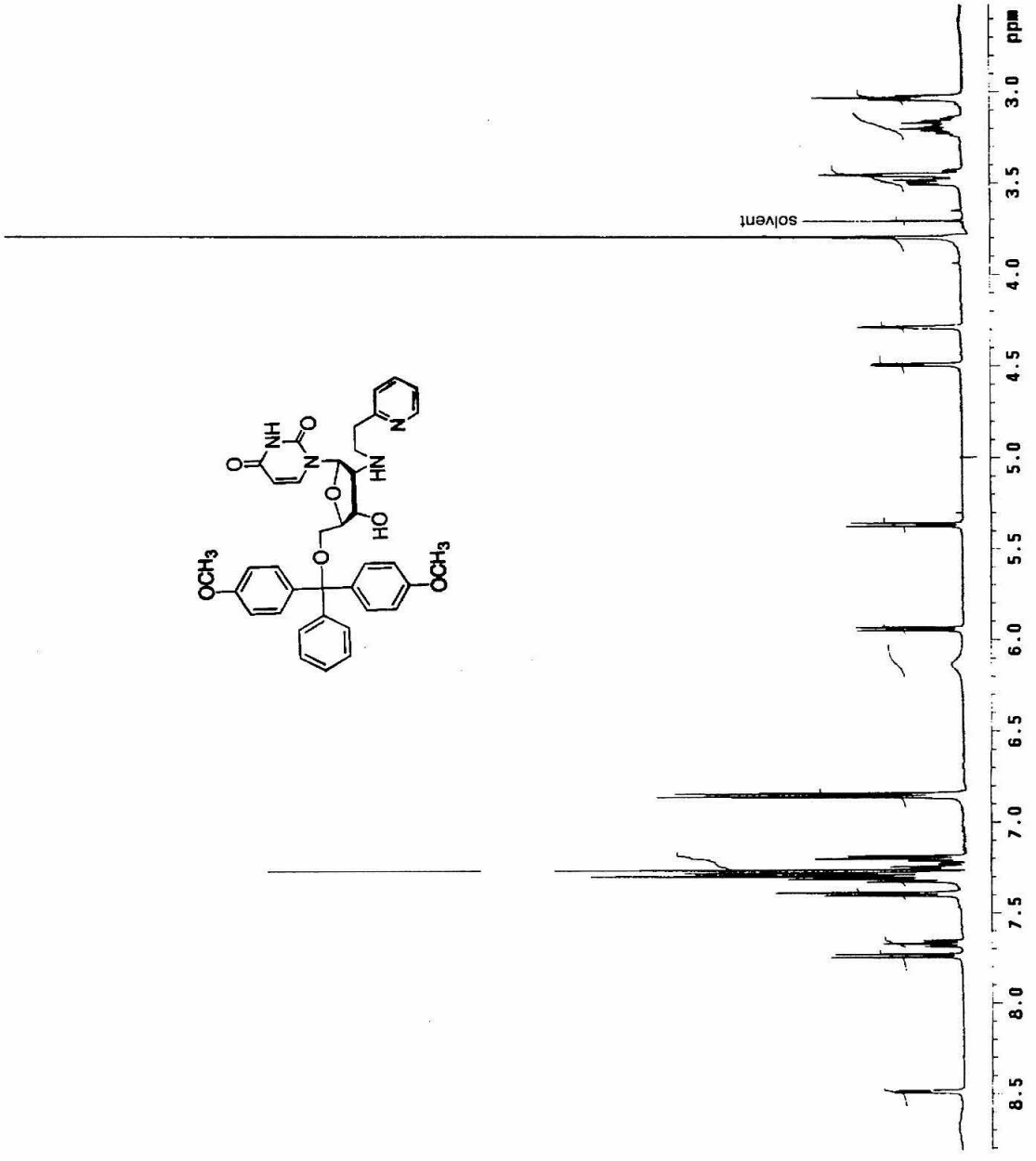
solvent
8.5
8.0
7.5
7.0
6.5
6.0
5.5
5.0
4.5
4.0
3.5
3.0
ppm
OCH3
OCH3
HO
HN
NH
O
N

Figure 2.17: ESI mass spectrum of **3b** conducted in positive ionization mode.

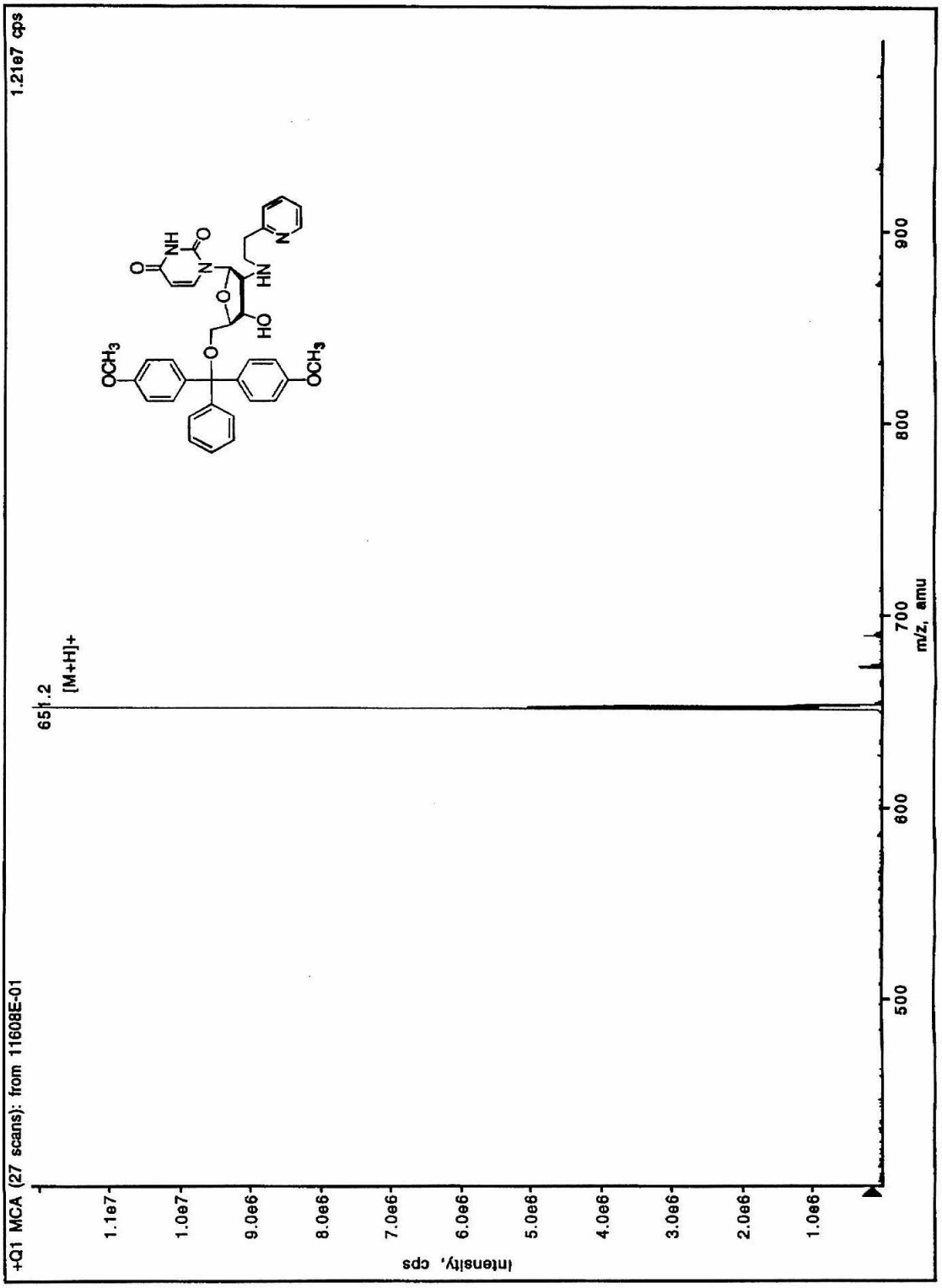
+Q1 MCA (27 scans): from 11608E-01
1.21e7 cps
651.2
[M+H]+
Intensity, cps
1.1e7
1.0e7
9.0e6
8.0e6
7.0e6
6.0e6
5.0e6
4.0e6
3.0e6
2.0e6
1.0e6
500
600
700
800
900
m/z, amu
NH
O
N
O
HN
N
HO
OCH3
OCH3

yield (69 mg, 0.094 mmol). ESI-MS mass calculated for $C_{40}H_{39}N_4O_{10}$ $[M-H]^-$: 735.27. Found: 735.2 (Figure 2.18).

5'-*O*-(4,4'-dimethoxytrityl)-$N^{2'}$-trifluoroacetamido-2'-deoxyuridine-3'-*O*-succinate, 6. Compound **4** (100 mg, 0.156 mmol), DMAP (9.4 mg, 0.5 eq), and succinic anhydride (17.2 mg, 1.1 equiv) were suspended in dry pyridine (2 ml) and stirred under argon for two hours. An additional 0.2-0.5 equivalents of succinic anhydride were added, and the reaction proceeded at room temperature overnight. The reaction was worked according to the procedure given for **5**. A white powder **7** was isolated in 74% yield (85 mg, 0.115 mmol). ESI-MS mass calculated for $C_{36}H_{33}N_3O_{11}$ $[M-H]^-$: 740.21. Found: 740.2 (Figure 2.19).

5'-*O*-(4,4'-dimethoxytrityl)-2'-aminomethylpyridyl-2'-deoxyuridine-3'-*O*-succinated support, 7. Compound **7** was prepared by suspending the solid support (controlled pore glass derivatized with long-chain alkyl amine, 500 Å pore size, 350 mg) in dry dichloromethane (5 ml) and adding TEA (250 µl) and **5** (180 mg, 245 µmol); HOBT (33 mg, 245 µmol) and BOP (119 mg, 270 µmol) were added to the suspension. The mixture was agitated for 16 hours at room temperature, filtered, and washed with dichloromethane (2 x 10 ml). The solid was transferred to a separate flask and suspended in pyridine (7.5 ml). Acetic anhydride (1-2 ml) and N-methylimidazole (100 µl) were added to the flask, and the mixture was agitated overnight. The solid was filtered, and washed with pyridine (3 x 10 ml), methanol (3 x 10 ml), dichloromethane (3 x 10 mL), and diethyl ether (3 x 10 mL). The white solid **7** was dried under vacuum. The nucleoside loading was determined spectrophotometrically to be 60 µmol/g.[17]

Figure 2.18: ESI mass spectrum of **5** conducted in negative ionization mode. Additional peaks observed at 771.2, $[M+Cl]^-$ and 635.2, $[M\text{-succinate}]^-$.

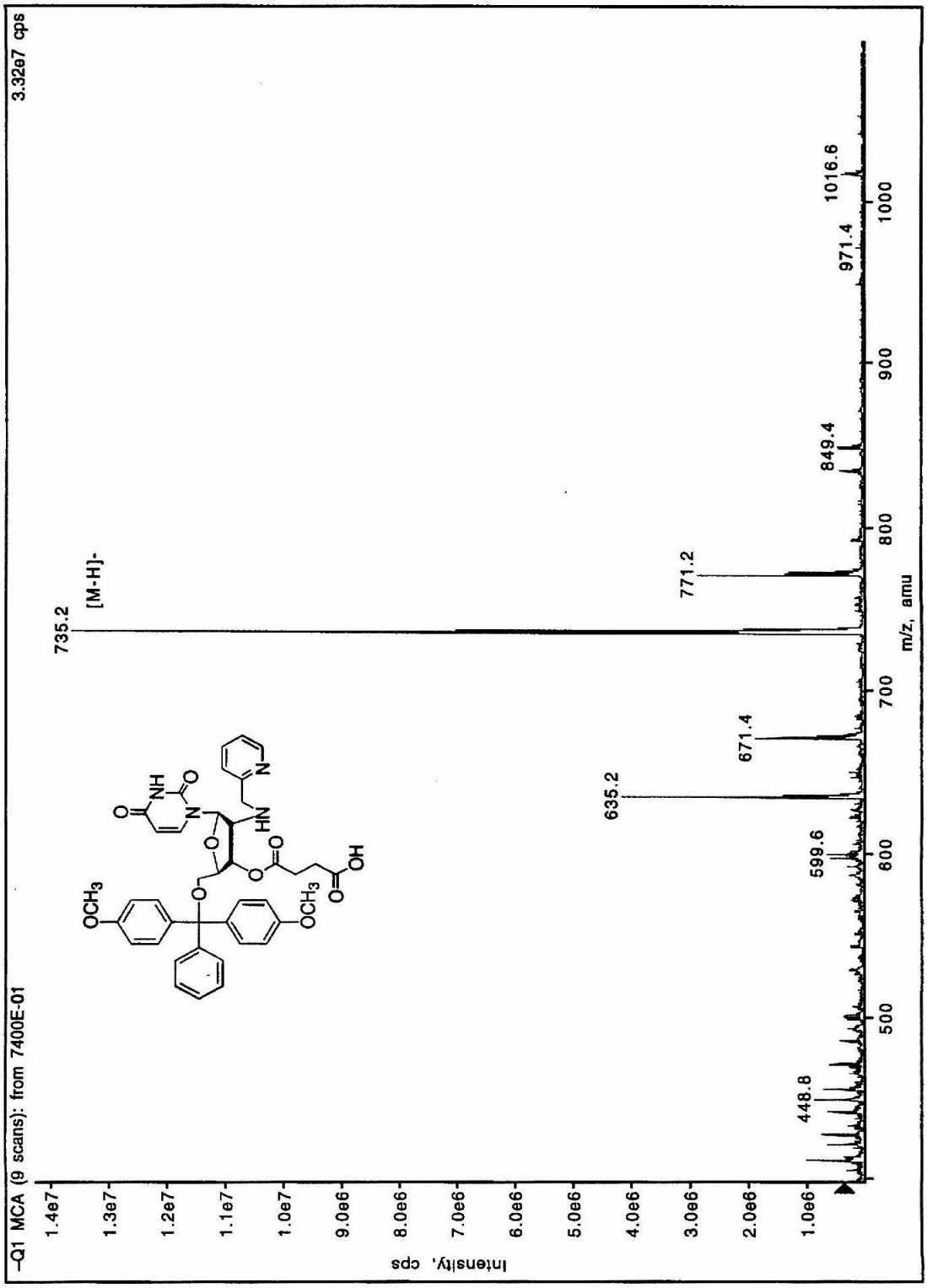
-Q1 MCA (9 scans): from 7400E-01
3.32e7 cps
Intensity, cps
m/z, amu
735.2
[M-H]-
771.2
635.2
671.4
599.6
448.8
849.4
971.4
1016.6
OCH3
OCH3
OH
NH
HN
N
O

Figure 2.19: ESI mass spectrum of **6** conducted in negative ionization mode.

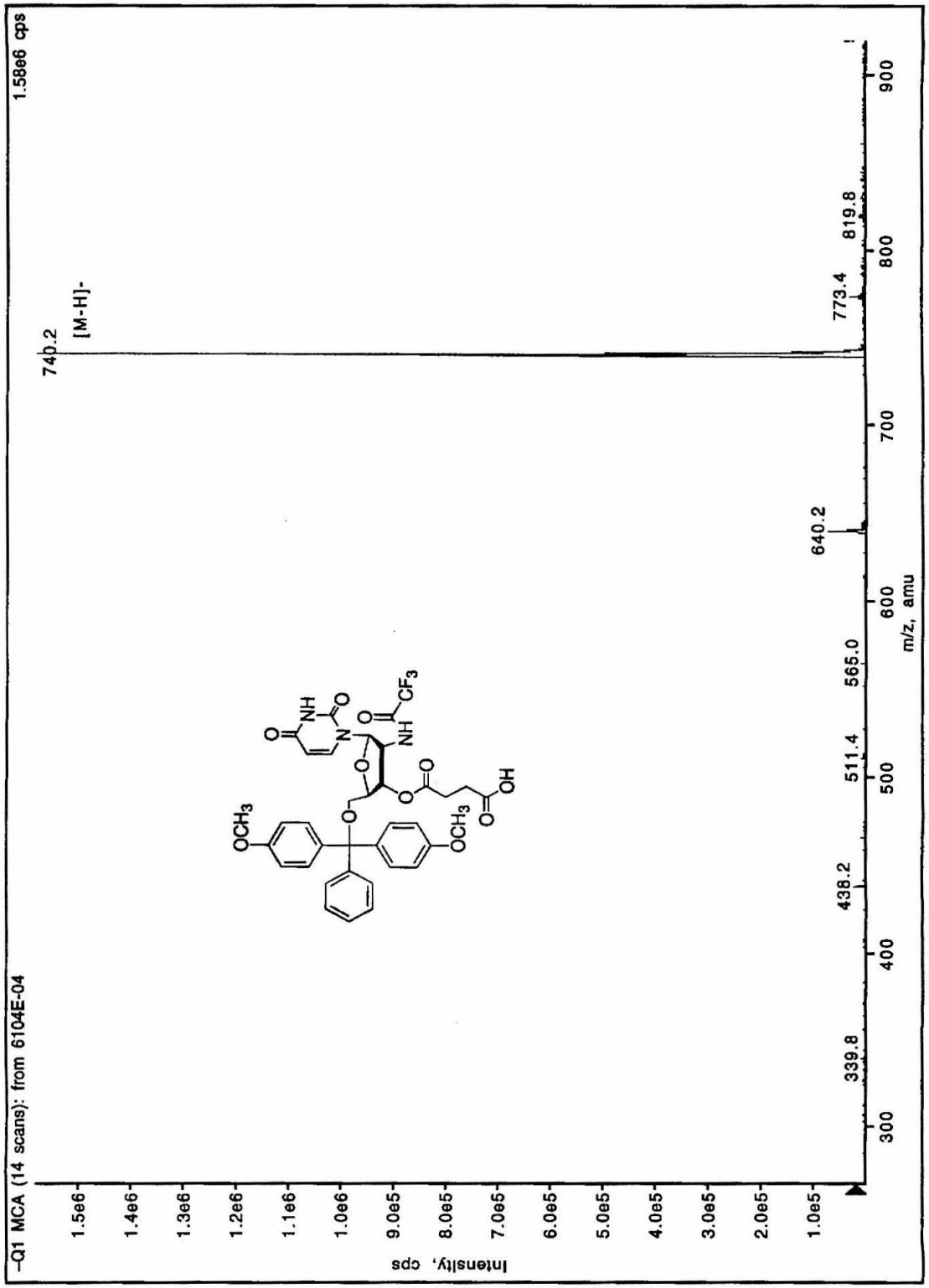
-Q1 MCA (14 scans): from 6104E-04
1.58e6 cps
740.2
[M-H]-
640.2
773.4
819.8
565.0
511.4
438.2
339.8
Intensity, cps
m/z, amu
1.5e6
1.4e6
1.3e6
1.2e6
1.1e6
1.0e6
9.0e5
8.0e5
7.0e5
6.0e5
5.0e5
4.0e5
3.0e5
2.0e5
1.0e5
300
400
500
600
700
800
900
NH
O
N
O
O
NH
CF3
O
O
OH
O
OCH3
OCH3

5'-*O*-(4,4'-dimethoxytrityl)-$N^{2'}$-trifluoroacetamido-2'-deoxyuridine-3'-*O*-succinated support, 8. Compound **8** was prepared using the same method described for **7**. The nucleoside loading for **8** was 52 μmol/g.

5'-*O*-(4,4'-dimethoxytrityl)-2'-aminomethylpyridyl-2'-deoxyuridine-3'-O-(2-cyanoethyl N,N-diisopropylaminophosphoramidite), 9. While under argon **3a** (200 mg, 0.314 mmol) was dissolved in dry dichloromethane (2 mL) containing DIEA (220 μL, 4 eq). The reaction vessel was de-gassed several times prior to the addition of 2-chlorocyanoethyl N,N-diisopropylaminophosphoramidite (105 μL, 1.5 eq) dropwise over 5 minutes. A positive ninhydrin test indicated formation of the desired product. After 50 minutes the reaction was diluted with 200 μL methanol and evaporated to dryness. The residue was applied to silica (eluting with 0-80% dichloromethane in hexane containing 1% TEA) to give an off-white powder **9** in 57% yield (151 mg, 0.180 mmol). ESI-MS mass calculated for $C_{45}H_{52}N_6O_8P$ $[M-H]^-$: 835.37. Found: 835.4.

5'-*O*-(4,4'-dimethoxytrityl)-$N^{2'}$-trifluoroacetamido-2'-deoxyuridine-3'-*O*-(2-cyanoethyl N,N-diisopropylaminophosphoramidite), 10. Compound **10** was prepared using the same method described for **9**, with the following workup procedure. After 90 minutes the reaction was diluted with ethyl acetate which had been previously washed with cold 10% sodium carbonate. The organic layer was extracted twice with cold 10% sodium carbonate and once with brine. The organic fraction was dried over sodium sulfate and evaporated to an oil. The residue was purified on silica (eluting with 0-80% dichloromethane in hexane containing 1% TEA) to yield an off-white powder **10** in 65% yield (88 mg, 0.10 mmol). ESI-MS mass calculated for $C_{41}H_{46}F_3N_5O_9P$ $[M-H^-]$: 840.31. Found: 840.4.

Oligonucleotide Synthesis. Protected deoxyribonucleoside phosphoramidites and other reagents required for solid-phase DNA synthesis were purchased from Applied Biosystems, Incorporated (ABI). All oligonucleotides were synthesized on a 1.0 μmole scale. Solid supports (**7**, **8**) were packed in column assemblies purchased from ABI, and contained approximately 23 mg of derivatized resin, depending on the nucleoside loading. The initial coupling steps in each synthesis were increased from 30 seconds to 2 minutes. The concentration of phosphoramidites (**9**, **10**) typically ranged from 0.1-0.18 M in dry acetonitrile. The coupling time for **9** and **10** was 15 minutes.

Oligonucleotides **11**, **13**, and **14** were synthesized with the terminal dimethoxytrityl (DMT) group retained. Oligonucleotide **12** was prepared with the 5′-DMT group removed prior to cleavage and deprotection. Oligonucleotides **11-13** were cleaved from the solid support with concentrated ammonia during the automated synthesis routine, and deprotected for either 16 hours at 55 °C or 4 hours at 65 °C. Oligonucleotide **14** was cleaved manually in 5 mL of concentrated ammonia for 16 hours at 55 °C. Oligonucleotides **15-18** were prepared by standard trityl-off procedures.

Oligonucleotide Purification. Deprotected oligonucleotides containing a 5′-DMT group were suspended in 20% triethylammonium bicarbonate buffer (1.0 M, pH 8.5) in water and injected onto a reverse phase VYDAC 201HS1022 C18 column. Preparative HPLC was performed with a Waters 600E Controller and 994 Diode Array Detecter, using the following gradient: 0-100% B over 50 minutes, where A = 0.1 M triethylamine acetate, 2% acetonitrile; B = 0.05 M triethylamine acetate, 50% acetonitrile. The collected peaks were dried *in vacuo* and further purified using Waters C18 Classic SepPak cartridges. The amount of purified oligonucleotide was determined

spectrophotometrically, with ε_{260} values given in parentheses: **11** (119,800 M^{-1} cm^{-1}), **12** (115,150 M^{-1} cm^{-1}), **13** (95,900 M^{-1} cm^{-1}), **14** (97,250 M^{-1} cm^{-1}).

Oligonucleotides **11**, **13**, and **14** were detritylated according to the procedure outlined by ABI manual and desalted using SepPak cartridges.[20] The detritylated oligonucleotides were further purified using a weak anion exchange column purchased from SynChroPak (AX-100, analytical, semiprep), using the following gradient: 0-90% B over 35 minutes, where A = 50 mM sodium phosphate (pH 5.9), 30% methanol; B = 50 mM sodium phosphate (pH 5.9), 30% methanol, 1 M ammonium sulfate. The collected peaks were desalted using SepPak cartridges and assayed as described above.

Oligonucleotide Yield. The overall yield of each modified oligonucleotide, following HPLC purification and workup, ranged from 30-40%, based on a 12-μmole synthesis. The detritylated, purified oligonucleotides **11-14** were characterized by MALDI-TOF mass spectrometry (Figures 2.20-2.23): **11**, calculated, 3355 [M], found, 3356.24 $[M-H]^-$; **12**, calculated, 3408 [M], found, 3407.17 $[M-H]^-$; **13**, calculated, 3230 [M], found, 3228.38 $[M-H]^-$; **14**, calculated, 3320 [M], found, 3319.43 $[M-H]^-$.

Enzymatic Digestion of Oligonucleotides and HPLC Analysis. Approximately 10-30 nanomoles of purified oligonucleotide was subjected to enzymatic digestion analysis. The digest cocktail (55 μL/sample) contained bacterial alkaline phosphatase (4 μL, 10 μL/unit) and snake venom phosphodiesterase (2.4 μL, 1 mL/mg), in 1 M $MgCl_2$ (0.8 μL), 0.5 M Tris buffer, pH 7.5 (3.5 μL). The reaction mixture was incubated at 37 °C for 8-16 hours. The reaction was stopped by adding 3 M sodium acetate (7 μL) and ethanol (155 μL) to the samples, which were then frozen on dry ice (10 minutes) and

Figure 2.20: MALDI-TOF mass spectrum of **11** conducted in negative ionization mode.

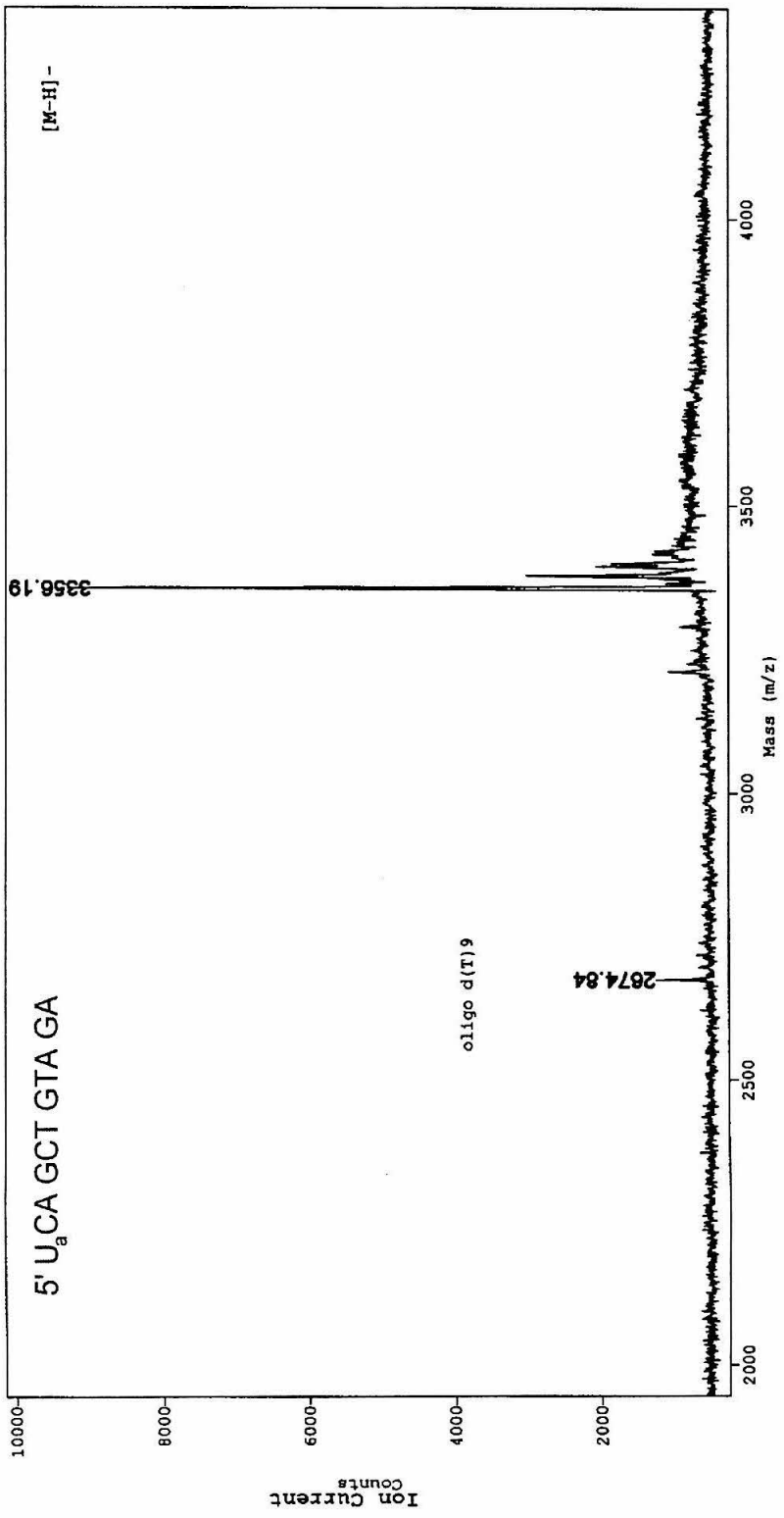
5' U$_a$CA GCT GTA GA
[M-H]-
3356.19
2874.84
oligo d(T)9
Ion Current
Counts
Mass (m/z)
10000
8000
6000
4000
2000
2000
2500
3000
3500
4000

Figure 2.21: MALDI-TOF mass spectrum of **12** conducted in negative ionization mode.

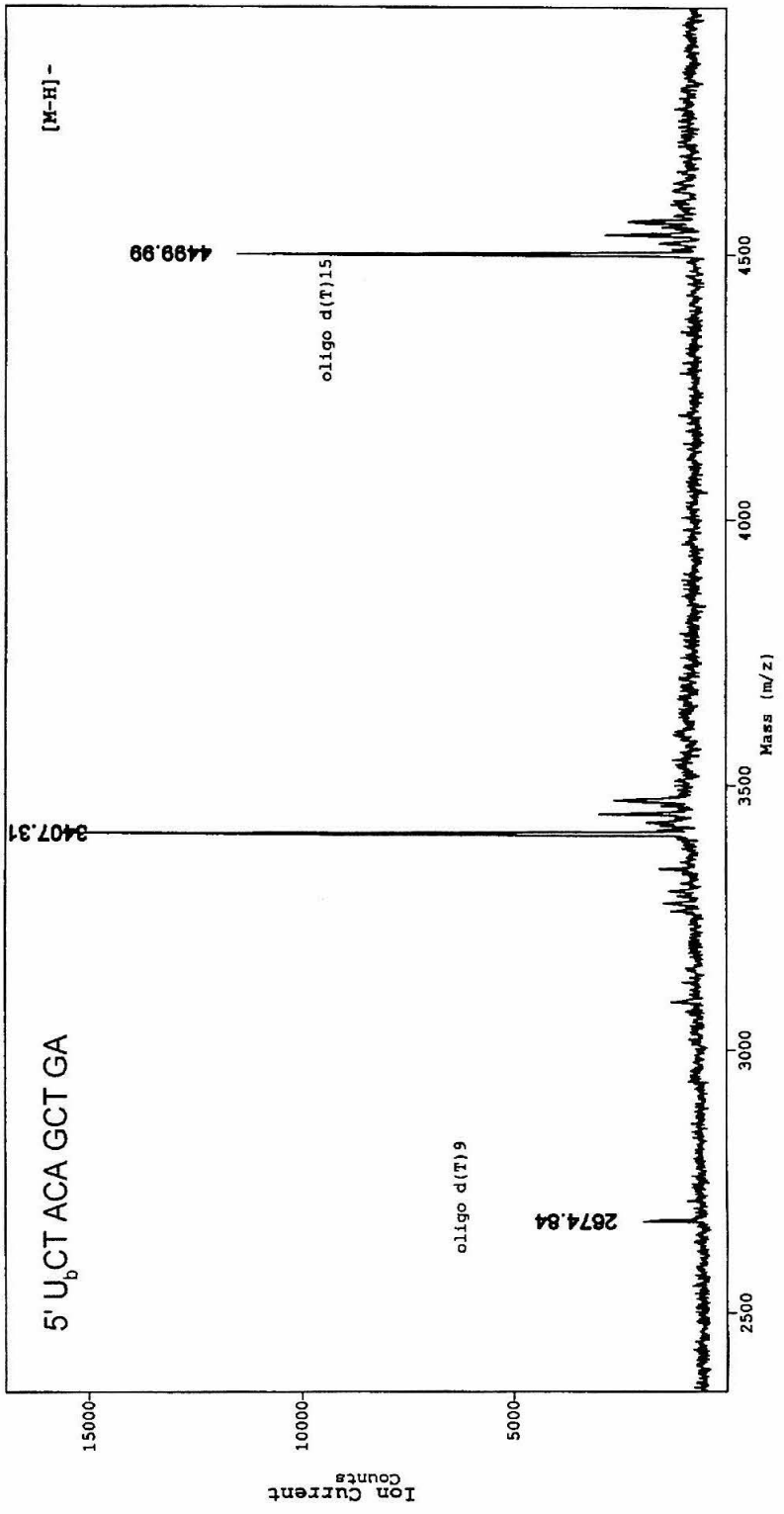
5' U$_b$CT ACA GCT GA
[M-H]-
4499.99
oligo d(T)15
3407.31
oligo d(T)9
2674.84
Ion Current Counts
15000
10000
5000
2500
3000
3500
4000
4500
Mass (m/z)

Figure 2.22: MALDI-TOF mass spectrum of **13** conducted in negative ionization mode.

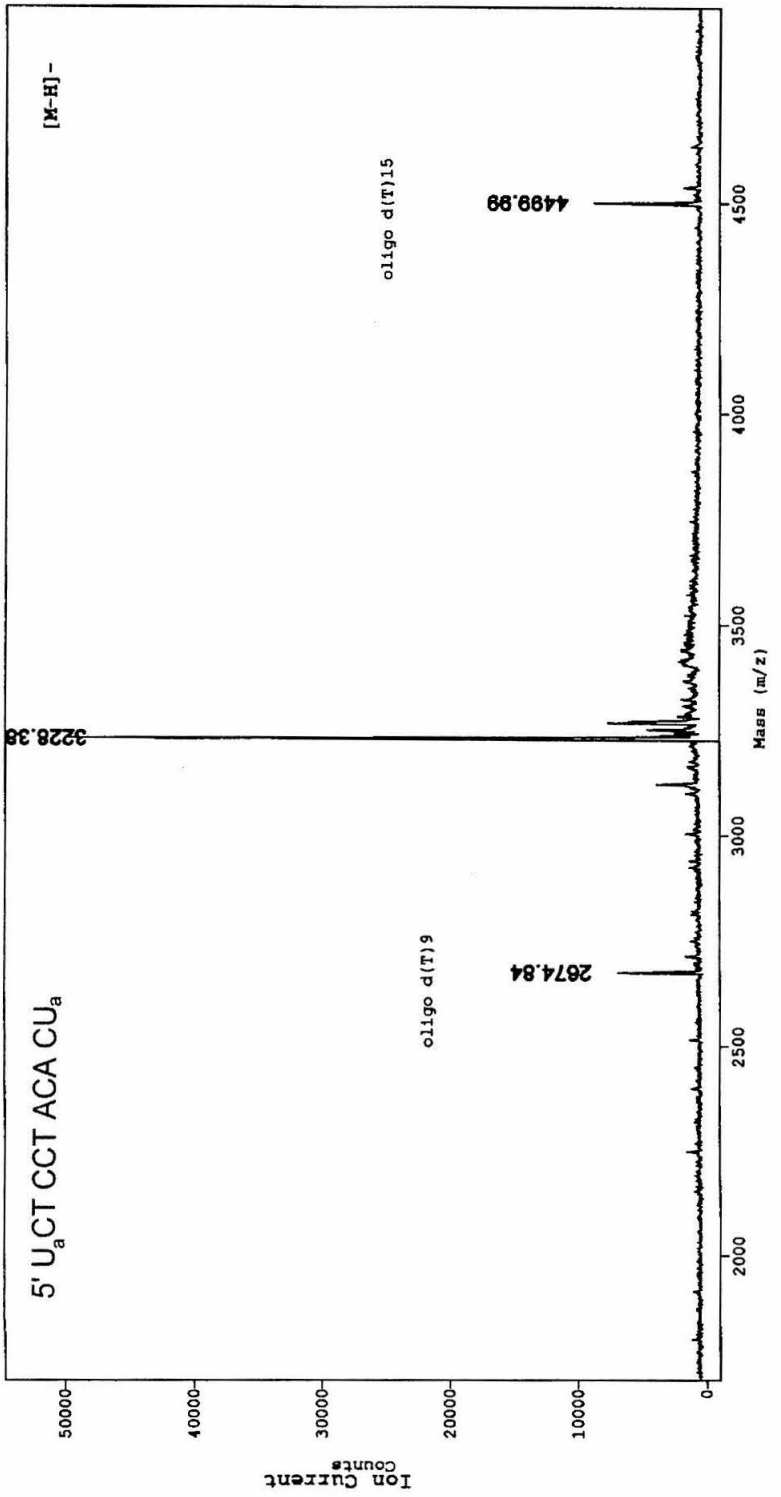
5' U$_a$CT CCT ACA CU$_a$
[M-H]-
3228.38
2674.84
4499.99
oligo d(T)9
oligo d(T)15
Ion Current Counts
Mass (m/z)
0
10000
20000
30000
40000
50000
2000
2500
3000
3500
4000
4500

Figure 2.23: MALDI-TOF mass spectrum of **14** conducted in negative ionization mode.

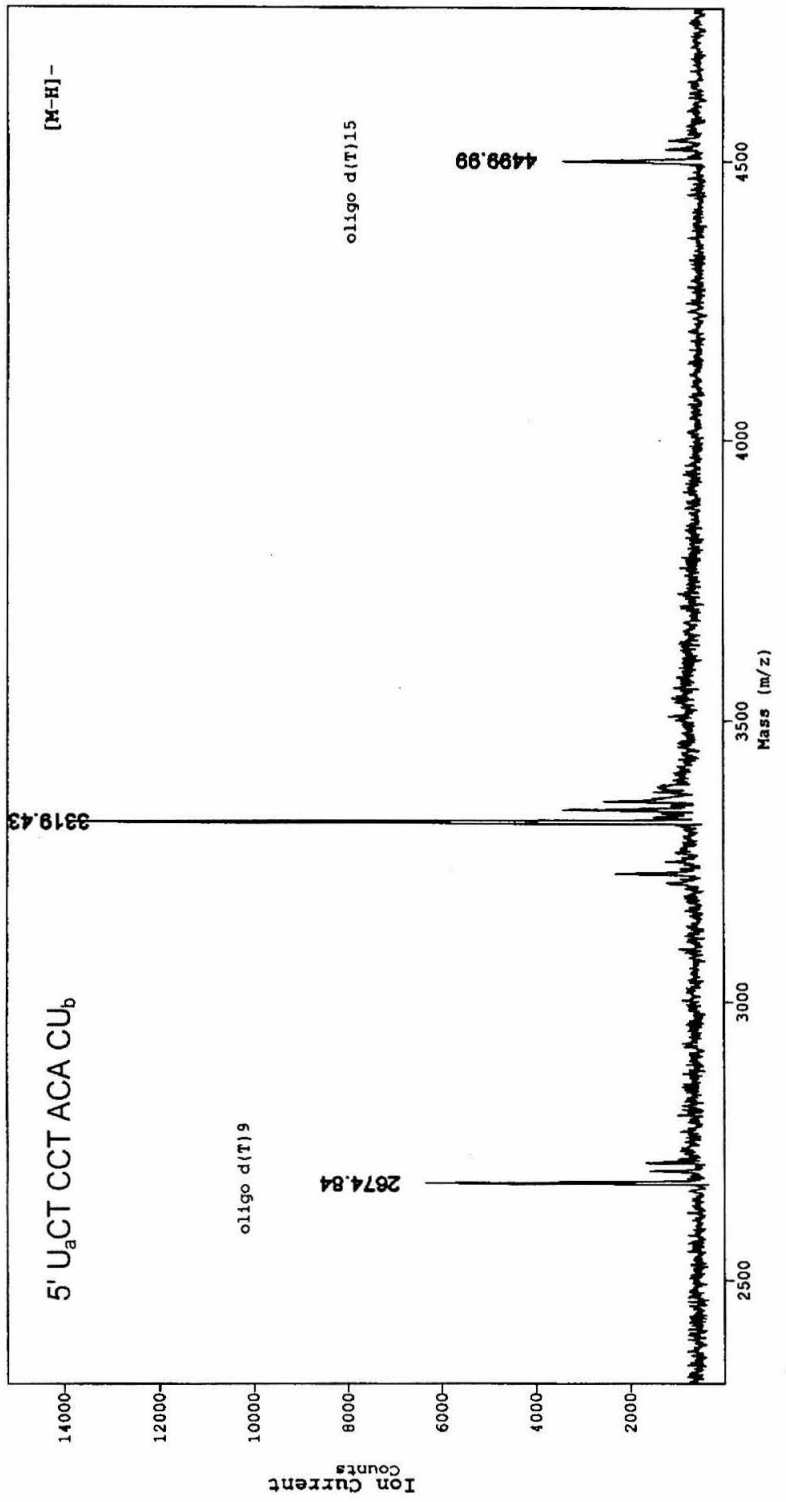
5' U$_a$CT CCT ACA CU$_b$
oligo d(T)9
2874.84
oligo d(T)15
4499.99
3319.43
[M-H]-
Ion Current Counts
Mass (m/z)
14000
12000
10000
8000
6000
4000
2000
2500
3000
3500
4000
4500

centrifuged (10 minutes) at 4 °C. The supernatants were removed and transferred to new tubes, each containing 452 μL ethanol. The samples were frozen and centrifuged; the resulting supernatants were removed and dried *in vacuo*. The samples were dissolved in water (200 μL) and injected onto a reverse phase Vydac (201HS54 4.6 mm x 25 cm, 5 micron, 90 angstrom) or Prism (Keystone Scientific, 4.6 x 250 mm, 5 micron, 100 angstrom) C18 column. The product nucleosides were eluted within twenty minutes, according to either of the following gradients: (Vydac) 0-30% B over twenty minutes then 30-100% B over 10 minutes, where A = 0.1 M triethylamine acetate, 2% acetonitrile, B = 0.05 M triethylamine acetate, 50% acetonitrile; (Prism) 0-17% B over 15 minutes then 17-75% B over 18 minutes, where A = 0.1 M triethylamine acetate, pH 7.0, 2% acetonitrile, B = 100% acetonitrile. The resulting peaks were compared against the appropriate set of nucleoside standards for a given oligonucleotide sequence. In all cases, the observed distribution of nucleosides matched the expected distribution (see Figures 2.5-2.8).

Thermal Denaturation Measurements. Individual oligonucleotides were hybridized to their complementary strands in 50 mM NaP_i buffer (pH 7.0), 0.5 M NaCl, to give solutions that were 2.7 μM in each strand. The samples were heated for 20 minutes at 70 °C and cooled to 4 °C overnight. Thermal denaturation profiles were measured at 260 nm with an Hewlett-Packard diode array UV-vis spectrophotometer equipped with a Peltier temperature controller and interfaced with a personal computer. Samples were equilibrated at 20 °C for 10-20 minutes prior to data collection. Absorbance values were taken over a temperature range of 20-70 °C, with measurements made every 0.5 °C with an equilibration time of 60 seconds for each point. Each hybrid

went through 2-4 separate heat-cool cycles, and the T_m values obtained from these heating and cooling traces were averaged to give the final T_m value. Standard deviations were calculated for each duplex.

Acknowledgment

This work was supported by NIST (ATP) Award 70NANB5H1031, Jet Propulsion Laboratory (JPL 67192), and the Beckman Institute Biological Imaging Center.

References and Notes

(1) Verma, S.; Eckstein, F. *Annu. Rev. Biochem.* **1998**, *67*, 99-134.

(2) Eaton, B. E.; Pieken, W. A. *Annu. Rev. Biochem.* **1995**, *64*, 837-863.

(3) Aurup, H.; Williams, D. M.; Eckstein, F. *Biochem.* **1992**, *31*, 9636-9641.

(4) Tuerk, C.; Gold, L. *Science* **1990**, *249*, 505-510.

(5) Lin, Y.; Qiu, Q.; Gill, S. C.; Jayasena, S. D. *Nucleic Acids Res.* **1994**, *22*, 5229-5234.

(6) Aurup, H.; Tuschi, T.; Benseler, F.; Ludwig, J.; Eckstein, F. *Nucleic Acids Res.* **1994**, *22*, 20-24.

(7) Sigurdsson, S. T.; Eckstein, F. *Nucleic Acids Res.* **1996**, *24*, 3129-3133.

(8) Kuznetsova, K. G.; Romanova, E. A.; Volkov, E. M.; Tashlitsky, V. N.; Oretskaya, T. S.; Krynetskaya, N. F.; Shabarova, Z. A. *J. Bioorg. Chem. (Moscow)* **1993**, *19*, 455-466.

(9) Sigurdsson, S. T.; Tuschl, T.; Eckstein, F. *RNA-Publ. RNA Soc.* **1995**, *1*, 575-583.

(10) Meade, T. J.; Kayyem, J. F. *Angew. Chem. Int. Ed. Engl.* **1995**, *34*, 352-353.

(11) Rack, J. J.; Krider, E. S.; Meade, T. J. *J. Am. Chem. Soc.* **2000**, *122*, 6287-6288.

(12) Abbreviations: AMPy, aminomethylpyridine; AEPy, aminoethylpyridine; BOP, benzotriazol-1-yloxytris(dimethylamino)phosphonium hexafluorophosphate; DBU, 1,8-Diazabicyclo[5.4.0]undec-7-ene (1,5-5); DCC, dicyclohexylcarbodiimide; DIEA, diisopropylethanolamine; DMAP, dimethylaminopyridine; DMT, 4,4′-dimethoxytrityl; EtOAC, ethyl acetate; HOBT, hydroxybenzotriazole; TEA, triethylamine; THF, tetrahydrofuran.

(13) Sebesta, D. P.; O'Rourke, S. S.; Martinez, R. L.; Pieken, W. A.; McGee, D. P. C. *Tetrahedron* **1996**, *52*, 14385-14402.

(14) McGee, D. P. C.; Sebesta, D. P.; O'Rourke, S. S.; Martinez, R. L.; Jung, M. E.; Pieken, W. A. *Tet. Lett.* **1996**, *37*, 1995-1998.

(15) McGee, D.; Vaughn-Settle, A.; Vargeese, C.; Zhai, Y. *J. Org. Chem.* **1996**, *61*, 781-785.

(16) Pieken, W. A.; Olsen, D. B.; Benseler, F.; Aurup, H.; Eckstein, F. *Science* **1991**, *253*, 314-317.

(17) *Oligonucleotide Synthesis: A Practical Approach*; Gait, M., Ed.; Oxford Univ. Press: Oxford, 1984.

(18) Caruthers, M. H.; Barone, A. D.; Beaucage, S. L.; Dodds, D. R.; Fisher, E. F.; McBride, L. J.; Matteucci, M.; Stabinsky, Z.; Tang, J.-Y. In *Methods in*

Enzymology: Recombinant DNA; Grossman, R. W. a. L., Ed.; Academic Press, Inc.:, 1987; Vol. 154.

(19) Knorr, R.; Trzeciak, A.; Bannwarth, W.; Gillessen, D. *Tet. Lett.* **1989**, *30*, 1927-1930.

(20) "Evaluating and Isolating Synthetic Oligonucleotides: The Complete Guide," Applied Biosystems, 1992.

(21) Brown, G. M.; Weaver, T. R.; Keene, F. R.; Meyer, T. J. *Inorg. Chem.* **1976**, *15*, 190-196.

(22) Juris, A.; Balzani, V.; Barigelletti, F.; Campagna, S.; Belser, P.; Vonzelewsky, A. *Coord. Chem. Rev.* **1988**, *84*, 85-277.

(23) Hurley, D. J.; Tor, Y. *J. Am. Chem. Soc.* **1998**, *120*, 2194-2195.

(24) Fu, P. K. L.; Turro, C. *J. Am. Chem. Soc.* **1999**, *121*, 1-7.

(25) Bannwarth, W.; Pfleiderer, W.; Muller, F. *Helv. Chim. Acta* **1991**, *74*, 1991-1999.

(26) Bannwarth, W.; Muller, F. *Helv. Chim. Acta* **1991**, *74*, 2000-2008.

(27) Tierney, M. T.; Sykora, M.; Khan, S. I.; Grinstaff, M. W. *J. Phys. Chem. B* **2000**, *104*, 7574-7576.

(28) Holmlin, R. E.; Dandliker, P. J.; Barton, J. K. *Angew. Chem. Int. Ed.* **1997**, *36*, 2715-2730.

(29) Arkin, M. A.; Stemp, E. D.; Holmlin, R. E.; Barton, J. K.; Hormann, A.; Olson, E. J.; Barbara, P. F. *Science* **1996**, *273*, 475.

(30) Bannwarth, W. *Anal. Biochem.* **1989**, *181*, 216-219.

(31) Goodchild, J. *Bioconj. Chem.* **1990**, *1*, 165-191.

(32) Ueno, Y.; Mikawa, M.; Matsuda, A. *Bioconj. Chem.* **1998**, *9*, 33-39.

(33) Haralambidis, J.; Duncan, L.; Angus, K.; Tregear, G. W. *Nucleic Acids Res.* **1990**, *18*, 493-499.

(34) Asseline, U.; Thuong, N. T. *Tet. Lett.* **1990**, *31*, 81-84.

(35) Reed, M. W.; Adams, A. D.; Nelson, J. S.; Meyer, R. B. *Bioconj. Chem.* **1991**, *2*, 217-225.

(36) Petrie, C. R.; Reed, M. W.; Adams, A. D.; Meyer, R. B. *Bioconj. Chem.* **1992**, *3*, 85-87.

(37) Thaden, J.; Miller, P. S. *Bioconj. Chem.* **1993**, *4*, 395-401.

(38) Nelson, P. S.; Frye, R. A.; Liu, E. *Nucleic Acids Res.* **1989**, *17*, 7187-7194.

(39) Nelson, P. S.; Kent, M.; Muthini, S. *Nucleic Acids Res.* **1992**, *20*, 6253-6259.

(40) Hovinen, J.; Guzaev, A.; Azhayeva, E.; Azhayev, A.; Lonnberg, H. *J. Org. Chem.* **1995**, *60*, 2205-2209.

(41) Mullah, B.; Andrus, A. *Tet. Lett.* **1997**, *38*, 5751-5754.

(42) Mullah, B.; Livak, K.; Andrus, A.; Kenney, P. *Nucleic Acids Res.* **1998**, *26*, 1026-1031.

(43) McMinn, D. L.; Matray, T. J.; Greenberg, M. M. *J. Org. Chem.* **1997**, *62*, 7074-7075.

(44) McMinn, D. L.; Greenberg, M. M. *J. Am. Chem. Soc.* **1998**, *120*, 3289-3294.

(45) Kahl, J. D.; Greenberg, M. M. *J. Org. Chem.* **1999**, *64*, 507-510.

(46) Benseler, F.; Williams, D.; Eckstein, F. *Nucleosides and Nucleotides* **1992**, *11*, 1333-1351.

Chapter 3

Post-Synthetic Modification of Oligonucleotides with Ruthenium(II) Reagents

Introduction

A general method for preparing oligonucleotides containing redox-active complexes was recently reported.[1] This method employed oligonucleotides that contained 2′-amino-2′-deoxyuridine nucleosides at the 5′ termini (Figure 3.1). These modified oligonucleotides were hybridized to complementary strands and subsequently treated with ruthenium(II) complexes. The extent of labeling at sites other than the 2′ position of the terminal ribose was minimized by the presence of the complementary strand, which served as a large hydrogen-bonded blocking group. This strategy to protect reactive sites on the bases from metallation was an important advance in the preparation of metal-containing oligonucleotides.

This post-synthetic modification method was employed to synthesize a series of ruthenium-modified oligonucleotides. The objective of this work was to prepare oligonucleotides containing the desired metal complex at a single, pre-determined location. Several oligonucleotides containing 2′-modified nucleosides were prepared as described in Chapter 2. The 2′-modified nucleosides and their positions in the target oligonucleotides are shown in Figure 3.2. Several unmodified oligonucleotides containing a single guanine base were also prepared for metallation reactions.

The following ruthenium(II) reagents were used: $[Ru(bpy)_2(CO_3]$, $[Ru(NH_3)_5(OH_2)]^{2+}$, and $[Ru(acac)_2(CH_3CN)_2]$, where bpy = 2,2′-bipyridine, acac = acetylacetonate. The first two reagents have been used extensively in the modification of redox-active proteins at reactive histidine sites.[2-7] The third reagent has not been used to label biological structures; however, the substitution chemistry of $[Ru(acac)_2(CH_3CN)_2]$ has been described in several reports.[8-10] These metal complexes were selected based on

Figure 3.1: Reaction scheme for preparing metal-containing oligonucleotides as described in Reference 1.

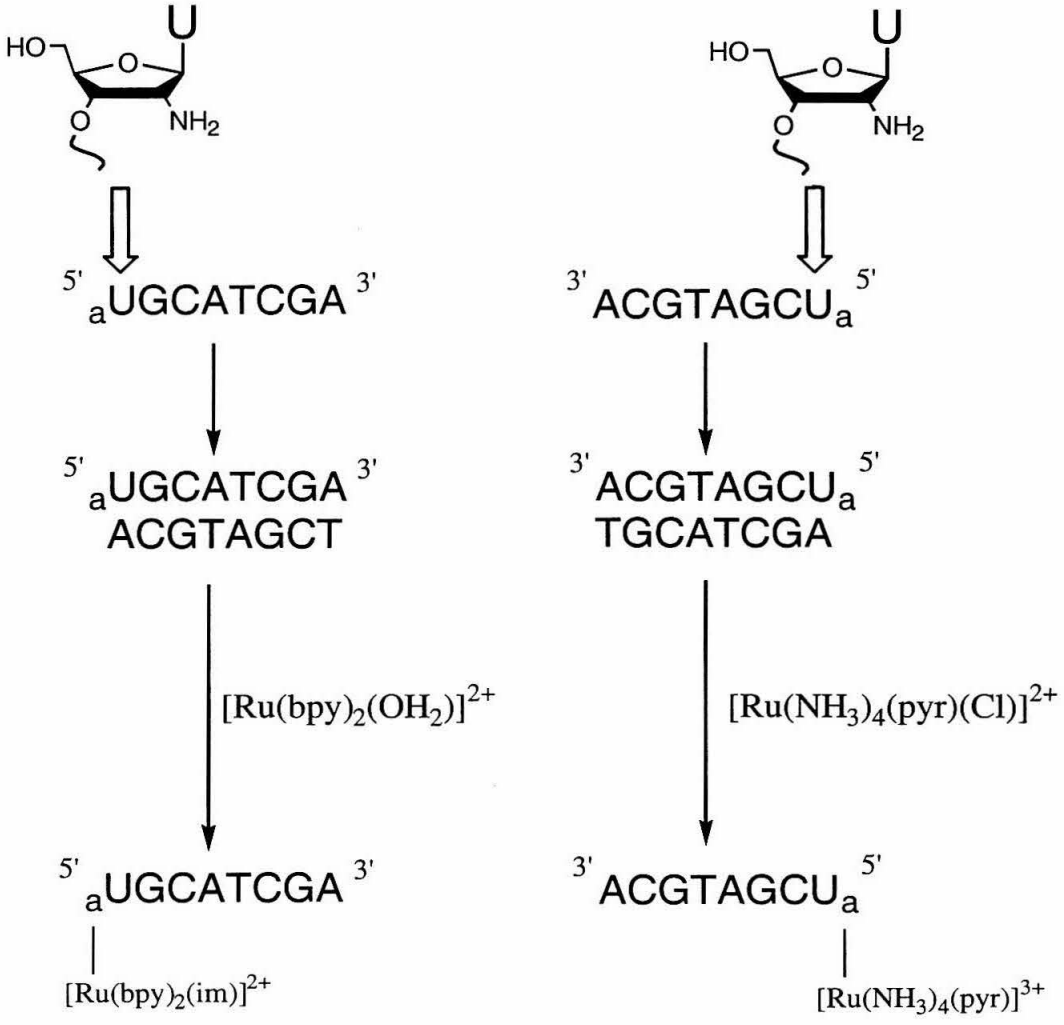
HO
U
O
O
NH2
5' aUGCATCGA 3'
5' aUGCATCGA 3'
ACGTAGCT
[Ru(bpy)2(OH2)]2+
5' aUGCATCGA 3'
[Ru(bpy)2(im)]2+
HO
U
O
O
NH2
3' ACGTAGCUa 5'
3' ACGTAGCUa 5'
TGCATCGA
[Ru(NH3)4(pyr)(Cl)]2+
3' ACGTAGCUa 5'
[Ru(NH3)4(pyr)]3+

Figure 3.2: Structures of 2′-modified nucleosides and their positions in 11-mer oligonucleotides.

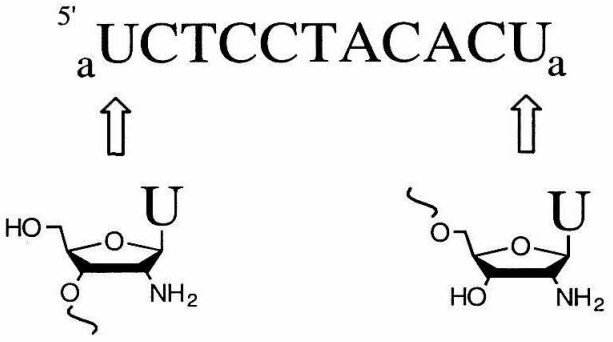
5'
aUCTCCTACACUa
HO
O
U
O
NH2
HO
O
U
O
NH2

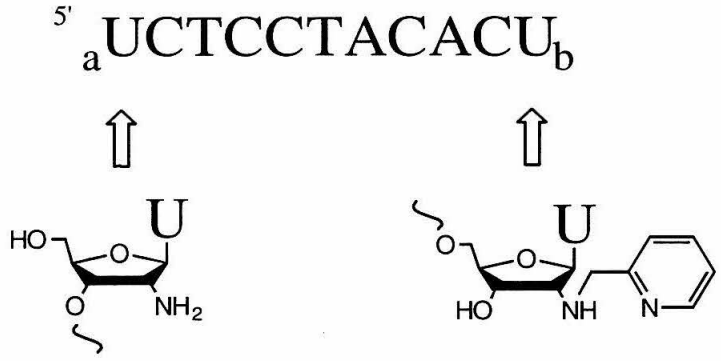
5'
aUCTCCTACACUb
HO
O
U
O
NH2
HO
O
U
O
NH
N

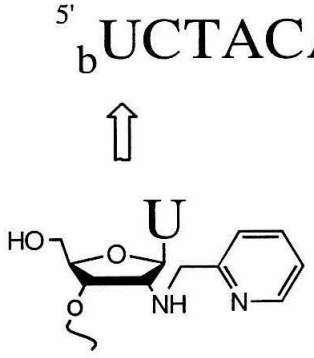
5'
bUCTACAGCTGA
HO
O
U
O
NH
N

the absorption and electrochemical features displayed by the anticipated products after metallation (Table 3.1).[11-14] The metal-containing oligonucleotides were expected to have features similar to the model complexes shown in Figure 3.3.

The remainder of Chapter 3 contains three sections summarizing results from metallation reactions involving $[Ru(bpy)_2CO_3]$, $[Ru(NH_3)_5(OH_2)]^{2+}$, and $[Ru(acac)_2(CH_3CN)_2]$. For each section, the target oligonucleotides are given in figures and the reaction procedures are described schematically. Several parameters (reaction duration, temperature, pH) were investigated in the course of the metallation studies. The conditions leading to substantial metallation are summarized in the Experimental Procedure. Sample HPLC traces showing the distribution of products are given for each metal reagent. HPLC columns and buffers are summarized in Appendix E.

Results: *Metallation Reactions with $[Ru(bpy)_2CO_3]$*

The target 11-mer oligonucleotides contained 2′-amino-2′-deoxyuridine nucleosides at either 5′ or 3′ termini or both (Figure 3.4). Typically, the oligonucleotide was hybridized to its complementary strand in buffer containing 0.5 M sodium chloride. The duplex solution was deaerated under argon and the metal reagent was added (Figure 3.5). The reaction proceeded at room temperature or slightly elevated temperatures.

Several reaction conditions were explored to maximize the yield of oligonucleotide metallation (Table 3.2). The reactions were monitored by analytical HPLC to determine optimal reaction conditions. Substantial metallation (~60%) was observed under the following conditions: 0.2 mM DNA, 2.0 mM $[Ru(bpy)_2CO_3]$, 50 mM

Table 3.1. Electrochemical and Absorption Data for Model Complexes.

Complex	$E_{1/2}$, V[a] vs. NHE	λ_{max}, nm[a] ($\varepsilon \times 10^{-3}$, M^{-1} cm^{-1})	Refs.
$[Ru(bpy)_2(im)(NH_2R)]^{2+}$	1.26[b]	480[b]	11
$[Ru(NH_3)_5(pyr)]^{2+}$	0.35	407 (7.7)	12
$[Ru(NH_3)_4(ampy)]^{2+}$	0.30	414 (6.3)	12
$[Ru(NH_3)_4(impy)]^{2+}$	0.56	520 (6.1) 378 (4.4)	12
$[Ru(acac)_2(impy)]$	0.23[c]	576 (4.6) 402 (4.6)	13
$[Ru(NH_3)_5(N^7(G))]^{2+}$	0.15	565 (0.44)	14

[a] Ru(III)/Ru(II) potentials measured in aqueous solution (unless otherwise noted).
[b] CH_3CN
[c] EtOH

Figure 3.3: Structures of nucleoside model complexes.

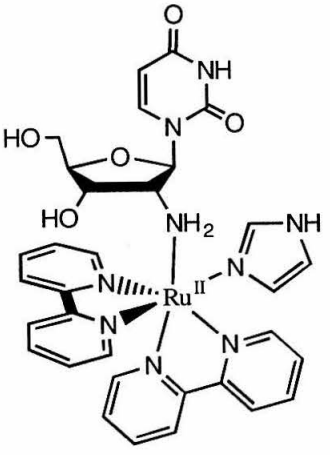

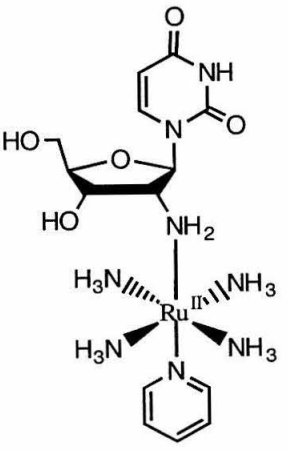

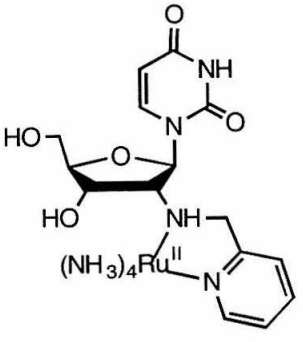

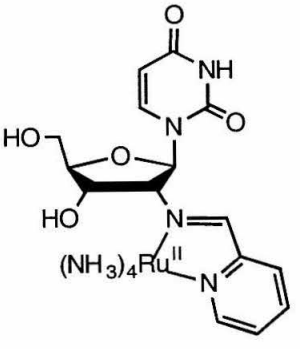

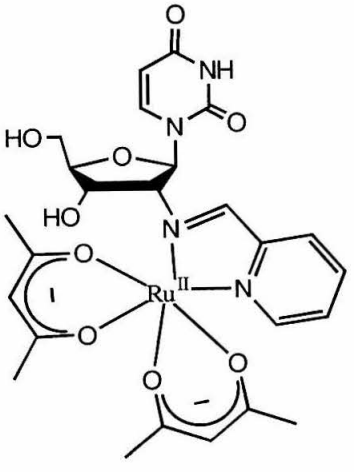

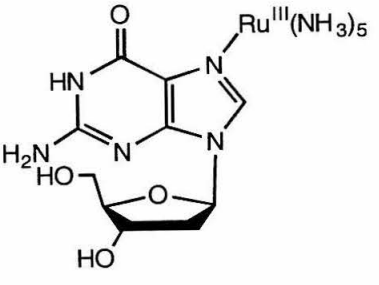

Figure 3.4: Oligonucleotide sequences used in metallation reactions with $[Ru(bpy)_2CO_3]$.

Oligonucleotide	*Abbreviation*
$^{5'}{}_{a}$UCTCCTACACU$_{a}$	$_{a}$**UU**$_{a}$
$^{5'}{}_{a}$UCTCCTACACT	$_{a}$**UT**
$^{5'}$TCTCCTACACU$_{a}$	**TU**$_{a}$

Figure 3.5: Reaction scheme for metallation of duplexed $_{a}\mathbf{UU}_{a}$ with $[Ru(bpy)_2CO_3]$.

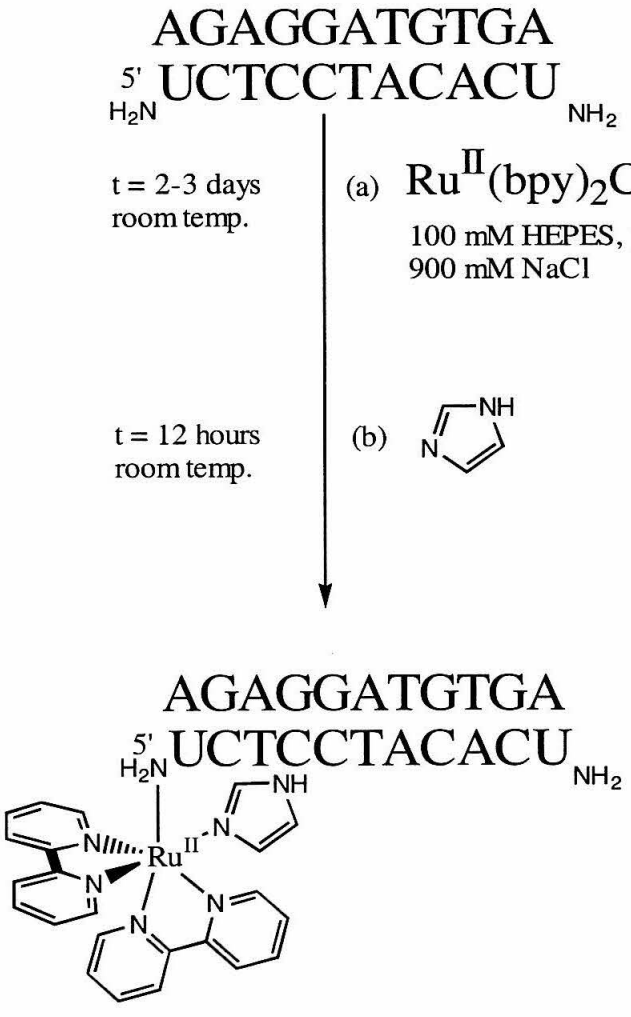
AGAGGATGTGA
5'
H2N
UCTCCTACACU
NH2
t = 2-3 days
room temp.
(a) Ru^II(bpy)2CO3
100 mM HEPES, pH 8.5
900 mM NaCl
t = 12 hours
room temp.
(b)
NH
N
AGAGGATGTGA
5'
H2N
UCTCCTACACU
NH2
NH
N
N
Ru^II
N
N
N

Table 3.2. Summary of Conditions for Metallations with $[Ru(bpy)_2(CO_3]$.

rxn #	sample	workup procedure	yield
	$^{5'}{}_{a}$UCTCCTACACU$_a$ AGAGGATGTGA	C18 RP HPLC	low
	$^{5'\,DMT}{}_{a}$UCTCCTACACU$_a$ AGAGGATGTGA	C18 RP HPLC	low
	$^{5'\,DMT}{}_{a}$UCTCCTACACU$_a$	gel filtration; C18 RP HPLC	low
	$^{5'}{}_{a}$UCTCCTACACU$_a$	SepPak; ion exchange HPLC	moderate
	$^{5'}{}_{a}$UCTCCTACACT	SepPak; ion exchange HPLC	moderate
	$^{5'}$TCTCCTACACU$_a$	SepPak; ion exchange HPLC	moderate

HEPES (pH 8.5), 35 °C, 48 hours. A sample HPLC trace is shown in Figure 3.6. The yield after HPLC purification was <10%.

Reactions with oligonucleotides containing a single 2′-amino-2′-deoxyuridine nucleoside at either the 5′ or 3′ end ($_a$**UT**, **TU**$_a$) highlighted the need for a complementary strand serving as a large blocking group. Experiments involving separate reactions of $_a$**UT** and **TU**$_a$ with [$Ru(bpy)_2CO_3$] showed the formation of a multi-ruthenated oligonucleotide. HPLC and mass spectrometry indicated the presence of two ruthenium complexes attached to each oligonucleotide. A sample HPLC trace of the $_a$**UT** metallation reaction is shown in Figure 3.7.

Efforts to isolate the desired metal-containing oligonucleotide were hindered by the large amounts of unreacted metal reagent in the reaction mixture. Attempts to remove the excess metal included: (a) HPLC purification, (b) gel filtration, (c) dialysis, and (d) SepPak C18 elution. The most effective means of eliminating excess metal reagent was achieved by the last method.

Further isolation of the metal-containing oligonucleotides employed both reverse-phase and ion-exchange HPLC methods. Two reverse-phase columns were used: C18 201HS54 (Vydac) and OligoR3 C18 (Perseptive Biosystems). Since the complementary strand was present in some of the reaction samples, it was necessary to separate it from the modified oligonucleotide. This was achieved by pre-heating the sample prior to injection into the HPLC system and by heating the column to 60 °C during the course of the chromatography. Heating the column proved effective for separating the two complementary strands when C18 RP columns were used. However, purification of the reaction mixture with C18 RP columns produced very small amounts of product.

Figure 3.6: HPLC trace of metallation reaction involving $_{a}\mathbf{UU}_{a}$ and $[Ru(bpy)_2CO_3]$. Column: AX-100 weak anion exchange. Gradient: 0-90% B over 35 minutes. Buffer A: 50 mM sodium phosphate (pH 5.9), 30% methanol. Buffer B: 50 mM sodium phosphate (pH 5.9), 30% methanol, 1 M ammonium sulfate. Wavelength monitored: 260 nm. Absorption spectra for the peaks are given in the upper part of the figure.

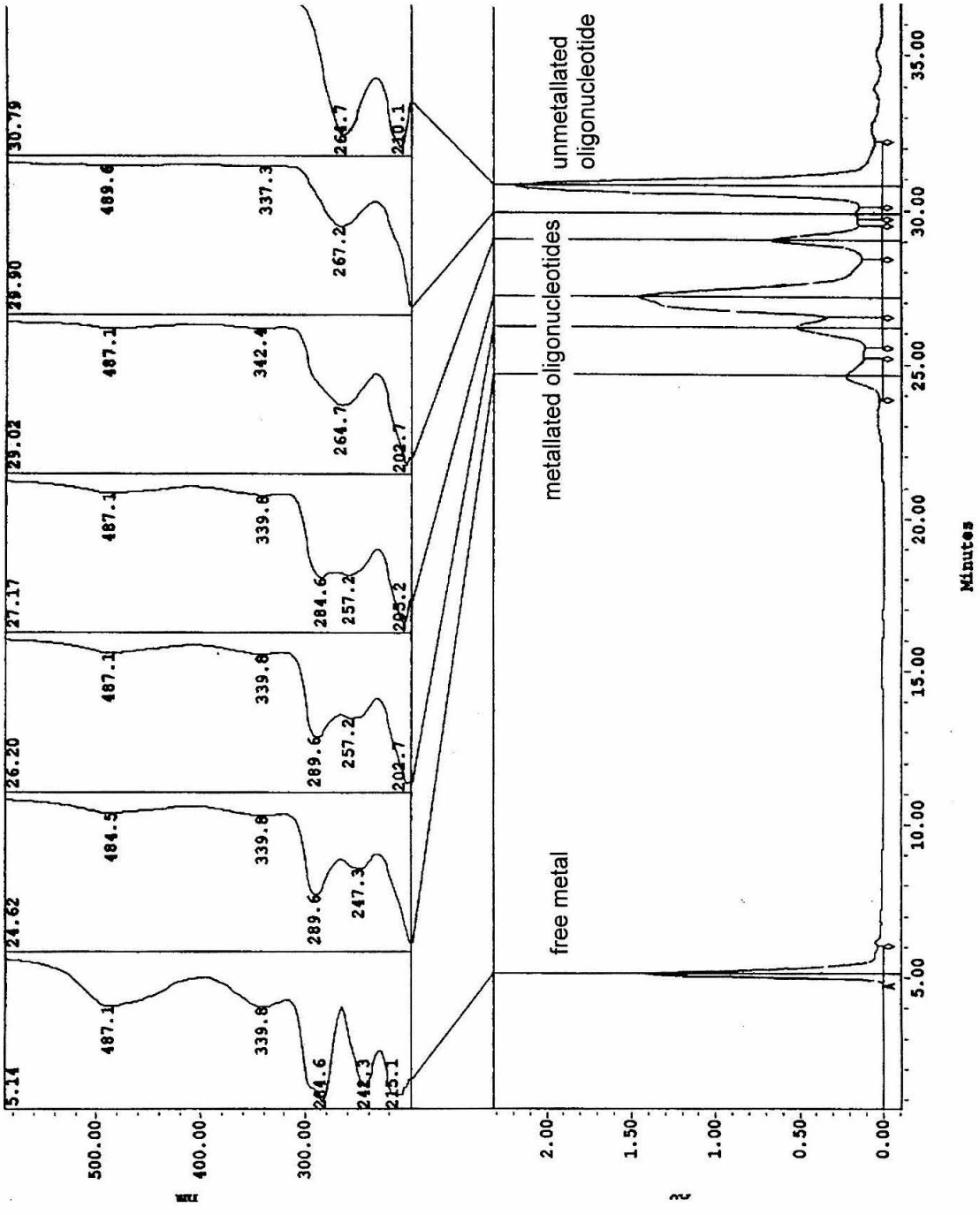
free metal
metallated oligonucleotides
unmetallated
oligonucleotide
Minutes

Figure 3.7: HPLC trace of metallation reaction involving $_{a}$**UT** and [$Ru(bpy)_2CO_3$]. Column: AX-100 weak anion exchange. Gradient: 0-90% B over 35 minutes. Buffer A: 50 mM sodium phosphate (pH 5.9), 30% methanol. Buffer B: 50 mM sodium phosphate (pH 5.9), 30% methanol, 1 M ammonium sulfate. Wavelength monitored: 260 nm. Absorption spectra for the peaks are given in the upper part of the figure.

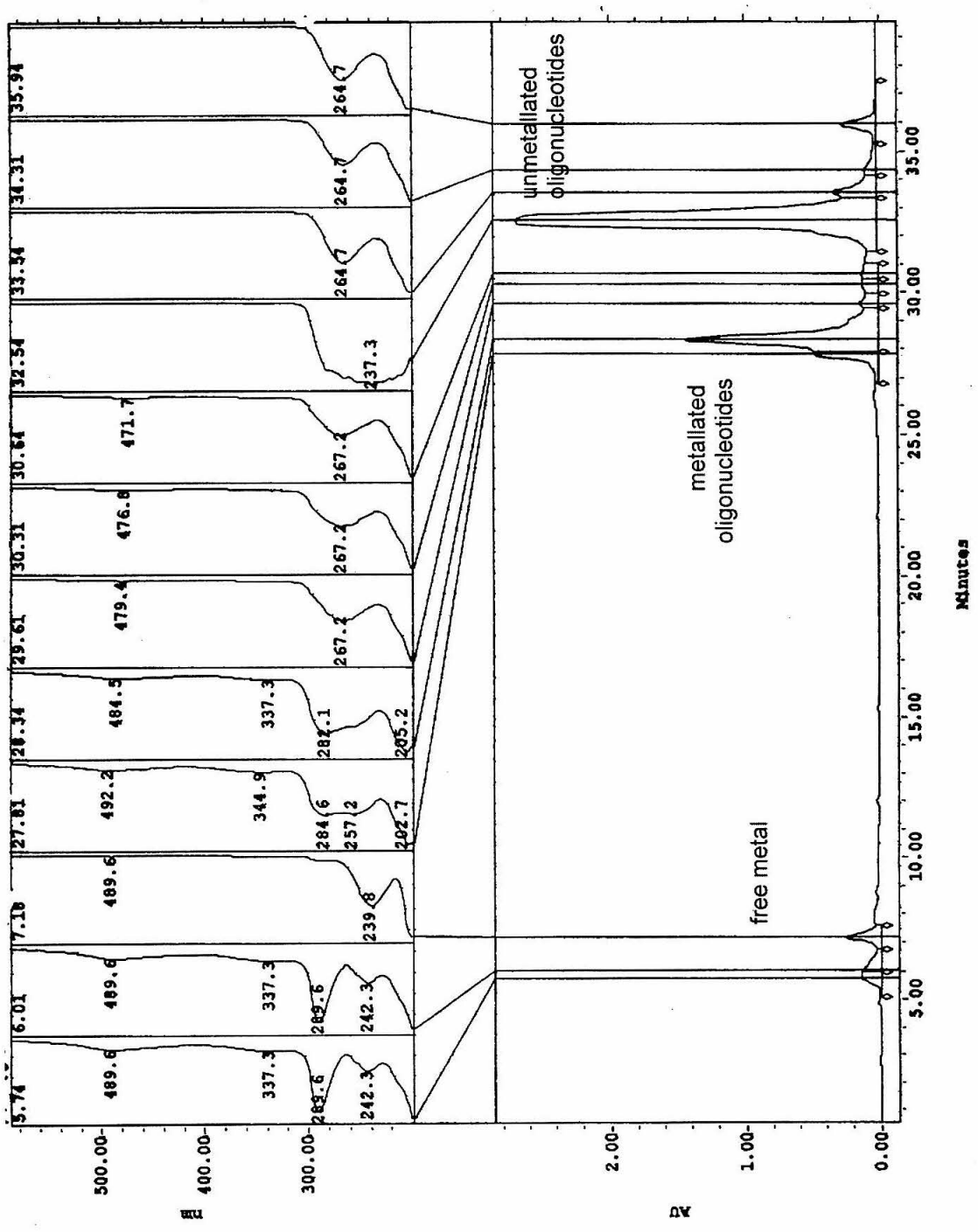
unmetallated
oligonucleotides
metallated
oligonucleotides
free metal
Minutes
nm
AU
5.00
10.00
15.00
20.00
25.00
30.00
35.00
0.00
1.00
2.00
300.00
400.00
500.00

Ion-exchange HPLC columns were more effective than C18 RP columns for separating the metallated oligonucleotides from the unmetallated strands. Three weak-anion exchange columns were used: AX-100 (SynchroPak), MonoQ (Pharmacia), and NucleoPac PA-100 (Dionex). Initially, the AX-100 column provided product separation that was far better than any results obtained with C18 columns. Further purification of metallation reactions was achieved with several solvent systems using the Dionex column.

Experimental Procedure. For all metallation reactions involving duplex DNA, the individual oligonucleotides were quantitated and combined in the desired ratio (target strand:complementary strand). The solution of DNA contained either 100 mM Tris (pH 7.2) or 100 mM HEPES (pH 8.5), plus 900 mM NaCl. Hybridization of the complementary strands involved heating the solution at 70-80 °C for 20 minutes and gradually cooling it to 4 °C over 6 hours in the cold room. The sample was deaerated under argon and equilibrated to the reaction temperature prior to the addition of the metal reagent.

Metallation with $[Ru(bpy)_2CO_3]\bullet 4H_2O$ of duplexes $_a\mathbf{UU}_a$ typically involved a final solution of 0.2 mM DNA and 2.0 mM Ru^{II}. The metal complex was added dropwise under argon to the reaction vessel over thirty minutes. The reaction proceeded for approximately 48 hours at 35 °C, with aliquots removed periodically and reacted with 10-fold excess of imidazole for 12 hours. The reaction's progress was monitored by RP HPLC performed at 60 °C to prevent any duplex formation. Unreacted metal complex was removed using a C18 SepPak cartridge (0.35g). The resulting metal-DNA fractions were injected on a Synchropak AX100 weak anion exchange column using the following

gradient: 0-90% B over 35 minutes, where A = 50 mM sodium phosphate (pH 5.9), 30% methanol; B = 50 mM sodium phosphate (pH 5.9), 30% methanol, 1 M ammonium sulfate. The collected fractions were dried down and desalted using a C18 SepPak cartridge. The amount of ruthenated $_{a}\mathbf{UU}_{a}$ was determined spectrophotometrically (20-100 nmol). An analytical sample of ruthenated $_{a}\mathbf{UU}_{a}$ analyzed by electrospray mass spectrometry indicated the presence of two $[Ru^{II}(bpy)_2(im)]$ fragments covalently attached to $_{a}\mathbf{UU}_{a}$.

Metallation reactions involving unduplexed $_{a}\mathbf{UU}_{a}$ were conducted in 50 mM HEPES (pH 8.5) at 35 °C at the DNA/Ru concentrations given above. An analytical sample of ruthenated $_{a}\mathbf{UU}_{a}$ analyzed by MALDI-TOF mass spectrometry indicated the presence of two $[Ru^{II}(bpy)_2(im)]$ fragments covalently attached to $_{a}\mathbf{UU}_{a}$: 3641, [M-imidazole]$^-$ and 4193, [M-(imidazole)$_2$ + matrix]$^-$.

Separate metallation reactions of $_{a}\mathbf{UT}$ and $\mathbf{TU}_{a}$ (each unduplexed) followed the same procedure described above for unduplexed target strands, with the following modifications: 10 eq. of $[Ru(bpy)_2CO_3]$, 100 nmol of oligonucleotide, 2-day reaction time, T = 40 °C; 12 eq. of imidazole, 2-day reaction time; workup by SepPak; AX-100 HPLC purification. The samples were preheated for 10 minutes at 60 °C prior to injection. The column was heated to 60 °C during the chromatography. An analytical sample of ruthenated $_{a}\mathbf{UT}$ analyzed by MALDI-TOF mass spectrometry indicated the presence of two $[Ru^{II}(bpy)_2(im)]$ fragments covalently attached to $_{a}\mathbf{UT}$: 3640, [M-imidazole]$^-$, and 4194 [M-(imidazole)$_2$ + matrix]$^-$. Likewise an analytical sample of ruthenated $\mathbf{TU}_{a}$ indicated two $[Ru^{II}(bpy)_2(im)]$ fragments covalently attached to the oligo: 3640, [M-imidazole]$^-$, and 4195 [M-(imidazole)$_2$ + matrix]$^-$.

Results: *Metallation Reactions with* $[Ru(NH_3)_5(OH_2)]^{2+}$

Modified Oligonucleotides. The oligonucleotides targeted for metallation by $[Ru(NH_3)_5(OH_2)]^{2+}$ are shown in Figure 3.8. They consist of 11-mer strands containing 2′-modified nucleosides, as well as oligonucleotides that contain a single guanine overhang at the 5′ terminus when hybridized to its complement. All reactions with $[Ru(NH_3)_5(OH_2)]^{2+}$ contained the target oligonucleotides hybridized to complementary strands to minimize ruthenium labeling at multiple sites. Overall, this blocking method was ineffective and the ruthenium reagent was incorporated at several locations on the target oligonucleotides.

Metallation reactions with $[Ru(NH_3)_5(OH_2)]^{2+}$ of samples containing duplexed $_aUU_b$ and **11B** took place at neutral pH, lasting for 3-16 hours at room temperature under an argon atmosphere (Figure 3.9). During this time, the solution changed from yellow to orange-brown. Exposure to air caused the solution to become a dark purple. Subsequent workup and HPLC purification produced an oligonucleotide pellet that was purple. A solution of the sample displayed broad absorption bands at 330 and 545 nm (Figure 3.10). Mass spectral analysis of this material gave results suggestive of an oligonucleotide modified with one or more Ru-ammine complexes (data not shown). However, the precise identity of the metal-containing oligonucleotide was not clear.

Model Complexes. Model reactions were conducted with *N*-(isopropyl)-aminomethylpyridine and $[Ru(NH_3)_5(OH_2)]^{2+}$ under conditions similar to the oligonucleotide metallation (Figure 3.11). The reaction was monitored by absorption spectroscopy; an aliquot from the reaction taken after 12 hours of stirring at room temperature displayed absorption bands at 206, 254, and 402 nm (Figure 3.12). (The

Figure 3.8: Oligonucleotides used in metallation reactions with $[Ru(NH_3)_5(OH_2)]^{2+}$.

Oligonucleotide	*Abbreviation*
$^{5'}{}_{a}$UCTCCTACACU$_{b}$	**$_{a}$UU$_{b}$**
$^{5'}{}_{b}$UCTACAGCTGA	**11B**
$^{5'}$ GTCTACAGCTGA	**12G**
$^{5'}$ GTCTACAGC	**9G**

Figure 3.9: Reaction scheme for metallation reactions with $[Ru(NH_3)_5(OH_2)]^{2+}$.

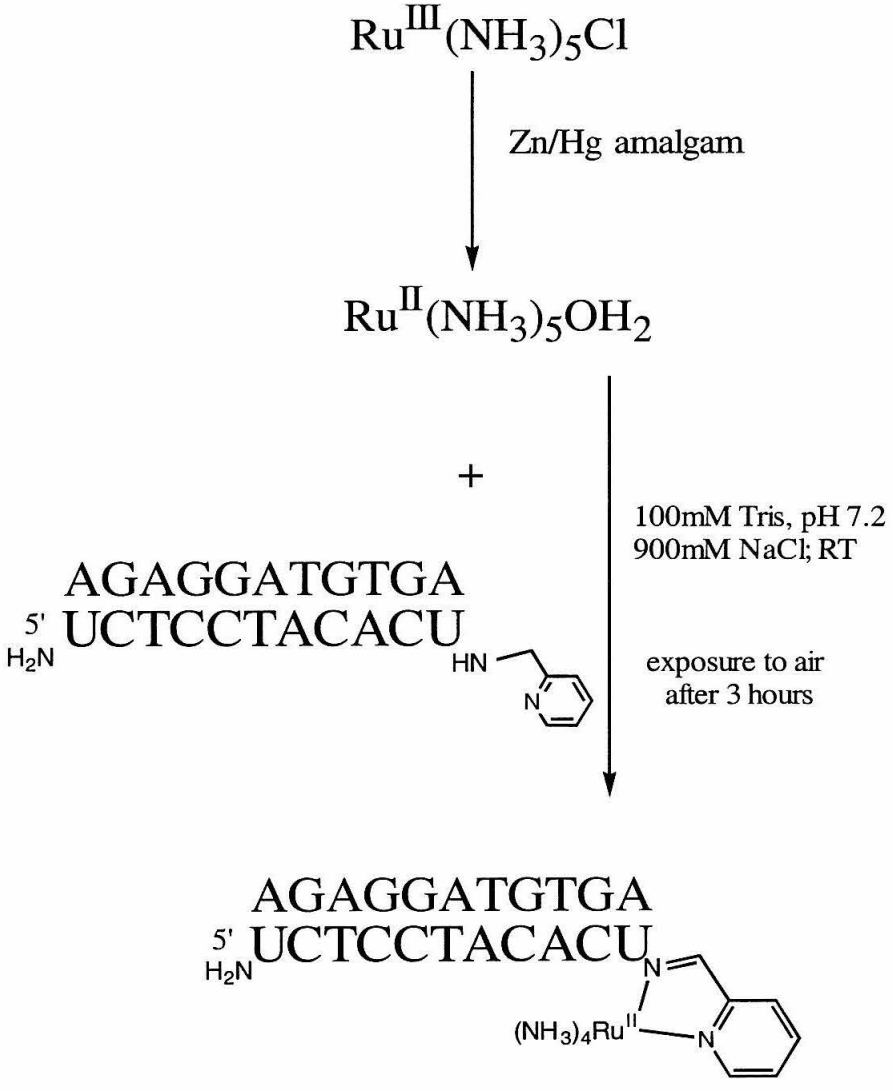
Ru^III(NH3)5Cl
Zn/Hg amalgam
Ru^II(NH3)5OH2
+
100mM Tris, pH 7.2
900mM NaCl; RT
AGAGGATGTGA
5' UCTCCTACACU
H2N
HN
N
exposure to air
after 3 hours
AGAGGATGTGA
5' UCTCCTACACU
H2N
N
(NH3)4Ru^II
N

Figure 3.10: Absorption spectrum of purified oligonucleotide **11B** following metallation with $[Ru(NH_3)_5(OH_2)]^{2+}$.

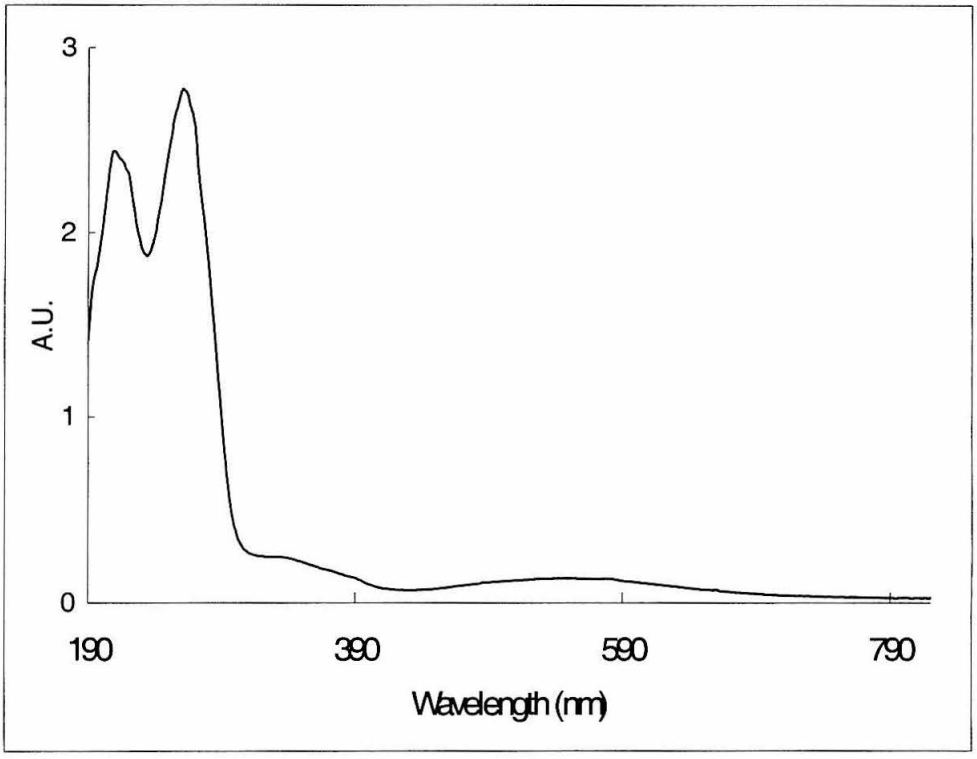
3
2
1
0
A.U.
190
390
590
790
Wavelength (nm)

Figure 3.11: Reaction scheme for the synthesis of $[Ru(NH_3)_4(impy)]^{2+}$ (where impy = iminomethylpyridine).

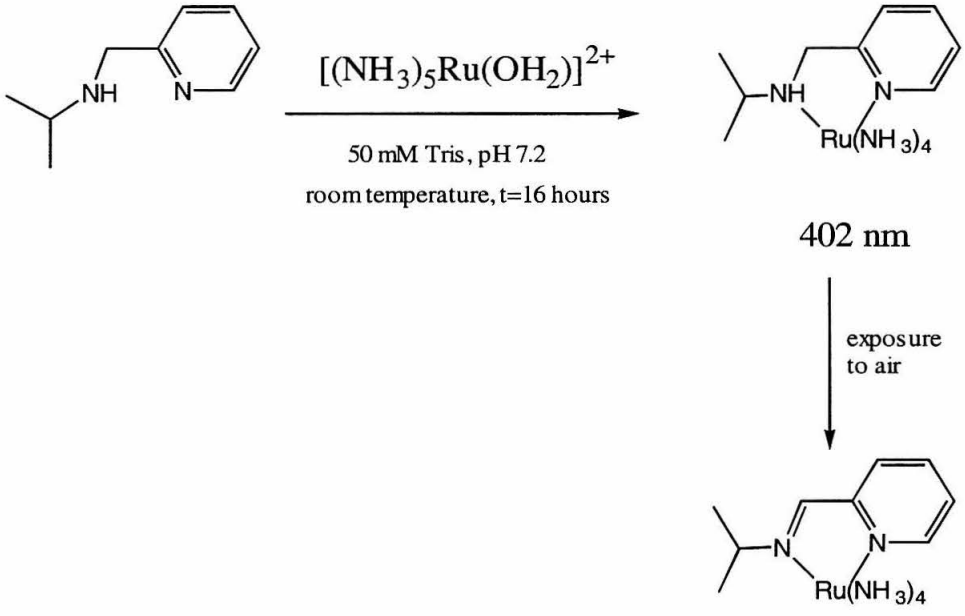
NH
N
$[(NH_3)_5Ru(OH_2)]^{2+}$
50 mM Tris, pH 7.2
room temperature, t=16 hours
NH
N
$Ru(NH_3)_4$
402 nm
exposure
to air
N
N
$Ru(NH_3)_4$
330, 528 nm

Figure 3.12: Absorption spectra of (a) $[Ru(NH_3)_4(ampy')]^{2+}$ (solid line) and (b) $[Ru(NH_3)_4(impy')]^{2+}$ (dashed line) in 50 mM Tris, pH 7.2. Abbreviations: ampy′ = N-substituted aminomethypyridine; impy′ = N-substituted iminomethylpyridine.

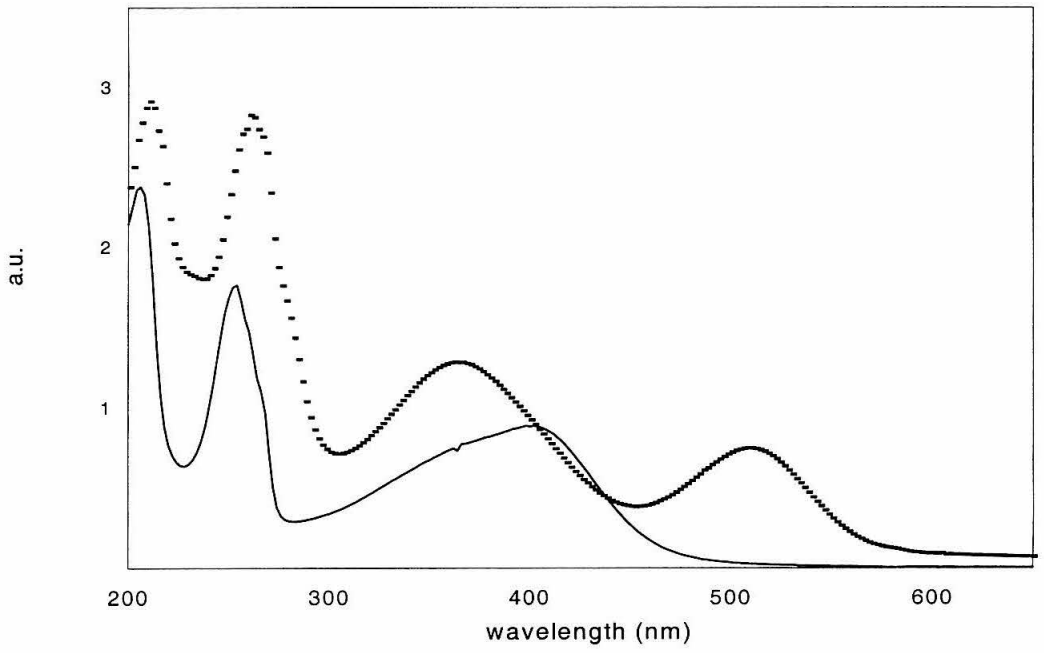
a.u.
3
2
1
200
300
400
500
600
wavelength (nm)

high-energy bands represent internal π-π^* ligand transitions; the feature at 402 nm is a MLCT from the Ru(II) to the pyridine ligand.)[12] Exposure of the sample to air caused several changes in the absorption spectrum. The band at 402 nm disappeared, and the spectrum was marked by the appearance of two additional bands with maxima at 366 and 502 nm (Figure 3.12). Kinetic analysis of the changes at λ = 402 nm and λ = 528 nm gave virtually equivalent rate constants (k_{402} = 3.4 x 10^{-4} s^{-1}; k_{528} = 5.0 x 10^{-4} s^{-1}). Isosbestic points were observed at 386 and 455 nm.

These results were consistent with reports describing the products from the oxidative dehydrogenation of amine ligands coordinated to ruthenium.[12,15-19] Ford and coworkers showed that air-exposure of $[Ru(NH_3)_4(ampy)]^{2+}$ (ampy = aminomethylpyridine) leads to the formation of $[Ru(NH_3)_4(impy)]^{2+}$ (impy = iminomethylpyridine).[12] Subsequent work by Keene and Meyer outlined the mechanism of oxidative dehydrogenation for a related complex, $[Ru(bpy)_2(ampy)]^{2+}$ (Figure 3.13).[17-19] The key intermediate in this mechanism is the Ru(IV) species that is formed upon disproportionation of the initial product of air-exposure, Ru(III). The high oxidation state facilitates a low-energy pathway for the transfer of two electrons needed for the dehydrogenation reaction.[18]

Additional model complex reactions involving oxidative dehydrogenation of coordinated ligands are described in Appendix B.

G-containing Oligonucleotides. Additional metallation reactions involved oligonucleotides containing a single guanine base overhanging on one end of the duplex (Figure 3.14). The guanine base was used as a metal attachment site. Reports by Clarke and coworkers describe the selective coordination of $[Ru(NH_3)_5(OH_2)]^{2+}$ to N^7 of guanine

Figure 3.13: Scheme showing the mechanism of oxidative dehydrogenation of amines coordinated to Ru(II) bis(bipyridine). Taken from Reference 18. Abbreviation: bpy, 2,2′-bipyridine.

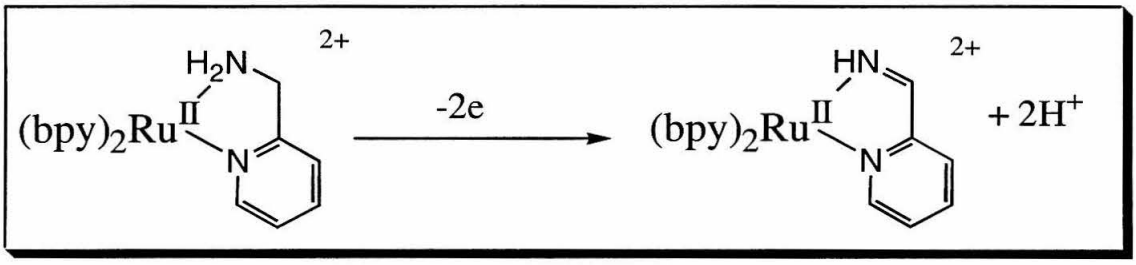
2+
H2N
(bpy)2Ru II
N
-2e
HN
2+
(bpy)2Ru II
N
+ 2H+

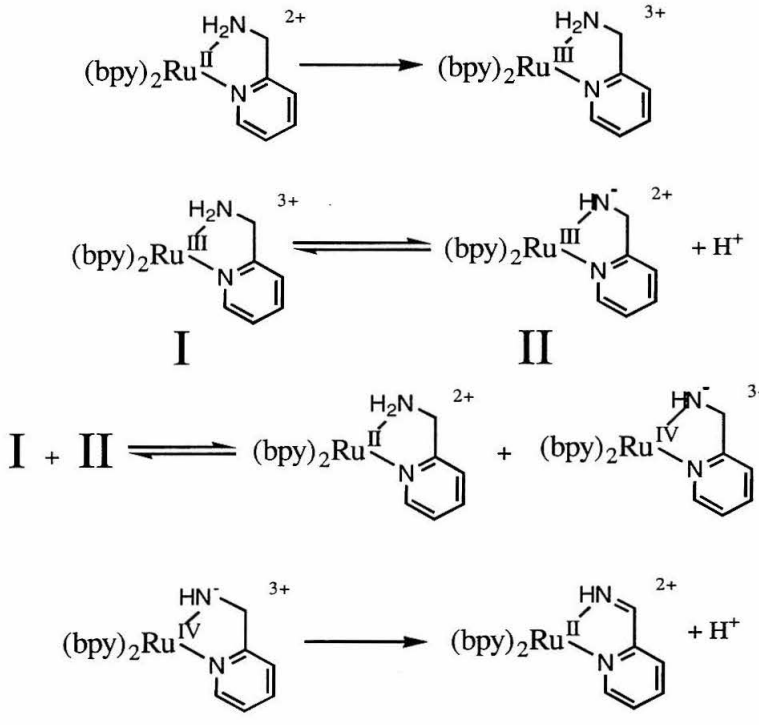
H2N
2+
(bpy)2Ru II
N
3+
(bpy)2Ru III
N
H2N
3+
(bpy)2Ru III
N
HN-
2+
(bpy)2Ru III
N
+ H+
I
II
I + II
H2N
2+
(bpy)2Ru II
N
+
HN-
3+
(bpy)2Ru IV
N
HN-
3+
(bpy)2Ru IV
N
HN
2+
(bpy)2Ru II
N
+ H+

Figure 3.14: Reaction scheme for metallation of duplexes containing an overhanging guanine base at the 5′ end.

Guanine as Metal Attachment Site

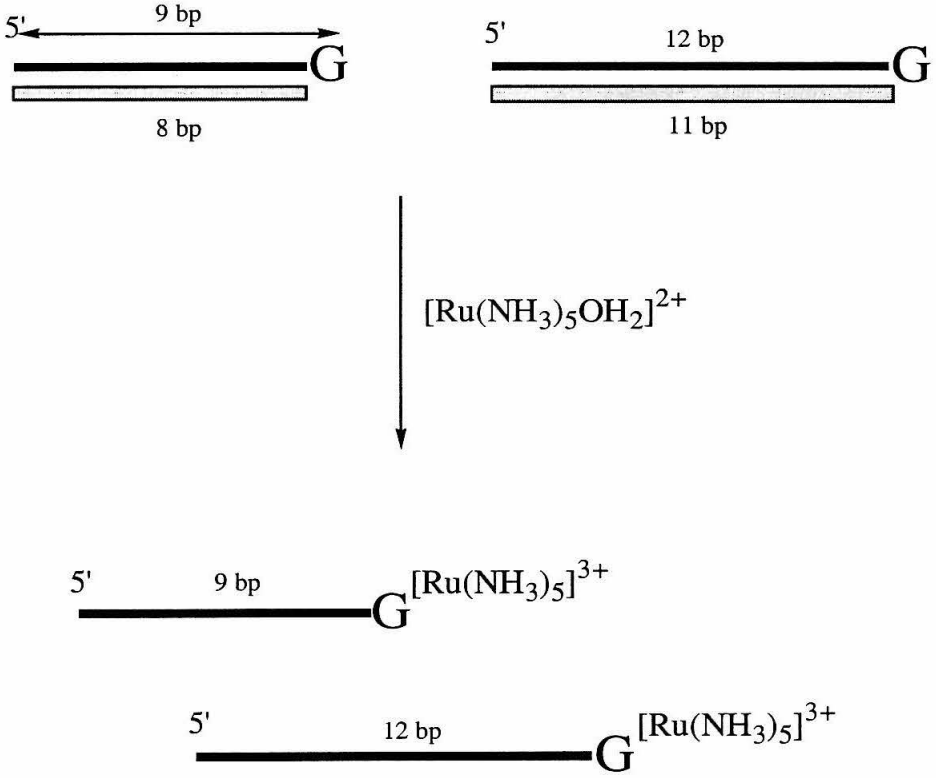

bases contained in calf-thymus DNA.[20-22] Studies of ruthenium(II) guanine complexes have demonstrated this selectivity.[23-26]

Metallation of G-containing oligonucleotides was pursued to avoid preparing oligonucleotides modified with a metal-binding ligand. The discouraging results obtained from metallations of $_{a}\mathbf{UU}_{b}$ and **11B** motivated this change in the type of oligonucleotides targeted. The reactions were conducted according to the procedure described for metallation of $_{a}\mathbf{UU}_{b}$ and **11B**. However, metallations of G-containing oligonucleotides failed to be selective for the single guanine. This conclusion is supported by the number of metallated products indicated in the HPLC traces. Attempts to control the metallation of duplexed G-containing oligonucleotides by limiting the amount of $[Ru(NH_3)_5(OH_2)]^{2+}$ present in the reaction did not minimize the complexity of the resulting solution (Figure 3.15). Reactions lasting as short at 15 minutes resulted in multi-ruthenated oligonucleotides. Separation of these products by HPLC was unsuccessful.

Experimental Procedure. Metallation of $_{a}\mathbf{UU}_{b}$ hybridized to its complementary strand involved a final solution of 0.1 mM DNA duplex and 1 mM $[Ru(NH_3)_5(OH_2)]Cl_2$ that had been freshly reduced over Zn/Hg amalgam in 100 mM Tris buffer (pH 7.2). The reaction mixture turned from yellow to an orange-brown over 3 hours under argon at room temperature, at which time the reaction vessel was opened up to air. Within 15 minutes the reaction solution changed to a dark purple. The solution was dried down or desalted right away by gel filtration, followed by ion exchange HPLC analysis.

Metallation of G-containing oligonucleotides proceeded as follows. Duplexes were prepared in 100 mM Tris (pH 7.2) containing 900 mM sodium chloride. Typical

Figure 3.15: HPLC trace of metallation reaction involving duplexed **9G** and $[Ru(NH_3)_5(OH_2)]^{2+}$ (1:1.5 DNA:Ru, t = 35 minutes, 50 mM Tris (pH 7.2), 900 mM sodium chloride). Column: Dionex NucleoPac 100. Gradient: 0-15% B over 4 minutes, 15-30% B over 33 minutes. Buffer A: 25 mM Tris (pH 8.0), 0.5% acetonitrile. Buffer B: 25 mM Tris (pH 8.0), 0.5% acetonitrile, 1.5 M ammonium chloride. Wavelength monitored: 260 nm. Absorption spectra for the peaks are given in the upper part of the figure.

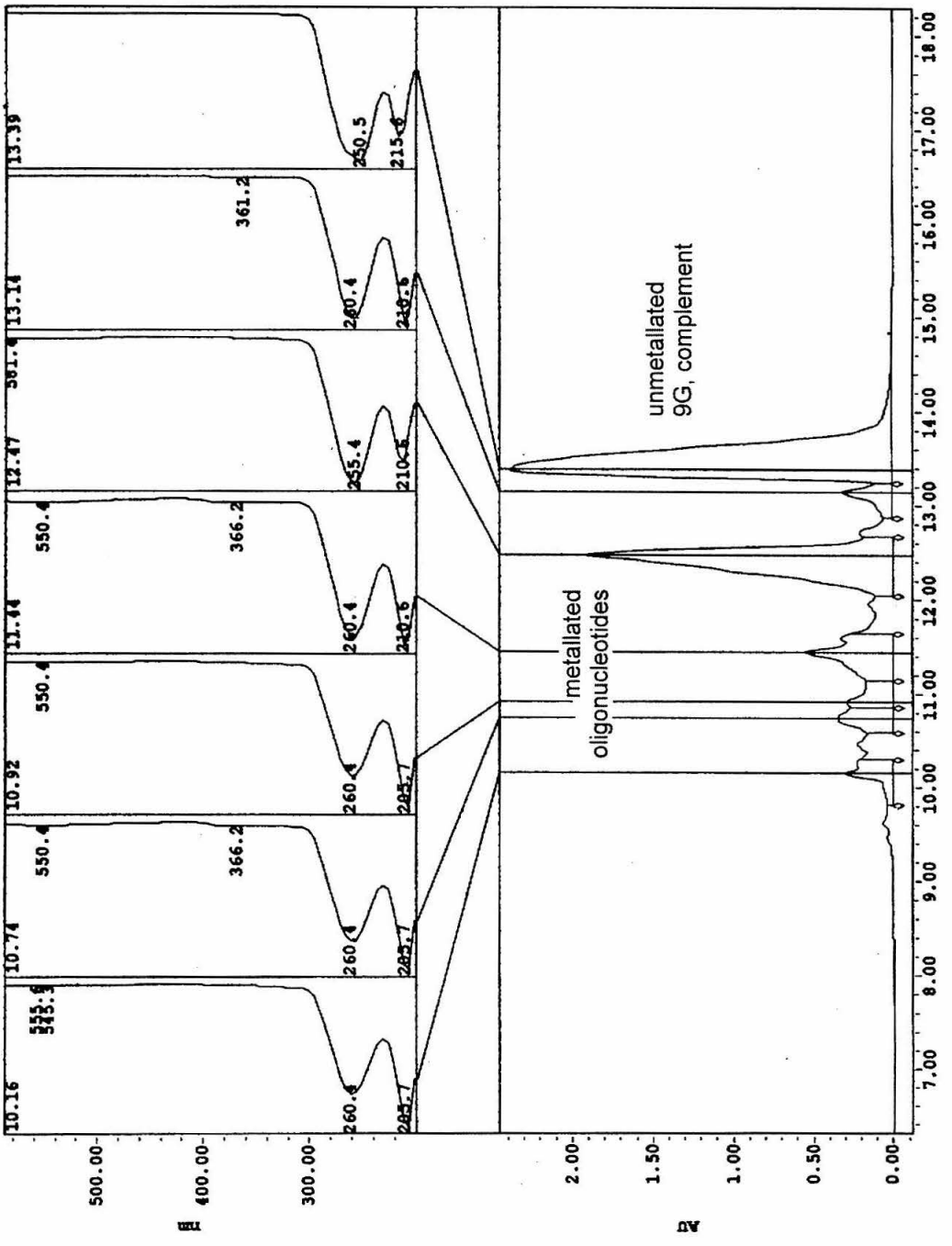
metallated
oligonucleotides
unmetallated
9G, complement
Minutes
AU
mV

reactions contained 0.95 mM DNA and 0.95-4.8 mM $[Ru]^{2+}$ and were stirred at room temperature for 30-60 minutes. Air was bubbled through the solution until the solution was purple. The sample was dialyzed, dried to a pellet, and purified by ion-exchange HPLC methods (Dionex column). A sample HPLC trace showing the reaction after 30 minutes is given in Figure 3.15.

Results: *Metallation Reactions with Ruthenium(II) Acetylacetonate Reagents*

The oligonucleotides targeted for metallation with $[Ru(acac)_3]$, $[Ru(acac)_2(CH_3CN)_2]$, and $[Ru(acac)_2(tmen)]^+$ (where tmen = tetramethylethylene diamine) included $_aUU_b$ and **11B** (see Figure 3.8). Metallations of $_aUU_b$ took place in absence of a complementary strand; therefore, these solutions did not contain sodium chloride. Metallations of **11B** contained duplexed samples of this target oligonucleotide, thus requiring that a high concentration of sodium acetate be present in the solution. All reactions were conducted under an argon atmosphere. Typically $[Ru(acac)_3]$ and $[Ru(acac)_2(tmen)]^+$ were reduced over Zn/Hg and then transferred under argon to the oligonucleotide sample. Some reactions took place in the presence of solid Zn/Hg. Metallations performed with $[Ru(acac)_2(CH_3CN)_2]$, did not require reduction prior to addition to the DNA.

Model Complexes. Reactions with a 2′-modified nucleoside assisted in designing suitable oligonucleotide metallation conditions (Figure 3.16). The 5′-DMT protected form of $N^{2'}$-(2-pyridylmethyl)-2′-amino-2′-deoxyuridine was reacted with either $[Ru(acac)_3]$ or $[Ru(acac)_2(CH_3CN)_2]$ to give the metallonucleoside shown in Figure

Figure 3.16: Reaction scheme for the synthesis of [$Ru(acac)_2$(impy′)] (where acac = acetylacetonate; impy′ = iminomethylpyridine containing 2′-modified nucleoside on the imino nitrogen).

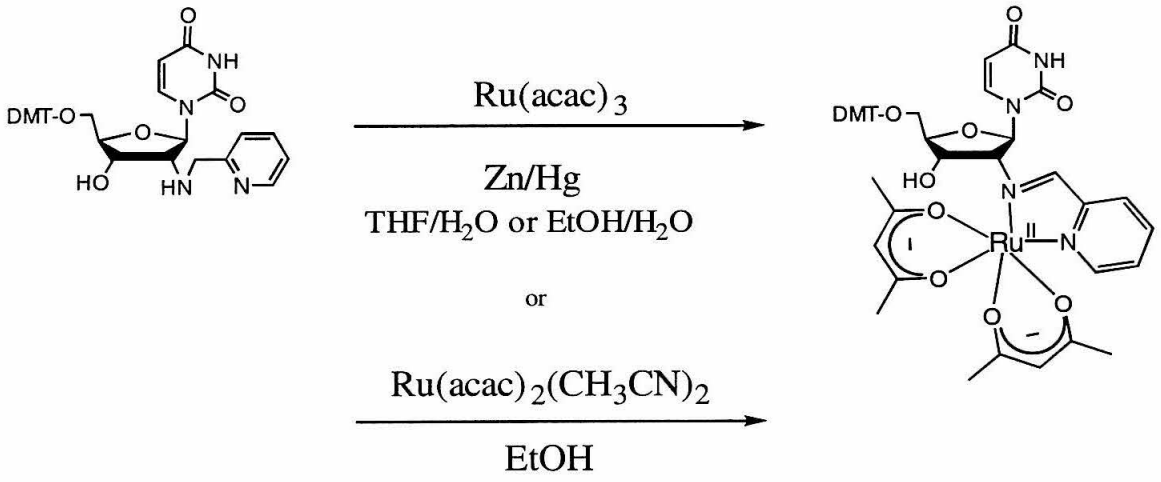
DMT-O
HO
HN
N
NH
O
Ru(acac)3
Zn/Hg
THF/H2O or EtOH/H2O
or
Ru(acac)2(CH3CN)2
EtOH
Ru
II
I

3.16. Details of the model complex synthesis are given in Appendix B. Full characterization of the metallonucleoside is given in Chapter 5.

Modified Oligonucleotides. Several reactions were performed with $_aUU_b$ under different conditions (Table 3.3). Metallations conducted with $[Ru(acac)_2(CH_3CN)_2]$ were more successful than those using $[Ru(acac)_3]$ or $[Ru(acac)_2(tmen)]^+$. Solutions containing $[Ru(acac)_2(CH_3CN)_2]$ remained a clear yellow or yellow-brown throughout the course of the metallation. Analytical HPLC was used to monitor the progress of the reactions and employed both ion-exchange and reverse-phase columns. Sample chromatograms for metallations of $_aUU_b$ and **11B** are shown in Figures 3.17 and 3.18. Because the peaks displaying absorption spectra suggestive of $Ru(acac)_2$-containing oligonucleotides eluted closely to other unmetallated peaks, separation of the desired peaks was difficult. Mass spectral results for such peaks are given in Figures 3.19 and 3.20. Overall, approximately 15-25 nmoles of $Ru(acac)_2$-modified $_aUU_b$ were isolated.

Experimental Procedure. Metallation of $_aUU_b$ and duplexes **11B** involved final solutions of 0.17 mM DNA and 0.17-3 mM ruthenium(II) reagent. $[Ru(acac)_3]$ and $[Ru(acac)_2(tmen)]^+$ were reduced over Zn/Hg amalgam in 25-50 mM Tris buffer (pH 7.2) and transferred via syringe to the reaction vessel. The solutions were deaerated under argon or degassed by the freeze-pump-thaw method. Reaction mixtures were typically red-pink in the presence of $[Ru(acac)_3]$ or $[Ru(acac)_2(tmen)]^+$. Reactions containing $[Ru(acac)_2(CH_3CN)_2]$ were yellow, yellow-brown, or orange. Aliquots were desalted by dialysis or SepPak elution. HPLC purification was performed by either ion-exchange (Dionex column) or reverse-phase (Oligo R3, T = 60 °C) chromatography. The collected fractions were dried down and desalted by SepPak elution.

Table 3.3. Conditions for Metallation Reactions involving Ruthenium(II) Acetylacetonate Reagents

reagent	Ru:DNA	oligo	buffer[a]	temp (°C)	length (hrs)	prodt
$Ru(acac)_3$	10:1	$_aUU_b$	Tris, pH 7.2 50% EtOH 25	25	96	
$Ru(acac)_3$	10:1	$_aUU_b$	Tris, pH 7.2 50% EtOH	80	96	
$Ru(acac)_3$, Zn/Hg		$_aUU_b$	Tris, pH 7.2	90	24	
$Ru(acac)_3$, Zn/Hg		$_aUU_b$	Tris, pH 7.2	25	10	
$Ru(acac)_2(CH_3CN)_2$	1:1	$_aUU_b$	Tris, pH 7.4	75	14	
$Ru(acac)_2(CH_3CN)_2$	10:1	$_aUU_b$	Tris, pH 7.4	75	3	*
$Ru(acac)_2(CH_3CN)_2$	10:1	$_aUU_b$	Tris, pH 7.4	75	3	*
$Ru(acac)_2(CH_3CN)_2$	10:1	$_aUU_b$	Tris, pH 7.4	75	1	*
$Ru(acac)_2(CH_3CN)_2$	3:1	$_aUU_b$	Tris, pH 7.4	65	40	*
$Ru(acac)_2(CH_3CN)_2$	1:1	$_aUU_b$	Tris, pH 7.4	65	30	*
$Ru(acac)_2(CH_3CN)_2$	3:1	$_aUU_b$	Tris, pH 7.4	65	26	*
$Ru(acac)_2$(tmen)	15:1	$_aUU_b$	Tris, pH 7.4	70	18	
$Ru(acac)_2$(tmen) + Zn/Hg	18:1	$_aUU_b$	Tris, pH 7.4	70	18	
$Ru(acac)_2(CH_3CN)_2$	1.2:1	**11B**[b]	Tris, pH 7.4 0.9 M NaOAc	40	48-120	*

[a] Buffer concentration: 25-50 mM.
[b] 11B hybridized to its complementary strand.

Figure 3.17: HPLC trace of metallation reaction involving $_{a}\mathbf{UU}_{b}$ and $[Ru(acac)_2(CH_3CN)_2]$ (1:3 DNA:Ru ratio, 25 mM Tris (pH 7.4), T = 65 °C, t = 26 hours). Column: Dionex NucleoPac 100. Gradient: 10-60% B over 3 minutes, 60-67% B over 25 minutes. Buffer A: 10% acetonitrile. Buffer B: 10% acetonitrile, 1.5 M ammonium acetate. Wavelength monitored: 260 nm. Absorption spectra for the peaks are given in the upper part of the figure.

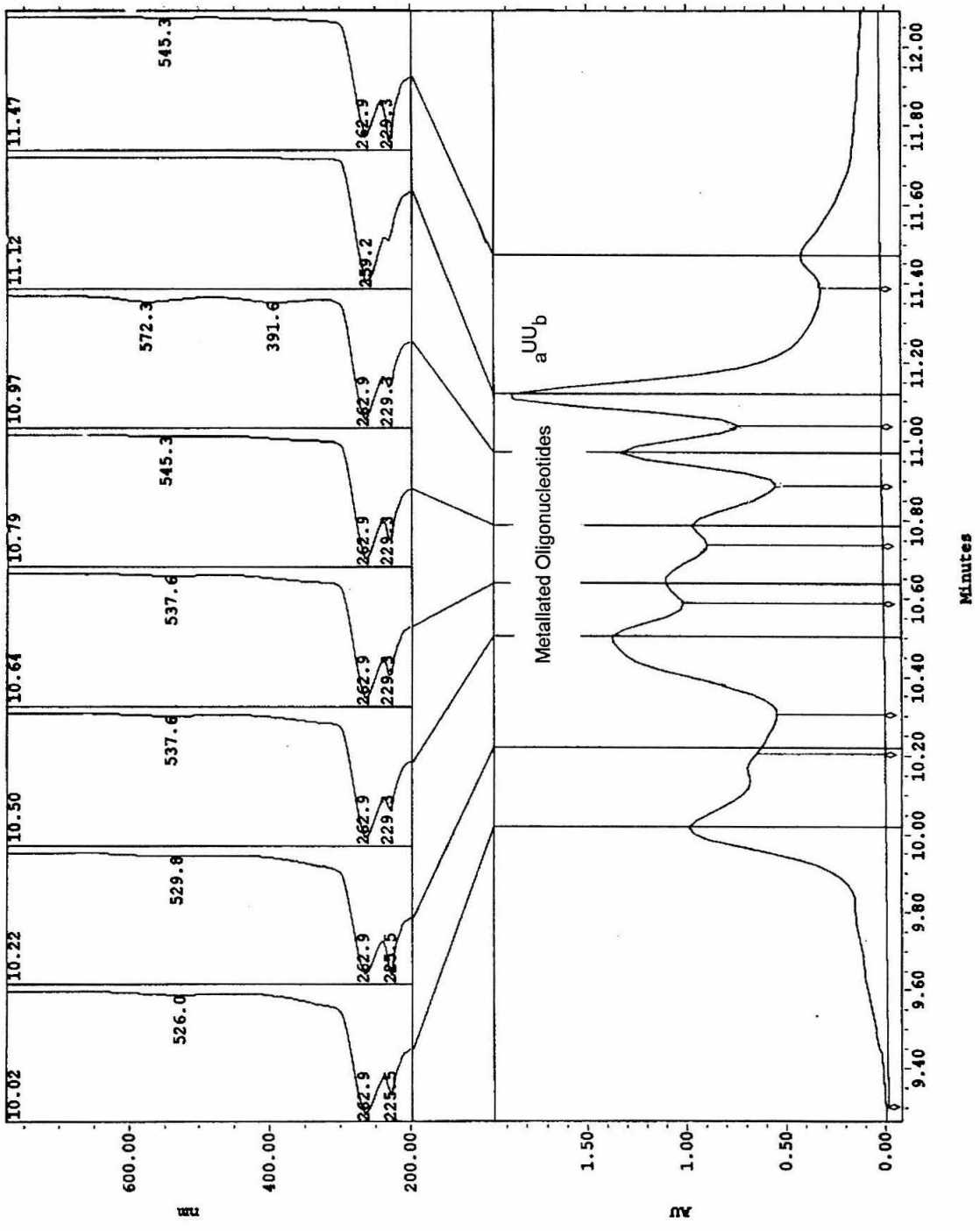
Metallated Oligonucleotides
aUUb
nm
AU
Minutes
10.02
526.0
262.9
225.5
10.22
529.8
262.9
225.5
10.50
537.6
262.9
229.2
10.64
537.6
262.9
229.2
10.79
545.3
262.9
229.2
10.97
572.3
391.6
262.9
229.2
11.12
259.2
11.47
545.3
262.9
229.2
600.00
400.00
200.00
1.50
1.00
0.50
0.00
9.40
9.60
9.80
10.00
10.20
10.40
10.60
10.80
11.00
11.20
11.40
11.60
11.80
12.00

Figure 3.18: HPLC trace of metallation reaction involving duplexed **11B** and $[Ru(acac)_2(CH_3CN)_2]$ (1:1.2 DNA:Ru ratio, 50 mM Tris (pH 7.4), 900 mM sodium acetate, T = 40 °C, t = 5 days). HPLC sample was pre-heated at 65 °C for 15 minutes. Column: Oligo R3, T = 65 °C. Gradient: 10-60% B over 3 minutes, 60-67% B over 25 minutes. Buffer A: 100 mM ammonium acetate (pH 8.5), 2% acetonitrile. Buffer B: 100% acetonitrile. Wavelength monitored: 260 nm. Absorption spectra for the peaks are given in the upper part of the figure.

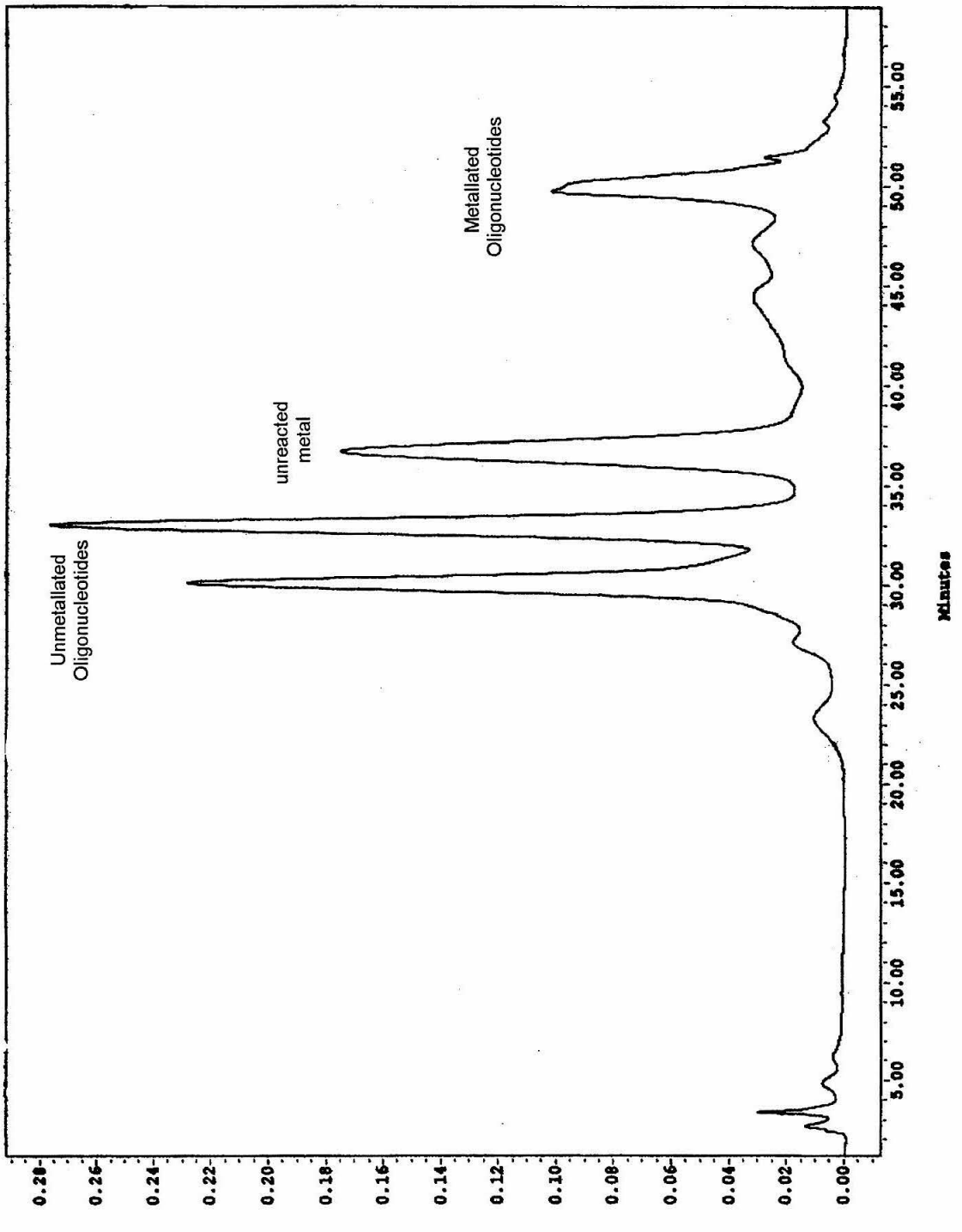
Unmetallated
Oligonucleotides
unreacted
metal
Metallated
Oligonucleotides
AU
Minutes
0.28
0.26
0.24
0.22
0.20
0.18
0.16
0.14
0.12
0.10
0.08
0.06
0.04
0.02
0.00
5.00
10.00
15.00
20.00
25.00
30.00
35.00
40.00
45.00
50.00
55.00

Figure 3.19: MALDI-TOF mass spectrum of fractions collected after HPLC purification of reaction involving $_{a}\mathbf{UU}_{\mathbf{b}}$ and $[Ru(acac)_2(CH_3CN)_2]$. See Figure 3.17 for HPLC trace. The molecular weight calculated for the desired metal-containing oligonucleotide {[M] = $_{a}\mathbf{UU}_{\mathbf{b}}$- $Ru(acac)_2$}is 3617; found, 3618.69 $[M-H]^-$.

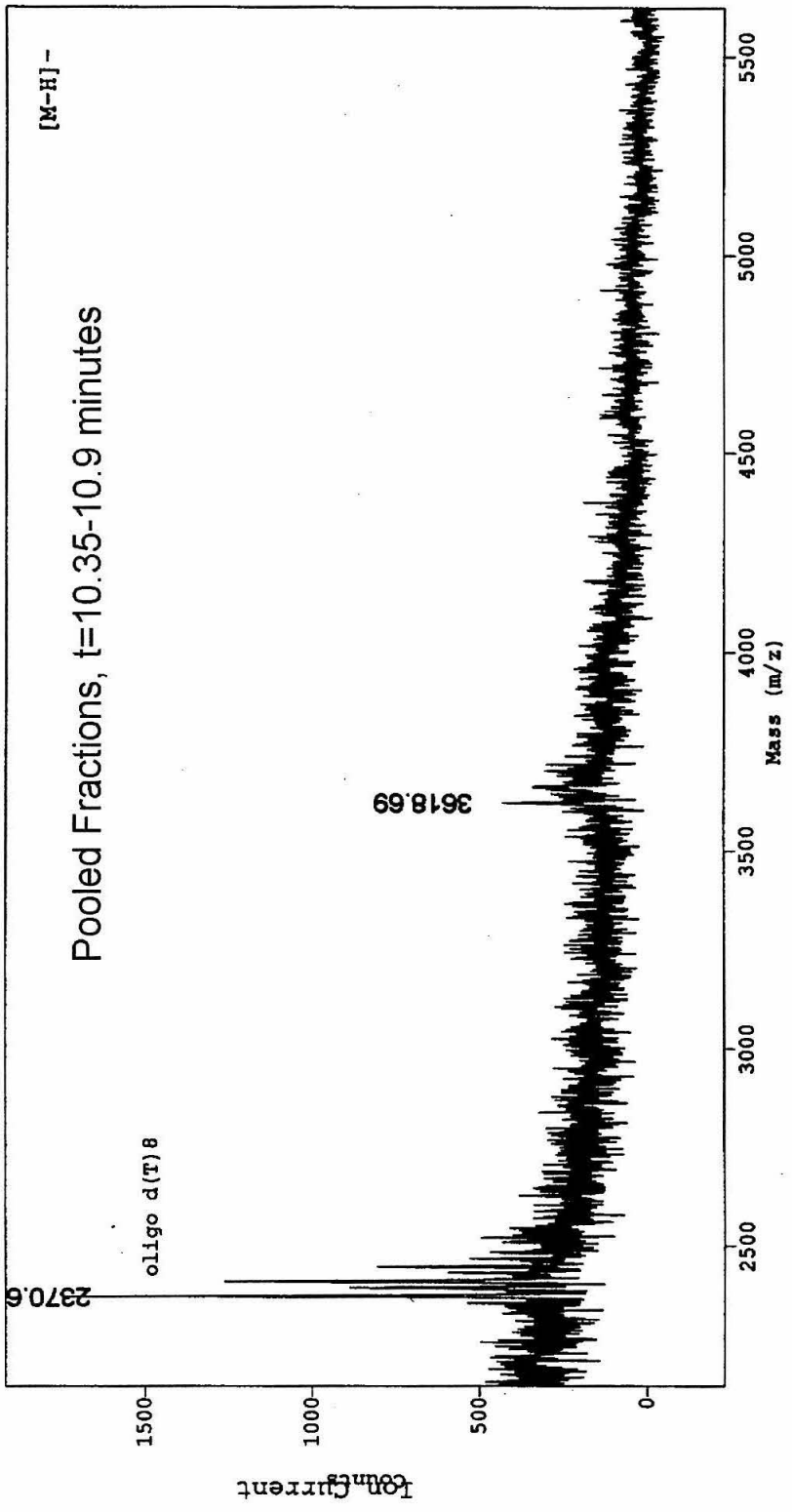
[M-H]-
Pooled Fractions, t=10.35-10.9 minutes
oligo d(T)8
2370.6
3618.69
Ion Current
Mass (m/z)
0
500
1000
1500
2500
3000
3500
4000
4500
5000
5500

Figure 3.20: MALDI-TOF mass spectrum of fractions collected after HPLC purification of reaction involving duplexed **11B** and $[Ru(acac)_2(CH_3CN)_2]$. See Figure 3.18 for HPLC trace. The molecular weight calculated for the desired metal-containing oligonucleotide {[M] = **11B**/$Ru(acac)_2$}is 3705; found, 3705.95 $[M-H]^-$.

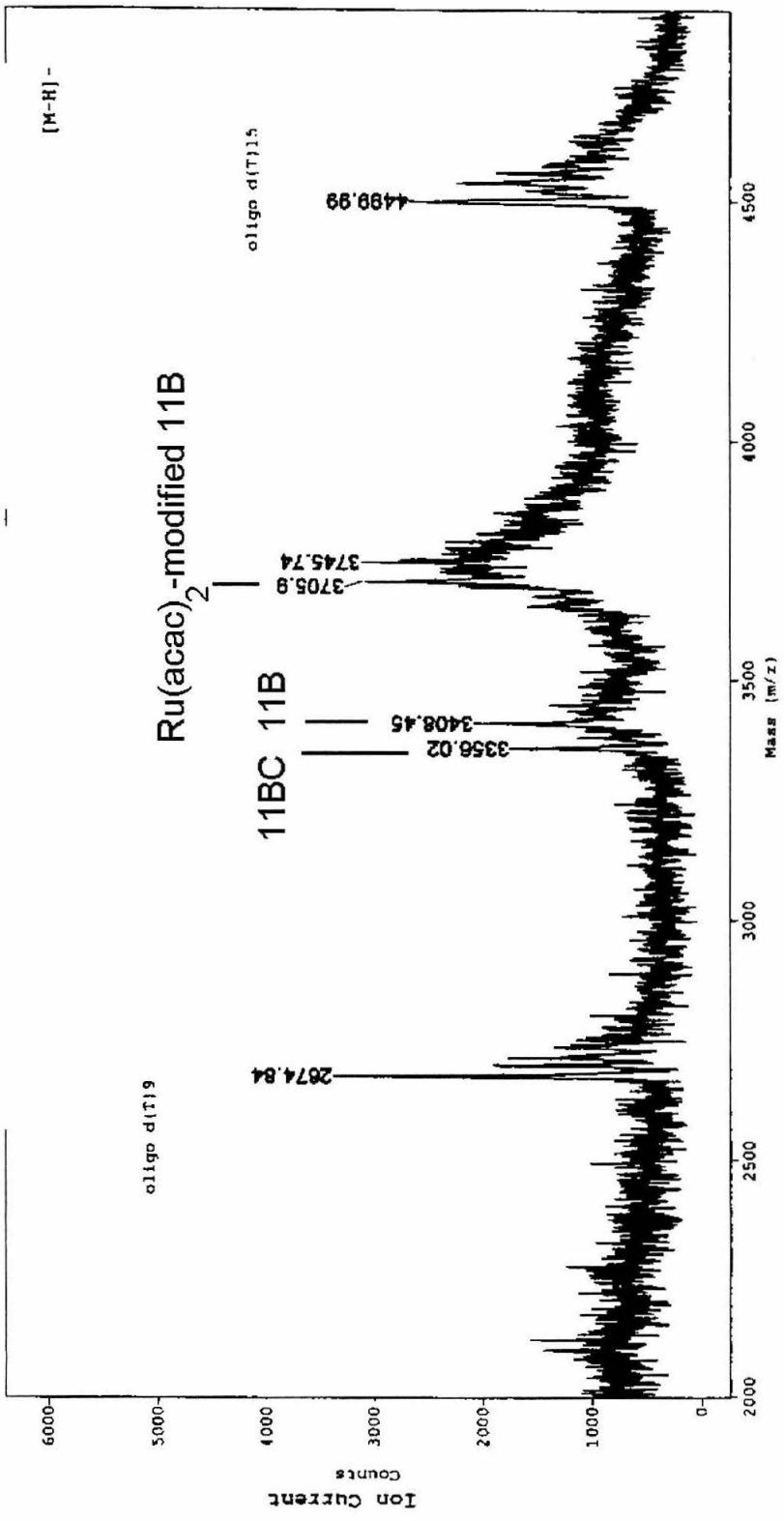
Ion Current
Counts
6000
5000
4000
3000
2000
1000
0
2000
2500
3000
3500
4000
4500
Mass (m/z)
[M-H]-
oligo d(T)19
oligo d(T)15
2674.84
11BC 11B
3356.02
3408.45
Ru(acac)2-modified 11B
3705.9
3745.74
4489.99

Discussion

Metallations with [Ru(bpy)$_2$CO$_3$]

Attempts to incorporate [Ru(bpy)$_2$CO$_3$] into oligonucleotides modified with amine ligands were complicated by several factors. Effective purification methods were difficult to develop due to the multiple components in the reaction mixture. Commercially available resins provided inadequate separation of the metallated oligonucleotides from unreacted starting materials. Identification of product fractions was hampered by the lack of high-recovery methods suited for desalting short oligonucleotides containing cationic metal complexes. These issues thwarted efforts to properly optimize the reaction conditions.

The lengthy reaction times needed for significant metallation further exacerbated efforts to optimize the reaction conditions. The substitution chemistry of the Ru(II) center was hindered by the presence of the near-molar quantities of sodium chloride required to stabilize the short duplex. However, conditions of low ionic strength did not lead to selective modification of the target oligonucleotide.

Metallation of oligonucleotides with [Ru(bpy)$_2$CO$_3$] is a complicated reaction for several reasons. The desired "ligand"—the 2′ amine group on the terminal nucleoside of an oligonucleotide—is attached to a highly charged oligonucleotide. It is not intended for this oligonucleotide to participate in the substitution reaction. However, single-stranded oligonucleotides—such as $_{a}$**UT** and **TU**$_{a}$—containing a single "ligand" are modified with more than one metal complex upon metallation with [Ru(bpy)$_2$CO$_3$]. These results confirm that metal complexation is not exclusive for the targeted ligand.

These results are consistent with those reported by Netzel and coworkers for incorporating $[Ru(bpy)_2(OH_2)_2]^{2+}$ into oligonucleotides using post-synthetic modification methods (Chapter 1). An equimolar amount of this ruthenium reagent was incubated in the presence of a bpy-bearing oligonucleotide that was unhybridized. This led to multiple ruthenium-containing oligonucleotides despite the fact that the DNA bases are poor ligands compared to bpy in this context. The lack of selective labeling precludes the wide-spread applicability of this method to certain metal complexes.

Metallation Reactions with $[Ru(NH_3)_5(OH_2)]^{2+}$

Reactions with $[Ru(NH_3)_5(OH_2)]^{2+}$ provided additional insight into the challenges of incorporating ruthenium complexes at single sites within several oligonucleotides. Oligonucleotides containing the nucleoside $\mathbf{U_b}$ were targeted initially, since the anticipated product would display features characteristic of the model complex, $[Ru(NH_3)_5(pyr)]^{2+}$. However, the results indicated the formation of a species displaying absorption features different from those of the expected product. Observations from a reaction between $[Ru(NH_3)_5(OH_2)]^{2+}$and a small molecule analogue of $\mathbf{U_b}$-type oligonucleotides aided in understanding these results. A comparison of the absorption features of the products isolated from both reactions suggested that the metallated oligonucleotide contained a metal complex at the desired $\mathbf{U_b}$ site; however, the nature of the complex was of the type $[Ru(NH_3)_4(impy)]^{2+}$. While a metallated oligonucleotide in this form has many desireable features, we concluded that the absorption bands displayed by this species were too broad and weak for the transient absorption studies we envisioned.

In addition to this result, there were several reasons why metallation with $[Ru(NH_3)_5(OH_2)]^{2+}$ was unsuccessful. Efforts to minimize ruthenation at multiple sites by using the complement as a blocking group were ineffective. We predicted that the multi-metallated oligonucleotides contained guanine bases modified with this ruthenium reagent. This assessment was based on the work by Clarke involving the selective coordination of $[Ru(NH_3)_5(OH_2)]^{2+}$ to N^7 of guanine.[20-22] The presence of these other metal-containing oligonucleotides complicated the isolation of the $[Ru(NH_3)_4(impy)]^{2+}$-modified oligonucleotide. Additionally, mass spectral characterization of such oligonucleotides was unreliable since the metallated species were not stable in the conditions of MALDI-TOF analysis. Efforts to characterize the products using a more gentle mass spectral method (ESI-MS) were hindered by the presence of salt unsuccessfully removed from the HPLC fraction.

The likelihood of guanine labeling by $[Ru(NH_3)_5(OH_2)]^{2+}$ motivated further attempts to obtain oligonucleotides containing a single metal complex. Since unmodified strands of any sequence could be prepared commercially, we investigated using duplexes containing an overhanging guanine at the 5′ end in subsequent metallation reactions. If prepared, these metal-containing oligonucleotides would serve as complementary strands to oligonucleotides separately metallated with $[Ru(bpy)_2CO_3]$. (The sequence of the G-containing oligonucleotide was constrained by the sequence of complementary oligonucleotides already containing $[Ru(bpy)_2CO_3]$).[27] However, the results from metallations of G-containing oligonucleotides showed that controlling the substitution of $[Ru(NH_3)_5(OH_2)]^{2+}$ was difficult. At 1:1 Ru:DNA concentrations, substantial metallation was observed after only a few minutes. HPLC traces indicated that multiple products

were formed under these conditions. After several attempts to limit the metallation to the single guanine base in solution, experiments with $[Ru(NH_3)_5(OH_2)]^{2+}$ were discontinued.

Metallation Reactions with Ruthenium(II) Acetylacetonate Reagents

Reactions involving three Ru(II) acac reagents demonstrated the difficulty of incorporating redox-active complexes into oligonucleotides. Metallations of $_{a}\mathbf{UU}_{b}$ with $[Ru(acac)_3]$ were unsuccessful due to the extreme oxygen sensitivity of the reduced metal complex. $[Ru(acac)_2(CH_3CN)_2]$ was a desireable reagent for metallation since (a) it was not as air-sensitive as $[Ru(acac)_3]^+$, (b) it did not require reduction over Zn/Hg prior to addition to the oligonucleotide solution, and (c) the substitution chemistry of $[Ru(acac)_2(CH_3CN)_2]$ could be managed by the reaction temperature. Model complex reactions performed with $[Ru(acac)_2(CH_3CN)_2]$ assisted in designing optimal reaction conditions for oligonucleotide metallation. Reactions involving $[Ru(acac)_2(CH_3CN)_2]$ and **11B** provided the desired metal-containing oligonucleotide, although there were several metallated oligonucleotides also produced in the course of the reaction.

Conclusion

Overall, incorporating ruthenium(II) complexes into the oligonucleotides using the post-synthetic modification method was unsuccessful. While this method originally provided metallated oligonucleotides under conditions similar to those described here,[1] its application to oligonucleotides of different length and sequence proved ineffective. The systematic variation of several reaction parameters (reaction time, temperature, pH, ionic strength, concentration, ratio of reactants, presence of complement, presence of

reductant, oligonucleotide sequence) did not yield large amounts of metallated oligonucleotides.

Despite these disappointing results, the insight gained from these studies has value. There are multiple factors controlling the successful incorporation of metal complexes into oligonucleotides using post-synthetic modification. One important factor is the association of the ruthenium complex with oligonucleotides, whether they be single- or double-stranded. The overall charge of the complex and the affinity of the ruthenium center for the binding sites available within DNA contribute to this association. Since multiple ruthenium-containing oligonucleotides were generated in reactions involving both dicationic and neutral ruthenium reagents, no correlation between yield of labeling and overall charge on the ruthenium complex emerges from these experiments.

Examining these factors contributes to our understanding of how metal complexes interact with nucleic acids. Such an understanding can aid in the design and development of metal reagents as drug candidates. For instance, promising candidates would behave like $[Ru(NH_3)_5(OH_2)]^{2+}$, as opposed to $[Ru(bpy)_2CO_3]$, due to the different rates of substitution displayed by these complexes in the presence of DNA. Unlike the conditions of solid-phase incorporation of metal complexes, the metallation experiments like those described in this chapter more closely mimic the biological setting in which metal-DNA interactions become important.

References and Notes

(1) Meade, T. J.; Kayyem, J. F. *Angew. Chem. Int. Ed. Engl.* **1995**, *34*, 352-353.

(2) Winkler, J. R.; Nocera, D. G.; Yocom, K. M.; Bordignon, E.; Gray, H. B. *J. Am. Chem. Soc.* **1982**, *104*, 5798-5800.

(3) Nocera, D. G.; Winkler, J. R.; Yocom, K. M.; Bordignon, E.; Gray, H. B. *J. Am. Chem. Soc.* **1984**, *106*, 5145-5150.

(4) Bowler, B. E.; Raphael, A. L.; Gray, H. B. *Prog. in Inorg. Chem.* **1990**, *38*, 259-322.

(5) Winkler, J. R.; Gray, H. B. *Chem. Rev.* **1992**, *92*, 369-379.

(6) Bjerrum, M. J.; Casimiro, D. R.; Chang, I.-J.; Bilio, A. J. D.; Gray, H. B.; Hill, M. G.; Langen, R.; Mines, G. A.; Skov, L. K.; Winkler, J. R.; Wuttke, D. S. *J. Bioenerg. Biomemb.* **1995**, *27*, 295-302.

(7) Winkler, J. R.; Gray, H. B. *J. Biol. Inorg. Chem.* **1997**, *2*, 399-404.

(8) Kobayashi, T.; Nishina, Y.; Shimizu, K.; Sato, G. P. *Chem. Lett.* **1988**, 1137-1140.

(9) Kasahara, Y.; Hoshino, Y.; Shimizu, K.; Sato, G. P. *Chem. Lett.* **1990**, 381-384.

(10) Hasegawa, T.; Lau, T. C.; Taube, H.; Schaefer, W. P. *Inorg. Chem.* **1991**, *30*, 2921-2928.

(11) Juris, A.; Balzani, V.; Barigelletti, F.; Campagna, S.; Belser, P.; Vonzelewsky, A. *Coord. Chem. Rev.* **1988**, *84*, 85-277.

(12) Alvarez, V. E.; Allen, R. J.; Matsubara, T.; Ford, P. C. *J. Am. Chem. Soc.* **1974**, *96*, 7686-7692.

(13) Rack, J. J.; Krider, E. S.; Meade, T. J. *J. Am. Chem. Soc.* **2000**, *122*, 6287-6288.

(14) Clarke, M. J.; Taube, H. *J. Am. Chem. Soc.* **1974**, *96*, 5413-5419.

(15) Lane, B. C.; Lester, J. E.; Basolo, F. *Chem. Commun.* **1971**, 1618-1619.

(16) Mahoney, D. F.; Beattie, J. K. *Inorg. Chem.* **1973**, *12*, 2561-2565.

(17) Brown, G. M.; Weaver, T. R.; Keene, F. R.; Meyer, T. J. *Inorg. Chem.* **1976**, *15*, 190-196.

(18) Ridd, M. J.; Keene, F. R. *J. Am. Chem. Soc.* **1981**, *103*, 5733-5740.

(19) Keene, F. R.; Ridd, M. J.; Snow, M. R. *J. Am. Chem. Soc.* **1983**, *105*, 7075-7081.

(20) Clarke, M. J.; Jansen, B.; Marx, K. A.; Kruger, R. *Inorg. Chim. Acta-Bioinorg. Chem.* **1986**, *124*, 13-28.

(21) Clarke, M. J.; Stubbs, M. In *Metal Ions in Biological Systems, Vol 32*, 1996; Vol. 32.

(22) Clarke, M. J. In *Electron Transfer Reactions*, 1997; Vol. 253.

(23) Clarke, M. J.; Bailey, V. M.; Doan, P. E.; Hiller, C. D.; LaChanceGalang, K. J.; Daghlian, H.; Mandal, S.; Bastos, C. M. *Inorg. Chem.* **1996**, *35*, 4896-4903.

(24) LaChanceGalang, K. J.; Zhao, M.; Clarke, M. J. *Inorg. Chem.* **1996**, *35*, 6021-6026.

(25) Zhao, M.; Clarke, M. J. *J. Biol. Inorg. Chem.* **1999**, *4*, 318-324.

(26) Zhao, M.; Clarke, M. J. *J. Biol. Inorg. Chem.* **1999**, *4*, 325-340.

(27) Meade, T. J., unpublished results.

Chapter 4

Automated Synthesis of 3′-Metallated Oligonucleotides

Introduction

Recent studies of electron transfer (ET) through DNA have employed redox-active probes bound to single- and double-stranded oligonucleotides.[1-8] An important objective in this area continues to be the facile and site-specific incorporation of metal complexes into DNA. One method to achieve this involves the synthesis of oligonucleotides possessing metal-binding ligands, followed by incorporation of the metal complexes at these sites.[8-21] While this method enables the preparation of various metal-containing oligonucleotides from the same strand, it requires large amounts of metal reagent, lengthy reaction times, and multiple chromatographic separations. A second method entails the preparation of metal-containing monomers that can be incorporated during solid-phase DNA synthesis using standard phosphoramidite coupling techniques.[22-32] Advantages of this method include: rapid preparation of metal-containing oligonucleotides, high yields of metal incorporation, and routine product isolation. The success of this approach depends on the construction of individual metallated monomers that are compatible with automated DNA synthesis techniques.

Several groups have introduced metal complexes into DNA using metallated phosphonate and phosphoramidite monomers, where the metal complex (containing either Pt^{II}, Ru^{II}, or Os^{II}) is attached to the nucleoside base (Chapter 1).[23,24,27,28,32,33] Other examples include nonnucleosidic phosphoramidite monomers where the metal complex is tethered to the terminal phosphate group of the oligonucleotide.[25,29] We designed two modified nucleosides containing low- and high-potential metal complexes, as introduced in Chapter 1 (Figure 4.1).[31] Because the site of modification is the 2′ position (as opposed to other ring positions), it is possible to

Figure 4.1: Synthesis of metallonucleosides and metal-containing solid support: (a) 2-pyridinecarboxaldehye, EtOH, 2h; (b) $Ru(acac)_2(CH_3CN)_2$, EtOH, 1h, 79% yield; (c) $Ru(bpy)_2Cl_2$, EtOH, 4 h, 19% yield; (d) succinic anhydride, DMAP, pyridine, 18 h, 54% yield; (e) solid support, TEA, HOBT, BOP, CH_2Cl_2, rt, 16 h; acetic anhydride, N-methylimidazole, pyridine, rt, 12 h.

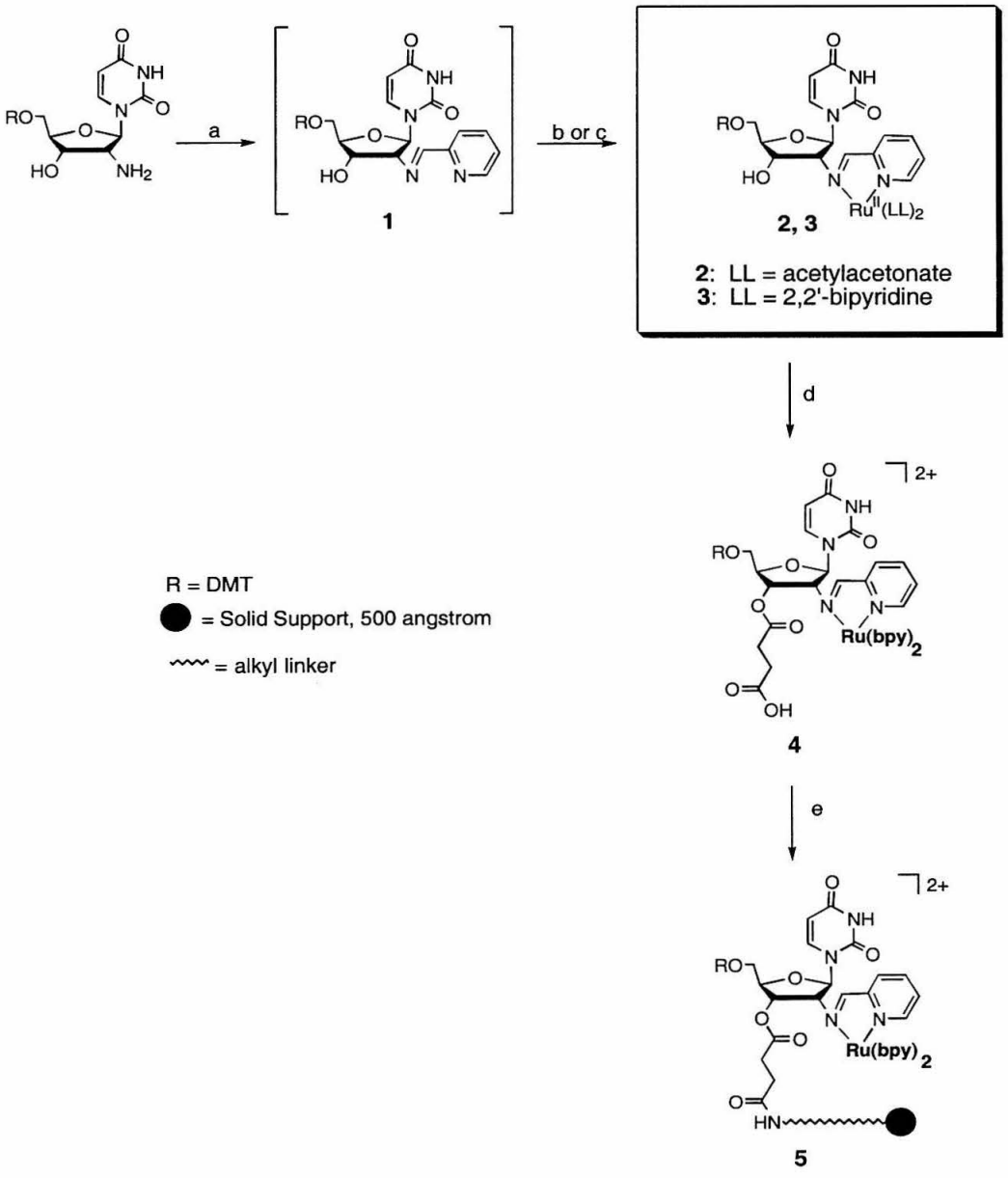
a
b or c
1
2, 3
2: LL = acetylacetonate
3: LL = 2,2'-bipyridine
d
4
e
5
R = DMT
= Solid Support, 500 angstrom
= alkyl linker

prepare these metallonucleosides as monomers that can be delivered during automated DNA synthesis.

We predicted that the presence of a metal complex at the 2′ ribose position would decrease the coupling of phosphoramidite derivatives of **2** and **3**. Therefore, we prepared customized solid supports containing the desired metallonucleoside and used these solid supports to initiate DNA synthesis. Because oligonucleotide synthesis proceeds step-wise in a 3′ → 5′ direction beginning with the nucleoside pre-derivatized to the solid support, all products isolated from the DNA synthesizer contain the metal complex. This method enables the rapid production of 3′-metallated oligonucleotides. The overall yield is not compromised by the coupling of a metallated phosphoramidite. Most importantly, the combination of both phosphoramidite and solid support-bound metallonucleosides affords the synthesis of an oligonucleotide containing metal complexes at the 3′ *and* 5′ ends (Appendix D).

Here we report the first synthesis of a metallonucleoside bound to a solid support and subsequent oligonucleotide synthesis with this precursor. Due to its stability in both the mildly acidic and strongly basic solutions that are routinely encountered during solid-phase DNA synthesis, **3** is an excellent candidate for conjugation to the solid support. However, the acid sensitivity of **2** precludes its use as a solid support-bound metallonucleoside. Large-scale syntheses of metal-containing oligonucleotides are achieved with the solid support modified with **3**. Interestingly, the yield is comparable to the values obtained for oligonucleotides synthesized with unmodified solid supports. A duplex formed with the purified metal-containing oligonucleotide exhibits superior thermal stability when compared to the corresponding unmetallated duplex. The

spectroscopic properties of the single- and double-stranded metal-containing oligonucleotides are unchanged from those of the metallonucleoside.

Results

Synthesis of Ruthenium-Containing Solid Support. The metal-binding nucleoside **1**, 5′-O-(4,4′-dimethoxytrityl)-2′-iminomethylpyridyl-2′-deoxyuridine, was prepared in situ by condensation of 5′-O-(4,4′-dimethoxytrityl)-2′-amino-2′-deoxyuridine and 2-pyridinecarboxaldehyde (Figure 4.1). The ruthenated nucleoside **2** was synthesized by addition of $Ru(acac)_2(CH_3CN)_2$ to **1** and isolated in 79% yield (see Chapter 5 for synthetic details and full characterization). Addition of $Ru(bpy)_2Cl_2$ to the intermediate **1** gave **3**, which was isolated in 19% yield.

The preparation of the ruthenium-containing solid support was based on our work involving the derivatization of solid supports with 2′-substituted uridine nucleosides (Chapter 2). Treatment of **3** with succinic anhydride in the presence of DMAP[34] yielded the hemisuccinate **4** in 43% yield.[35] Derivatization of the solid support with an excess of **4** using the coupling agent BOP, followed by capping of the unreacted sites, produced the ruthenium-containing solid support **5** with high nucleoside loading (~ 30 μmol/g).[36] The derivatization yield was comparable to those observed in the preparation of solid supports with similar 2′-modified nucleosides (Chapter 2).

Oligonucleotide Synthesis with 5. The preparation of 10- and 11-mer oligonucleotides containing the Ru-modified nucleoside at the 3′ terminus was done on a 1.0 μmol scale. Automated DNA synthesis with **5** is illustrated in Figure 4.2; the length

Figure 4.2: Oligonucleotide synthesis with the metal-containing solid support: (a) detritylation of **5**; monomer coupling; normal synthesis cycle; (b) detritylation of nascent oligonucleotide, monomer coupling; normal synthesis cycle; (c) cleavage of oligonucleotide from solid support and removal of protecting groups. Oligonucleotides **6** and **7** were synthesized separately.

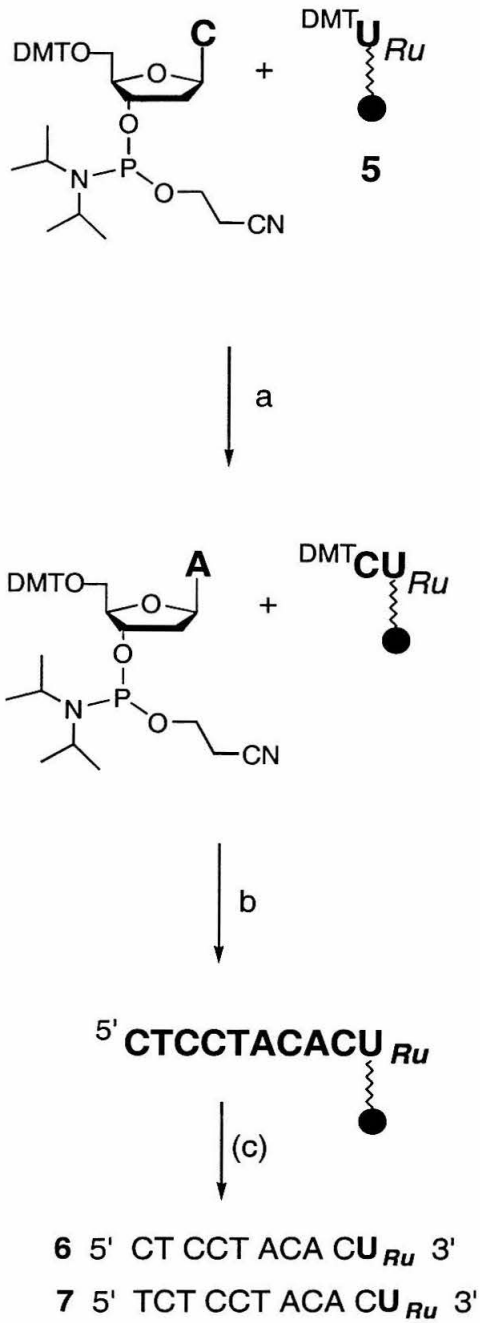
DMTO
C
O
O
N
P
O
CN
+
DMT
U
Ru
5
a
DMTO
A
O
O
N
P
O
CN
+
DMT
CU
Ru
b
5' CTCCTACACU Ru
(c)
6 5' CT CCT ACA CU Ru 3'
7 5' TCT CCT ACA CU Ru 3'

of the first coupling step lasted from 2-10 minutes. Cleavage of the products from the solid support was performed manually using concentrated aqueous ammonia. Incubation at room temperature for 15 hours followed by 3 hours at 55 °C provided optimal cleavage and deprotection conditions. Figure 4.3 shows the HPLC profile of the crude mixture of deprotected oligonucleotide **7**. The purity and composition of oligonucleotides **6** and **7** were verified by mass spectrometry and enzymatic digestion. MALDI-TOF (matrix-assisted laser desorption ionization/time-of-flight) mass spectra of **6** and **7** showed a single peak representing the singly charged species and having *m/e* ratios equal to 3425.73 (calc. 3425.56) and 3728.55 (calc. 3730.76), respectively (Figure 4.4). HPLC analysis of the enzymatic digestion products of **6** and **7** confirmed the presence of a single metallonucleoside **3** in each oligonucleotide (Figures 4.5 and 4.6).

Absorption. The electronic spectrum of **3** displays intense UV transitions (210, 238, 256, 284 nm) and a broad absorption band in the visible region (480 nm). The high-energy bands represent the bipyridine- and nucleoside-based π-π^* transitions. The feature at 480 nm represents multiple metal-to-ligand charge-transfer (MLCT) transitions due to the presence of the bipyridine and iminomethylpyridine groups coordinated to the ruthenium center (Chapter 5).[37-39] The electronic spectra of **6** and **7** display the same broad band in the visible region, verifying that **3** was successfully incorporated into these oligonucleotides (Figure 4.7). The π-π^* transitions of the oligonucleotide bases are unaffected by the presence of the metal complex.

Thermal Denaturation Studies. We investigated the thermal stability of a ruthenium-containing duplex to assess the influence of the metal complex on the overall DNA structure. Table 4.1 contains the sequences of the duplexes prepared in 50 mM

Figure 4.3: Ion-exchange HPLC trace of the crude mixture following synthesis, cleavage, and deprotection of oligonucleotide **7** (denoted by *; λ = 260 nm). Column type: Dionex NucleoPac 100. Gradient: 10-33% B over 1 minute, 33-44% B over 17 minutes (A = 10% acetonitrile; B = 10% acetonitrile, 1.5 M ammonium acetate). Flow rate: 1.0 mL/min; absorption monitored at 260 nm.

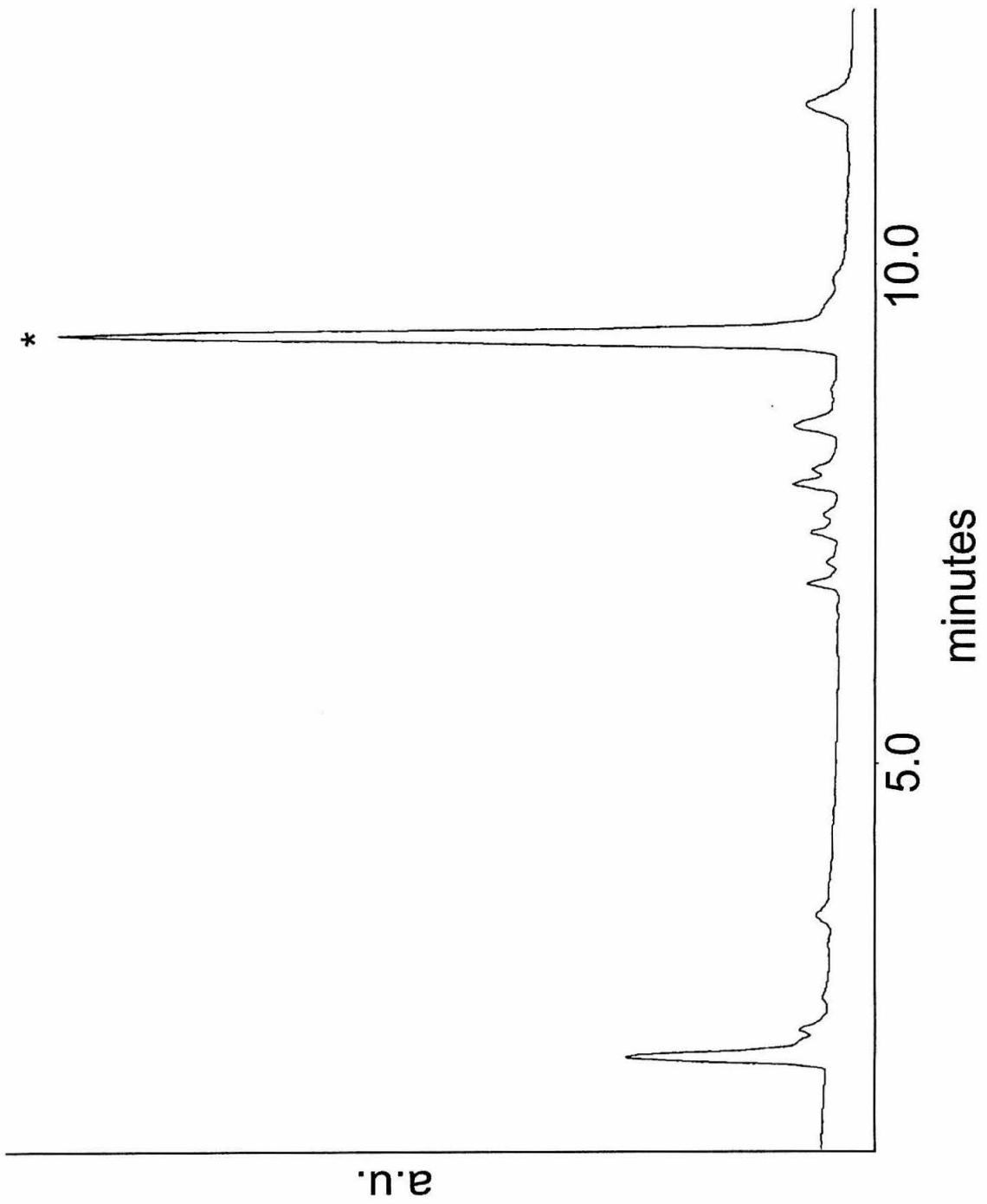
a.u.
*
5.0
10.0
minutes

Figure 4.4: MALDI-TOF mass spectra for ruthenium-containing oligonucleotides, **6** (top) and **7** (bottom). Calculated for **6**: 3425.56 $[M-H]^-$. Calculated for **7**: 3730.76 $[M-H]^-$.

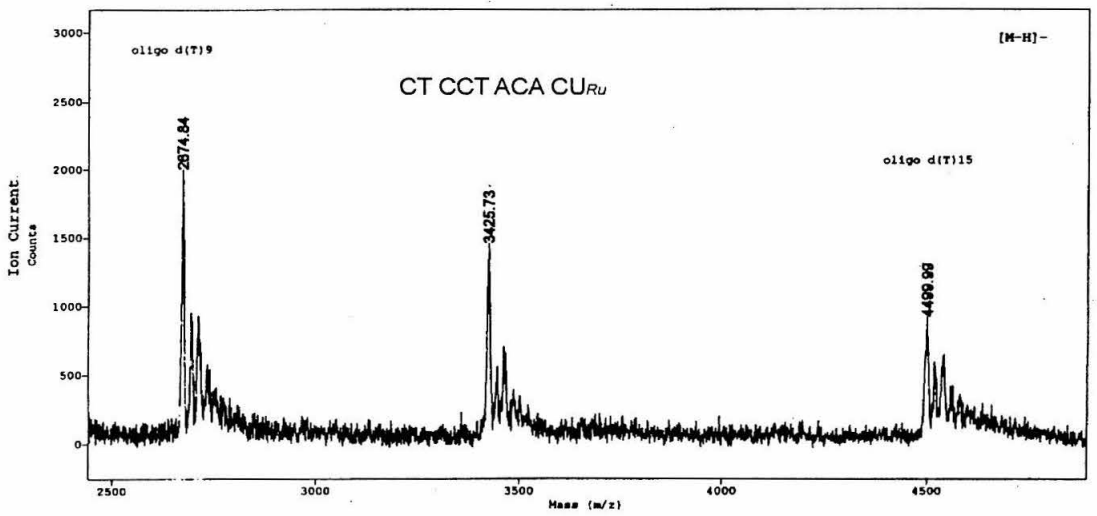
oligo d(T)9
[M-H]-
CT CCT ACA CURu
2874.84
3425.73
oligo d(T)15
4499.99
Ion Current
Counts
Mass (m/z)

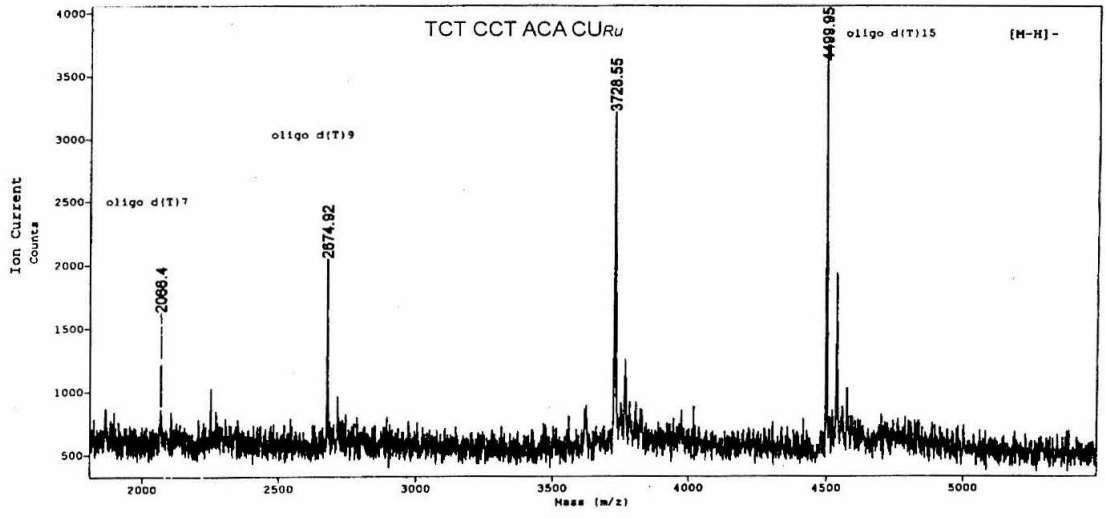
TCT CCT ACA CURu
4499.95
oligo d(T)15
[M-H]-
3728.55
oligo d(T)9
oligo d(T)7
2874.82
2088.4
Ion Current
Counts
Mass (m/z)

Figure 4.5: Products of enzymatic digestion of **6** as analyzed by reverse-phase HPLC. Sequence: 5′-CTCCTACACU$_{Ru}$. Integration of the peak areas gives 5C:2T:2A:1U$_{Ru}$ (λ = 260 nm). The peaks observed at t = 18.57 and 19.07 minutes display identical absorption spectra and represent the diastereomers of the ruthenium-containing nucleoside generated after complete digestion. See Experimental Section for additional information. The extinction coefficient for U$_{Ru}$ at 260 nm is 23300 M^{-1} cm^{-1}. Column: Prism C18. Gradient: 0-17% B over 15 minutes, then 17-75% B over 15 minutes. Solvent A = 0.1 M triethylamine acetate, pH 7.0, 2% acetonitrile; Solvent B = acetonitrile.

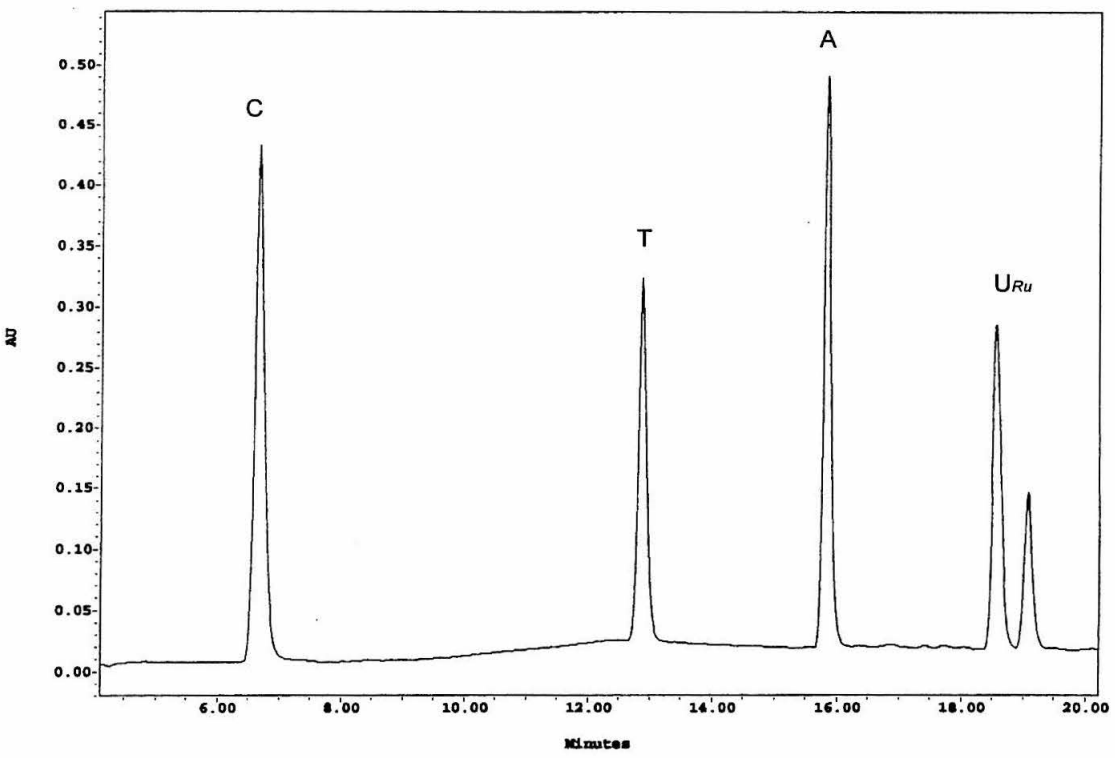
C
T
A
URu
AU
0.50
0.45
0.40
0.35
0.30
0.25
0.20
0.15
0.10
0.05
0.00
6.00
8.00
10.00
12.00
14.00
16.00
18.00
20.00
Minutes

Figure 4.6: Products of enzymatic digestion of **7** as analyzed by reverse-phase HPLC. Sequence: 5′-TCTCCTACACU$_{Ru}$. Integration of the peak areas gives 5C:3T:2A:1U$_{Ru}$ (λ = 260 nm). The peaks observed at t = 18.85 and 19.45 minutes display identical absorption spectra and represent the two diastereomers of the ruthenium-containing nucleoside generated after complete digestion. See Experimental Section for additional information. The extinction coefficient for U$_{Ru}$ at 260 nm is 23300 M^{-1} cm^{-1}. Column: Prism C18. Gradient: 0-17% B over 15 minutes, then 17-75% B over 15 minutes. Solvent A = 0.1 M triethylamine acetate, pH 7.0, 2% acetonitrile; Solvent B = acetonitrile.

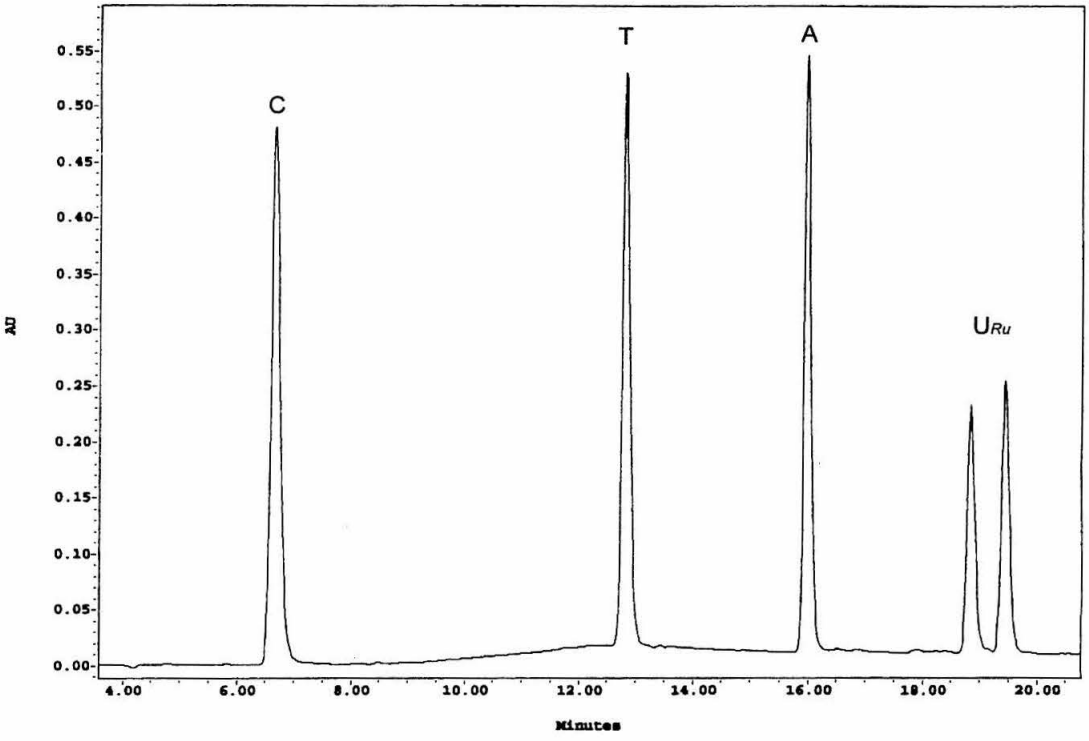
C
T
A
URu
AU
0.55
0.50
0.45
0.40
0.35
0.30
0.25
0.20
0.15
0.10
0.05
0.00
4.00
6.00
8.00
10.00
12.00
14.00
16.00
18.00
20.00
Minutes

Figure 4.7: Absorption spectra of **3** (top; methanol) and **7** (bottom; 0.05 M sodium phosphate, pH 7.0, 0.5 M sodium chloride) at room temperature. λ_{max} (ε, M^{-1} cm^{-1}) for **7**: 260 (109000), 480 (9100).

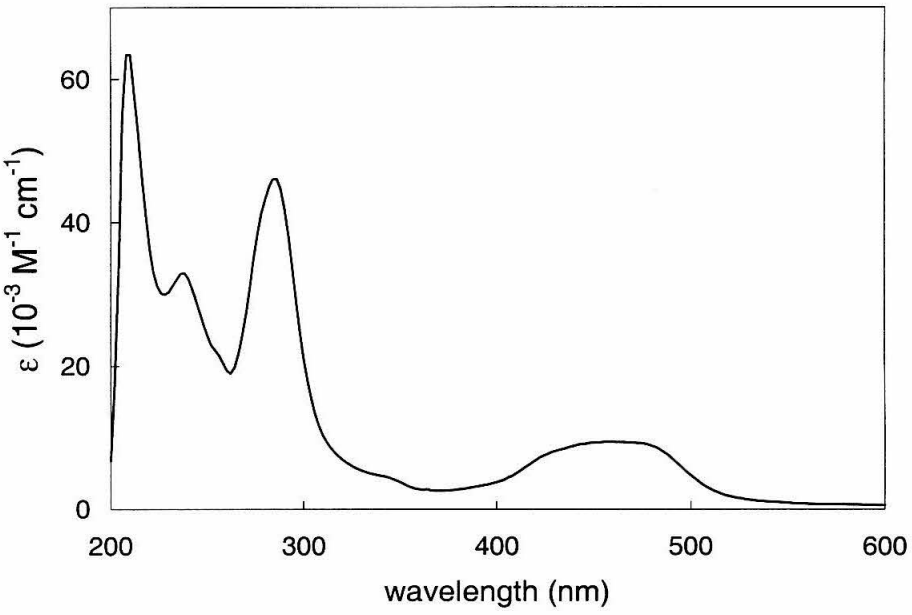
60
40
20
0
ε (10-3 M-1 cm-1)
200
300
400
500
600
wavelength (nm)

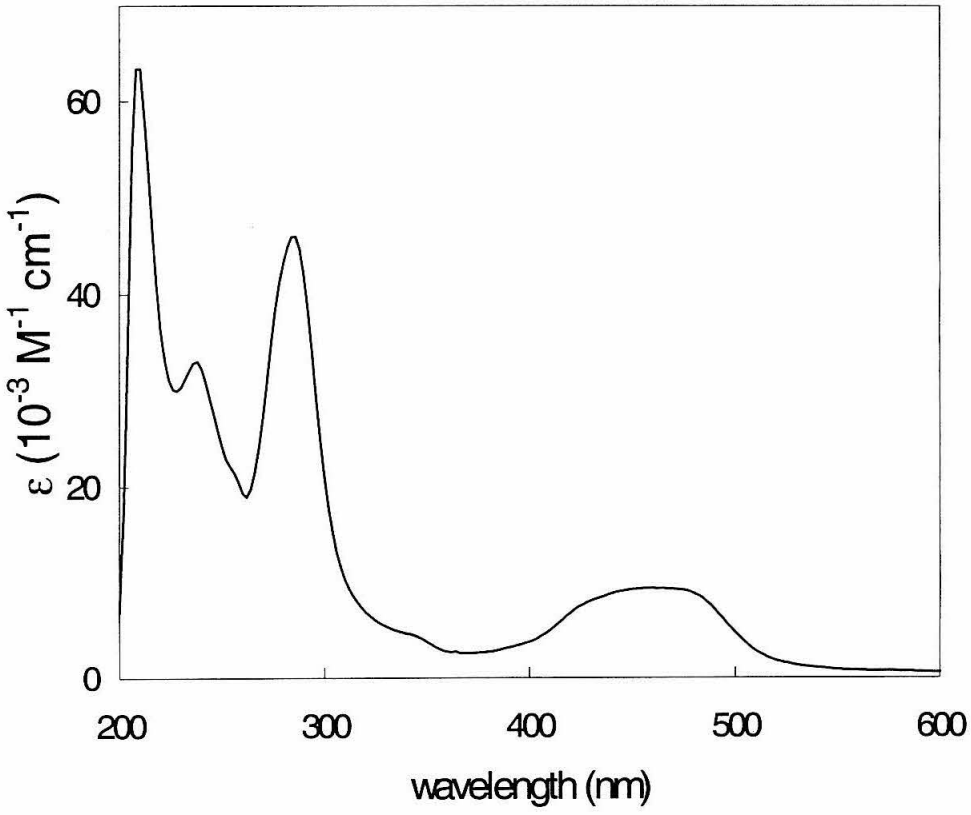
60
40
20
0
ε (10-3 M-1 cm-1)
200
300
400
500
600
wavelength (nm)

Table 4.1. Thermal Denaturation Temperatures for Metallated and Modified Oligonucleotides.[a]

sequence	abbreviation	modification	duplex	T_m (°C)[b]
5′ -TCTCCTACAC**U$_{Ru}$**	**7**	3′ **U$_{Ru}$**	**7•9**	49.5 ± 0.6
5′ -TCTCCTACACT	**8**	none	**8•9**	47.6 ± 0.2
5′ -AGTGTAGGAGA	**9**	none	-	-
5′-$_a$**U**CTCCTACAC**U$_a$**	**10**	3′ **U$_a$**, 5′ **U$_a$**	**10•9**	45.8 ± 0.5
5′-$_a$**U**CTCCTACAC**U$_b$**	**11**	3′ **U$_b$**, 5′ **U$_a$**	**11•9**	46.2 ± 0.5

[a] The symbol **U$_a$** denotes 2′-amino-2′-deoxyuridine; **U$_b$** denotes $N^{2'}$-(2-pyridylmethyl)-2′-amino-2′-deoxyuridine. [b] Values were determined in 0.05 M sodium phosphate buffer (pH 7.0) containing 0.5 M sodium chloride.

sodium phosphate buffer (pH 7.0) containing 0.5 M sodium chloride. The melting temperature (T_m) of the duplex formed by the unmodified oligonucleotide **8** and its complement **9** is 47.6 °C (Figure 4.8). The ruthenium-containing duplex formed by **7** and **9** exhibits a single, cooperative melting transition similar to the transition observed for the unmodified duplex. The T_m of **7·9** is 50.0 °C, 2 °C *higher* than that of **8·9**. Differences of a few degrees in the T_m values of metal-containing vs. unmodified duplexes are observed for duplexes containing other metal complexes.[12,19,27,32,33]

Electrochemistry. Voltammograms of **3** in dichloromethane display a reversible one-electron oxidation (1.6 V vs. normal hydrogen electrode, NHE), which represents the Ru(III/II) couple. This reduction potential compares well with that reported for the model system $[Ru(bpy)_2(impy)]^{2+}$, where impy = iminomethylpyridine (1.5 V vs. NHE, acetonitrile).[37] The Ru(III/II) reduction potential for **3** is slightly more positive than that of the model complex, suggesting that the proximity of the nucleoside to the metal center may be responsible for the small positive shift. This effect is observed for metallonucleoside **2** ($E_{1/2}$ = 0.29 V vs. NHE, ethanol) and $Ru(acac)_2(impy)$, where acac = acetylacetonate ($E_{1/2}$ = 0.23 V vs. NHE, ethanol).[31] Incorporation of **3** into an oligonucleotide, **7**, results in a Ru(III/II) couple of 1.3 V in aqueous solution (Figure 4.9).

Multiple ligand-centered reductions are observed (-0.8, -1.1, -1.3 V vs. NHE) for **3**; the most positive reduction is irreversible. Similar results have been reported for a series of $Ru(bpy)_2(\alpha,\alpha'\text{-diimine})^{2+}$ complexes.[37] Based on these values, estimates of the excited-state potentials of **3** are ($E^{3+/2+*}$) ~ -0.18 V and ($E^{2+*/1+}$) ~ 1.0 V vs. NHE, respectively.[40]

Additional discussion of these electrochemistry results can be found in Chapter 5.

Figure 4.8: Thermal denaturation curves for duplex **8·9** (□) and metal-containing duplex **7·9** (♦). Sequences are given in Table 4.1. Buffer: 50 mM sodium phosphate (pH 7.0), 500 mM sodium chloride.

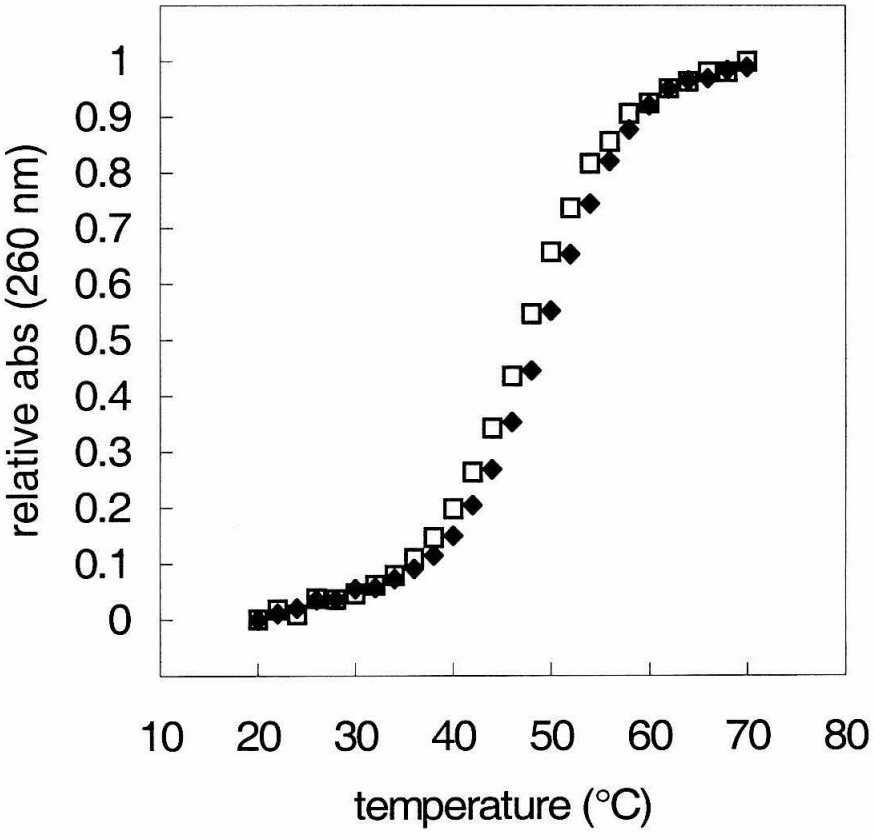
relative abs (260 nm)
1
0.9
0.8
0.7
0.6
0.5
0.4
0.3
0.2
0.1
0
10
20
30
40
50
60
70
80
temperature (°C)

Figure 4.9: Square-wave voltammogram of oligonucleotide **7** in 50 mM sodium phosphate (pH 7.0) containing 500 mM sodium chloride.

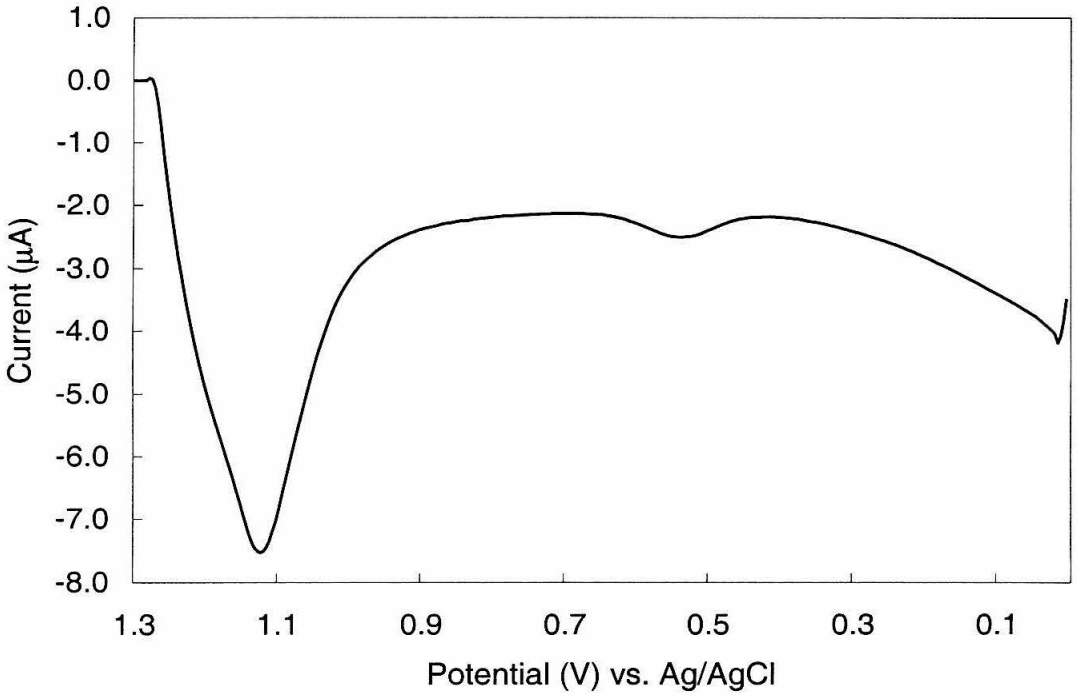
1.0
0.0
-1.0
-2.0
-3.0
-4.0
-5.0
-6.0
-7.0
-8.0
Current (µA)
1.3
1.1
0.9
0.7
0.5
0.3
0.1
Potential (V) vs. Ag/AgCl

Emission. Steady-state emission spectra of metallonucleoside **3** and oligonucleotide **7** show similar profiles. Excitation of either **3** or **7** at 480 nm produces an emission maximum at 730 nm, with a shoulder near 810 nm (Figure 4.10). The excited-state lifetimes are strictly monoexponential and are independent of solvent: 44 ns for **3** (aqueous methanol) and 42 ns for **7** (phosphate buffer). However, the quantum yield of **3** is slightly greater than that of **7** (Table 4.2). These observations support the assertion that the lowest electronically excited state is the same for both the metallonucleoside and ruthenium-containing oligonucleotide (Chapter 5).[31]

The absence of any significant differences in the lifetimes of **3** and **7** demonstrates that the bases contained in **7** (adenine, cytosine, thymine) do not quench the luminescent MLCT state. The addition of the guanine-rich complementary strand **9** to **7** does not alter the excited-state lifetime, suggesting that (1) hybridization does not influence the emissive properties of the incorporated ruthenium complex and (2) the photoexcited species does not oxidize guanine, the most easily oxidized base ($E^{+\bullet/0}$ = 1.3 V vs. NHE, pH 7).[41] Absorption spectra recorded at various time points after initial excitation confirm this assessment. Data collected at multiple wavelengths did not indicate guanine oxidation (Appendix C).

The addition of quenchers known to generate potent Ru(III) oxidants from photoexcited Ru(II) polypyridyl species does not lead to detectable guanine oxidation.[42] For example, oxidative quenching of photoexcited **7**·**9** by $[Ru(NH_3)_6]^{3+}$ is described by linear plots of the observed decay rate constant (k_{obs}) vs. quencher concentration under conditions of high ionic strength (bimolecular quenching constant, k_q =1.1 x 10^8 M^{-1} s^{-1}). However, high concentrations of quencher (150-1500-fold excess of $[Ru(NH_3)_6]^{3+}$ or

Figure 4.10: Steady-state emission spectrum of **3** in aerated methanol (λ_{exc} = 480 nm, λ_{max} = 730 nm).

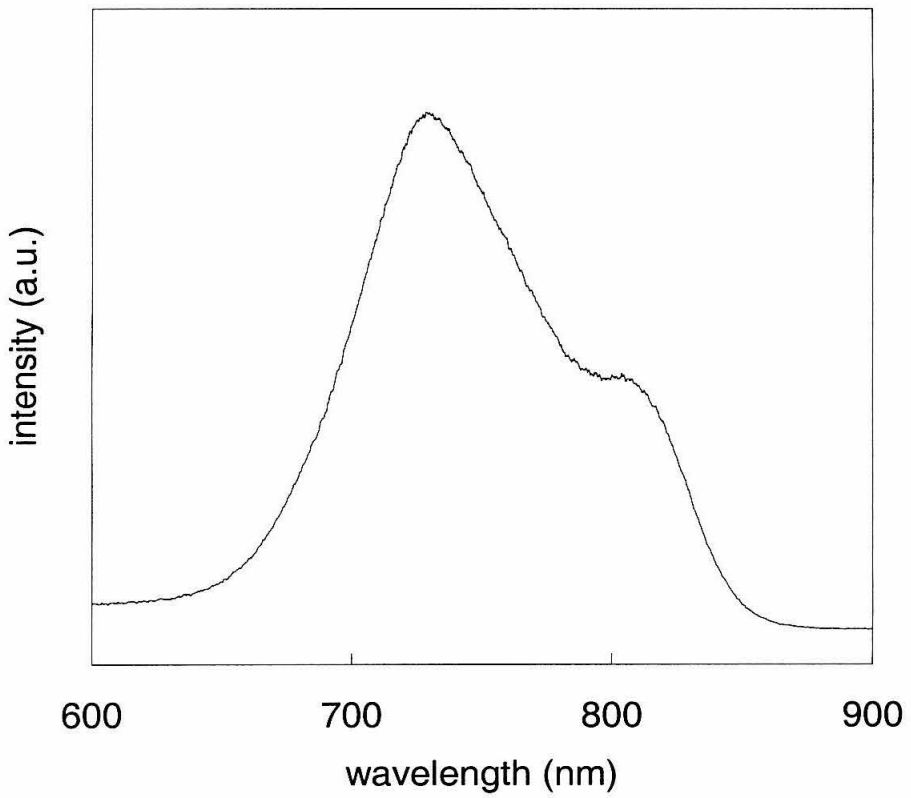
intensity (a.u.)
600
700
800
900
wavelength (nm)

Table 4.2. Absorption and Emission Data for $Ru(bpy)_2(impy)^{2+}$ Derivatives at Room Temperature.[a]

compd	λ_{max} (abs)[b]	λ_{max} (em)[c]	τ [d]	ϕ_{em} [e] x 10^{-3}
$Ru(bpy)_2(impy)^{2+}$	470	-	-	-
3	480	730	44	0.53
7	480	725	42	0.11
7•9	480	725	42	-

[a] Concentrations ranged from 10-40 μM. [b] Measured in aqueous solution or methanol. [c] Emission maxima determined from steady-state emission spectra collected with aerated solutions (in MeOH for **3**, in water for samples containing **7**). [d] Lifetimes determined from monoexponential fits of the luminescence decay observed at 720 nm in degassed solutions (in 25% MeOH for **3**, in 0.05 M sodium phosphate, pH 7.0, 0.5 M NaCl for all samples containing **7**). [e] Quantum yields for emission calculated using $Ru(bpy)_3Cl_2$ as an actinometer.

methyl viologen) are required to effect a ~ 10% decrease in the excited-state lifetime of **7**. Absorption spectra recorded 5 μs after excitation indicate that the yield of generating Ru(III) following oxidative quenching is low (Appendix C).

Discussion

Incorporation Strategy. The solid-phase incorporation of nucleoside monomers containing metal complexes attached directly to the ribose ring has gone unexplored until recently.[31,32] This is primarily due to the difficulty of introducing substituents to the ribose ring of the nucleoside (Chapter 2). Nevertheless, this site is an attractive location for modifications since reporter molecules incorporated here may cause fewer perturbations to the secondary duplex structure than those attached to the nucleoside base. Additionally, the selective placement of metal complexes at various locations on the nucleoside (base and ribose positions) allows for comparative studies regarding electron transfer pathways in nucleic acids.

There are numerous constraints associated with incorporating modified nucleosides during automated solid-phase DNA synthesis.[43-46] The most demanding of these include the mildly acidic and strongly basic conditions to which the solid support is repeatedly exposed during synthesis. The choice of metallonucleoside **3** is motivated by its observed stability under these conditions. While higher yields (60-74%) for succination are observed for unmetallated nucleosides containing 2′ substituents (Chapter 2), the modest yield for succination of **3** (43%) indicates that the metal complex inhibits this reaction (Figure 4.1). The successful derivatization of the solid support with the succinated metallonucleoside demonstrates that a large, cationic metal complex can be tolerated in the conjugation reaction.

The utility of solid supports pre-derivatized with metallonucleosides is validated by the rapid, large-scale synthesis of 10- and 11-mer oligonucleotides containing $[Ru(bpy)_2(impy')]^{2+}$ (impy′ = nucleoside **1**) complexes at the 3′ termini. Analysis of the crude oligonucleotide mixture following cleavage from the solid support reveals an efficient synthesis (integration at 260 nm indicates a yield of 70% prior to HPLC purification, as shown in Figure 4.3). Clearly, this methodology may be extended to other transition metal complexes incorporated into nucleosides at either ribose or base positions, provided that the metal complex is stable to the conditions of oligonucleotide synthesis.

Effect of Metal Complexes on Duplex Stability. Thermal denaturation studies serve as an indication of how the incorporated label influences the duplex stability. In the case of metal-containing duplexes, it is difficult to ascertain from the T_m value if the cationic nature of a non-intercalating metal complex partially offsets the destabilization caused by the modification. For the metal-containing duplex **7·9**, the T_m value is slightly higher than the T_m of the unmodified duplex **8·9** (50 °C vs. 48 °C, respectively). Modified duplexes of similar sequence serve as a useful comparison to duplex **7·9**; they contain nucleosides with unmetallated substituents at the same ribose position (Table 4.1). The duplexes **10·9** and **11·9** contain the modified nucleosides at both the 3′ and 5′ ends of the strands, whereas duplex **7·9** contains a single metal complex at the 3′ end. Despite the fact that the nucleosides with unmetallated 2′-substituents favor the same sugar conformation adopted by 2′-deoxynucleosides, the T_m values of the resulting duplexes are slightly below the melting temperature of the unmodified duplex (Chapter

2).[47] This comparison suggests that the presence of the cationic metal complex compensates for some of the destabilizing effects induced by the 2′ modification.

Our observation that the T_m for duplex **7·9** is two degrees *higher* than the T_m of the unmodified duplex **8·9** contrasts with reports describing T_m values of duplexes end-labeled with other metal complexes (Chapter 1).[12,19,27,32,33] All of these duplexes contain metallonucleosides at the 5′ end, as opposed to the 3′ end. The T_m values are either essentially unchanged or lower by a few degrees relative to the melting temperatures of the unmodified duplexes.[21,27,29,32,48] An exception to this trend occurs when $[Ru(bpy)_2(bpy')]^{2+}$ is tethered to the 5′-terminal phosphate group: the T_m of the metal-containing duplex is 18 degrees lower than the value of the unmodified duplex (42 °C vs. 60 °C).[29] This result suggests that tethering a cationic metal complex to the 5′-terminal phosphate group has a large destabilizing influence on the duplex; the absence of a nucleoside at the end of the duplex may be responsible for the lowered duplex stability.

Absorption. The electronic spectrum of metallonucleoside **3** displays a broad absorption band with maximum at 480 nm (ε = 9100 M^{-1} cm^{-1}) that is red-shifted from λ_{max} = 470 nm (ε = 13600 M^{-1} cm^{-1}) for the model complex $[Ru(bpy)_2(impy)]^{2+}$ (Table 4.2).[38] The slight difference in λ_{max} for the model complex and the metallonucleoside reveals the effect of replacing the impy ligand with an impy derivative possessing a ribose substituent on the imino nitrogen. The metal-containing oligonucleotides **6** and **7** display visible absorption bands identical to those of **3**, demonstrating that incorporation does not alter the electronic properties of the metallonucleoside.

Similar trends are observed for oligonucleotides containing derivatives of $[Ru(bpy)_3]^{2+}$. Changes in the absorption maximum occur when the model complex (i.e., $[Ru(bpy)_3]^{2+}$) is modified to accommodate linkers required for oligonucleotide attachment (Table 4.3). The resulting monomer complex (i.e., $[Ru(bpy)_2(bpy')]^{2+}$, where bpy′ denotes a substituted bipyridine ligand containing the linker) displays an absorption maximum that is unchanged or slightly red-shifted from λ_{max} for $[Ru(bpy)_3{}^{2+}]$.[49] Typically, incorporation of the monomer complex into an oligonucleotide does not alter λ_{max} for the metal-containing oligonucleotides (Table 4.3).

Emission. The emission spectra of **7** and **7·9** are virtually identical to that of the precursor **3**, indicating that both incorporation into an oligonucleotide and hybridization of the metal-containing strand do not alter the emissive properties of the metal complex (Table 4.1). This result is in contrast to the changes in the emissive behavior of monomer complexes based on $[Ru(bpy)_3]^{2+}$ (Table 4.3). In most cases, these complexes exhibit emission maxima shifted from 628 nm to lower energy (660-675 nm). When the monomer complexes are incorporated into oligonucleotides, the emission maxima are unchanged or shifted to lower energy. An exception to this trend is a 16-mer oligonucleotide containing a $[Ru(bpy)_2(bpy')]^{2+}$ complex attached to the base of a nucleoside located mid-strand; the emission maximum is centered at 660 nm, blue-shifted from the corresponding value of the monomer complex (675 nm).[28,48]

The excited-state lifetime of **3** does not change upon incorporation into an oligonucleotide and subsequent duplex formation. This result contrasts with observations made for many of the metal-containing oligonucleotides in Table 4.3. The lifetimes of both single- and double-stranded oligonucleotides are dramatically different from those

Table 4.3. Absorption and Emission Data for Ru(II) Polypyridyl Complexes Incorporated into Oligonucleotides.[a]

compd	λ_{max} (abs)	λ_{max} (em)	τ (μsec)	Ref.
$Ru(bpy)_3^{2+}$	452	628	0.65	49
$Ru(bpy)_2(impy)^{2+}$	470	-	-	37
3[b]	480	730	0.044	
7	480	725	0.042	
7•9	480	725	0.042	
$Ru(bpy)_2(bpy')^{2+}$	460	670	0.407	29
5′-^{X}TCAACAGTTTGTAGCA	465	670	0.616	
Duplex			0.629	
$Ru(bpy)_2(bpy')^{2+}$	454	675	0.485	28,48
5′-TCAACAG**X**TTGTAGCA	450	660	0.544	
Duplex			0.594	
$Ru(bpy)_2(bpy')^{2+}$	450	666	0.430	32
5′-**X**TCAACAGTTTGT	450	677	0.572	
Duplex			0.586	
$Ru(bpy)_2(bpy')^{2+}$[c]	468	665	0.850	30
5′-TTTT-**X**-AAAA	468	665	0.815	
5′-GGG-**X**-CCC	468	665	0.790	
5′-GCAATTGC-**X**-GCAATTGC	468	665	0.608	
$Ru(bpy)_2(phen')^{2+}$[d]	450	629	-	27
5′-TCGGCGCGAA**X**TCGCGTGCC	456	630	-	
Duplex			-	
$Ru(bpy)_2(bpy')^{2+}$	460	660	-	12
5′-GCAC^{X}TCAG	460	660	-	
Duplex			-	

[a] Values measured in buffered aqueous solution (pH 7.0) at room temperature unless otherwise noted. **X** denotes metal attachment to oligonucleotide via linker to nucleoside base, ribose, or phosphate. Please see individual references for details of metal attachment for each system. [b] Measured in aqueous methanol solution. [c] Measured in unbuffered aqueous solution. [d] Monomer complex values measured in acetonitrile.

of the monomer complexes, despite identical experimental conditions. Lewis and coworkers observe a decrease in the lifetime of single-stranded oligonucleotides containing a $[Ru(bpy)_2(bpy')]^{2+}$ label.[30] The lifetimes of two short strands are within 10% of the value for the monomer complex; a third strand forms a hairpin structure at high ionic strength and exhibits a lifetime that is 30% shorter compared to the lifetime of the monomer complex. Conversely, Grinstaff and coworkers report an increase in the lifetime values upon both incorporation and hybridization of three separate $[Ru(bpy)_2(bpy')]^{2+}$ derivatives, regardless of the attachment linkage or placement of the metal complex within the duplex.[29,32,48]

A rationale for the contrasting changes in the excited-state lifetime values of the metal-containing oligonucleotides summarized in Table 4.3 is unclear. The decrease in excited-state lifetime reported by Lewis for the single-stranded vs. hairpin oligonucleotides could be attributed to structural differences between the conformations available to the strands. The two 8-mer strands do not form well-defined hairpin structures at high ionic strength; therefore, the emission lifetimes for these oligonucleotides are expected to resemble that of the monomer complex.[30] The 16-mer oligonucleotide forms a stable hairpin structure, and this structural difference may cause the observed decrease in the excited-state lifetime.[50] However, the increase in lifetime values upon both incorporation and hybridization reported by Grinstaff may be due to interactions between the metal complex and the duplex not operative in Lewis' hairpin assembly. Subtle factors involving duplex conformation and ionic strength may be responsible for these trends.

Guanine Oxidation. The absence of any significant differences in the lifetimes of **3**, **7**, and **7·9** demonstrates that the bases contained in **7** or **9** do not quench the photoexcited $[Ru(bpy)_2(impy')]^{2+}$. Although guanine is the most facile electron donor of the DNA bases ($E^{+\bullet/0}$ = 1.3 V vs. NHE, pH 7),[41] oxidation by photoexcited **7** is not favored thermodynamically ($E^{2+*/1+}$ ~ 1 V vs. NHE). Even the addition of oxidative quenchers fails to result in any oxidative damage to the DNA bases of **7·9**, despite generating a Ru(III) species that is a powerful oxidant ($E_{1/2}$ = 1.3 V).

Modest decreases in the excited-state lifetimes of **7** and **7·9** are observed in the presence of large excess of oxidative quenchers. In the case of $[Ru(NH_3)_6]^{3+}$, the bimolecular quenching constant determined for the quenching of photoexcited **7·9** is one order of magnitude smaller compared to the value measured for the quenching of $[Ru(bpy)_3]^{2+}$ (1.1×10^8 vs. 2×10^9 M^{-1} s^{-1}, respectively).[42] However, the driving force estimate (ΔG_q) for the single electron transfer from $[Ru(NH_3)_6]^{3+}$ to photoexcited **7·9** is approximately –0.24 eV, much smaller than the value calculated for $[Ru(bpy)_3]^{2+*}$ (–0.92 eV).[42,51] Oxidative quenching by methyl viologen is thermodynamically unfavorable (ΔG_q = 0.26 eV). Despite the large difference in ΔG_q for the two quenchers, the addition of either quencher in large excess to **7** or **7·9** generates small amounts of oxidized product.

Conclusion

We report the first method of synthesizing a metal-containing solid support for use in automated DNA synthesis. This achievement represents a significant advance in the development of metal-containing oligonucleotides. While the solid support employed here is glass-based, the method is applicable to other solid supports containing any long-

chain alkylamine linker. Succination yields for nucleosides containing metal complexes at locations other than the 2′ position are expected to be much higher, due to the absence of steric constraints. This methodology may be extended to other transition metal complexes, provided that the metal complex is stable to the conditions of oligonucleotide synthesis. The preparation of a metal-containing solid support provides the opportunity to generate oligonucleotides with metal complexes placed at 3′, intervening, and 5′ positions of the duplex when combined with other solid-phase incorporation methods (Appendix D).[21-25,27-29,32]

Thermal denaturation studies of the modified duplexes indicate that the presence of metallonucleoside **3** at the 3′ terminus compensates for part of the destabilizing effects induced by placing a chelating ligand at the 2′ ribose position. The metal-containing strands exhibit electrochemical and spectroscopic features nearly identical to those of the individual metallonucleoside. The absence of any change in these properties upon metallonucleoside incorporation into oligonucleotides and subsequent hybridization suggests that the $Ru(bpy)_2(impy)^{2+}$ chromophore is a valuable probe for DNA-mediated ET studies.

Experimental Section

General Materials and Methods. All reagents were of the highest purity available from commercial sources and used as received. All solvents were of spectrophotometric quality or better. Aqueous solutions were prepared from Millipore purified water with resistivity of 18 MΩ-cm. Flash chromatography was performed on alumina (basic, activated Brockmann I, 150 mesh) from Aldrich. Thin-layer chromatography (TLC) was

performed on Merck precoated silica plates (60 F_{254}, 5 x 7.5 cm). Analytical HPLC was performed using reverse phase Prism C18 column (Keystone Scientific, 4.6 x 250 mm, 5 μm, 100 angstrom), using one of the following gradients: (1) 0-17% B over 15 minutes, then 17-75% B over 15 minutes; (2) 0-100% B over 30 minutes; (3) 0-40% B over 15 minutes (where A = 0.1 M triethylamine acetate, pH 7.0, 2% acetonitrile; B = acetonitrile). Controlled pore glass (LCAA-CPG, 500-angstrom pore size) was obtained from Peninsula Laboratories. Oligonucleotide synthesis was carried out on an Applied Biosystems Incorporated 394 DNA synthesizer using standard protocols. DNA synthesis reagents were purchased from Glen Research. Enzymes were purchased from Pharmacia.

Instrumentation. Steady-state absorption spectra were obtained using a Hewlett-Packard HP8452A diode array spectrophotometer. HPLC was performed using a Waters 600E Controller equipped with a 994 Diode Array Detecter. Steady-state emission spectra were obtained with a Hitatchi F-4500 Fluorescence Spectrophotometer using a Xe arc lamp as the light source and the following instrumental parameters: 10 nm slits, 750 V PMT, 480 nm excitation, and 500-900 nm observation range. All spectra are blank-subtracted. Quantum yield measurements were calculated using $[Ru(bpy)_3]^{2+}$ as an actinometer. Time-resolved measurements (emission and transient absorption) were conducted in the Beckman Institute Laser Resource Center as previously described.[52] Electrochemical measurements were conducted at room temperature with a CH Instruments 660 electrochemical workstation. Data were collected in a traditional two-compartment cell using a polished and sonicated 3 mm-diameter glassy carbon or platinum disk working electrode, Pt wire auxiliary electrode, and Ag/AgCl reference

electrode. Solutions for electrochemical measurements were performed either in dichloromethane containing 0.1 M n-tetrabutylammonium hexafluorophosphate or in sodium phosphate buffer (50 mM, pH 7.0, 0.5 M sodium chloride, nanopure water), and were deaerated under argon.

Approximately 10-30 nanomoles of purified oligonucleotide was subjected to enzymatic digestion analysis. The digest cocktail (55 μL/sample) contained bacterial alkaline phosphatase (4 μL, 10 μL/unit) and snake venom phosphodiesterase (2.4 μL, 1 mL/mg), in 1 M $MgCl_2$ (0.8 μL), 0.5 M Tris buffer, pH 7.5 (3.5 μL). The reaction mixture was incubated at 37 °C for 8-16 hours. The reaction was quenched by the addition of 200 μL of Buffer A (see HPLC section above). The products were analyzed by reverse-phase HPLC. The resulting peaks were compared against the appropriate set of nucleoside standards for that given oligonucleotide sequence. Two peaks with identical absorption spectra were observed for the ruthenium-containing nucleoside; the sum of the integrated areas of these peaks corresponds to one ruthenium-containing nucleoside relative to the other nucleosides (ε_{260} for **3** = 23300 M^{-1} cm^{-1}). This observation of two peaks is explained by the fact that the isomers of **3** and **4** were not separated prior to coupling to the solid support. Independent synthesis of the detritylated form of **3** produced two diastereomers that elute as two peaks upon HPLC injection under similar conditions (see Appendix B for synthetic details).

Thermal denaturation curves were collected using a Hewlett-Packard HP 8452A diode array spectrophotometer equipped with a Peltier temperature controller (20-70 °C range). Individual oligonucleotides were hybridized to their complementary strands in 50 mM sodium phosphate (pH 7.0) containing 0.5 M sodium chloride, to give solutions that

were 2.7 μM in each strand. The samples were heated for 20 minutes at 70 °C and slowly cooled to 4 °C overnight. Thermal denaturation values were calculated from absorbance changes at 260 nm as the average of the heating and cooling traces collected for each hybrid; values were obtained from 2-4 separate heat-cool cycles.

Synthesis of $[Ru(bpy)_2(1)](PF_6)_2$ (3): 2'-amino-5'-O-(4,4'-dimethoxytrityl)-2'-deoxyuridine (1.8 g, 3.31 mmol) was dissolved in ethanol (30 mL) containing molecular sieves, and the solution was flushed with argon for 15 minutes. 2-pyridinecarboxaldehyde (295 uL, 3.1 mmol) was added incrementally, and the reaction was refluxed for 6 hours. The solution was cooled, filtered to remove the molecular sieves, and evaporated to dryness under reduced pressure to give the intermediate nucleoside **1**. (Electrospray mass spectral analysis of an aliquot of crude **1** found 635.2 $[M+H]^+$; calculated for $[M+H]^+$, 635.14. See Appendix A for additional details.) The residue was re-dissolved in EtOH (180 mL) and $Ru(bpy)_2Cl_2$ (1.6 g, 3.31 mmol) was added to the solution. The reaction was refluxed over molecular sieves for 4 hours under argon. The solution was filtered, and the solvent was removed under reduced pressure. The residue was purified by flash chromatography [(a) silica, 2% saturated aqueous KNO_3, 7% water in acetonitrile; (b) basica alumina after conversion to the PF_6^- salt, 0.5% saturated aqueous KPF_6, 2.5% water in acetonitrile]. The product fractions were concentrated, dissolved in dichloromethane, and filtered to remove excess salt. The product was obtained as a red film (yield 19%). ^{1}H-NMR (500 MHz, CD_3CN, Figure 4.11) δ 7.15-8.5 (mm, 31H), 6.89 (d, 4H), 6.60 (d, 1H), 6.35 (d, 1H), 5.39 (d, 1H), 4.77 (d, 1H), 4.18-4.20 (m, 2H), 3.79-3.84 (m, 6H), 2.87-3.04 (m, 2H). UV-vis (MeOH) nm

Figure 4.11: 500 MHz NMR spectrum of **3** in CD_3CN. (Asterisks denote peaks for which the integration is less than 0.8/H).

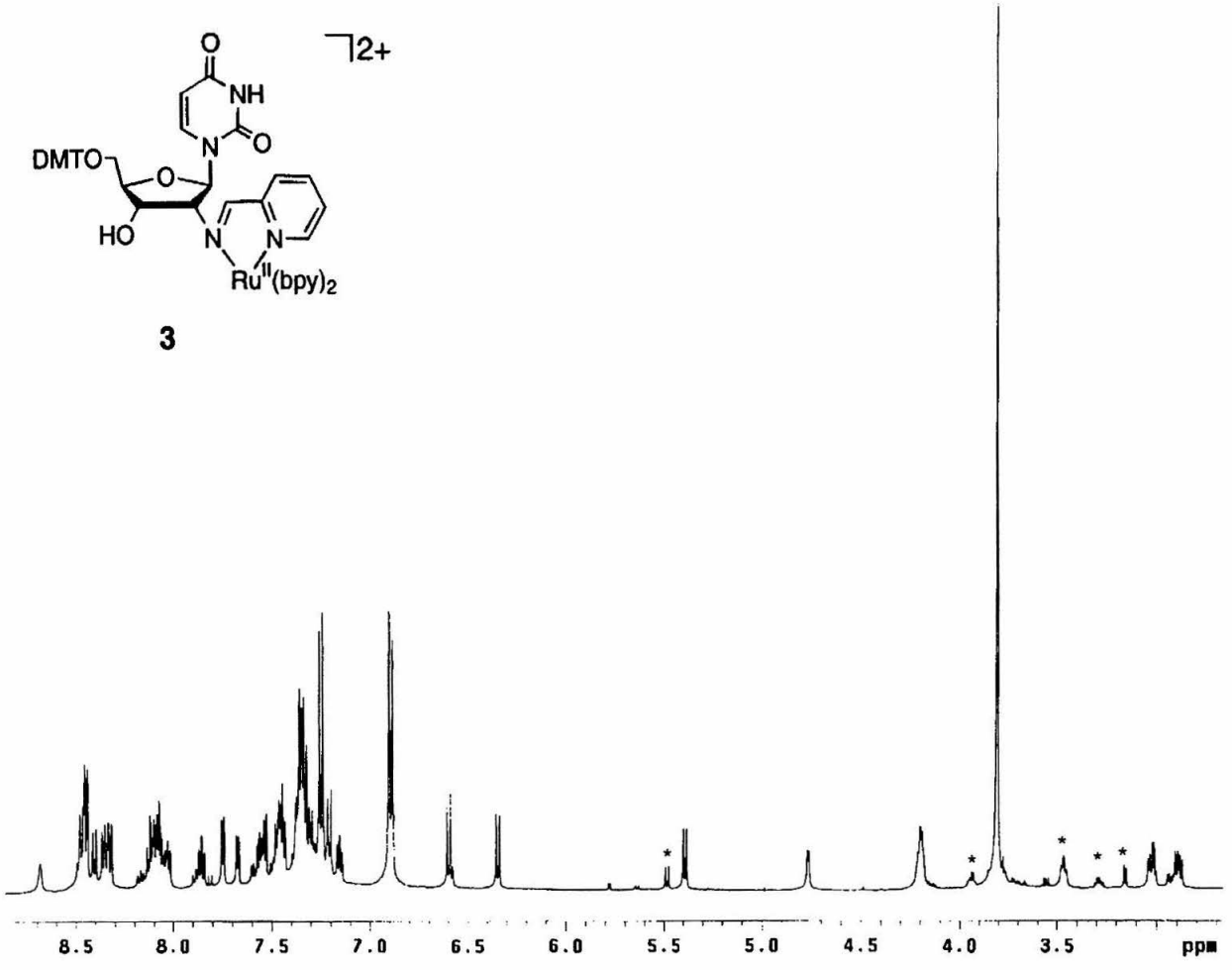
O
NH
O
N
DMTO
O
HO
N
N
Ru^II(bpy)2
2+
3
8.5
8.0
7.5
7.0
6.5
6.0
5.5
5.0
4.5
4.0
3.5
ppm

(ε, M^{-1} cm^{-1}): 210 (70100), 238 (38900), 256 (25800), 284 (51900), 480 (9100). ESI-MS calculated for $C_{56}H_{50}N_8O_7RuPF_6$ $[M]^+$ 1193.08, found 1193.0 $[M]^+$ (Figure 4.12). Analytical HPLC with gradient 3: t = 24.09 minutes (Figure 4.13).

Synthesis of Ru(bpy)$_2$(1-succinate)(PF$_6$)$_2$ (4): To a solution of **3** (46.5 mg, 35 μmol) and dimethylaminopyridine (2.1 mg, 17.5 μmol) in 0.5 mL anydrous pyridine was added succinic anhydride (3.1 mg, 31.5 μmol). The reaction was stirred for 19 hours at room temperature under an argon atmosphere. The solvent was removed under reduced pressure and the residue was co-evaporated with toluene. The residue was purified by flash chromatography (basic alumina, 1% saturated aqueous KNO_3, 19% water in acetonitrile). The product fractions were combined and the acetonitrile was removed. A saturated aqueous solution of ammonium hexafluorophosphate was added to the resulting solution to precipitate the product. The red solid was collected by filtration and dried under vacuum (yield 54%). ESI-MS calculated for $C_{60}H_{54}N_8O_{10}RuPF_6$ $[M]^+$ 1293.26, found 1293.2 $[M]^+$ (Figure 4.14). Several attempts to obtain a ^1H NMR spectrum of **4** were unsuccessful due to the presence of trace amounts of **3** in the sample. Preliminary results showed peaks diagnostic of the protons on the succinate arm in the region 2.6-2.95 ppm (CD_3CN, 500 MHz).

Synthesis of Ru-Solid Support (5): To a solution of **4** (179 mg, 125 μmol) in 4 mL of anhydrous dichloromethane was added anhydrous triethylamine (350 μL), HOBT (22.6 mg, 166 μmol), and BOP (91, 205 μmol). This solution was transferred to a flask containing long-chain alkylamine-controlled pore glass (LCAA-CPG) (250 mg, 500 Å

Figure 4.12: ESI mass spectra of **3** obtained in positive ionization mode.

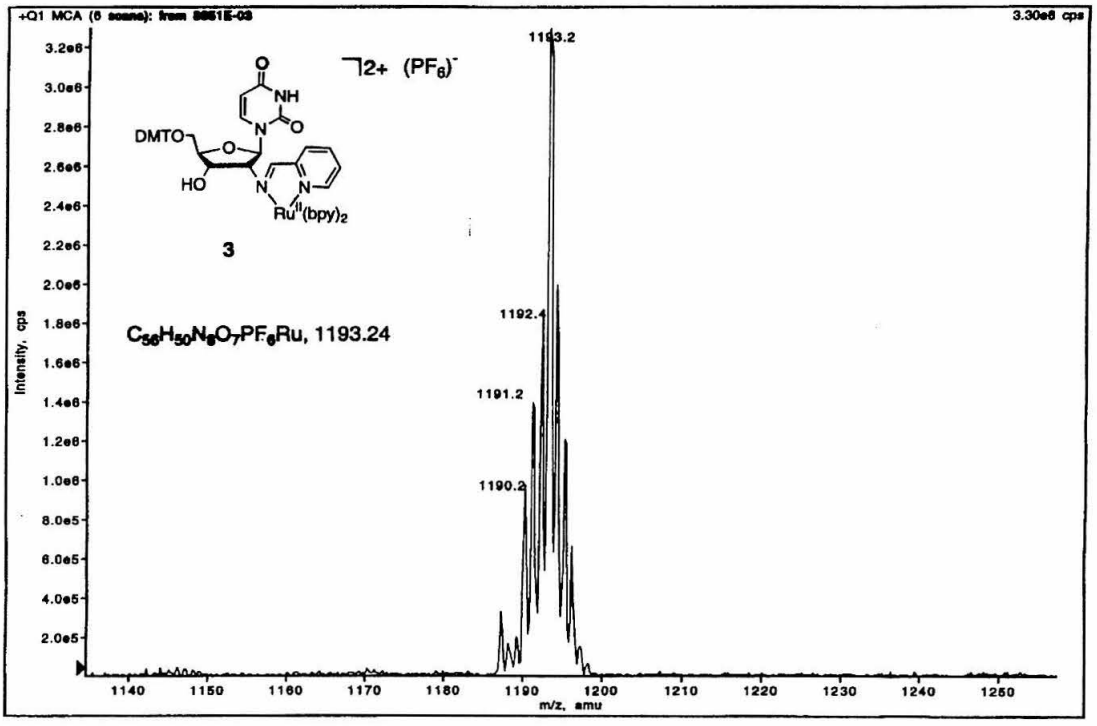
+Q1 MCA (6 scans): from 8851E-03
3.30e6 cps
1193.2
2+ (PF6)-
DMTO
HO
NH
O
N
Ru(bpy)2
3
C56H50N8O7PF6Ru, 1193.24
1192.4
1191.2
1190.2
Intensity, cps
m/z, amu

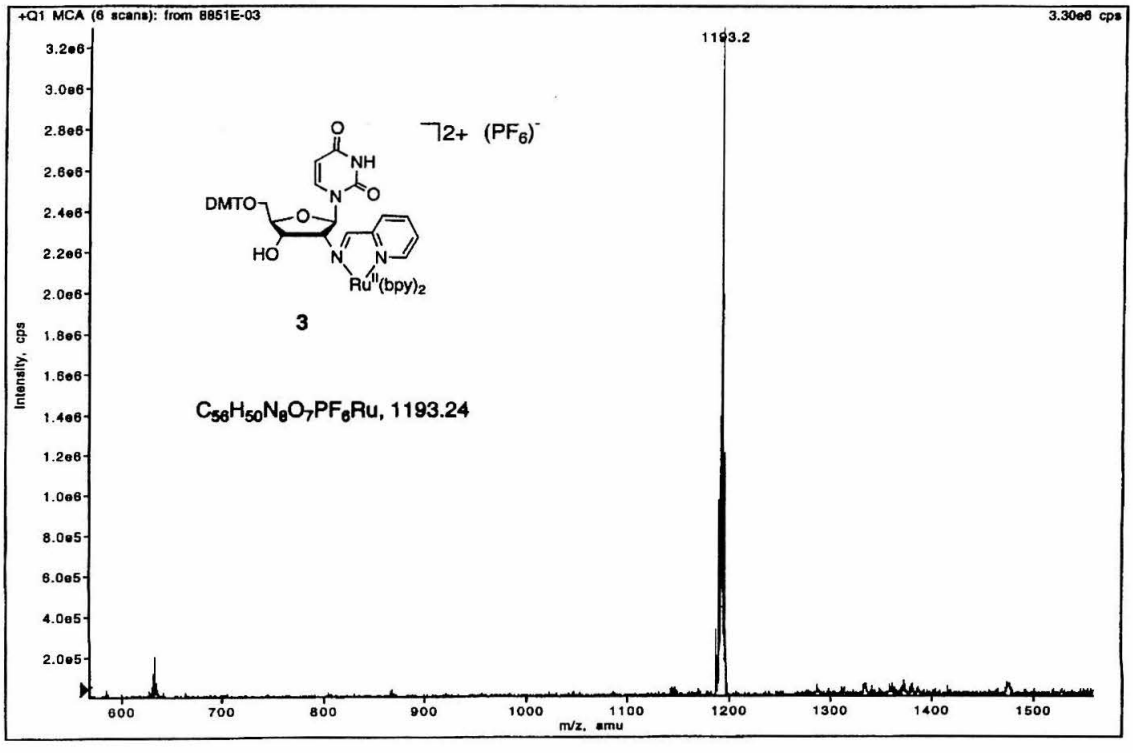
+Q1 MCA (6 scans): from 8851E-03
3.30e6 cps
1193.2
2+ (PF6)-
DMTO
HO
NH
O
N
Ru(bpy)2
3
C56H50N8O7PF6Ru, 1193.24
Intensity, cps
m/z, amu

Figure 4.13: Analytical HPLC trace of **3**. Column: Prism C18. Gradient: 0-40% B over 15 minutes. Solvent A = 0.1 M triethylamine acetate, pH 7.0, 2% acetonitrile; Solvent B = acetonitrile.

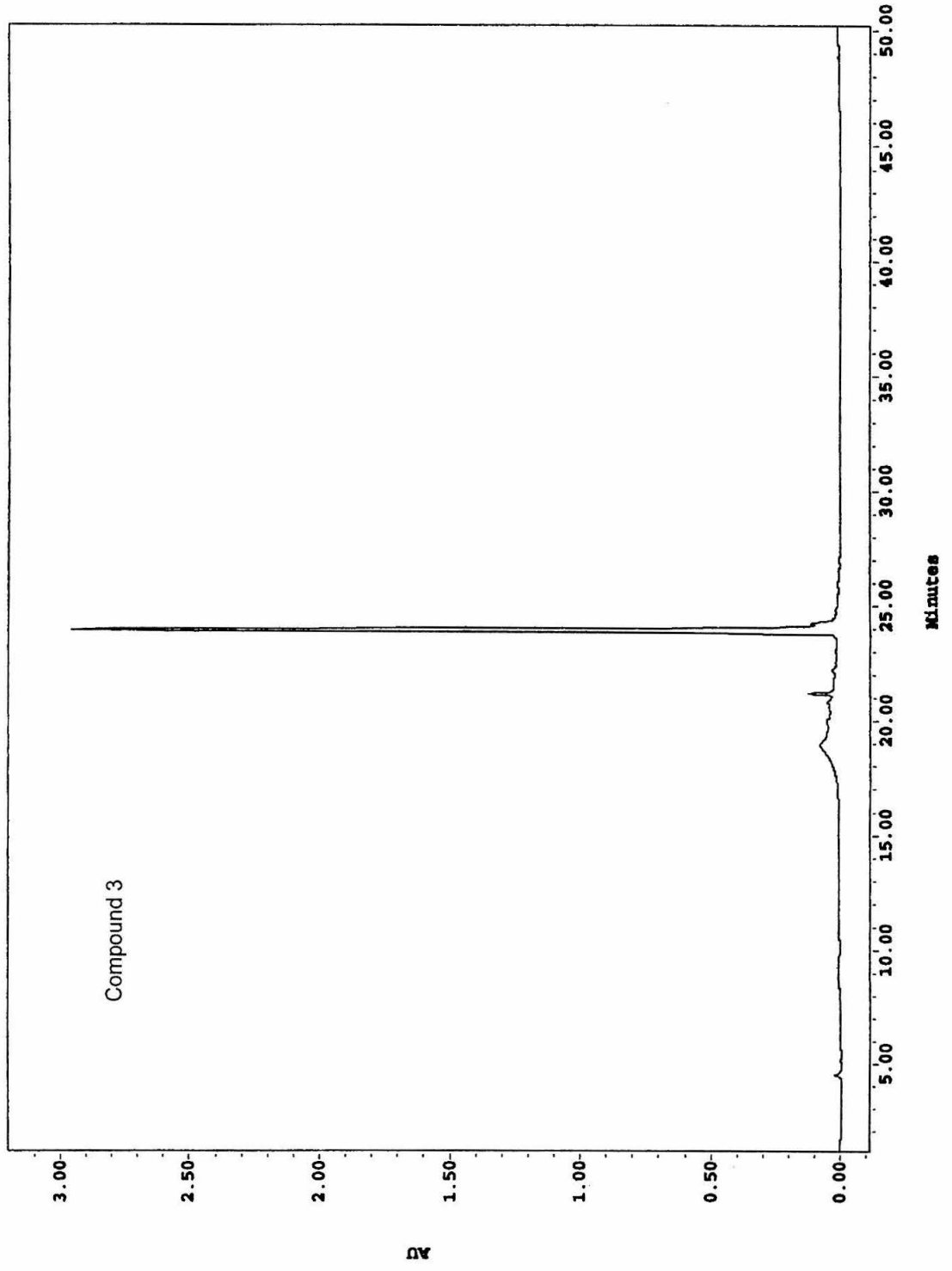
Compound 3
AU
3.00
2.50
2.00
1.50
1.00
0.50
0.00
5.00
10.00
15.00
20.00
25.00
30.00
35.00
40.00
45.00
50.00
Minutes

Figure 4.14: ESI mass spectra of **4** obtained in positive ionization mode.

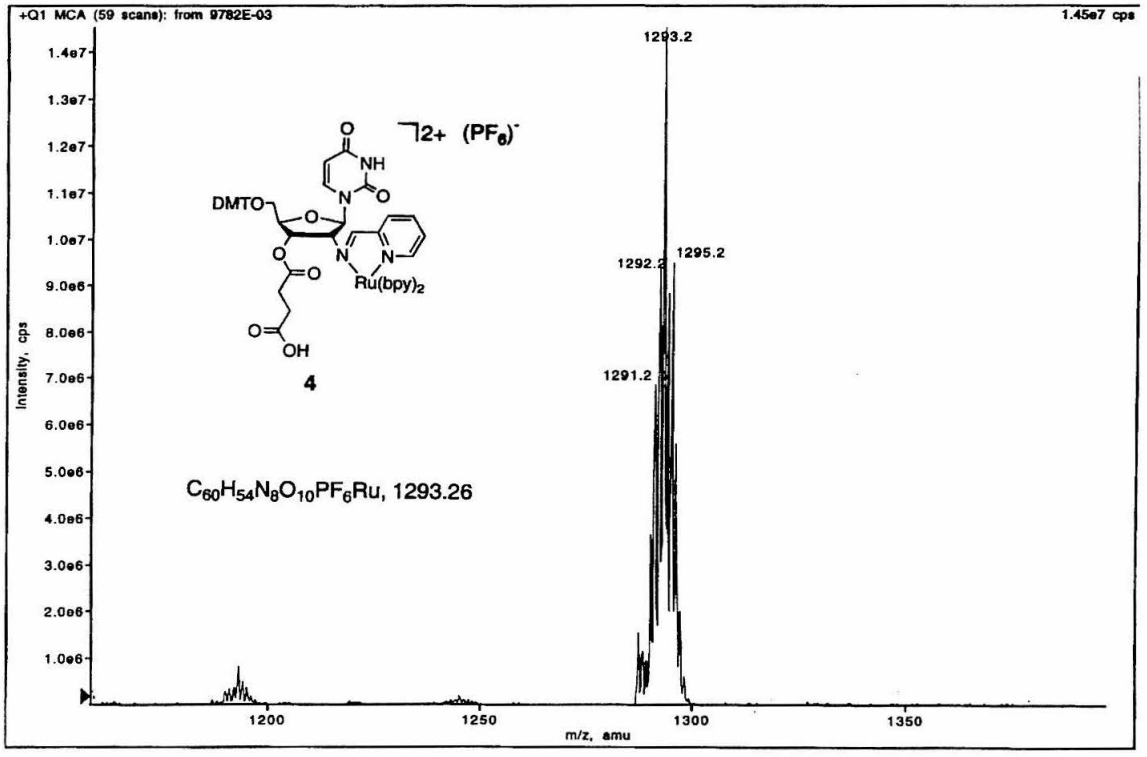
+Q1 MCA (59 scans): from 9782E-03
1.45e7 cps
1293.2
1295.2
1292.2
1291.2
2+ (PF6)-
DMTO
NH
Ru(bpy)2
OH
4
C60H54N8O10PF6Ru, 1293.26
Intensity, cps
m/z, amu

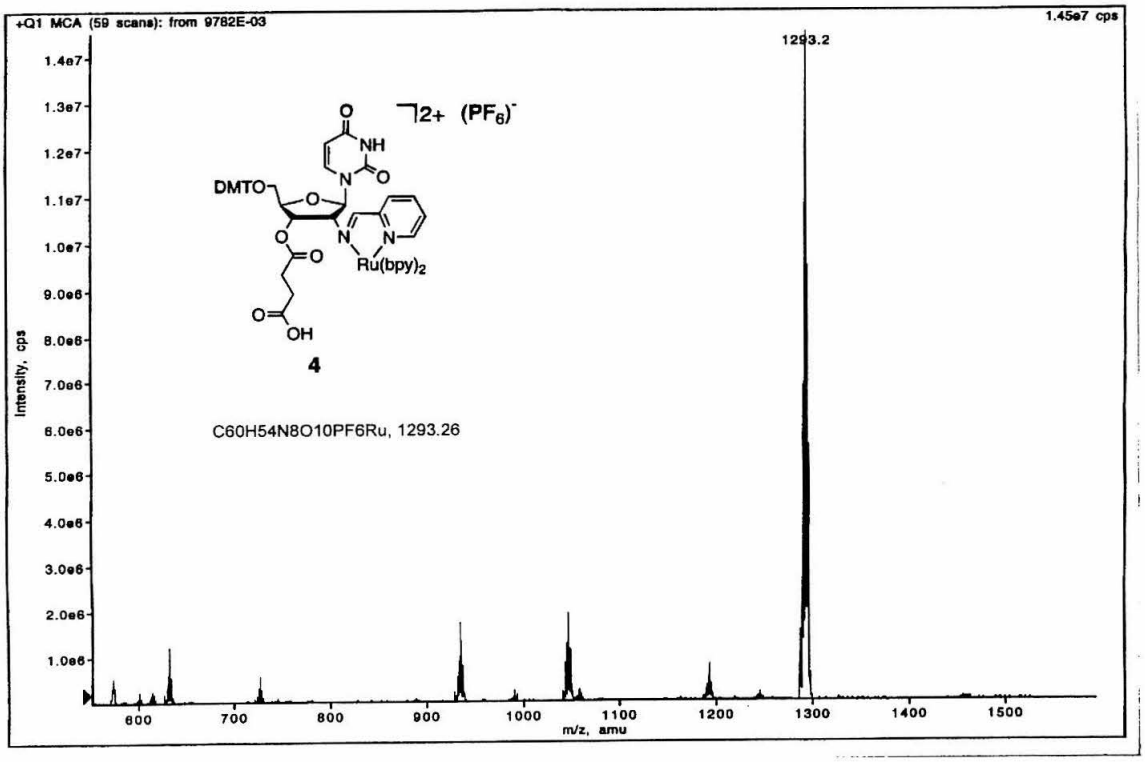
+Q1 MCA (59 scans): from 9782E-03
1.45e7 cps
1293.2
2+ (PF6)-
DMTO
NH
Ru(bpy)2
OH
4
C60H54N8O10PF6Ru, 1293.26
Intensity, cps
m/z, amu

pore size) and agitated gently overnight at room temperature. The resin was filtered and washed with fresh dichloromethane. A portion of the rinsed CPG was removed, washed with methanol and ether, and assayed for nucleoside loading (38-47 μmol/g resin). The remaining resin was rinsed with methanol and ether and dried under vacuum. The washed resin was resuspended in 2 mL of acetic anhydride/pyridine/THF solution (supplied by ABI) and 1 mL 1-methyl-imidazole/THF solution (ABI) and was agitated for 30 minutes. The resin was filtered, washed with pyridine (3 x 20 mL), methanol (3 x 20 mL), dichloromethane (3 x 20 mL), and ether (3 x 20 mL), and dried under vacuum. The nucleoside loading of the solid support after capping was 28 μmol/g resin.

Synthesis of CT CCT ACA CUimpyRu(bpy)$_2$ (6) and **TCT CCT ACA CUimpyRu(bpy)$_2$ (7):** Ru-solid support (40 mg, 1 μmol) was packed into an ABI column; two-four columns were used for each oligonucleotide synthesis. The reaction time for the first coupling was 2-10 minutes: the yield of the first coupling step was routinely > 95%. Upon completion of the synthesis (trityl off), the contents of the columns were transferred to two glass tubes and suspended in 30% aqueous ammonia (5 mL/tube). The oligonucleotide solutions were incubated either at room temperature for 15 hours followed by 3 hours at 55°C. The solvent was evaporated in a speed vacuum and the red pellets were purified by ion-exchange HPLC (Dionex NucleoPac PA-100 column; A = 10% acetonitrile in water, B = 10% acetonitrile in water, 1.5 M NH_4OAc, pH = 6, 37-47% B over 17 minutes). The product fractions were collected and the solvent was removed under vacuum. The resulting pellets were desalted using Waters C18 SepPak cartridges. Yield of **6** after isolation: 30%. MALDI-TOF mass

spectrometry: found: 3425.73 $[M-H]^-$; calculated: 3425.56 $[M-H]^-$ (Figure 4.4) Yield of **7** after isolation: 28%. MALDI-TOF mass spectrometry: found: 3728.55 $[M-H]^-$; calculated: 3730.76 $[M-H]^-$ (Figure 4.4).

Acknowledgment

We thank Harry B. Gray and Jay R. Winkler for helpful discussions. E.S.K. wishes to thank Timothy Hubin and Pratip Bhattacharya for NMR assistance. This work was supported by NIST (ATP) Award 70NANB5H1031, Jet Propulsion Laboratory (JPL 67192), and the Beckman Institute Biological Imaging Center.

References and Notes

(1) Lewis, F. D.; Wu, T. F.; Liu, X. Y.; Letsinger, R. L.; Greenfield, S. R.; Miller, S. E.; Wasielewski, M. R. *J. Am. Chem. Soc.* **2000**, *122*, 2889-2902.

(2) Tierney, M. T.; Sykora, M.; Khan, S. I.; Grinstaff, M. W. *J. Phys. Chem. B* **2000**, *104*, 7574-7576.

(3) Kelley, S. O.; Barton, J. K. *Science* **1999**, *283*, 375-381.

(4) Harriman, A. *Angew. Chem. Int. Ed.* **1999**, *38*, 945-949.

(5) Okahata, Y.; Kobayashi, T.; Tanaka, K.; Shimomura, M. *J. Am. Chem. Soc.* **1998**, *120*, 6165-6166.

(6) Fukui, K.; Tanaka, K. *Angew. Chem. Int. Ed.* **1998**, *37*, 158-161.

(7) Holmlin, R. E.; Dandliker, P. J.; Barton, J. K. *Angew. Chem. Int. Ed.* **1997**, *36*, 2715-2730.

(8) Meade, T. J.; Kayyem, J. F. *Angew. Chem. Int. Ed. Engl.* **1995**, *34*, 352-353.

(9) Ledoan, T.; Perrouault, L.; Chassignol, M.; Thuong, N. T.; Helene, C. *Nucleic Acids Res.* **1987**, *15*, 8643-8659.

(10) Bannwarth, W.; Schmidt, D.; Stallard, R. L.; Hornung, C.; Knorr, R.; Muller, F. *Helv. Chim. Acta* **1988**, *71*, 2085-2099.

(11) Chen, C. H. B.; Sigman, D. S. *J. Am. Chem. Soc.* **1988**, *110*, 6570-6572.

(12) Telser, J.; Cruickshank, K. A.; Schanze, K. S.; Netzel, T. L. *J. Am. Chem. Soc.* **1989**, *111*, 7221-7226.

(13) Modak, A. S.; Gard, J. K.; Merriman, M. C.; Winkeler, K. A.; Bashkin, J. K.; Stern, M. K. *J. Am. Chem. Soc.* **1991**, *113*, 283-291.

(14) Jenkins, Y.; Barton, J. K. *J. Am. Chem. Soc.* **1992**, *114*, 8736-8738.

(15) Bashkin, J. K.; Frolova, E. I.; Sampath, U. S. *J. Am. Chem. Soc.* **1994**, *116*, 5981-5982.

(16) Arkin, M. R.; Stemp, E. D. A.; Pulver, S. C.; Barton, J. K. *Chem. & Biol.* **1997**, *4*, 389-400.

(17) Inoue, H.; Furukawa, T.; Shimizu, R.; Tamura, T.; Matsui, M. N.; Ohtsuka, E. *Chem. Commun.* **1999**, 45-46.

(18) Wiederholt, K.; McLaughlin, L. W. *Nucleic Acids Res.* **1999**, *27*, 2487-2493.

(19) Ortmans, I.; Content, S.; Boutonnet, N.; Kirsch-De Mesmaeker, A.; Bannwarth, W.; Constant, J. F.; Defrancq, E.; Lhomme, J. *Chem. Eur. J.* **1999**, *5*, 2712-2721.

(20) Holmlin, R. E.; Dandliker, P. J.; Barton, J. K. *Bioconj. Chem.* **1999**, *10*, 1122-1130.

(21) Khan, S. I.; Grinstaff, M. W. *J. Am. Chem. Soc.* **1999**, *121*, 4704-4705.

(22) Bannwarth, W.; Schmidt, D. *Tet. Lett.* **1989**, *30*, 1513-1516.

(23) Manchanda, R.; Dunham, S. U.; Lippard, S. J. *J. Am. Chem. Soc.* **1996**, *118*, 5144-5145.

(24) Schliepe, J.; Berghoff, U.; Lippert, B.; Cech, D. *Angew. Chem. Int. Ed.* **1996**, *35*, 646-648.

(25) Magda, D.; Crofts, S.; Lin, A.; Miles, D.; Wright, M.; Sessler, J. L. *J. Am. Chem. Soc.* **1997**, *119*, 2293-2294.

(26) Meggers, E.; Kusch, D.; Giese, B. *Helv. Chim. Acta* **1997**, *80*, 640-652.

(27) Hurley, D. J.; Tor, Y. *J. Am. Chem. Soc.* **1998**, *120*, 2194-2195.

(28) Khan, S. I.; Beilstein, A. E.; Smith, G. D.; Sykora, M.; Grinstaff, M. W. *Inorg. Chem.* **1999**, *38*, 2411-2415.

(29) Khan, S. I.; Beilstein, A. E.; Sykora, M.; Smith, G. D.; Hu, X.; Grinstaff, M. W. *Inorg. Chem.* **1999**, *38*, 3922-3925.

(30) Lewis, F. D.; Helvoigt, S. A.; Letsinger, R. L. *Chem. Commun.* **1999**, 327-328.

(31) Rack, J. J.; Krider, E. S.; Meade, T. J. *J. Am. Chem. Soc.* **2000**, *122*, 6287-6288.

(32) Hu, X.; Smith, G. D.; Sykora, M.; Lee, S. J.; Grinstaff, M. W. *Inorg. Chem.* **2000**, *39*, 2500-2504.

(33) Khan, S. I.; Beilstein, A. E.; Grinstaff, M. W. *Inorg. Chem.* **1999**, *38*, 418-419.

(34) Abbreviations: BOP, benzotriazol-1-yloxytris(dimethylamino)phosphonium hexafluorophosphate; DBU, 1,8-diazabicyclo[5.4.0]undec-7-ene; DIEA, diisopropylethanolamine; DMAP, dimethylaminopyridine; DMT, 4,4′-dimethoxytrityl; EtOAC, ethyl acetate; HOBT, hydroxybenzotriazole; TEA, triethylamine; THF, tetrahydrofuran.

(35) Caruthers, M. H.; Barone, A. D.; Beaucage, S. L.; Dodds, D. R.; Fisher, E. F.; McBride, L. J.; Matteucci, M.; Stabinsky, Z.; Tang, J.-Y. In *Methods in Enzymology: Recombinant DNA*; Grossman, R. W. a. L., Ed.; Academic Press, Inc.:, 1987; Vol. 154.

(36) Knorr, R.; Trzeciak, A.; Bannwarth, W.; Gillessen, D. *Tet. Lett.* **1989**, *30*, 1927-1930.

(37) Brown, G. M.; Weaver, T. R.; Keene, F. R.; Meyer, T. J. *Inorg. Chem.* **1976**, *15*, 190-196.

(38) Ridd, M. J.; Keene, F. R. *J. Am. Chem. Soc.* **1981**, *103*, 5733-5740.

(39) Keene, F. R.; Ridd, M. J.; Snow, M. R. *J. Am. Chem. Soc.* **1983**, *105*, 7075-7081.

(40) $E^*_{red} = E_{red} + E^{00}$; $E^*_{ox} = E_{ox} - E^{00}$.

(41) Steenken, S.; Jovanovic, S. V. *J. Am. Chem. Soc.* **1997**, *119*, 617-618.

(42) Bock, C. R.; Meyer, T. J.; Whitten, D. G. *J. Am. Chem. Soc.* **1974**, *96*, 4710-4712.

(43) *Oligonucleotide Synthesis: A Practical Approach*; Gait, M., Ed.; Oxford Univ. Press: Oxford, 1984.

(44) Goodchild, J. *Bioconj. Chem.* **1990**, *1*, 165-191.

(45) *Oligonucleotides and Analogues: A Practical Approach*; Eckstein, F., Ed.; Oxford Univ. Press: Oxford, 1991.

(46) Detailed descriptions of oligonucleotide synthesis are given in Ref. 43-45.

(47) Saenger, W. *Principles of Nucleic Acid Structure*; Springer-Verlag: New York, 1984.

(48) Khan, S. I.; Beilstein, A. E.; Tierney, M. T.; Sykora, M.; Grinstaff, M. W. *Inorg. Chem.* **1999**, *38*, 5999-6002.

(49) Juris, A.; Balzani, V.; Barigelletti, F.; Campagna, S.; Belser, P.; Vonzelewsky, A. *Coord. Chem. Rev.* **1988**, *84*, 85-277.

(50) An estimate of the excited-state reduction potential of $[Ru(bpy)_2(bpy')]^{2+}$, based on data collected for $[Ru(bpy)_3]^{2+}$, suggests that guanine oxidation from the excited-state is not likely (Ref.49).

(51) $\Delta G_q = -[E_{1/2}^{Q/Q-} - E_{1/2}^{Ru3+/Ru2+*}]$

(52) Low, D. W.; Winkler, J. R.; Gray, H. B. *J. Am. Chem. Soc.* **1996**, *118*, 117-120.

Chapter 5:

Spectroscopy of Ruthenium-Modified Nucleic Acids

Introduction

Several reports have described the preparation of mixed-chelate ruthenium(II) polypyridine complexes bound at specific sites in single- and double-stranded oligonucleotides.[1-15] Typically, these ruthenium complexes contain two types of ligands: an unmodified polypyridine ligand (pp) and a substituted polypyridine ligand containing a linker required for oligonucleotide attachment (pp′). These $[Ru(pp)_2(pp')]^{2+}$ complexes attain relatively long-lived (triplet) metal-to-ligand charge-transfer (^{3}MLCT) excited states upon excitation.[2,3,5,6,10,16,17] In a few cases, the $Ru(pp)_2(pp')]^{2+}$ complexes incorporated into oligonucleotides have been used in studies investigating DNA-mediated energy and electron transfer reactions.[11,12,18-21]

Further tuning of the probes for such reactions depends on a detailed understanding of both the ground- and excited-state properties of these complexes. Extensive correlations between photophysical and electrochemical data for mixed-chelated complexes demonstrate the dependence of these properties on the π^* energies of the pp and pp′ ligands.[22-24] Multiple charge-transfer transitions from the filled $d\pi(Ru^{II})$ levels to the low-lying π^* (ligand) orbitals are expected.[25] Emission energies reflect the population of the π^* orbital that is lowest in energy.[26-28] Likewise, the redox behavior of mixed-chelate Ru(II) complexes is influenced by the π^* energies of the ligands. The absorption, emission, and electrochemical properties correlate well since the metal-centered and ligand-centered orbitals involved in MLCT transitions are also the orbitals involved in the redox processes.

We have prepared mixed-chelate Ru(II) complexes for use in ground-state electron transfer studies involving DNA.[1,21] These complexes consist of low-(**1**) and high-potential (**2**) metallonucleosides (Figure 5.1). Their absorption and electrochemical features are similar to those of the closely related complexes, $[Ru(acac)_2(bpy)]$ and $[Ru(bpy)_3]^{2+}$, respectively (acac = acetylacetonate, bpy = 2,2′-bipyridine).[23,29] However, subtle differences in these properties are observed for **1** and **2** relative to the reference complexes. These changes reflect the presence of the substituted iminomethylpyridine (impy′) ligand present in the coordination sphere of the metallonucleosides. We utilized resonance Raman spectroscopy to document the influence of the impy′ ligand on the ground-state properties of **1** and **2**.

Results

Electrochemistry. Cyclic voltammograms of **1** in ethanol show a reversible one-electron oxidation (48 mV vs. SCE) that represents the Ru(III/II) couple (Table 5.1). This value is slightly more positive than the reduction potentials measured for the model system $[Ru(acac)_2(impy)]$, and the closely related complexes, $[Ru(acac)_2(bpy)]$ and $[Ru(acac)_2(dppz)]$ (Table 5.1).[1,30-32] These differences in $E_{1/2}$ suggests that the presence of the nucleoside is responsible for the positive shift in the reduction potential for **1**.

Voltammograms of **2** in dichloromethane display a reversible one-electron oxidation at 1.38 V attributable to the Ru(III/II) couple (Table 5.2). The oxidation process is not completely reversible at slow scan rates (0.1 – 1.0 V/sec). Studies of the electrochemical behavior of a series of $[Ru(bpy)_2(\alpha,\alpha'\text{-diimine})]^{2+}$ complexes show that fast scan rates (> 5 V/sec) are required in order for these complexes to display reversible, or nearly reversible, one-electron oxidation processes in acetonitrile.[33] The reduction

Figure 5.1: Structure and sequence of ruthenium-modified nucleic acids.

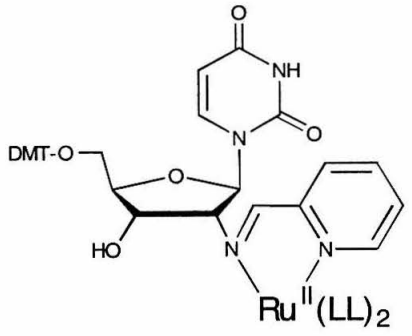

1: LL = acetylacetonate

2: LL = 2,2'-bipyridine

3: 5'-TCT CCT ACA CU $_{(impy)Ru^{II}(bpy)_2}$

Table 5.1: Reduction Potentials and Absorption Data for Ru(II) Acetylacetonate Complexes.

Compd	$E_{1/2}$, mV[a] vs. SCE	λ_{max}, nm[b] ($\varepsilon \times 10^{-3}$, M^{-1} cm^{-1})	Ref.
1	48	592 (3.6) 396 (3.6) 276 (27.0) 234 (33.4)	1
$[Ru(acac)_2(impy)]$	-11	576 (4.6) 402 (4.6) 274 (16.8) 206 (21.8)	1
$[Ru(acac)_2(bpy)]$	-94[c]	621 (16.1) 416 (24.0) 278 (sh) (33.7) 257 (sh) (38.9) 246 (sh) (40.6)	29,31
$[Ru(acac)_2(dppz)]$	-9	547 (6.4) 375 (10.5) 365 (9.0)	32

[a] EtOH containing 0.1 M NH_4PF_6 at room temperature (unless otherwise noted).
[b] EtOH (unless otherwise noted); λ_{max} values ± 2 nm; ε values ± 5%.
[c] CH_2Cl_2 containing 0.5 M $TBABF_4$, 20 °C.

Table 5.2. Ground and Excited State Properties in Acetonitrile at Room Temperature.

	$E_{1/2}$, V vs. SCE[a]		λ_{max}, nm (±2 nm)	λ_{em}	ϕ_{em}	τ (ns)
	oxidn	redn	($\varepsilon \times 10^{-3}$, M^{-1} cm^{-1})	nm (±5 nm)	$\times 10^3$ (±5%)	ns (±%)
2	+1.38[b]	-1.08	480 (9.1) [c]	730 [c]	0.53 [c]	44 [c]
		-1.39	284 (51.9)			
		-1.61	256 (25.8)			
			238 (38.9)			
			210 (70.1)			
3	+1.12 [d]		260 (109) [d]	725 [d]	0.11 [d]	42 [d]
			480 (9.1)			
$[Ru(bpy)_2(impy)]^{2+}$ [e]		+1.27	470 (13.0)			
			430 (sh)			
			345 (sh)			
			315 (sh)			
			286 (51.0)			
			245 (18.0)			
			242 (20.0)			
$[Ru(bpy)_2(ampy)]^{2+}$ [e]		+1.12	471 (10.0)	625 [f,g]		192 [g]
			422 (sh) (6.3)			
			339 (11.0)			
			298 (55.0)			
			244 (23.0)			
$[Ru(bpy)_3]^{2+}$ [h]	+1.29	-1.33	451 (14.0)	628	4.5	650
		-1.52	345 (6.5)			
		-1.78	323 (6.5)			
			285 (87.0)			

[a] Values obtained in acetonitrile containing 0.1 M $[N(n\text{-}C_4H_9)_4]PF_6$ unless otherwise noted. [b] CH_2Cl_2. [c] CH_3OH. [d] 50 mM sodium phosphate buffer (pH 7.0), 500 mM sodium chloride. [e] Reference 33. [f] 1 M $HClO_4$. [g] Reference 35. [h] Reference 34.

potential of **2** is more positive than $E_{1/2}$ for the model system $[Ru(bpy)_2(impy)]^{2+}$ as well as $E_{1/2}$ for $[Ru(bpy)_3]^{2+}$ (Table 5.2).[33,34]

Multiple ligand-centered reductions are observed in acetonitrile for **2** (-1.08, -1.39, -1.61 V). The most positive reduction potential is irreversible and represents reduction of the impy′ ligand, by analogy to the $[Ru(bpy)_2(\alpha,\alpha'\text{-diimine})]^{2+}$ complexes described above.[33] The other two ligand-centered potentials observed for **2** are shifted to more positive values relative to the ligand-based reductions observed for $[Ru(bpy)_3]^{2+}$ (Figure 5.2).[34]

Absorption. The visible absorption features of **1** and **2** are shown in Figure 5.3. The electronic spectrum of **1** in ethanol displays maxima at 234, 276, 396, and 592 nm (Table 5.1). The high-energy bands represent acac- and nucleoside-based π-π^* transitions. The transitions in the visible region shift slightly in dichloromethane (392 nm, ε = 3600 M^{-1} cm^{-1}; 602 nm, ε = 3700 M^{-1} cm^{-1}). These bands are similar to the maxima reported for $[Ru(acac)_2(impy)]$ in ethanol: 206, 274, 402, and 576 nm.[1] Comparison of the absorption maxima of **1** and of the closely related complexes, $[Ru(acac)_2(bpy)]$ and $[Ru(acac)_2(dppz)]$, reveals notable differences (Table 5.1).[29,32] Two visible absorption maxima are observed for $[Ru(acac)_2(bpy)]$ at lower energy (416, 621 nm), whereas $[Ru(acac)_2(dppz)]$ displays a single band (547 nm).

The absorption maxima of **2** in methanol are 210, 238, 256, and 284, with a broad absorption band at 480 nm (ε = 9100 M^{-1} cm^{-1}) (Table 5.2). The high-energy bands represent bpy- and nucleoside-based π-π^* transitions. For comparison, $[Ru(bpy)_2(impy)]^{2+}$ exhibits a maximum in the visible region at 470 nm (ε = 13600 M^{-1} cm^{-1}) with a shoulder at 430 nm.[33,35] The slight difference in λ_{max} for the model

Figure 5.2: Differential pulse voltammograms showing ligand centered reductions of **3** (solid) and $[Ru(bpy)_3]^{2+}$ (dashed) in acetonitrile containing 0.1 M TBAH.

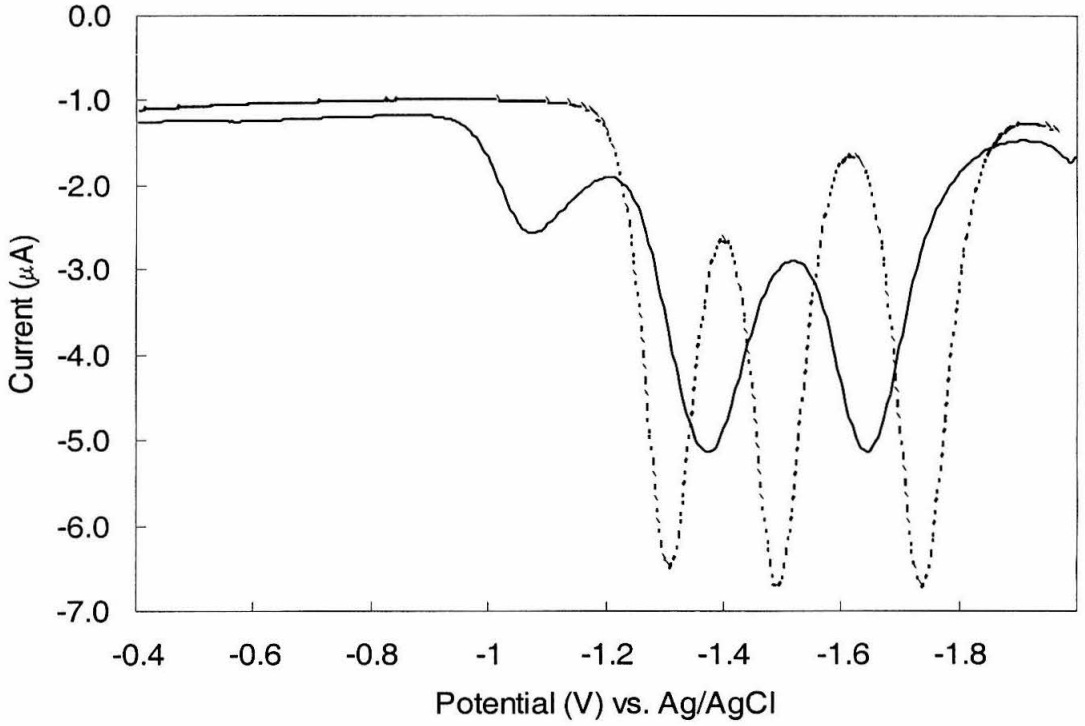
0.0
-1.0
-2.0
-3.0
-4.0
-5.0
-6.0
-7.0
Current (μA)
-0.4
-0.6
-0.8
-1
-1.2
-1.4
-1.6
-1.8
Potential (V) vs. Ag/AgCl

Figure 5.3: Absorption spectra of **2** (dotted line) and **3** (solid line) in ethanol and methanol, respectively.

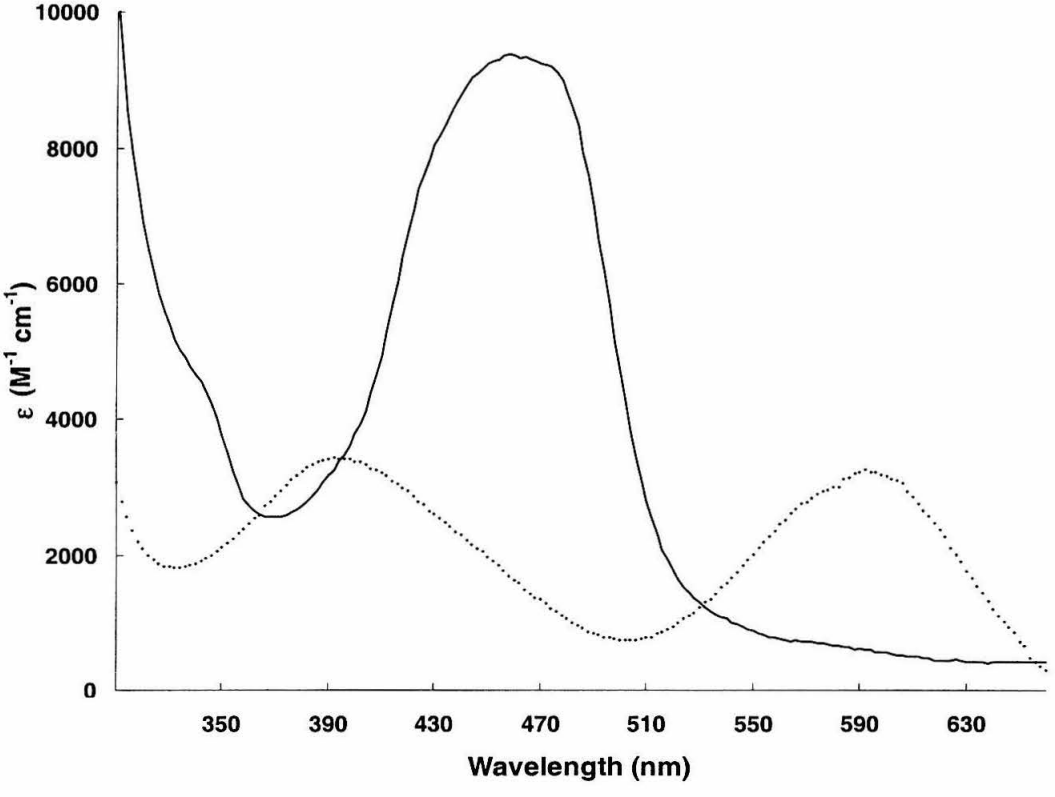
10000
8000
6000
4000
2000
0
ε (M-1 cm-1)
350
390
430
470
510
550
590
630
Wavelength (nm)

Figure 5.4: Resonance Raman spectrum of **1** in dichloromethane (441.6 nm excitation). Solvent peaks are noted in parentheses. Laser source: He-Cd Liconix. Dwell time of 10 sec/cm^{-1} at 1 cm^{-1} intervals.

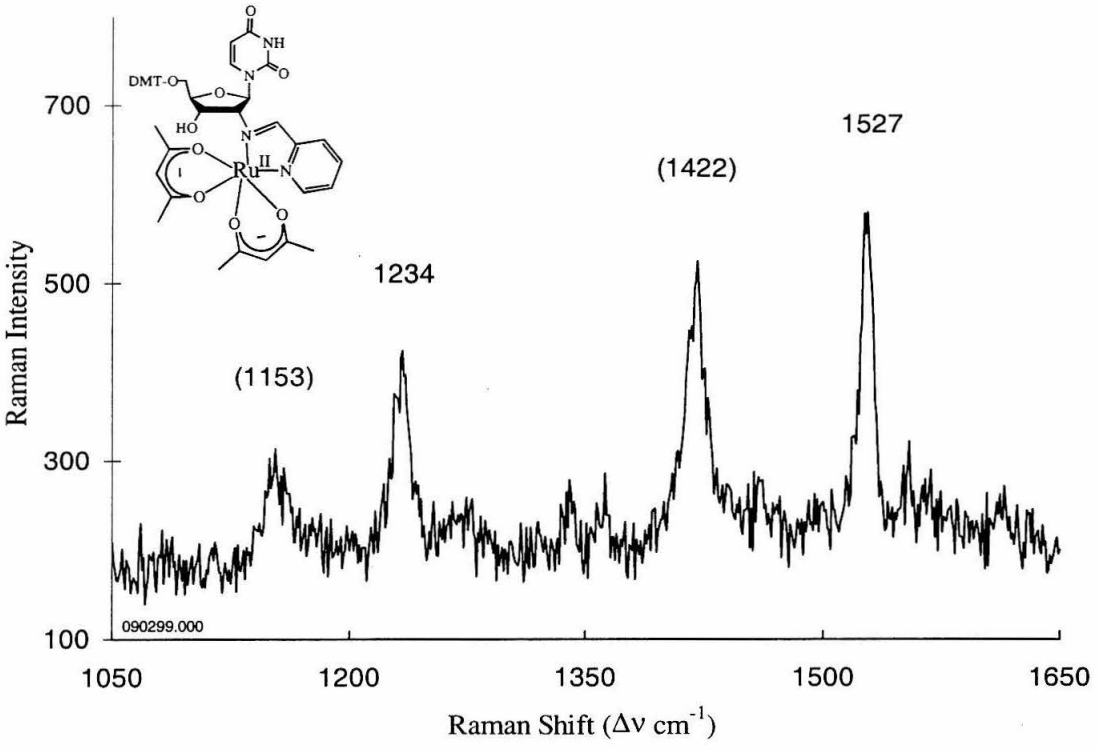
DMT-O
HO
O
NH
N
O
Ru
II
N
O
O
O
O
O
-
700
500
300
100
Raman Intensity
1234
(1153)
(1422)
1527
090299.000
1050
1200
1350
1500
1650
Raman Shift (Δν cm-1)

complex and **2** shows the effect of replacing the impy ligand with an impy derivative possessing a ribose substituent on the imino nitrogen.

Resonance Raman. Ground-state resonance Raman spectra of **1** in dichloromethane were recorded at multiple excitation wavelengths (441.6, 457.9, and 514.5 nm). Spectra obtained at the first two excitation frequencies both display peaks at 1234 and 1527 cm^{-1} (Figures 5.4-5.6). An exception occurs upon 514.5 nm excitation: the peak observed at 1234 cm^{-1} is absent, with peaks at 1249 and 1286 cm^{-1} observed instead (Figure 5.6). Multiple vibrational modes are enhanced despite the weak absorption of **1** at this excitation frequency.

Ground-state rR spectra of **2** (d_4-methanol) and **3** (water) were recorded at 441.6 nm excitation and displayed nearly identical peaks (Figures 5.7 and 5.8). The rR spectra of $[Ru(bpy)_3]^{2+}$ and **3** in water are shown in Figure 5.8 (441.6 nm excitation). Comparison of these two spectra enables the identification of bpy-associated vibrations observed in the spectrum of **3** at 1023, 1173, 1276, 1315, 1488, 1552, and 1604 cm^{-1}. However, additional vibrations at 1471 and 1242 cm^{-1} are observed. The feature at 1552 cm^{-1} is broader than the corresponding vibration in the spectrum of $[Ru(bpy)_3]^{2+}$.

Additional rR spectra of **2** were obtained with 457.9 and 488.0 nm excitation wavelengths (Figures 5.9 and 5.10). These rR spectra resemble the spectra obtained with 441.6 nm excitation. However, significant changes in the intensity of peaks were observed between 1400-1700 cm^{-1}. Figure 5.11 shows the striking changes in the intensity of two modes (1470 and 1488 cm^{-1}) as a function of excitation wavelength. In addition to these changes, the broad feature at 1552 cm^{-1} observed with 441.6 nm

Figure 5.5: Resonance Raman spectrum of **1** in dichloromethane (457.9 nm excitation). Solvent peaks are noted in parentheses. Laser source: Ar^+ Coherent Innova 70. Dwell time of 10 sec/cm^{-1} at 1 cm^{-1} intervals.

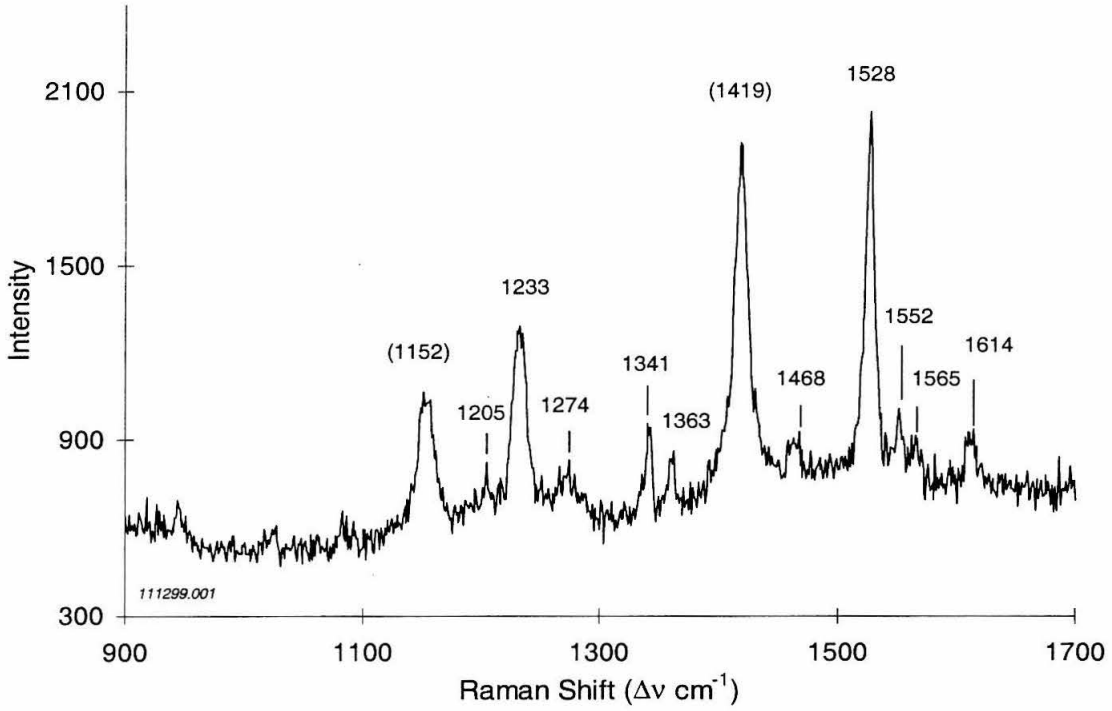
2100
1500
900
300
Intensity
(1152)
1205
1233
1274
1341
1363
(1419)
1468
1528
1552
1565
1614
111299.001
900
1100
1300
1500
1700
Raman Shift (Δν cm-1)

Figure 5.6: Resonance Raman spectrum of **1** in dichloromethane (514.5 nm excitation). Solvent peaks are noted in parentheses. Laser source: Ar^+ Coherent Innova 70. Power at the sample: 130 mW. Dwell time of 10 sec/cm^{-1} at 1 cm^{-1} intervals.

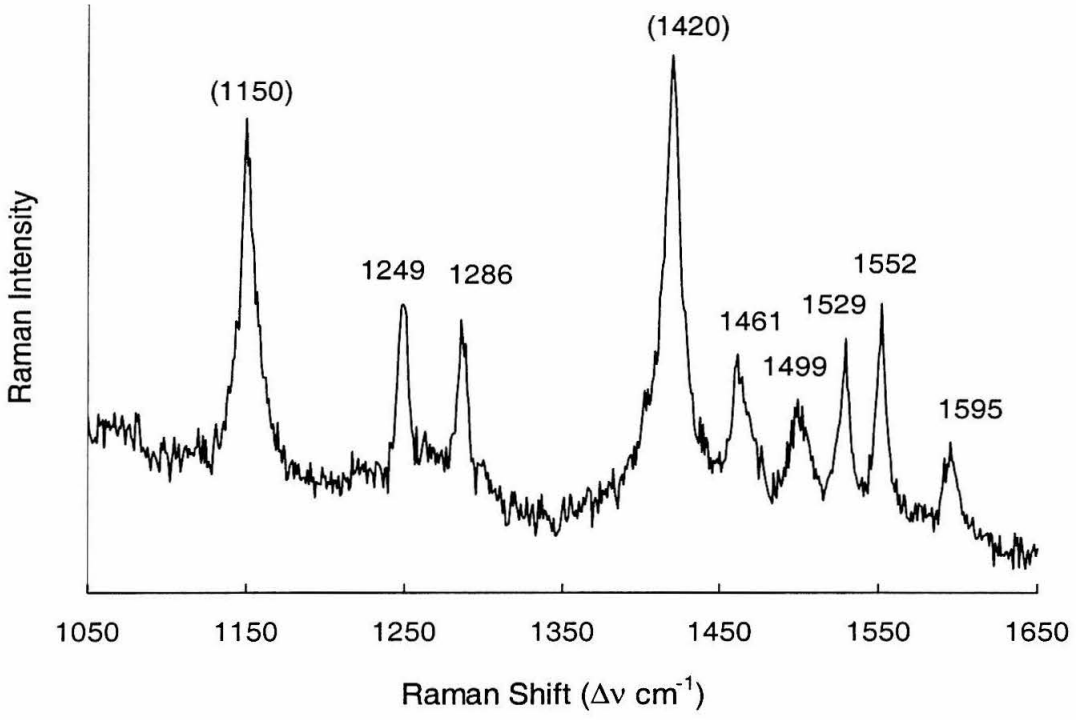
(1420)
(1150)
1249
1286
1552
1529
1461
1499
1595
Raman Intensity
1050
1150
1250
1350
1450
1550
1650
Raman Shift (Δν cm-1)

Figure 5.7: Resonance Raman spectrum of **2** in deuterated methanol (441.6 nm excitation). Solvent peaks are noted in parentheses. Laser source: He-Cd Liconix. 300 micron slits. Dwell time of 10 sec/cm^{-1} at 1 cm^{-1} intervals.

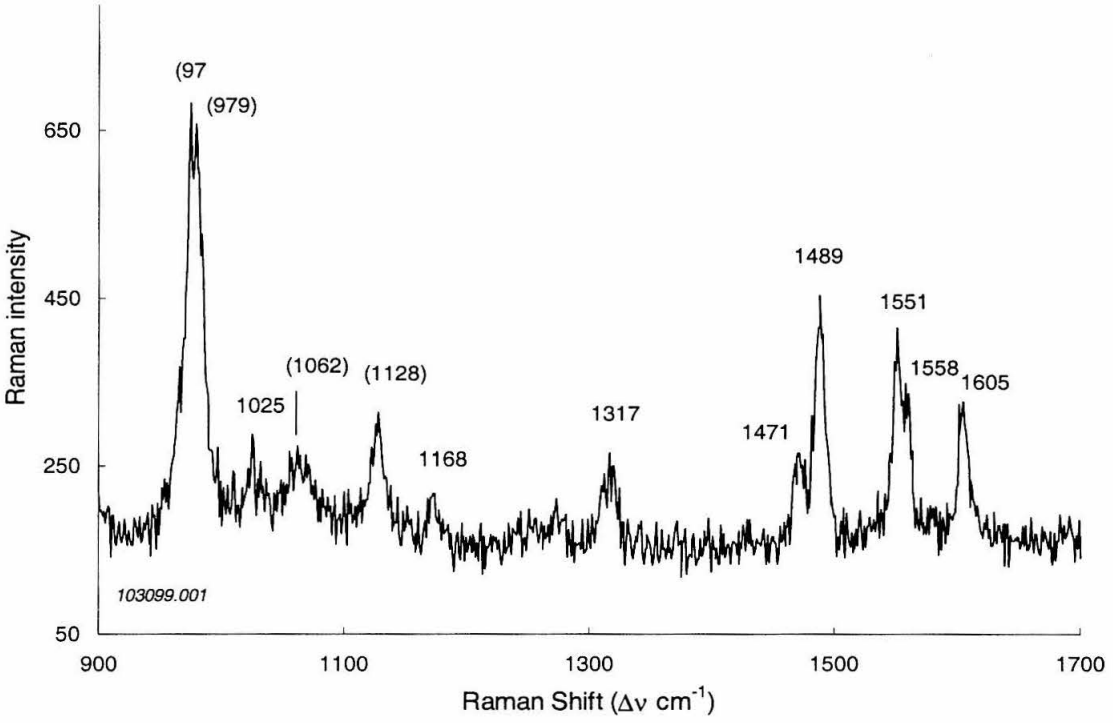
(97
(979)
650
450
250
50
Raman intensity
1025
(1062)
(1128)
1168
1317
1471
1489
1551
1558
1605
103099.001
900
1100
1300
1500
1700
Raman Shift (Δν cm-1)

Figure 5.8: Resonance Raman spectrum obtained with 441.6 nm excitation of $[Ru(bpy)_3]^{2+}$ (top) and **3** (bottom) in water. Laser source: He-Cd Liconix. Dwell time of 10 sec/cm^{-1} at 1 cm^{-1} intervals.

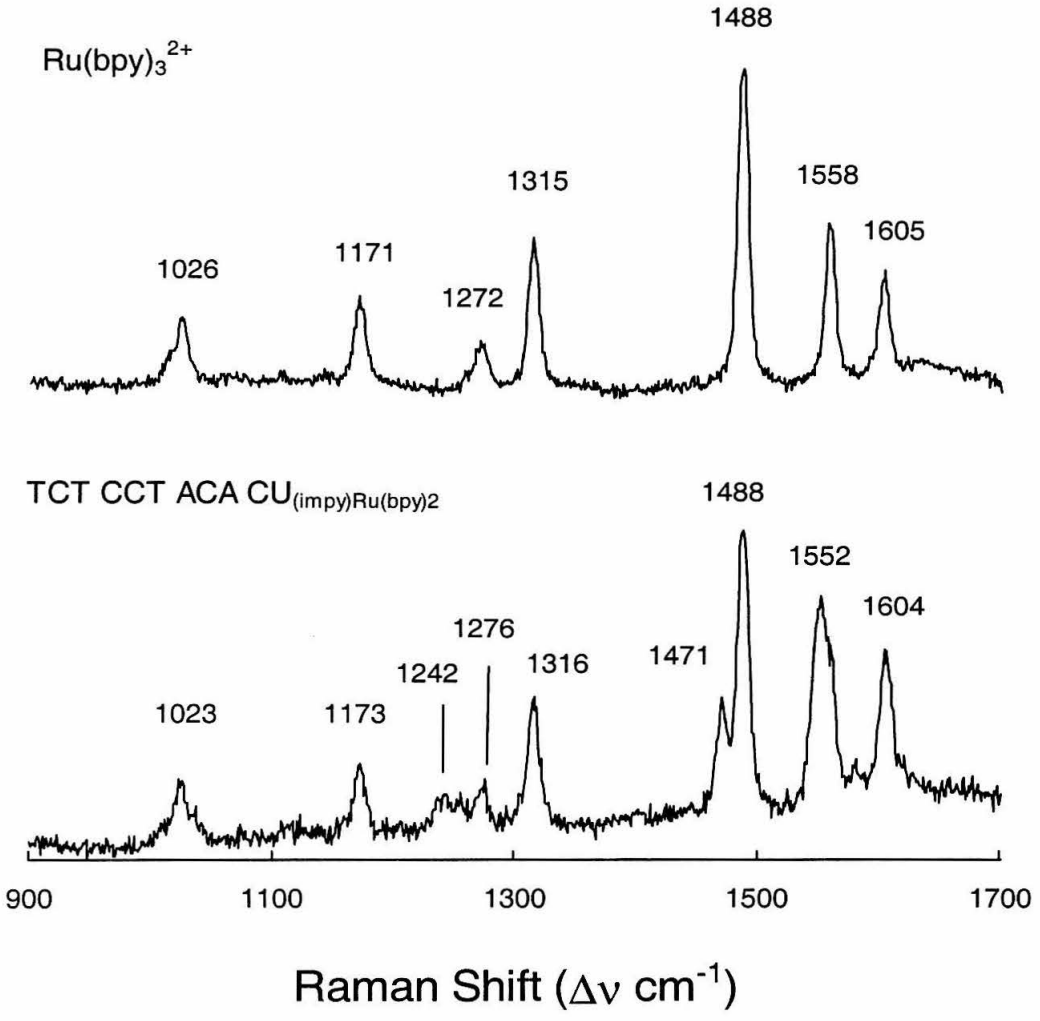
Ru(bpy)3 2+
1488
1315
1558
1605
1026
1171
1272
TCT CCT ACA CU(impy)Ru(bpy)2
1488
1552
1604
1276
1242
1316
1471
1023
1173
900
1100
1300
1500
1700
Raman Shift (Δν cm-1)

Figure 5.9: Resonance Raman spectrum of **2** in deuterated methanol (457.9 nm excitation). Laser source: Ar^+ Coherent Innova 70. Dwell time of 10 sec/cm^{-1} at 1 cm^{-1} intervals.

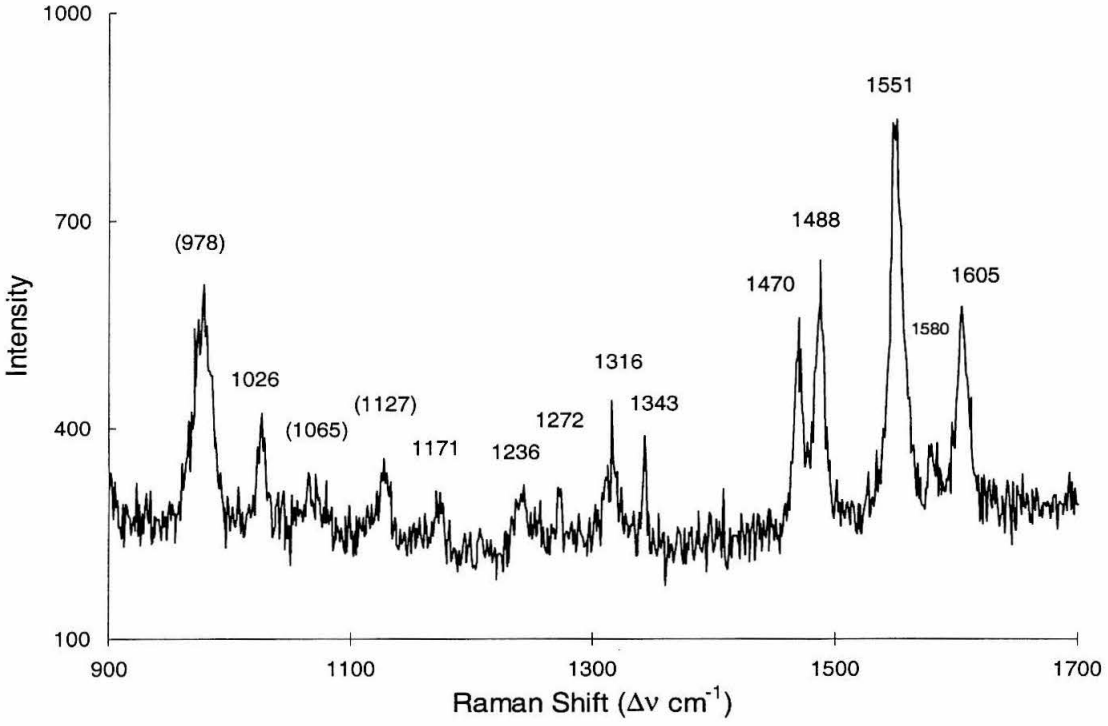
1000
700
400
100
Intensity
(978)
1026
(1065)
(1127)
1171
1236
1272
1316
1343
1470
1488
1551
1580
1605
900
1100
1300
1500
1700
Raman Shift (Δν cm-1)

Figure 5.10: Resonance Raman spectrum of **2** in deuterated methanol (488.0 nm excitation). Solvent peaks are noted in parentheses. Laser source: Ar^+ Coherent Innova 70. Dwell time of 10 sec/cm^{-1} at 1 cm^{-1} intervals.

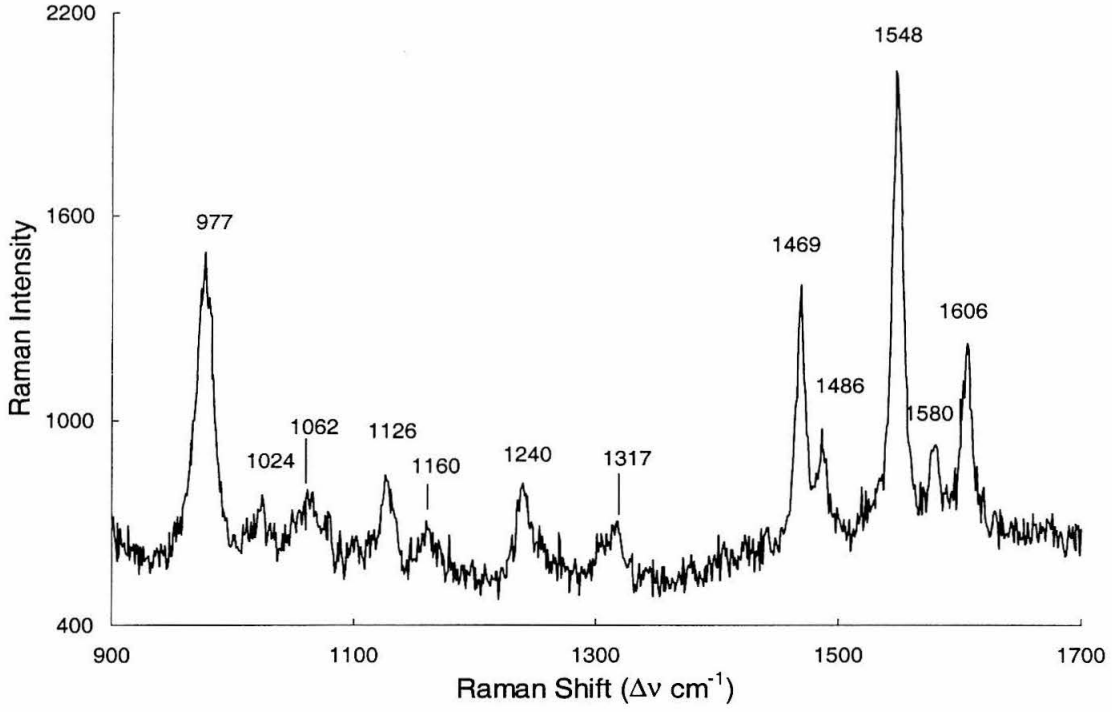
2200
1600
1000
400
Raman Intensity
977
1024
1062
1126
1160
1240
1317
1469
1486
1548
1580
1606
900
1100
1300
1500
1700
Raman Shift (Δν cm-1)

Figure 5.11: Resonance Raman spectrum of **2** in deuterated methanol at three excitation wavelengths: 441.6 (bottom), 457.9 (middle), and 488.0 nm (top). Laser sources: He-Cd Liconix and Ar^+ Coherent Innova 70. Dwell time of 10 sec/cm^{-1} at 1 cm^{-1} intervals.

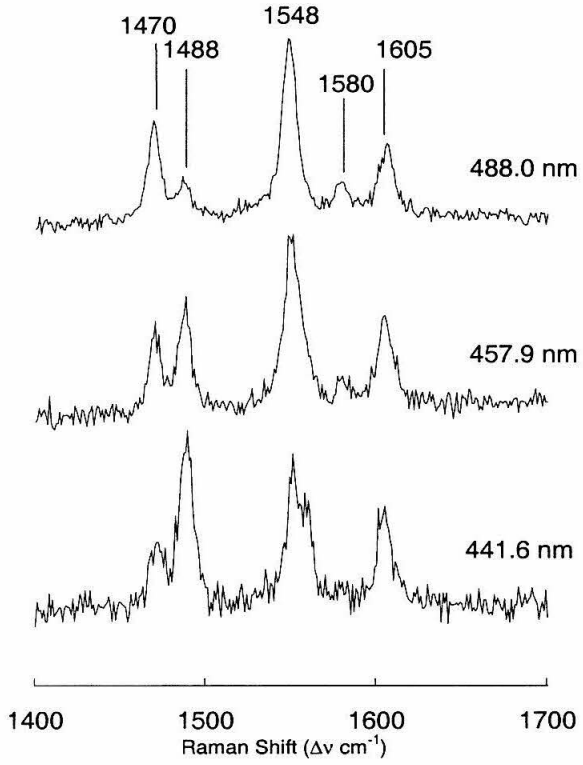
1470
1488
1548
1580
1605
488.0 nm
457.9 nm
441.6 nm
1400
1500
1600
1700
Raman Shift (Δν cm-1)

Figure 5.12: Steady-state emission spectrum of **2** in aerated methanol (480.0 nm excitation). Emission maximum = 730 nm.

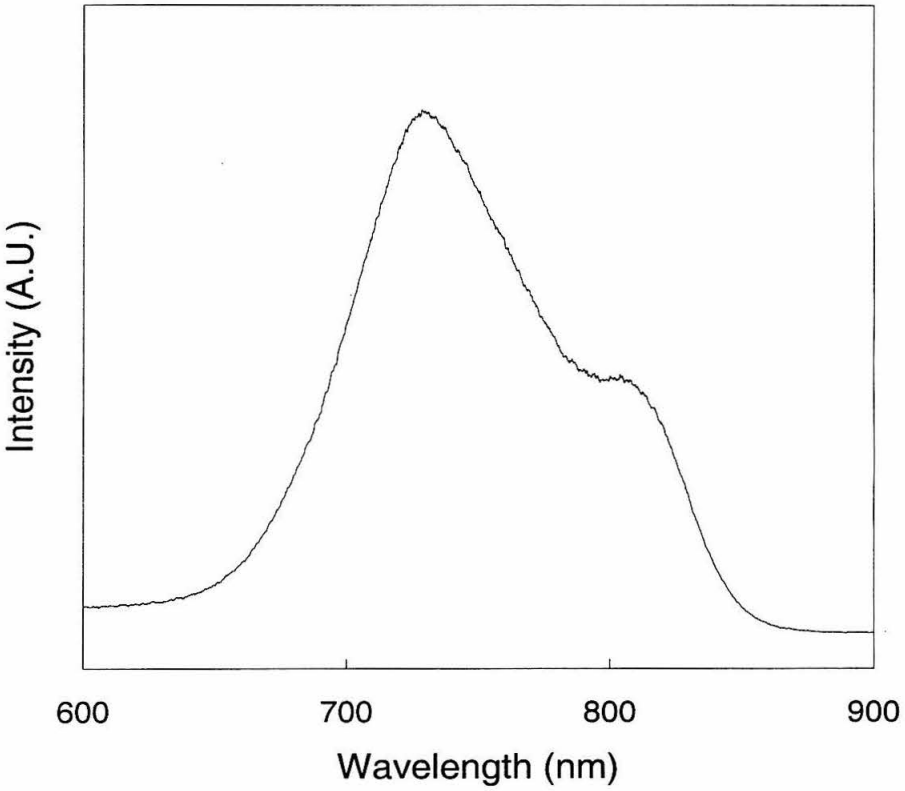
Intensity (A.U.)
600
700
800
900
Wavelength (nm)

excitation becomes resolved at longer excitation wavelengths. A weak feature at 1580 cm^{-1} becomes apparent with 488.0 nm excitation.

Emission. Steady-state emission spectra of metallonucleoside **2** and oligonucleotide **3** show similar profiles at room temperature. Irradiation of **2** and **3** at 480 nm produces an emission maximum at 730 nm, with a shoulder near 810 nm (Figure 5.12). The excited-state lifetimes are strictly monoexponential and are independent of solvent: 44 ns for **2** (aqueous methanol) and 42 ns for **3** (phosphate buffer). However, the quantum yield of **2** is slightly greater than that of **3** (Table 5.2).

Variable-temperature emission spectra were obtained with **2** suspended in a polymer matrix. While the shape of the emission spectrum of the solid sample closely resembles that of the solution sample, the emission maximum is shifted to higher energy (707 nm). However, lowering the temperature does not appreciably alter the position of λ(em). The emission maximum at 181K and 64K is 700 nm.

Discussion

Electrochemistry. The reduction potentials of **1** and **2** are more positive than those of the corresponding impy model complexes by 60 and 110 mV, respectively (Tables 5.1 and 5.2). While this comparison isolates the contribution of the impy′ ligand to the reduction potential, it does not explain why the shift in $E_{1/2}$ is larger for **2** than for **1**. Reduction of the imine linkage in **2** and in $[Ru(bpy)_2(\alpha,\alpha'\text{-diimine})]^{2+}$ complexes occurs at potentials more positive than bpy-based reductions; this implies that the π^* orbital energy for impy is lower than that of bpy.[36]

Based on the values measured for metal- and ligand-centered processes (Table 5.2), estimates of the excited-state couples for **2** can be made using equations (1) and (2):

$$E^{3+/2+*} = E_{ox} - E_{em} \quad (1)$$

$$E^{2+*/1+} = E_{red} + E_{em} \quad (2)$$

For values of E_{em}, $E_{0\text{-}0}$ measured at 64K in a polymer matrix was used. These values give estimates for $E^{3+/2+*} \sim -0.4$ and $E^{2+*/1+} \sim 0.7$ V vs. SCE. For comparison, the reduction and oxidation potentials for $*[Ru(bpy)_3]^{2+}$ are 0.77 and –0.81 V (acetonitrile).[23] The differences in the reduction potentials of these complexes is highlighted by inspecting the Latimer diagrams in Figure 5.13. This comparison reveals the effect of replacing one bpy ligand with impy′.

Absorption of 1. Assigning the transitions of **1** by comparison with other complexes is difficult since only a limited number of Ru(II) acetylacetonate complexes have been prepared. The low-energy feature at 621 nm in the spectrum of $[Ru(acac)_2(bpy)]$ has been assigned as a $d\pi(Ru) \rightarrow \pi^*(bpy)$ transition.[29] A tentative assignment of MLCT was given to the band at 416 nm for $[Ru(acac)_2(bpy)]$, although the nature of the π^* orbital of this transition was not specified.[29] Transitions in other Ru(II) acetylacetonate complexes – such as *cis*- and *trans*-$[Ru(acac)_2(L)_2]$ complexes (where L = CH_3CN, pyrazine, Cl) – appear near 400 nm, which have been described as $d\pi(Ru) \rightarrow \pi^*(acac)$ transitions.[37] The single absorption band at 547 nm exhibited by $[Ru(acac)_2(dppz)]$ was assigned as a $d\pi(Ru) \rightarrow \pi^*(dppz)$ transition based solely on its energy and intensity.[32]

Based on the assignments given for the reference complexes above, the absorption bands at 592 and 396 nm displayed by **1** can be described as $d\pi(Ru) \rightarrow \pi^*(impy')$ and

Figure 5.13: Latimer diagrams for $[Ru(bpy)_2(impy')]^{2+}$ (top) and $[Ru(bpy)_3]^{2+}$ (bottom). Adapted from Reference 23.

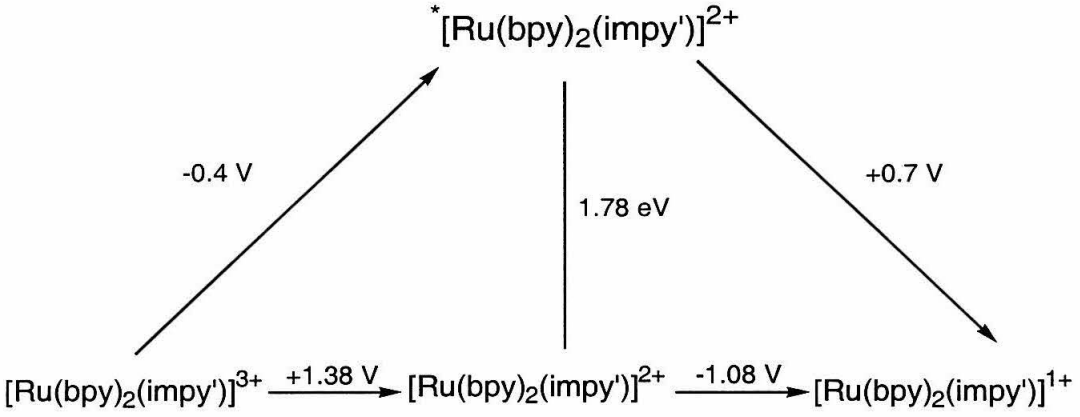

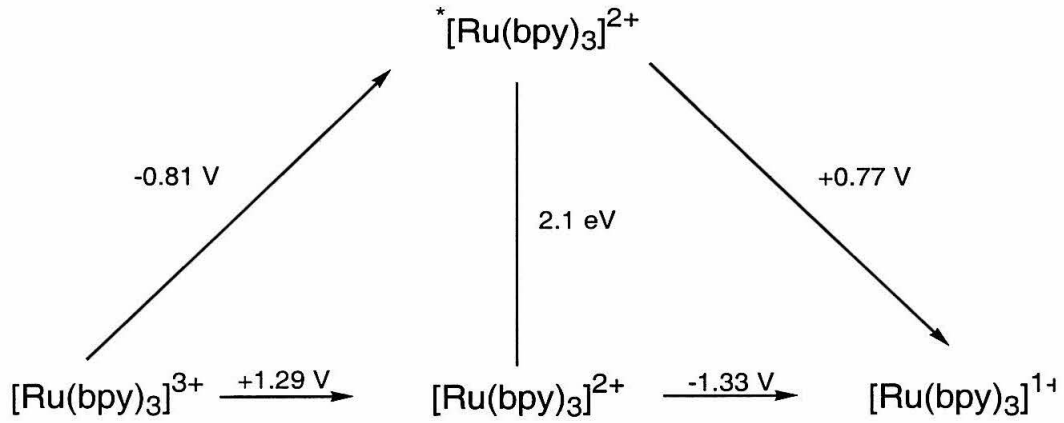

(All potentials vs. SCE, in acetonitrile.)

$d\pi(Ru) \rightarrow \pi^*(acac)$ transitions, respectively. An analogous assignment is given for the visible bands displayed by $[Ru(acac)_2(impy)]$. Such a description is consistent with the relative ordering of the ligand reduction potentials. Reduction of impy′ occurs at a –1.08 V, with reduction of the acac ligand expected to occur at more negative potentials due to the electron-rich nature of this ligand.

Interestingly, the energy of the $d\pi(Ru) \rightarrow \pi^*$(ligand) transition increases over the series: $[Ru(acac)_2(bpy)]$ (621 nm), $[Ru(acac)_2(impy')]$ (592 nm), $[Ru(acac)_2(impy)]$ (576 nm), $[Ru(acac)_2(dppz)]$ (547 nm). This trend suggests that impy′ and impy ligands stabilize the $d\pi(Ru)$ level to a greater degree than the bpy ligand in Ru(II) acetylacetonate complexes. Furthermore, it appears that the $d\pi(Ru) \rightarrow \pi^*(acac)$ transition in $[Ru(acac)_2(dppz)]$ complex has been blue-shifted to lie under the dppz intraligand (π-π^*) transition.

Similar to the low-energy bands in $[Ru(acac)(bpy)_2]^+$ and $[Ru(acac)_2(bpy)]$, the visible absorption maxima for **1** vary with solvent polarity.[29] However, these two bands do not shift in the same direction with increasing solvent polarity. For **1**, the absorption maxima are centered at 602 and 392 nm in dichloromethane, and at 592 and 396 nm in ethanol. This observed shift from 602 to 592 nm is not consistent with the MLCT description given to this transition.

Typically, MLCT bands of complexes like $[Ru(bpy)_3]^{2+}$ exhibit a positive solvatochromism, wherein λ_{max} shifts to lower energy as a function of increasing solvent polarity.[25] This trend is consistent with the molecule having a nonpolar ground state and a more polar excited state, consequences brought about by the removal of an electron

from a ruthenium-centered dπ orbital and subsequent population of an empty π* orbital of the bpy ligand. Thus, a shift of λ_{max} to *higher* energy in solvents of increasing polarity indicates a negative solvatochromism. This effect implies that the ground state is polar and that the dipole moment of the molecule is reversed or reduced upon excitation.

Negative solvatochromism is a hallmark of ligand-to-ligand charge-transfer (LLCT) transitions displayed by several metal diimine complexes.[38,39] The CT transition is directed to the vacant π* orbital of the diimine ligand, as verified by electrochemistry,[40,41] molecular orbital calculations,[42] resonance Raman spectroscopy,[43,44] and emission studies.[42,45] Of these LLCT complexes, Pt(diimine)(dithiolate) complexes have been studied by Eisenberg and coworkers, who present computational results indicating substantial metal character in the HOMO.[42] These findings support a revised assignment of the charge-transfer band to include the contribution of the Pt, which is described as follows: {d(Pt)/p(S)→π*(diimine)}. It is possible that the charge-transfer band in **1** near 600 nm represents a similarly metal-mixed LLCT transition. That this band exhibits negative solvatochromism suggests that it may originate in a mixed Ru/acac orbital and be directed to the π* orbital of the impy′ ligand.

Resonance Raman of 1. Probing the visible transitions of **1** by resonance Raman spectroscopy provides support for this revised description. The peaks observed at 1234 and 1528 cm^{-1} (441.6 nm excitation) have been recorded for other metal-acac complexes and represent ν(C-C) and ν(CO) vibrations, respectively.[46,47] No other modes are observed at this excitation frequency, implying that the transition near 400 nm involves only the acac ligand.

The rR spectrum of **1** obtained with 514.5 nm excitation shows enhancement of multiple vibrational modes (Figure 5.6). The vibrations at 1286, 1461, 1499, 1552, and 1595 cm^{-1} can be attributed to the presence of the impy′ ligand, based on comparisons with similar Ru(II) polypyridine complexes (see discussion of **2** below).[48] Interestingly, the mode at 1529 cm^{-1} is not observed in the rR spectra of these reference complexes. This mode experiences significant distortion upon low-energy excitation. Similarities between the rR spectra obtained at both 441.6 and 514.5 nm excitation suggest that this mode represents a ν(CO) vibration.

The origin of the mode at 1249 cm^{-1} observed upon 514.5 nm excitation is not immediately clear. Given the appearance of the strong Raman signal at 1529 cm^{-1} tentatively assigned as a ν(CO) vibration, the presence of an accompanying ν(C-C) vibration in the region of 1234 cm^{-1} is expected. However, the rR spectrum of **2** shows bpy- and impy′-associated vibrations in the same region (see discussion below). Therefore, the peak at 1249 cm^{-1} could represent an acac- or impy′-associated vibration.

The presence of modes characteristic of both acac- and impy′-associated vibrations in the 514.5 nm rR spectrum supports the LLCT assignment suggested earlier in the discussion. This description for the band near 600 nm in **1** — {d(Ru)/p(acac)→π*(diimine)}— is consistent with the observed negative solvatochromism. Regardless of the degree of metal involvement, a d(Ru)/p(acac)→π*(diimine) transition would be expected to cause resonance enhancement of vibrational modes on both ligands involved.

Absorption and Resonance Raman of 2. For mixed-chelate Ru(II) complexes, separate transitions to the π* orbital of each ligand may occur, resulting in an absorption

spectrum that is a composite of MLCT transitions. The broad absorption feature of **2** represents multiple MLCT transitions due to the presence of the bipyridine and iminomethylpyridine groups coordinated to the metal center.[33,35,49]

Resonance Raman data confirm this description (Figures 5.7-5.11). The rR spectra of both **2** and **3** show striking similarities with the spectrum obtained for $[Ru(bpy)_3]^{2+}$ upon 441.6 nm excitation (Figures 5.7 and 5.8). The peaks characteristic of bpy-associated vibrations are observed at 1023, 1173, 1276, 1316, 1488, 1552, and 1604 cm^{-1} for both **2** and **3**, which confirms the $d\pi(Ru) \rightarrow \pi^*(bpy)$ nature of the transition in this region. Additional peaks at 1242 and 1471 cm^{-1} represent distortions that are absent in $[Ru(bpy)_3]^{2+}$ and can be attributed to the presence of the impy′ ligand.

Typically, ground-state rR spectra of mixed-chelate Ru(II) complexes show features characteristic of the types of ligands present.[26,27] For example, the Raman signals reported for $[Ru(bpy)_2(Br_2bpy)]^{2+}$ are a combination of those observed for the homoleptic complexes, $[Ru(bpy)_3]^{2+}$ and $[Ru(Br_2bpy)_3]^{2+}$, at identical excitation frequency.[27] The relative intensities of the observed features reflect the number and type of pp ligand present in the complex.[26] Therefore, it is expected that the rR spectra of **2** and **3** to contain Raman signals characteristic of both bpy and impy′ vibrations.

Changes in the rR spectra of **2** (457.9 and 488.0 nm excitation) suggest that the low-energy side of the broad MLCT band is dominated by a $d\pi(Ru) \rightarrow \pi^*(impy')$ transition (Figures 5.9 and 5.10). This assignment is supported by the variation in the relative intensities of modes in the region of 1400-1700 cm^{-1}. The 1471 and 1488 cm^{-1} modes undergo a striking reversal in intensity as a function of excitation wavelength (Figure 5.11). While the peak at 1605 cm^{-1} remains essentially unchanged, the broad

peak at 1552 cm^{-1} (441.6 nm excitation) sharpens upon 488.0 nm excitation. The appearance of a peak at 1580 cm^{-1} implies that absorption at this excitation frequency involves a $d\pi(Ru) \rightarrow \pi^*(impy')$ transition in addition to the $d\pi(Ru) \rightarrow \pi^*(bpy)$ transition.

Emission of 2. Irradiation of **2** at 480 nm yields an emission spectrum with a maximum at 730 nm, which is red-shifted from the emission maximum of $[Ru(bpy)_3]^{2+}$ (625 nm) (Figure 5.12). This substantial shift to lower energy suggests that the emitting state is based on the impy′ ligand. Electrochemical data show that this ligand has the most positive reduction potential; consequently, impy′ is the ligand in **2** with the π^* orbital that is lowest in energy.[36] This assertion that the excited electron is localized on the most easily reduced ligand is consistent with the literature.[27]

The excited-state lifetime of **2** is 44 nsec, much shorter than those of similar complexes (Table 5.2). The decrease in the lifetime values over the series—$[Ru(bpy)_3]^{2+}$ (650 nsec), $[Ru(bpy)_2(ampy)]^{2+}$ (192 nsec), **2** (44 nsec)—reveals the effect of the ampy and impy linkages. The differences in the lifetime and quantum yield for $[Ru(bpy)_3]^{2+}$ vs. **2** correspond to an increase in the nonradiative rate constant (k_{nr}) from 1.54×10^6 s^{-1} to 2.38×10^7 s^{-1}, respectively. This increase is consistent with the additional vibrational modes observed by rR spectroscopy for **2**, which represent excited state distortions not operative in $[Ru(bpy)_3]^{2+}$.

Conclusion

We utilize several methods to investigate the visible transitions displayed by metallonucleosides **1** and **2**. Comparison of the ground-state properties of these complexes with those of reference complexes shows the effect of replacing one bipyridine ligand with a substituted impy ligand. The presence of the nucleoside

substituted on the impy ligand increases the metal-centered reduction potentials displayed by **1** and **2**. Resonance Raman spectroscopy assists in analyzing the absorption spectrum of each metallonucleoside. The rR results suggest that the low-energy transition displayed by **1** involves both the acac and impy′ ligands, tentatively assigned as a metal-mixed LLCT transition.

The broad visible band displayed by **2** represents multiple charge-transfer transitions, namely MLCT transitions to the π^* orbtials of the bpy and impy′ ligands. A description of this broad band as a composite of ligand-localized MLCT transitions is supported by rR data obtained at multiple excitation frequencies.[25] The electrochemical, absorption, and emission data of **2** indicate that the lowest energy π^* orbital available for occupation by an excited electron is that of the impy′ ligand.

The replacement of one bpy ligand with a substituted impy ligand causes minor alterations to the ground-state properties of the resulting mixed-chelate complex, **2**. However, profound changes in the excited-state properties are observed upon this bpy→ impy′ synthetic substitution. While the impy′ ligand enables facile incorporation of the ruthenium complex into oligonucleotides by solid-phase DNA syntheis,[1] it dominates the emissive behavior of the Ru(II) complex. This result illustrates how ligand replacements imposed for synthetic purposes can cause significant alterations in the excited-state properties of the resulting mixed-chelate complex.

Experimental Section

Synthesis of Ru(acac)$_2$(impy′) (1): 2'-amino-5'-O-(4,4'-dimethoxytrityl)-2'-deoxyuridine (93 mg, 0.17 mmol) was dissolved in ethanol (5 mL) containing molecular

sieves, and the solution was flushed with argon for 15 minutes. 2-pyridinecarboxaldehyde (15 μL, 0.16 mmol) was added incrementally, and the reaction was refluxed for 2 hours. The solution was cooled, filtered to remove the molecular sieves, and evaporated to dryness under reduced pressure to give the intermediate nucleoside impy′. (Electrospray mass spectral analysis of an aliquot of crude impy′ found 635.2 [M+H$^+$], as compared to 634.2 calculated for [M].) The nucleoside was redissolved in ethanol (5 mL) and the solution was deaerated. In a separate flask $Ru(acac)_2(CH_3CN)_2$ (0.17 mmol) was dissolved ethanol (25 mL) and the solution was deaerated. The two solutions were combined and heated to reflux for 1 hour. The solvent was removed under reduced pressure and the green residue was purified by flash chromatography on silica using 1.5:1 THF/hexanes mobile phase (yield 79%). ^{1}H-NMR (500 MHz, $CDCl_3$, Figure 5.14) δ 8.93 (s, 1H), 8.74 (d, 1H), 7.81 (d, 1H), 7.73 (d, 1H), 7.48 (t, 1H), 7.43 (d, 2H), 7.20-7.34 (mm, 7H), 7.11 (t, 1H), 6.81 (dd, 4H), 5.36 (dd, 1H), 5.28 (s, 1H), 5.02 (s, 2H), 4.88-4.92 (m, 1H), 4.84 (s (br), 1H), 4.68-4.76 (m, 1H), 3.79 (d, 6H), 3.41-3.56 (m, 2H), 2.20 (s, 3H), 2.12 (s, 3H), 1.82 (s, 3H), 1.60 (s, 3H). UV-vis (EtOH) nm (ε): 234 (33400), 276 (27000), 396 (3600), 592 (3600). ESI-MS calculated for $C_{46}H_{48}N_4O_{11}Ru$ [M+H$^+$] 934.96, found 934.4 [M+H$^+$] (Figure 5.15).

Synthesis of $Ru(acac)_2$(impy): The model complex was prepared by first reducing $Ru(acac)_3$ (99.6 mg, 0.25 mmol) over Zn/Hg amalgam under argon in 6:1 ethanol/water solution.[50] Following reduction, 2-(aminomethyl)pyridine (28.4 μL, 0.25 mmol) was added dropwise in 1 mL EtOH and the solution was refluxed for 2 hours. The reaction mixture was cooled, filtered and purified by flash chromatography on silica under argon using 1.5:1 THF/hexanes mobile phase (yield 58%). UV-vis (EtOH) nm (ε): 206

Figure 5.14: ^{1}H NMR spectrum of **1** in $CDCl_3$ (500 MHz).

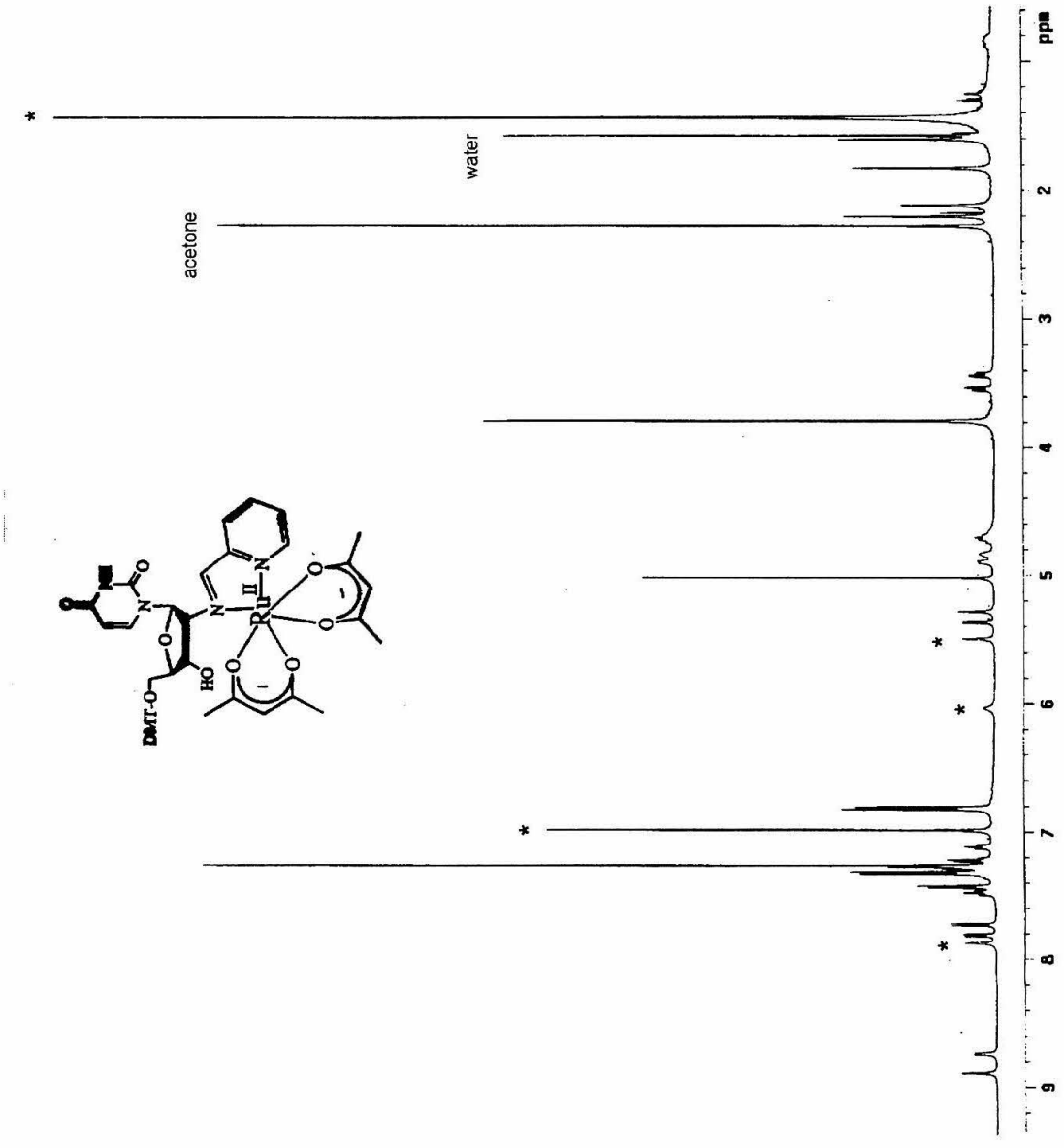
acetone
water
ppm
DMT-O
HO

Figure 5.15: ESI mass spectrum of **1** in positive ionization mode (top) and MALDI-TOF mass spectrum of **1** showing isotopic distribution (bottom).

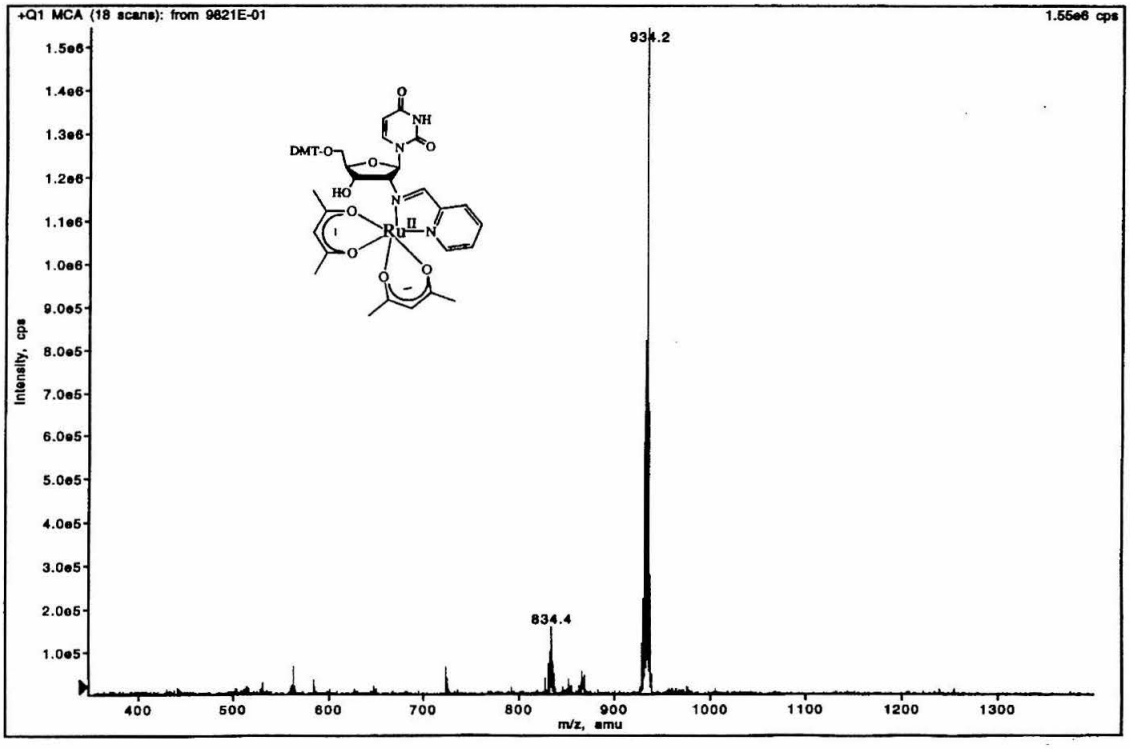
+Q1 MCA (18 scans): from 9821E-01
1.55e6 cps
934.2
834.4
Intensity, cps
m/z, amu
DMT-O
HO
NH
Ru
II

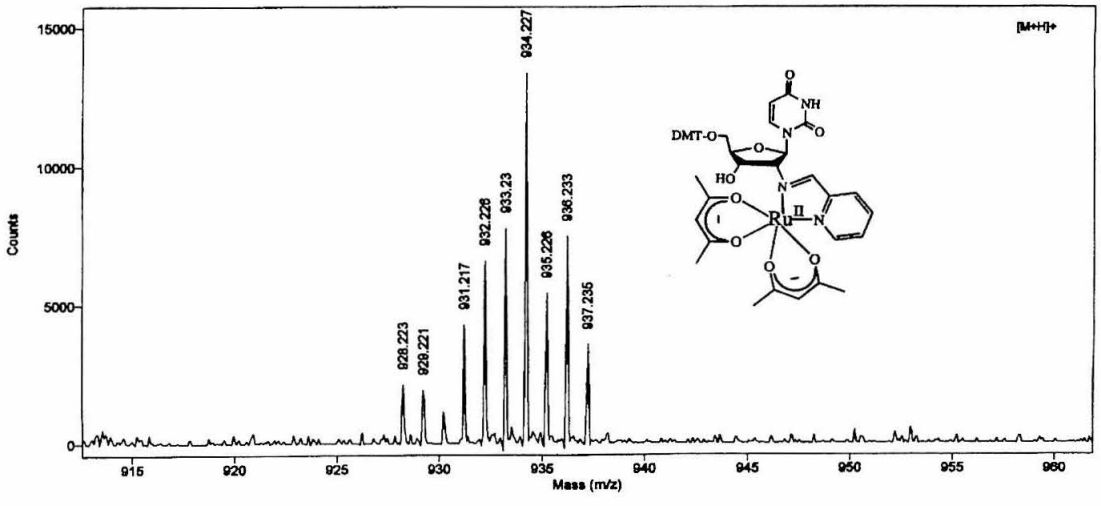
[M+H]+
934.227
933.23
932.226
931.217
936.233
935.226
937.235
928.223
928.221
Counts
Mass (m/z)
DMT-O
HO
NH
Ru
II

(21,800), 274 (16,800), 402 (4600), 576 (4600). ESI-MS calculated for $C_{16}H_{20}N_2O_4Ru$ [M+H$^+$] 406.41, found 406.2 [M+H$^+$] (Figure 5.16).

The ruthenium(II) compounds **2** and **3** were prepared and characterized as previously described in Chapter 4.[1]

Instrumentation

Electrochemical data were collected in a traditional two-compartment cell using a polished and sonicated 3 mm-diameter glassy carbon or platinum disk working electrode (BAS), Pt wire auxiliary electrode, and Ag/AgCl reference electrode. Values in the text are referenced to the saturated calomel electrode (SCE). Measurements were conducted at room temperature with a CH instruments 660 electrochemial workstation after the solutions were deaerated under argon. Data for **1** and [Ru(acac)$_2$(impy)] were recorded in ethanol containing 0.1 M ammonium hexafluorophosphate (Aldrich); measurements of **2** were collected in either acetonitrile or dichloromethane (Burdick and Jackson) containing 0.1 M n-tetrabutylammonium hexafluorophosphate (SACHEM). Square-wave voltammograms of **3** were recorded in phosphate buffer (50 mM, pH 7.0, 0.5 M NaCl) in nanopure water. Absorption spectra were obtained using a Hewlett-Packard 8452A diode array spectrophotometer.

Excitation of the rR samples was provided by 441.6 nm (He:Cd Liconix) or 514.5 nm (Ar$^+$ Coherent Innova 70) and scattered light was dispersed with a Spex 1403 Double Monochromator and intensities were measured by single-photon counting. Samples were prepared in NMR tubes and contained either water, d_4-methanol, or dichloromethane. The Raman signal was collected at 90° during irradiation with dwell times of 10 sec/cm^{-1}

Figure 5.16: ESI mass spectrum of [$Ru(acac)_2(impy)$] in positive ionization mode.

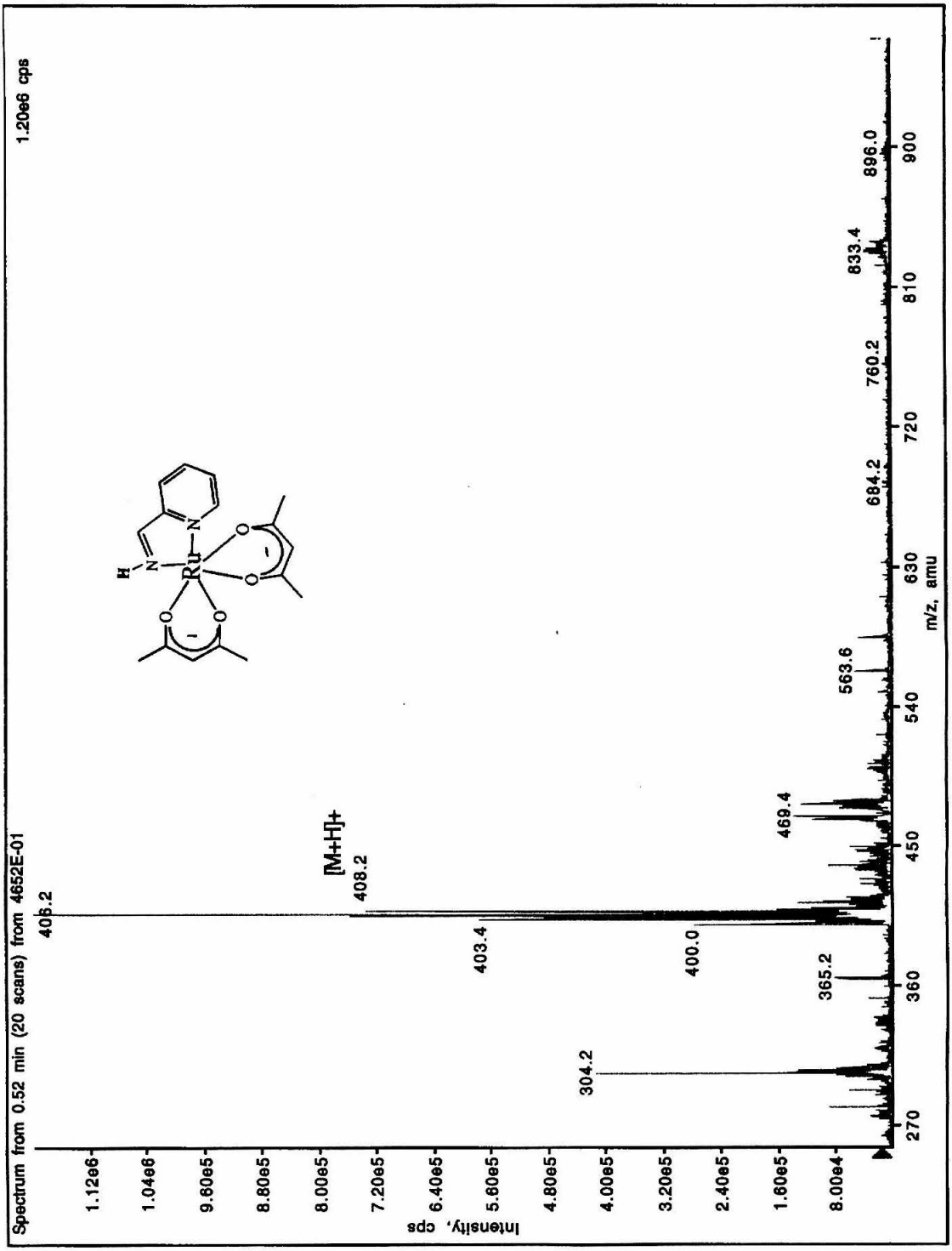
Spectrum from 0.52 min (20 scans) from 4652E-01
1.20e6 cps
406.2
[M+H]+
408.2
403.4
400.0
469.4
365.2
304.2
563.6
684.2
760.2
833.4
896.0
Intensity, cps
m/z, amu
1.12e6
1.04e6
9.60e5
8.80e5
8.00e5
7.20e5
6.40e5
5.60e5
4.80e5
4.00e5
3.20e5
2.40e5
1.60e5
8.00e4
270
360
450
540
630
720
810
900
Ru
N
O

at 1 cm^{-1} intervals.

Emission spectra were collected with a Hitachi F-4500 Fluorescence Spectrometer with the following instrumental parameters: 10 nm slits, 750 V PMT, 480 nm excitation, 500-900 nm scan wavelengths. Quantum yield measurements were calculated using $[Ru(bpy)_3]^{2+}$ as an actinometer. Lifetimes were collected as previously described.[51] Variable-temperature emission spectra were collected with **2** suspended in polymer matrix by Dr. Jeffrey J. Rack.

Acknowledgment

This work was supported by NIST (ATP) Award 70NANB5H1031, Jet Propulsion Laboratory (JPL 67192), and the Beckman Institute Biological Imaging Center.

References and Notes

(1) Rack, J. J.; Krider, E. S.; Meade, T. J. *J. Am. Chem. Soc.* **2000**, *122*, 6287-6288.

(2) Hu, X.; Smith, G. D.; Sykora, M.; Lee, S. J.; Grinstaff, M. W. *Inorg. Chem.* **2000**, *39*, 2500-2504.

(3) Lewis, F. D.; Helvoigt, S. A.; Letsinger, R. L. *Chem. Commun.* **1999**, 327-328.

(4) Holmlin, R. E.; Dandliker, P. J.; Barton, J. K. *Bioconj. Chem.* **1999**, *10*, 1122-1130.

(5) Khan, S. I.; Beilstein, A. E.; Tierney, M. T.; Sykora, M.; Grinstaff, M. W. *Inorg. Chem.* **1999**, *38*, 5999-6002.

(6) Khan, S. I.; Beilstein, A. E.; Sykora, M.; Smith, G. D.; Hu, X.; Grinstaff, M. W. *Inorg. Chem.* **1999**, *38*, 3922-3925.

(7) Khan, S. I.; Beilstein, A. E.; Grinstaff, M. W. *Inorg. Chem.* **1999**, *38*, 418-419.

(8) Khan, S. I.; Grinstaff, M. W. *J. Am. Chem. Soc.* **1999**, *121*, 4704-4705.

(9) Wiederholt, K.; McLaughlin, L. W. *Nucleic Acids Res.* **1999**, *27*, 2487-2493.

(10) Ortmans, I.; Content, S.; Boutonnet, N.; Kirsch-De Mesmaeker, A.; Bannwarth, W.; Constant, J. F.; Defrancq, E.; Lhomme, J. *Chem. Eur. J.* **1999**, *5*, 2712-2721.

(11) Hurley, D. J.; Tor, Y. *J. Am. Chem. Soc.* **1998**, *120*, 2194-2195.

(12) Holmlin, R. E.; Dandliker, P. J.; Barton, J. K. *Angew. Chem. Int. Ed.* **1997**, *36*, 2715-2730.

(13) Meggers, E.; Kusch, D.; Giese, B. *Helv. Chim. Acta* **1997**, *80*, 640-652.

(14) Telser, J.; Cruickshank, K. A.; Schanze, K. S.; Netzel, T. L. *J. Am. Chem. Soc.* **1989**, *111*, 7221-7226.

(15) Bannwarth, W.; Schmidt, D. *Tet. Lett.* **1989**, *30*, 1513-1516.

(16) Khan, S. I.; Beilstein, A. E.; Smith, G. D.; Sykora, M.; Grinstaff, M. W. *Inorg. Chem.* **1999**, *38*, 2411-2415.

(17) Bannwarth, W.; Schmidt, D.; Stallard, R. L.; Hornung, C.; Knorr, R.; Muller, F. *Helv. Chim. Acta* **1988**, *71*, 2085-2099.

(18) Bannwarth, W.; Pfleiderer, W.; Muller, F. *Helv. Chim. Acta* **1991**, *74*, 1991-1999.

(19) Bannwarth, W.; Muller, F. *Helv. Chim. Acta* **1991**, *74*, 2000-2008.

(20) Tierney, M. T.; Sykora, M.; Khan, S. I.; Grinstaff, M. W. *J. Phys. Chem. B* **2000**, *104*, 7574-7576.

(21) Meade, T. J.; Kayyem, J. F. *Angew. Chem. Int. Ed. Engl.* **1995**, *34*, 352-353.

(22) Lever, A. B. P. *Inorg. Chem.* **1990**, *29*, 1271-1285.

(23) Juris, A.; Balzani, V.; Barigelletti, F.; Campagna, S.; Belser, P.; Vonzelewsky, A. *Coord. Chem. Rev.* **1988**, *84*, 85-277.

(24) Barigelletti, F.; Juris, A.; Balzani, V.; Belser, P.; Vonzelewsky, A. *Inorg. Chem.* **1987**, *26*, 4115-4119.

(25) Kober, E. M.; Sullivan, B. P.; Meyer, T. J. *Inorg. Chem.* **1984**, *23*, 2098-2104.

(26) McClanahan, S. F.; Dallinger, R. F.; Holler, F. J.; Kincaid, J. R. *J. Am. Chem. Soc.* **1985**, *107*, 4853-4860.

(27) Mabrouk, P. A.; Wrighton, M. S. *Inorg. Chem.* **1986**, *25*, 526-531.

(28) Danzer, G. D.; Golus, J. A.; Kincaid, J. R. *J. Am. Chem. Soc.* **1993**, *115*, 8643-8648.

(29) Bryant, G. M.; Fergusson, J. E.; Powell, H. K. J. *Aust. J. Chem.* **1971**, *24*, 257-273.

(30) Bennett, M. A.; Chung, G. L.; Hockless, D. C. R.; Neumann, H.; Willis, A. C. *J. Chem. Soc. Dalt. Trans.* **1999**, 3451-3462.

(31) Bennett, M. A.; Heath, G. A., unpublished results.

(32) Nair, R. B.; Yeung, L. K.; Murphy, C. J. *Inorg. Chem.* **1999**, *38*, 2536-+.

(33) Brown, G. M.; Weaver, T. R.; Keene, F. R.; Meyer, T. J. *Inorg. Chem.* **1976**, *15*, 190-196.

(34) Strouse, G. F.; Anderson, P. A.; Schoonover, J. R.; Meyer, T. J.; Keene, F. R. *Inorg. Chem.* **1992**, *31*, 3004-3006.

(35) Ridd, M. J.; Keene, F. R. *J. Am. Chem. Soc.* **1981**, *103*, 5733-5740.

(36) Stufkens, D. J. *Coord. Chem. Rev.* **1990**, *104*, 39-112.

(37) Hasegawa, T.; Lau, T. C.; Taube, H.; Schaefer, W. P. *Inorg. Chem.* **1991**, *30*, 2921-2928.

(38) Vogler, A.; Kunkely, H. *Comments Inorg. Chem.* **1990**, *9*, 201-220.

(39) Acosta, A.; Zink, J. I.; Cheon, J. *Inorg. Chem.* **2000**, *39*, 427-432.

(40) Miller, T. R.; Dance, I. G. *J. Am. Chem. Soc.* **1973**, *95*, 6970-6979.

(41) Vogler, A.; Kunkely, H.; Hlavatsch, J.; Merz, A. *Inorg. Chem.* **1984**, *23*, 506-509.

(42) Zuleta, J. A.; Bevilacqua, J. M.; Proserpio, D. M.; Harvey, P. D.; Eisenberg, R. *Inorg. Chem.* **1992**, *31*, 2396-2404.

(43) Nieuwenhuis, H. A.; Stufkens, D. J.; Oskam, A. *Inorg. Chem.* **1994**, *33*, 3212-3217.

(44) Wootton, J. L.; Zink, J. I. *J. Phys. Chem.* **1995**, *99*, 7251-7257.

(45) Zuleta, J. A.; Chesta, C. A.; Eisenberg, R. *J. Am. Chem. Soc.* **1989**, *111*, 8916-8917.

(46) Handa, M.; Miyamoto, H.; Suzuki, T.; Sawada, K.; Yukawa, Y. *Inorg. Chim. Acta* **1993**, *203*, 61-65.

(47) Yukawa, Y.; Handa, M.; Hoshino, Y. *J. Sol. Chem.* **1995**, *24*, 19-24.

(48) Schoonover, J. R.; Strouse, G. F. *Chem. Rev.* **1998**, *98*, 1335-1355.

(49) Keene, F. R.; Ridd, M. J.; Snow, M. R. *J. Am. Chem. Soc.* **1983**, *105*, 7075-7081.

(50) Knowles, T. S.; Howells, M. E.; Howlin, B. J.; Smith, G. W.; Amodio, C. A. *Polyhedron* **1994**, *13*, 2197-2203.

(51) Low, D. W.; Winkler, J. R.; Gray, H. B. *J. Am. Chem. Soc.* **1996**, *118*, 117-120.

Appendix A:

Additional Nucleoside Synthesis

Part A. Synthesis of 2′-Modified Nucleoside, 3a.

An alternate approach to preparing nucleoside **3a** (Chapter 2) was pursued that utilized the 5′-protected form of 2′-amino-2′-deoxyuridine (**A1**). Condensation of **A1** with 2-pyridinecarboxaldehyde in absolute ethanol gave the 2′-imine nucleoside (nucleoside **1**, Chapter 4) in approximately 70% yield. Attempts to purify nucleoside **1** by flash chromatography were unsuccessful. Subsequent reduction of **1** with sodium cyanoborohydride gave **3a** in high yield as indicated by TLC. However, attempts to isolate **3a** by flash chromatography resulted in low yields (5-10%).

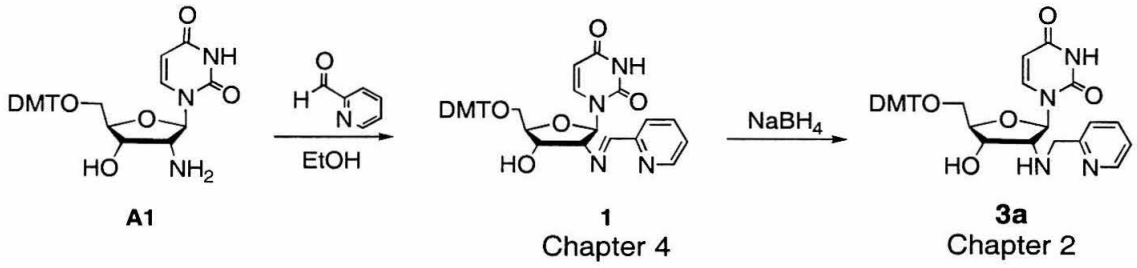

A1 **1** Chapter 4 **3a** Chapter 2

Experimental Notes

5′-O-(4,4′-dimethoxytrityl)-2′-aminomethylpyridyl-2′-deoxyuridine (3a). Compound **A1** was prepared as described.[1] **A1** (1.9 g, 3.5 mmol, 1.5 eq) was dissolved in absolute ethanol (25 mL) over molecular sieves; the reaction vessel was flushed with argon for 20 minutes while heated to reflux temperature. 1 eq of 2-pyridinecarboxaldehyde (220 μL, 2.3 mmol) was delivered to the solution in 1 mL of ethanol, and the solution was refluxed for 2-16 hours.

An aliquot from the reaction was filtered and evaporated to dryness by rotary evaporation. ESI-MS calculated for **1** $[M-H]^-$ (negative mode): 633.24. Found: 633.2.; calcd for **1** $[M+H]^+$ (positive mode): 635.24. Found: 635.2. Additional peaks were observed in positive mode: $[M+Na]^+$ 657.2, $[M+K]^+$ 673.2, (unassigned) 724.4. Data are shown in Figures A.1 and A.2. Purification on silica was unsuccessful; ^1H NMR analysis of the crude product was complicated by impurities.

The remaining solution was cooled and excess sodium borohydride was added to the solution. The reaction was stirred at room temperature for 12 hours and refluxed for an additional 2 hours. The solvent was removed and the residue was dissolved in dichloromethane and extracted with: 5% ammonia solution, saturated sodium chloride, water, and cold 5% citric acid. The organic phase was dried over sodium sulfate and the solvent evaporated to give **3a**. Purification on silica (45-45-10 dichloromethane-methanol-triethylamine) was unsuccessful and resulted in impure fractions of **3a**.

Figure A.1: ESI mass spectrum of crude **1** conducted in negative ionization mode.

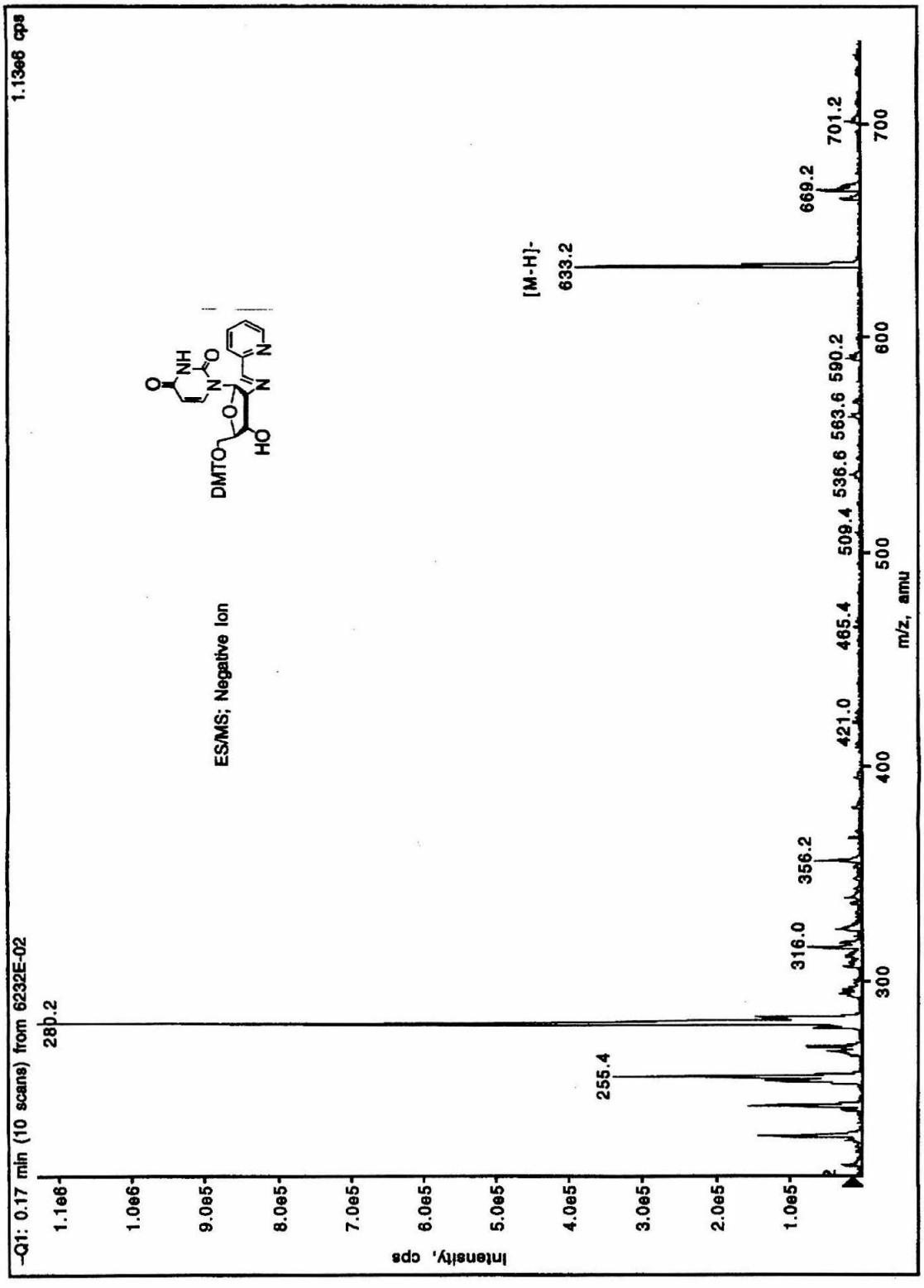
-Q1: 0.17 min (10 scans) from 6232E-02
1.13e6 cps
Intensity, cps
m/z, amu
ES/MS; Negative Ion
DMTO
HO
[M-H]-
633.2
669.2
701.2
590.2
563.6
536.6
509.4
465.4
421.0
356.2
316.0
255.4
280.2

Figure A.2: ESI mass spectrum of crude **1** conducted in positive ionization mode.

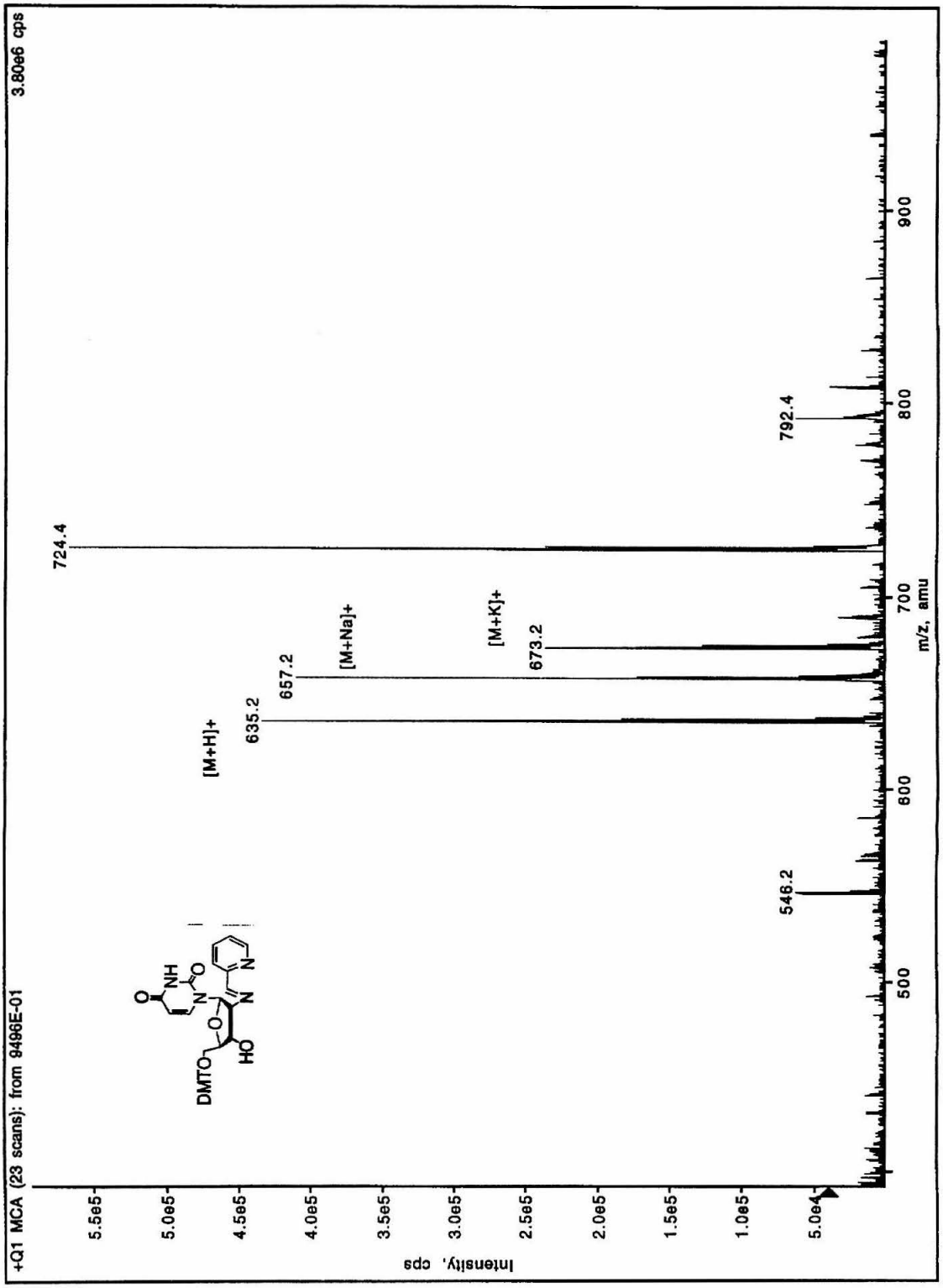
+Q1 MCA (23 scans): from 9496E-01
3.80e6 cps
Intensity, cps
m/z, amu
724.4
635.2
[M+H]+
657.2
[M+Na]+
673.2
[M+K]+
546.2
792.4
DMTO
HO
NH
O
N
O
N
N

Part B. Deprotection of 2′-Modified Nucleoside, 3b.

There are two methods for removing the trityl protecting group at the 5′ position. The first method involves stirring the solid in 80% acetic acid for 16-24 hours, followed by removal of the solvent and coevaporation with methanol. The residue is extracted in dichloromethane with water. The aqueous fraction is evaporated to dryness to give the deprotected nucleoside. The second method uses trichloroacetic acid and is complete in a very short period of time. The solid is dissolved in a 1:4 mixture of ethanol and dichloromethane, to which is added an equal volume of aqueous 5% trichloroacetic acid (para-toluene sulfonic acid may also be used). The mixture is shaken well and the reaction is complete within 15 minutes (as monitored by TLC). The organic phase is removed and the resulting solution is neutralized with 4 M sodium hydroxide. The remaining solvent is removed and the residue is dissolved in water, followed by extraction with either ethyl acetate or dichloromethane. The aqueous phase was evaporated to dryness to give the deprotected nucleoside.

Nucleoside **3b** from Chapter 2 was detritylated using the second method. ESI-MS calculated for $C_{16}H_{20}N_4O_5$: $[M+H]^+$: 349.14. Found: 349.2. Additional peaks were found: $[M+Na]^+$ 371.2, (unassigned) 393.2. The deprotected nucleoside was used in the model complex reactions summarized in Appendix B.

Part C. Synthesis of Modified Oligonucleotides.

Oligonucleotides containing the 2′ modified nucleosides shown below were synthesized and purified. The sequences of these oligonucleotides are tabulated. However, no data in addition to that presented in Chapters 2 and 3 are included here.

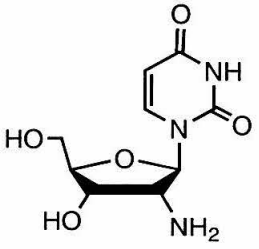

U_a

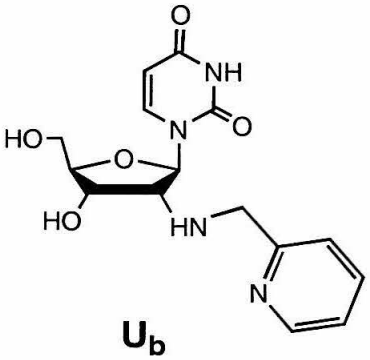

U_b

Abbreviation	Oligonucleotide Sequence
8A	5′-$\mathbf{U_a}$GCATCGA-3′
8B	5′-$\mathbf{U_a}$CGATGCA-3′
11A	5′-$\mathbf{U_a}$CAGCTGTAGA-3′
11B	5′-$\mathbf{U_b}$CTACAGCTGA-3′
14A	5′-$\mathbf{U_a}$GTGCTCCTGAGGA-3′

References

(1) McGee, D.; Vaughn-Settle, A.; Vargeese, C.; Zhai, Y. *J. Org. Chem.* 1996, *61*, 781-785.

Appendix B:

Synthesis of Ruthenium Model Complexes

Summary

Several ruthenium model complexes were evaluated as possible donor-acceptor candidates for use in DNA-ET studies (see Chapter 1 for discussion of criteria). The types of complexes considered included Ru(II) acetylacetonate, bipyridine, and amine complexes. Once prepared, the model complexes were evaluated for subsequent incorporation into oligonucleotides by either post-synthetic modification or solid-phase synthesis methods (Chapter 4). The synthesis and characterization of these complexes is summarized below.

Experimental Section

$Ru(acac)_2(impy)$. The model complex was prepared by first reducing $Ru(acac)_3$ (99.6 mg, 0.25 mmol) over Zn/Hg amalgam under argon in 6:1 ethanol/water solution. Following reduction, 2-(aminomethyl)pyridine (28.4 μL, 0.25 mmol) was added dropwise in 1 mL EtOH and the solution was refluxed for 2 hours. The solution was a deep orange. The reaction mixture was cooled and filtered. Upon exposure to air, the solution became a deep purple. The solution was evaporated to dryness and purified by flash chromatography on silica under argon using 1.5:1 THF/hexanes mobile phase (yield 58%). UV-vis (EtOH) nm (ε): 206 (21,800), 274 (16,800), 402 (4600), 576 (4600); (CH_2Cl_2) 232 (7800), 276 (11,800), 398 (4700), 592 (4800). ESI-MS calculated for $C_{16}H_{20}N_2O_4Ru$ [$M+H^+$] 406.05, found 406.2 [$M+H^+$]. See Chapter 5 for mass spectral data shown in Figure 5.15. Electrochemical data: $E_{1/2}$ = 33 mV vs. Ag/AgCl in EtOH, 0.1 M NH_4PF_6.

$Ru(acac)_2(impy')$. 5'-O-(4,4'-dimethoxytrityl)-2'-amino-2'-deoxyuridine (93 mg, 0.17 mmol) was dissolved in ethanol (5 mL) containing molecular sieves, and the solution was flushed with argon for 15 minutes. 2-pyridinecarboxaldehyde (15 μL, 0.16 mmol) was added incrementally, and the reaction was refluxed for 2 hours. The solution was cooled, filtered to remove the molecular sieves, and evaporated to dryness under reduced pressure to give the intermediate impy-modified nucleoside. (Electrospray mass spectral analysis of an aliquot of the crude nucleoside found 635.2 $[M+H^+]$, as compared to 634.2 calculated for [M].) The nucleoside was redissolved in ethanol (5 mL) and the solution was deaerated. In a separate flask $Ru(acac)_2(CH_3CN)_2$ (0.17 mmol) was dissolved ethanol (25 mL) and the solution was deaerated. The two solutions were combined and heated to reflux for 1 hour. The solvent was removed under reduced pressure and the green residue was purified by flash chromatography on silica using 1.5:1 THF/hexanes mobile phase (yield 79%). ^{1}H-NMR (500 MHz, $CDCl_3$, see Chapter 5, Figure 5.13) δ 8.93 (s, 1H), 8.74 (d, 1H), 7.81 (d, 1H), 7.73 (d, 1H), 7.48 (t, 1H), 7.43 (d, 2H), 7.20-7.34 (mm, 7H), 7.11 (t, 1H), 6.81 (dd, 4H), 5.36 (dd, 1H), 5.28 (s, 1H), 5.02 (s, 2H), 4.88-4.92 (m, 1H), 4.84 (s (br), 1H), 4.68-4.76 (m, 1H), 3.79 (d, 6H), 3.41-3.56 (m, 2H), 2.20 (s, 3H), 2.12 (s, 3H), 1.82 (s, 3H), 1.60 (s, 3H). UV-vis (EtOH) nm (ε): 234 (33400), 276 (27000), 396 (3600), 592 (3600); (CH_2Cl_2) 234 (21,500), 276 (18,600), 392 (3600), 602 (3700). ESI-MS calculated for $C_{46}H_{48}N_4O_{11}Ru$ $[M+H^+]$ 934.96, found 934.4 $[M+H^+]$ (see Figure 5.14). $E_{1/2}$ = 92 mV vs. Ag/AgCl in EtOH, 0.1 M NH_4PF_6. See Chapter 5 for additional characterization.

$Ru(acac)_2(aepy)^+$. The model complex was prepared by reducing $Ru(acac)_3$ (100 mg, 0.25 mmol) over Zn/Hg amalgam under argon in 6:1 ethanol/water solution.

Following reduction 2-(aminoethyl)pyridine (29 μL, 0.25 mmol, d = 1.049) was added dropwise in 1 mL EtOH and the solution was refluxed for 18 hours. The reaction mixture was cooled, filtered, and evaporated to dryness by rotary evaporation. An absorption spectrum of the crude material in ethanol showed bands at 332, 396, and 580 nm; the UV region was broad and ill-defined. ESI-MS (crude material) calculated for $C_{17}H_{24}N_2O_4Ru$ [M] 422, found 422.2 [M], in addition to other peaks at 474.2, 511.4, 562.4, and 835.4. The isotope pattern of the peak at 422.2 matched the predicted pattern for $C_{17}H_{24}N_2O_4Ru$.

[Ru(acac)$_2$(tmen)](NO$_3$). *Method 1.* The model complex was prepared by reducing $Ru(acac)_3$ (100 mg, 0.251 mmol) over Zn/Hg amalgam under argon in 100:1 THF/water solution. The tmen ligand (38 μL, 0.251 mmol, d = 0.77) was added and the solution was refluxed overnight. The progress of the reaction was monitored by TLC using a 3:1 THF:hexanes solvent system. The reaction was filtered and evaporated to dryness by rotary evaporation to give 135 mg of crude materal. This residue was resuspended in a minimal amount of THF, and a saturated solution of TBAH in THF was added to the sample and the solution was chilled overnight.

Method 2. The model complex was prepared by dissolving $Ru(acac)_2(CH_3CN)_2$ (20 mg, 0.052 mmol) in ethanol under argon and adding the tmen ligand (7.9 μL, 0.052 mmol, d = 0.77) to this solution. The reaction was heated to reflux and monitored by TLC using a 90:10 CH_3CN:water solvent system. Initially the solution was orange; 30 minutes after heating commenced, the solution was a dark orange-red. TLC showed a new spot near the origin. The reaction was cooled to room temperature after 10 hours of refluxing, evaporated to dryness (35 mg crude material), and purified by column chromatography on silica gel (80:20 CH_3CN:water containing 0.1% saturated KNO_3).

The sample was resuspended in ethanol and evaporated to dryness. UV-vis (EtOH, 0.1 M NH_4PF_6): 226, 284, 332, 514 nm. ESI-MS calculated for $C_{16}H_{30}N_2O_4Ru$ [M] 416, found 416.4 [M]. Electrochemical data: $E_{1/2}$ = -0.415 V vs. Ag/AgCl in EtOH, 0.1 M NH_4PF_6.

$[Ru(bpy)_2(U_{impy})](NO_3)_2$. 2'-amino-2'-deoxyuridine (0.5 g, 2.05 mmol) was dissolved in ethanol (140 mL) containing molecular sieves, and the solution was flushed with argon for 15 minutes. 2-pyridinecarboxaldehyde (196 uL, 2.05 mmol) was added dropwise, and the reaction was refluxed for 11 hours. The reaction was monitored by TLC using the following solvent systems: 70:30 CH_2Cl_2:MeOH; 85:12:3 CH_2Cl_2:MeOH:TEA; 3:1 EtOH:TEAAc. The solution was filtered and evaporated to dryness by rotary evaporation, giving ~ 700 mg of crude material. (ESI-MS (crude material) calculated for $C_{15}H_{16}N_4O_5$ [M] 332.3, found 333.0 [M+H^+], 355.0 [M+Na^+], in addition to small peaks at 304.2, 387.0, 422.2, 476.0, and 490.0.) The crude nucleoside was resuspended in ethanol (40 mL) and the solution was flushed with argon for 10 minutes. $Ru(bpy)_2Cl_2$ (0.904 g, 1.87 mmol) was dissolved in ethanol (40 mL) and stirred for 10 minutes prior to being delivered to the nucleoside solution. The combined solutions were flushed with argon for 10 minutes and heated to reflux for 4 hours. The reaction was monitored by TLC using a 90:8:2 CH_3CN:water:saturated KNO_3 solvent system. The reaction was cooled, filtered, and stripped to dryness by rotary evaporation to give 1.5 g of crude material, which was purified on basic alumina using a 88:10:2 CH_3CN:water:saturated KNO_3 solvent system. ESI-MS showed impurities contaminating the product, so the material was re-purified as follows. The sample was dissolved in MeOH, the excess KNO_3 was removed by filtration, the resulting solution

was stripped to dryness, and the residue was purified on alumina using a 90:8:2 CH_3CN:water:saturated KNO_3 solvent system. Fractions containing the product were evaporated to dryness, redissolved in MeOH to remove excess salt, and evaporated to dryness to give a red film (~500 mg). MALDI-TOF MS calculated for $C_{35}H_{32}N_8O_5Ru$ [M] 746.35, found 746.14 [$M+H^+$]. Additional peaks were observed at 633.11, which corresponds to the loss of the uracil base; the complex was deemed unstable in the absence of the matrix. Electrochemical data: $E_{1/2}$ = 1.38 V vs. Ag/AgCl in CH_3CN containing 0.1 M TBAH (scan rate, 1.0 V/sec). Emission decay at 720 nm (λ_{exc} = 480 nm): τ = 60 nsec (50 mM sodium phosphate, pH 7.0, 500 mM sodium chloride).

[$Re(CO)_3$(phen)(U_a)](OSO_2CF_3). The model complex was prepared (by Dr. Jeffrey J. Rack) by heating [$Re(CO)_3$(phen)(OSO_2CF_3)]$^+$ in water at 80 °C for 3 hours. The supernatant was removed and a portion of this solution (1 mL, ~0.4 mM) was added to a buffered solution (50 mM HEPES, pH 8.5) containing 2′-amino-2′-deoxyuridine (27 mg, 0.11 mmol). The solution was stirred for 24 hours. ESI-MS identified peaks at 239.0, 694.0 and 478.5, which correspond to U_{impy}, $Re(CO)_3$(phen)(U_{impy})$^+$, and $Re(CO)_3$(phen)(H_2O)$^+$, respectively. The excited state lifetimes of the two Re(I) complexes were determined using the crude solution (Figure B.1).

Figure B.1: Emission decay of a solution containing $Re(CO)_3(phen)(OH_2)^+$ and $Re(CO)_3(phen)(2'$-amino-$2'$-deoxyuridine$)^+$ (50 mM HEPES, pH 8.5; λ_{exc} = 396 nm; λ_{obs} = 575 nm).

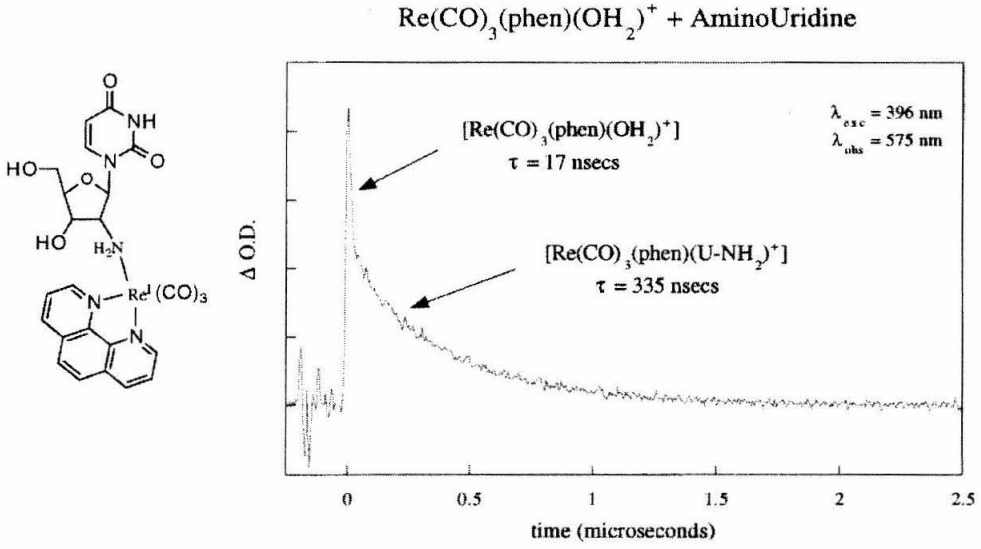
Re(CO)3(phen)(OH2)+ + AminoUridine
[Re(CO)3(phen)(OH2)+]
τ = 17 nsecs
[Re(CO)3(phen)(U-NH2)+]
τ = 335 nsecs
λexc = 396 nm
λobs = 575 nm
Δ O.D.
time (microseconds)
0
0.5
1
1.5
2
2.5
HO
NH
O
HO
H2N
Re(CO)3

Results and Discussion

Ru(II) acetylacetonate Complexes. Synthesis of the Ru(II) acetylacetonate complexes employed either $Ru(acac)_3$ or $Ru(acac)_2(CH_3CN)_2$ as starting reagents (Figure B.2).[1-3] Both complexes provided convenient routes to the model complexes that might qualify as donor-acceptor complexes suitable for DNA electron transfer experiments.

Initially, $Ru(acac)_2(ampy)^{1+}$ was selected as one of these targets, based on our interest in preparing ruthenium complexes that would bind the 2′-modified nucleosides previously synthesized (Chapter 2, Appendix A). We predicted that this particular complex would display a low reduction potential, due to the presence of the electron donating acac ligands. The tris-chelate nature of this complex made it an attractive candidate because of the enhanced stability that bidentate ligands confer on a metal complex.

Preparation of this complex was adapted from methods developed by Bennett and coworkers for synthesizing alkene derivatives of Ru(II) and Ru(III) acetylacetonate complexes (Figure B.3).[4] However, exposure to air resulted in a dramatic change in the solution color, reminiscent of the model complex work performed with $Ru(NH_3)_4(ampy')^{2+}$ in Chapter 3. Results with this acac derivative were consistent with reports describing the products from the oxidative dehydrogenation of amine ligands coordinated to ruthenium.[5-10] Ford and coworkers showed that air-exposure of $[Ru(NH_3)_4(ampy)]^{2+}$ leads to the formation of $[Ru(NH_3)_4(impy)]^{2+}$.[7] Subsequent work by Keene and Meyer outlined the mechanism of oxidative dehydrogenation for a related complex, $[Ru(bpy)_2(ampy)]^{2+}$ (see Chapter 3, Figure 3.13).[8-10] $Ru(acac)_2(impy)$ and $Ru(acac)_2(impy')$ can also be prepared from $Ru(acac)_2(CH_3CN)_2$ (Chapters 3 and 5).

Figure B.2: Scheme showing the synthetic route to various Ru(II) acetylacetonate complexes.

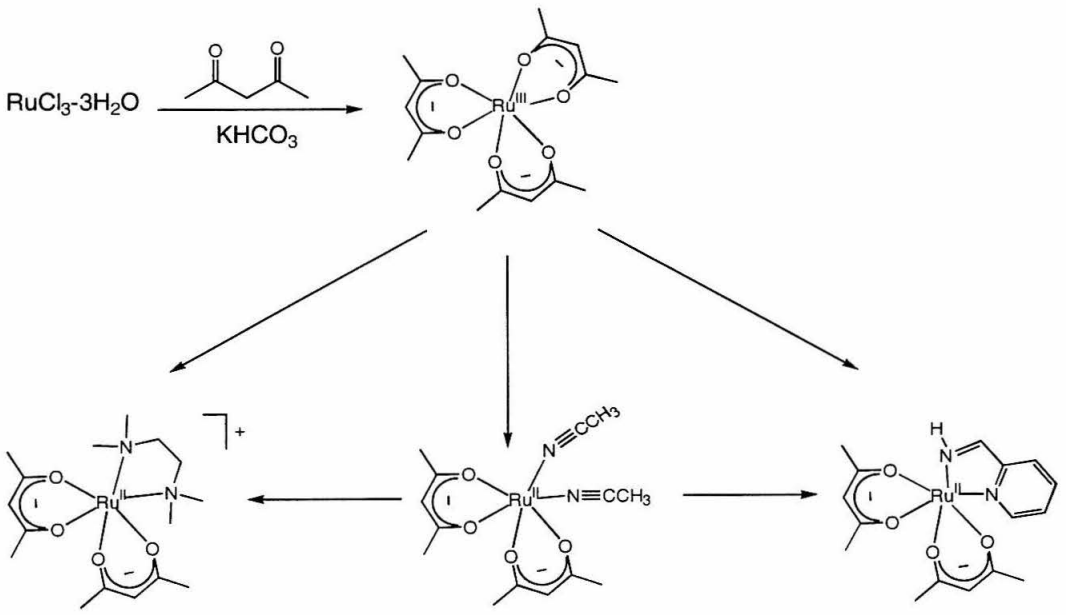
RuCl3-3H2O
KHCO3
Ru III
Ru II
N≡CCH3
H
N
+

Figure B.3: Synthesis of $Ru(acac)_2(impy)$, where acac = acetylacetonate; impy = iminomethylpyridine.

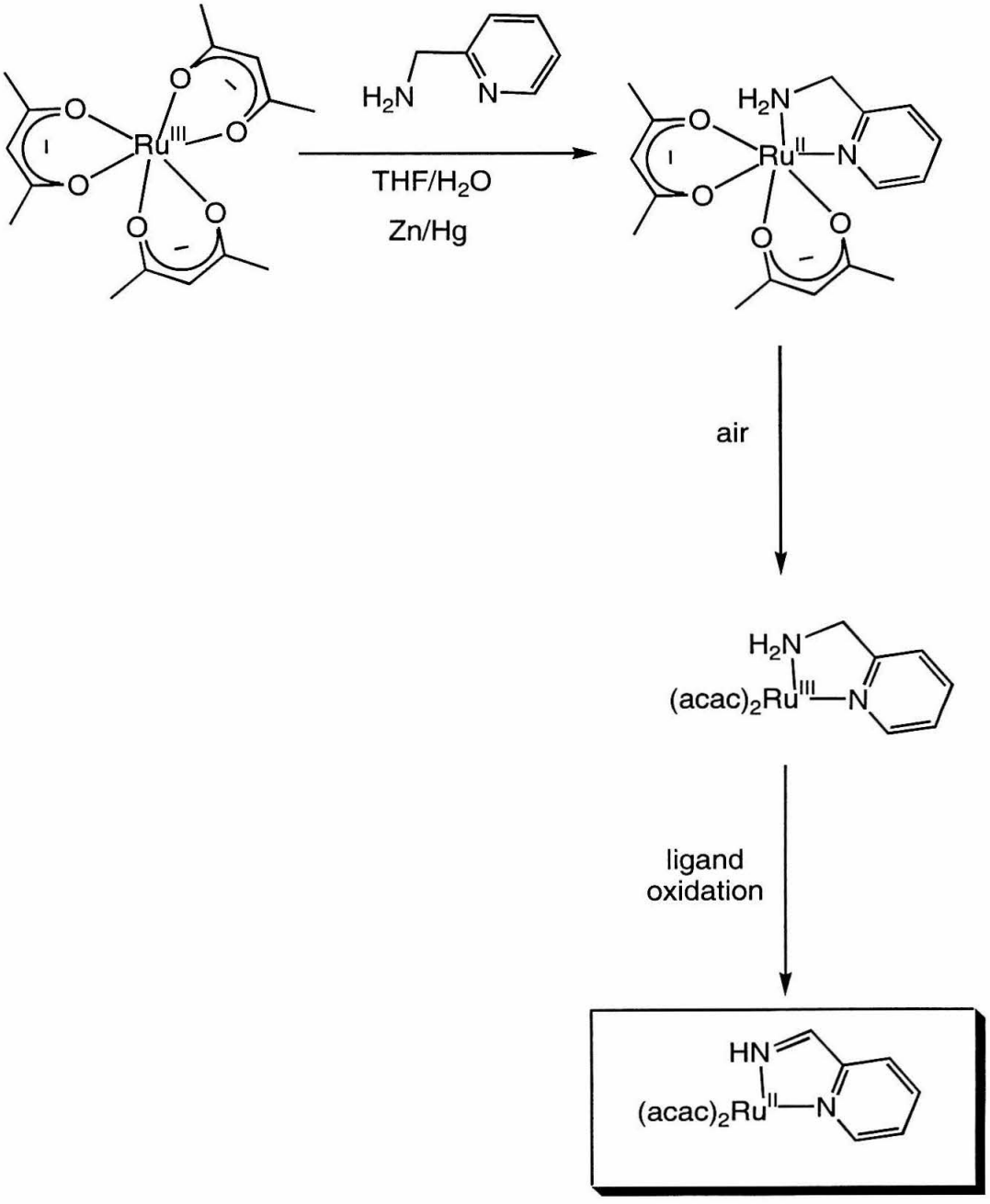
H2N
N
THF/H2O
Zn/Hg
Ru III
Ru II
air
(acac)2Ru III
ligand
oxidation
HN
(acac)2Ru II

A second target complex, $Ru(acac)_2(aepy)^+$, was selected based on the availability of a nucleoside containing a bidentate substituent at the 2′ position (**3b**, Chapter 2). The preparation of $Ru(acac)_2(aepy)^+$ relied on the method devised for synthesizing $Ru(acac)_2(impy)$. Although preliminary mass spectral data indicated formation of the desired product, the crude material was difficult to purify and the expected air-sensitivity of the product complicated these purification efforts. Synthesis of this complex using **3b** and a detritylated version of **3b** (Appendix A) were unsuccessful.

Synthesis of $[Ru(acac)_2(tmen)](NO_3)$ was pursued since this complex was a desireable precursor for use in the post-synthetic modification of oligonucleotides (Chapters 2 and 3). The complex was prepared from both $Ru(acac)_3$ and $Ru(acac)_2(CH_3CN)_2$ in reasonable yields (values not reported). However, metallation reactions employing this precursor were unsuccessful (Chapter 3).

Acid treatment of $Ru(acac)_2(impy)$ and $Ru(acac)_2(impy')$. To assess the stability of these complexes in the mildly acidic solution used in automated DNA synthesis, samples of each were dissolved in dichloromethane and treated with dichloromethane containing 0.15-3% trichloroacetic acid. Solutions of $Ru(acac)_2(impy)$ displayed absorption maxima at 398 and 592 nm prior to treatment; the addition of the acidic solution immediately caused changes in the absorption spectrum of each complex, such that no distinct absorption maxima were observed. Rather, a broad featureless band was observed in the visible region, suggestive of significant decomposition.

Likewise, treatment of $Ru(acac)_2(impy')$ resulted in rapid changes in the absorption spectrum of the sample. The absorption maxima at 392 and 602 nm decrease after acid treatment; the growth of two intense bands at 414 and 504 nm is observed.

These bands are identical to a dichloromethane solution of dimethoxytrityl chloride, which indicates that acid treatment of $Ru(acac)_2(impy')$ causes removal of the DMT protecting group on the nucleoside appended to the metal. The results obtained for $Ru(acac)_2(impy)$ and $Ru(acac)_2(impy')$ indicate that these complexes are not stable in the mildly acidic conditions employed during automated DNA synthesis.

Synthesis of $Ru(bpy)_2(U_{impy})^{2+}$. The metallonucleoside **3** prepared in Chapter 4 proved to be an attractive candidate for use in DNA electron transfer studies; this prompted interest in having a water-soluble version of the complex ($Ru(bpy)_2(U_{impy})^{2+}$) on-hand for additional study. The synthesis was achieved using a non-tritylated nucleoside, U_{impy}, that was prepared *in situ* by condensing 2-pyridinecarboxaldehyde and 2′-amino-2′-deoxyuridine. Addition of $Ru(bpy)_2Cl_2$ produced the desired complex. Purification, however, was lengthy and reduced the overall yield of the synthesis. HPLC analysis of the purified complex using a reverse-phase C18 column revealed the presence of two diastereomers, each eluting as separate peaks. This result clarified the identity of the products obtained upon enzymatic digestion of oligonucleotides containing metallonucleoside **3** (Chapter 4; Figures 4.5 and 4.6).

Interestingly, the excited-state lifetime of $Ru(bpy)_2(U_{impy})^{2+}$ in buffered aqueous solution is 60 nsec (λ_{exc} = 480 nm; λ_{obs} = 720 nm), which is slightly longer than the lifetime determined for the tritylated complex in aqueous methanol (τ(**3**) = 42 nsec; Chapter 5).

Synthesis of $Re(CO)_3(phen)(U_a)^+$. The Re(I) complex prepared with a 2′ modified nucleoside was investigated due the high reduction potential the target complex was expected to exhibit (~ 1.8 V vs. NHE). The limited solubility of the Re(I) precursor

in conditions conducive to complexation with 2′-amino-2′-deoxyuridine resulted in a low yield. That this result precluded further characterization of the target complex is unfortunate, especially since the complex displayed a long excited-state lifetime in buffered aqueous solution (Figure B.1).

Conclusion

The complexes described in this Appendix are representative of our efforts to develop ruthenium complexes that might qualify as promising candidates for use in DNA-mediated electron transfer studies.

References

(1) Knowles, T. S.; Howells, M. E.; Howlin, B. J.; Smith, G. W.; Amodio, C. A. *Polyhedron* **1994**, *13*, 2197-2203.

(2) Kobayashi, T.; Nishina, Y.; Shimizu, K.; Sato, G. P. *Chem. Lett.* **1988**, 1137-1140.

(3) Kasahara, Y.; Hoshino, Y.; Shimizu, K.; Sato, G. P. *Chem. Lett.* **1990**, 381-384.

(4) Bennett, M. A.; Chung, G. L.; Hockless, D. C. R.; Neumann, H.; Willis, A. C. *J. Chem. Soc. Dalt. Trans.* **1999**, 3451-3462.

(5) Lane, B. C.; Lester, J. E.; Basolo, F. *Chem. Commun.* **1971**, 1618-1619.

(6) Mahoney, D. F.; Beattie, J. K. *Inorg. Chem.* **1973**, *12*, 2561-2565.

(7) Alvarez, V. E.; Allen, R. J.; Matsubara, T.; Ford, P. C. *J. Am. Chem. Soc.* **1974**, *96*, 7686-7692.

(8) Brown, G. M.; Weaver, T. R.; Keene, F. R.; Meyer, T. J. *Inorg. Chem.* **1976**, *15*, 190-196.

(9) Ridd, M. J.; Keene, F. R. *J. Am. Chem. Soc.* **1981**, *103*, 5733-5740.

(10) Keene, F. R.; Ridd, M. J.; Snow, M. R. *J. Am. Chem. Soc.* **1983**, *105*, 7075-7081.

Appendix C:

Fluorescence Quenching Experiments with Ruthenium-Modified Nucleic Acids

Introduction

Inherent in the process of designing donor-acceptor complexes for use in DNA-ET studies is the evaluation of such candidates for their viability in the bimolecular quenching method (Figure C.1). Of the methods available to measure ET rate constants in biological assemblies, this method is attractive since it facilitates the determination of rate constants that vary over several orders of magnitude.[1] It also allows the experimenter to study ET reactions that have large thermodynamic driving forces. A potent oxidant (or reductant) is generated upon excited-state quenching by an exogenous quencher. The products of this quenching include the oxidized complex and reduced quencher. In the absence of an electron donor, the oxidized complex recombines with the quencher to form the starting reagents and the cycle is repeated. In the presence of an electron donor, ET from the donor to the oxidized complex (electron acceptor) takes place in competition with the charge recombination step. Thus, driving force values are estimated from the difference in the ground-state reduction potentials of the electron donor and electron acceptor.

The design and synthesis of donor-acceptor candidates involves evaluating these complexes under conditions that mimic the bimolecular quenching scheme described above. Suitable acceptor complexes must display an emission lifetime that is long enough to allow oxidative or reductive quenching. Additionally, the excited-state quenching must generate products that are detectable using transient absorption spectroscopy. There must be enough quenched product to undergo ET when the donor complex is present. This amount can be modulated by the concentration of exogenous quencher.

Figure C.1: Scheme outlining the bimolecular quenching cycle designed for studying electron transfer reactions in biological systems. The bis-metallated DNA duplex is excited at 480 nm in the presence of an added quencher, which oxidatively quenches the newly formed excited state. Quenching generates the mixed-valence intermediate that then undergoes electron transfer depending on the overall driving force for the ET step. Recombination of the ET product with the reduced quencher gives the initial starting materials. Abbreviations: acac = acetylacetonate, bpy = 2,2′-bipyridine.

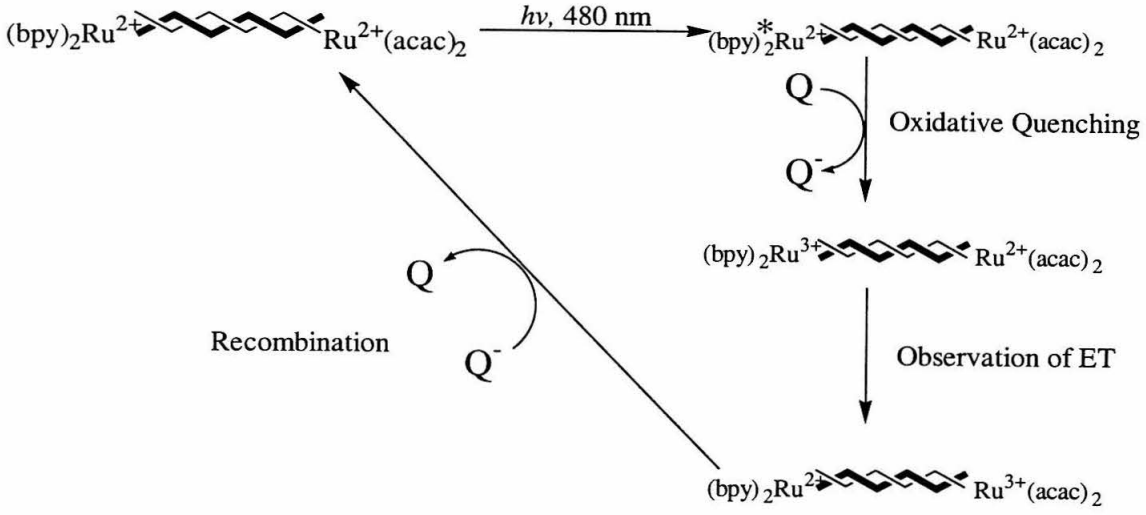
(bpy)2Ru2+
Ru2+(acac)2
hv, 480 nm
(bpy)*2Ru2+
Ru2+(acac)2
Q
Q-
Oxidative Quenching
(bpy)2Ru3+
Ru2+(acac)2
Observation of ET
(bpy)2Ru2+
Ru3+(acac)2
Q
Q-
Recombination

Some of the results from oxidative quenching experiments with ruthenium-modified nucleic acids are presented in Chapter 4. Included here is a summary of the quenching studies conducted with metallonucleoside **3**, oligonucleotide **7** (or **6**), and duplex **7:9**. The specialized reaction scheme shown in Figure C.2 outlines the experiments performed with these samples. Nanosecond transient absorption and emission spectroscopy were used to probe the nature of both oxidative and reductive quenching of the Ru-containing complexes by a variety of quenchers in aqueous solution.

Results

Samples were approximately 40 μM and included either the metallonucleoside **3** in methanol (25-100%) or Ru-oligonucleotides (**6** or **7** alone; or **7** hybridized to its complement **9**) in phosphate buffer (0.05 M sodium phosphate, pH 7.0, 0.5 M sodium chloride). The preparation of **3**, **6**, and **7** is described in Chapter 4. A non-tritylated version of **3** was prepared as described in Appendix B. Figure C.3 shows the structure and sequences of these ruthenium-modified nucleic acids. The abbreviation impy′ will be used throughout this section to denote either the impy-containing nucleoside or impy-containing oligonucleotides, where impy = iminomethylpyridine.

The oxidative quenchers employed in these studies included $[Ru(NH_3)_6]^{3+}$, methyl viologen (MV^{2+}), $[Fe(CN)_6]^{3-}$, and $[Ru(acac)_2(tmen)]^+$ (Figure C.4). A single reductive quencher, $[W(CN)_8]^{4-}$, was investigated. Changes in the optical density at 450 nm were monitored for the Ru^{III} species generated upon oxidative quenching of the $*Ru^{II}$-excited state, due to the differential absorbance of Ru^{III}- vs. Ru^{II}-diimine complexes at this wavelength. The isosbestic point determined in the absence of quencher was 406 nm (Figure C.5). Formation and decay of $[Ru(bpy)_2(impy')]^+$ was monitored at 510 nm,

Figure C.2: Scheme for Stern-Volmer analysis of quenching reactions.

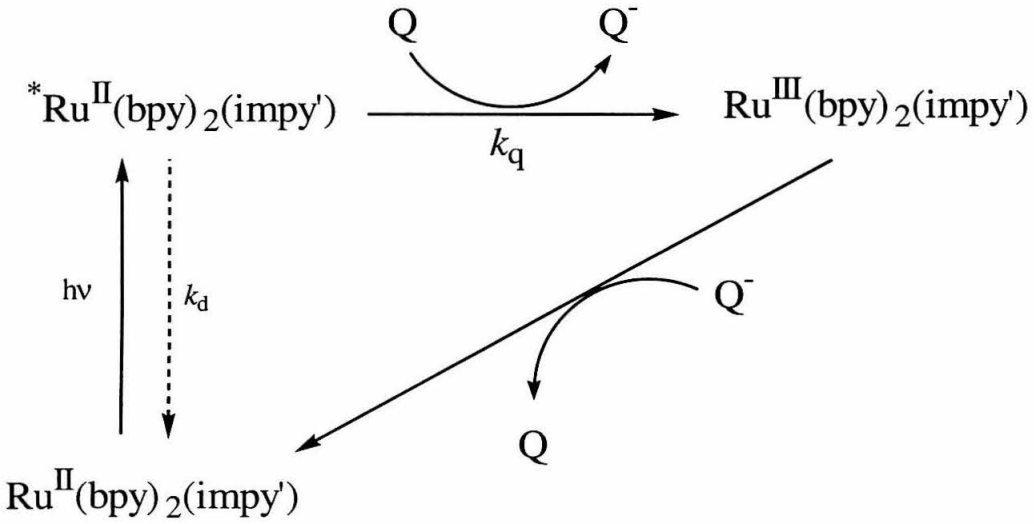

$$k_d = 1/\tau_0$$

$$k_{obs} = k_d + k_q[Q]$$

k_q = bimolecular quenching constant

k_d = emission lifetime decay rate in the absence of quencher

Figure C.3: Structure of ruthenium-containing nucleoside **3** and sequences of oligonucleotides **6**, **7**, and **9**.

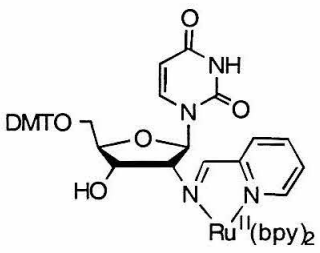

3

$^{5'}$CTCCTACACU$_{Ru(bpy)2}$ **6**

$^{5'}$TCTCCTACACU$_{Ru(bpy)2}$ **7**

AGTGTAGGAGA $^{5'}$
$^{5'}$TCTCCTACACU$_{Ru(bpy)2}$ **7:9**

Figure C.4: Scheme showing oxidative and reductive quenchers employed in quenching studies.

Oxidative Quenching:

$$*Ru^{II}(bpy)_2(impy') + Q \longrightarrow Ru^{III}(bpy)_2(impy') + Q^-$$

Q = $Ru(NH_3)_6^{3+}$
MV^{2+}
$Fe(CN)_6^{3-}$
$Ru(acac)_2(tmen)^+$

Reductive Quenching:

$$*Ru^{II}(bpy)_2(impy') + Q \longrightarrow Ru^{I}(bpy)_2(impy') + Q^+$$

Q = $W(CN)_8^{4-}$

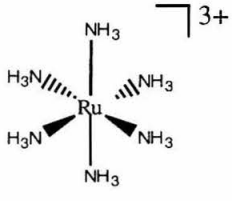

$Ru(NH_3)_6^{3+}$

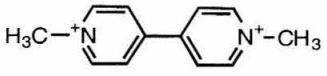

MV^{2+}

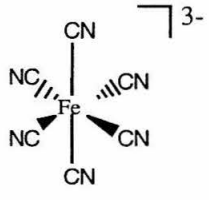

$Fe(CN)_6^{3-}$

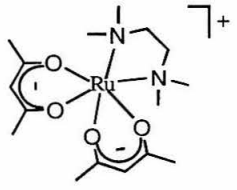

$Ru(acac)_2(tmen)^+$

Figure C.5: A sample Stern-Volmer plot derived from quenching experiments involving photoexcited **7:9** (35 μM) in the presence of $[Ru(NH_3)_6]^{3+}$ (12-52 mM). Buffer: 50 mM sodium phosphate (pH 7.0), 500 mM sodium chloride.

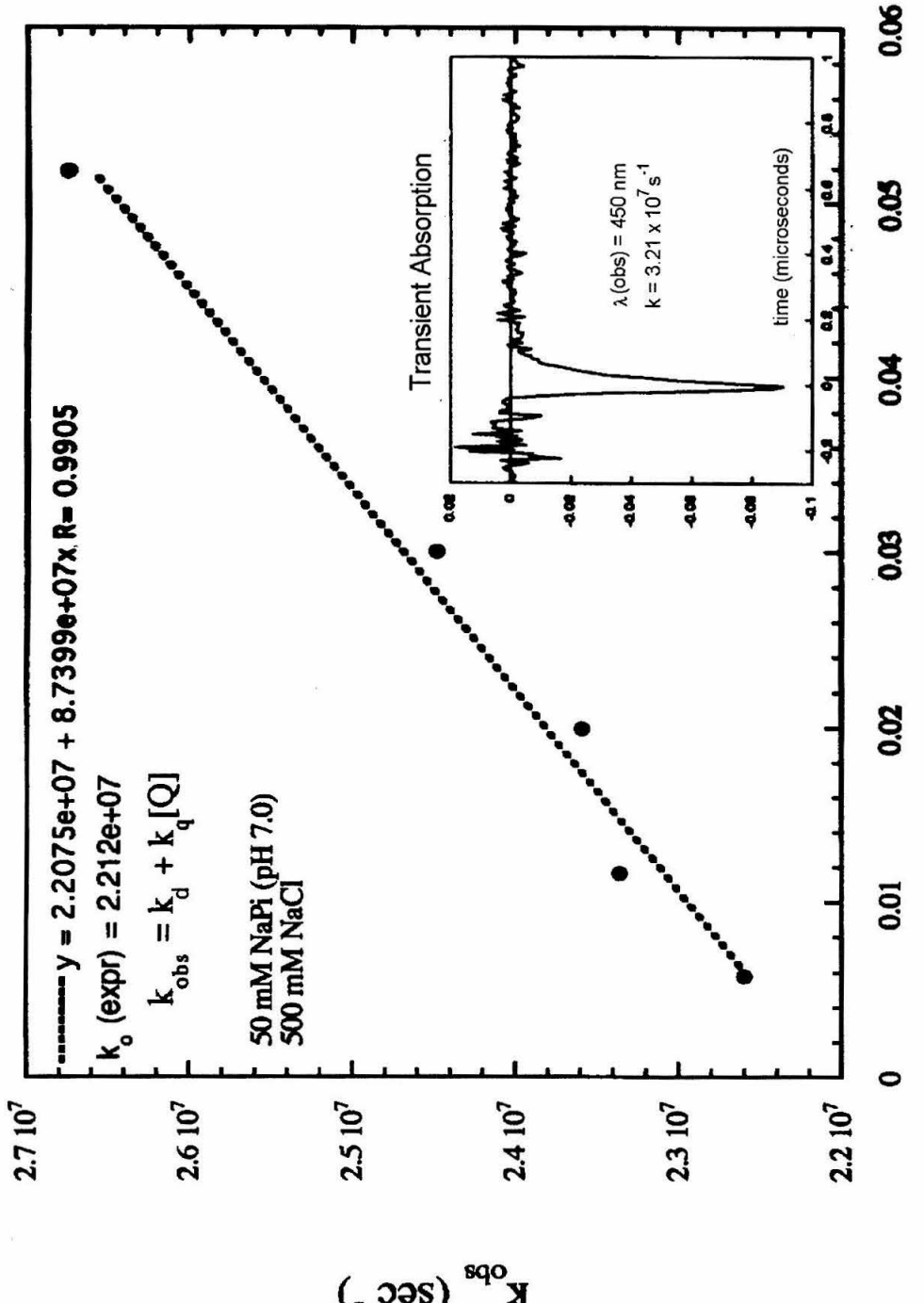
y = 2.2075e+07 + 8.7399e+07x R= 0.9905
k_o (expr) = 2.212e+07
k_obs = k_d + k_q[Q]
50 mM NaPi (pH 7.0)
500 mM NaCl
Transient Absorption
λ (obs) = 450 nm
k = 3.21 x 10^7 s^-1
time (microseconds)
K_obs (sec^-1)
Concentration (M) of Quencher, Ru(NH3/6)^3+

based on the intense absorption features of the Ru^{I} species at this wavelength.[2] Other wavelengths diagnostic of the reduced/oxidized quencher were employed where possible.

Reduction Potentials. $E_{1/2}$ (vs. NHE) values are given for the following quenchers: $[Ru(NH_3)_6]^{3+/2+}$, 0.06 V; $MV^{2+/1+}$, -0.44 V; $[Fe(CN)_6]^{3-/4-}$, 0.36 V; $[Ru(acac)_2(tmen)]^{+/0}$, -0.22 V; $[W(CN)_8]^{4-/5-}$, 0.50 V.

Emission Lifetimes. The excited-state lifetimes of **3**, **6**, **7**, and a non-tritylated version of **3** were determined by monitoring the emission decay at 720 nm. All decay traces are monoexponential, and no indications of decomposition were observed. The lifetimes are as follows: 43.7 nsec (**3**), 42.1 nsec (**6** or **7**), 42.1 nsec (duplexed **7**), 60 nsec (non-tritylated **3** in buffer).

Oxidative Quenching. The oxidative quenching of duplexed *Ru-oligonucleotide **7** by $[Ru(NH_3)_6]^{3+}$ gave linear plots of k_{obs}, the observed decay rate constant, vs. $[Ru(NH_3)_6]^{3+}$ under conditions of high ionic strength (Figure C.6). The average bimolecular quenching rate constant (k_q) derived from these plots was 1.1×10^8 M^{-1} s^{-1}. In all cases the presence of oxidative quenchers resulted in only modest reductions in the lifetime of $[*Ru(bpy)_2(impy')]^{2+}$. High concentrations of quencher (150-1500-fold excess) were required to effect a ~ 10% decrease in the lifetime values. Figure C.7 displays the lifetime of photoexcited **7:9** in the presence of 0, 30, and 52 mM $[Ru(NH_3)_6]^{3+}$ (τ = 45, 41, and 37 nsec, respectively). An exception to this general trend was observed with **3** (25% methanol) in the presence of $[Fe(CN)_6]^{3+}$ (1.8 mM), for which the lifetime decrease was greater than 50%.

Transient difference spectra showed rapid bleaching of the $[Ru(bpy)_2(impy')]^{2+}$ MLCT absorbance as observed at 450 nm, and the subsequent decay back to zero ΔOD

Figure C.6: Plot of excited-state lifetime of **7:9** (35 μM) in the presence of $[Ru(NH_3)_6]^{3+}$ (0, 30, and 52 mM). Buffer: 50 mM sodium phosphate (pH 7.0), 500 mM sodium chloride. Observation wavelength = 720 nm.

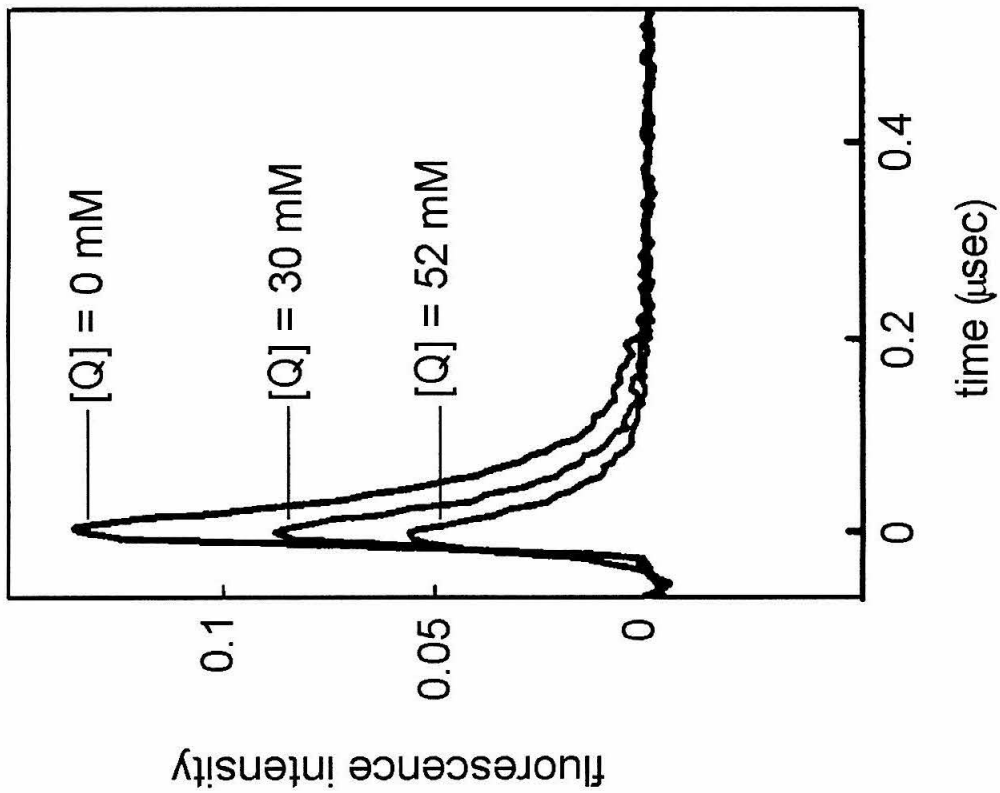
[Q] = 0 mM
[Q] = 30 mM
[Q] = 52 mM
0.1
0.05
0
0
0.2
0.4
time (µsec)
fluorescence intensity

Figure C.7: Transient absorption difference spectrum constructed for oligonucleotide **6** (35 μM) following irradiation at 480 nm. The spectrum was generated by plotting the ΔOD at t = 5 μsec at wavelengths 350-550 nm, excluding the wavelengths overlapping with the excitation source. Buffer: 50 mM sodium phosphate buffer (pH 7.0), 500 mM sodium chloride.

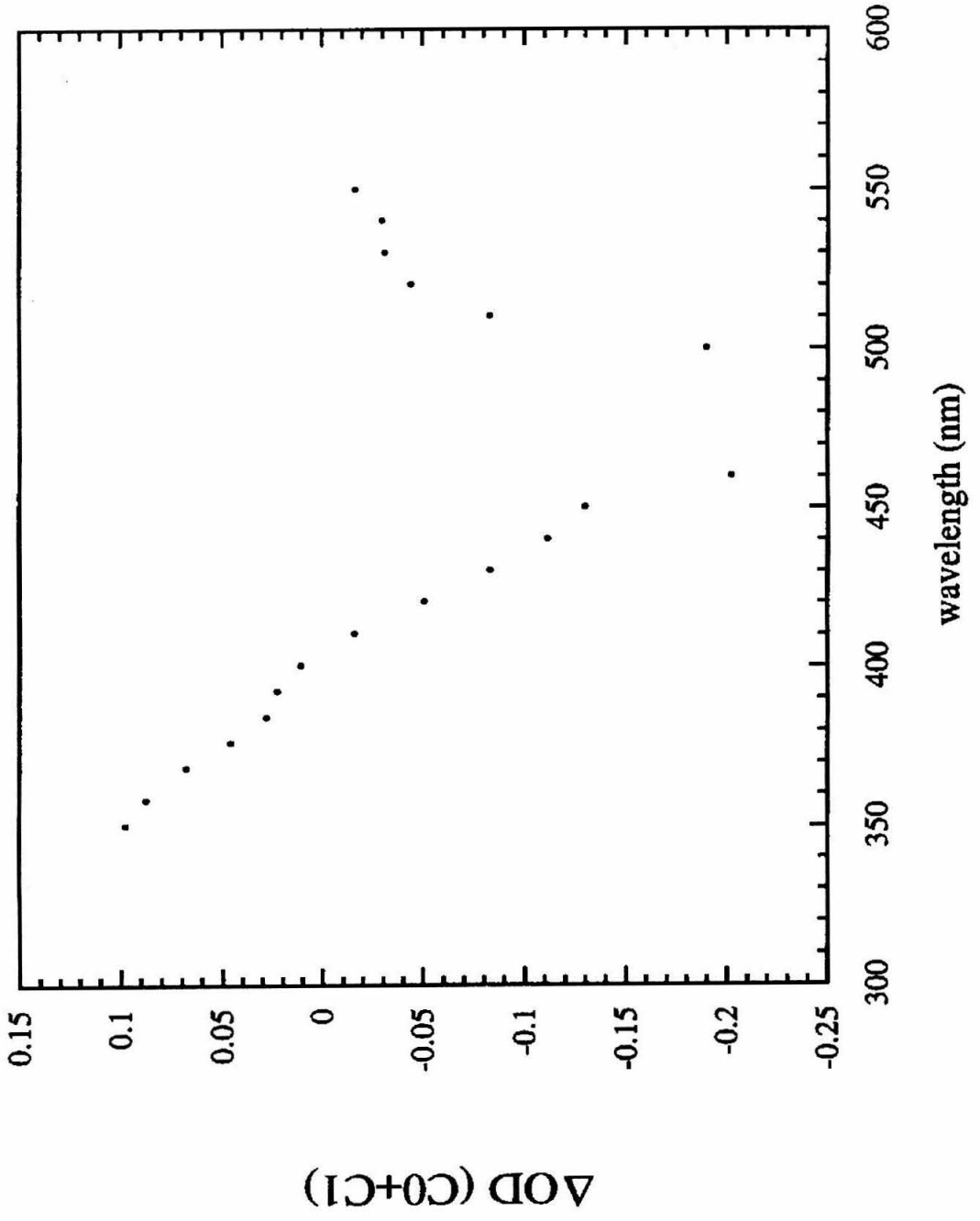
ΔOD (C0+C1)
0.15
0.1
0.05
0
-0.05
-0.1
-0.15
-0.2
-0.25
300
350
400
450
500
550
600
wavelength (nm)

was complete within nearly 5 μseconds in most samples. Only in samples of **3** with high concentrations of oxidative quencher was a detectable amount of the Ru^{III} product observed within this 5-μsecond window. The highest apparent yield of $[Ru(bpy)_2(impy')]^{3+}$ product was recorded in 25% methanol with $[Ru(NH_3)_6]^{3+}$ (27 mM) present.

A sample of non-tritylated **3** (0.1 mM) was suspended in 50 mM sodium phosphate (pH 7.0) containing 500 mM sodium chloride, to which was added $[Ru(acac)_2(tmen)]^+$ (~ 1mM). Determination of the lifetime of the non-tritylated **3** in the presence and absence of the oxidative quencher gave identical values (60 nsec).

Reductive Quenching. The nature of reductive quenching of $*[Ru(bpy)_2(impy')]^{2+}$ by $[W(CN)_8]^{4-}$ was unclear. Samples of **6** in the presence of $[W(CN)_8]^{4-}$ (1.8 mM) exhibited a modest decrease in the lifetime (~ 13%); transient difference spectra collected at 350 and 510 nm 5 μseconds after excitation were suggestive of a Ru^I species. Parallel experiments with **3** and $[W(CN)_8]^{4-}$ (1 mM) in 25% methanol revealed a significant reduction in the lifetime (~ 30%) and gave similar spectra. However, the positive ΔOD change observed at 510 nm persisted longer than 5 μseconds and did not return to zero at longer time points (50 μs – 1 ms), suggestive of an irreversible reaction between photoexcited **3** and $[W(CN)_8]^{4-}$.

Discussion and Conclusion

The absence of any significant differences in the lifetimes of **3**, **7**, and **7·9** demonstrates that the bases contained in **7** or **9** do not quench the photoexcited $[Ru(bpy)_2(impy')]^{2+}$. Although guanine is the most facile electron donor of the DNA

bases ($E^{+\bullet/0}$ = 1.3 V vs. NHE, pH 7),[3] oxidation by photoexcited **7** is not favored thermodynamically ($E^{2+*/1+}$ ~ 1 V vs. NHE; Chapter 4). Even the addition of oxidative quenchers fails to result in any oxidative damage to the DNA bases of **7·9**, despite generating a Ru(III) species that is a powerful oxidant ($E_{1/2}$ = 1.3 V).

Modest decreases in the excited-state lifetimes of **7** and **7·9** are observed in the presence of large excess of oxidative quenchers. In the case of $[Ru(NH_3)_6]^{3+}$, the bimolecular quenching constant determined for the quenching of photoexcited **7·9** is one order of magnitude smaller compared to the value measured for the quenching of $[Ru(bpy)_3]^{2+}$ (1.1 x 10^8 vs. 2 x 10^9 M^{-1} s^{-1}, respectively).[4] However, the driving force estimate (ΔG_q) for the single electron transfer from $[Ru(NH_3)_6]^{3+}$ to photoexcited **7·9** is approximately –0.24 eV, much smaller than the value calculated for $[Ru(bpy)_3]^{2+*}$ (–0.92 eV).[4,5] Oxidative quenching by methyl viologen is thermodynamically unfavorable (ΔG_q = 0.26 eV). Despite the large difference in ΔG_q for the two quenchers, the addition of either quencher in large excess to **7** or **7·9** generates small amounts of oxidized product.

Interestingly, the largest percentage decrease in the excited-state lifetime of **3** was generated by the addition of $[Fe(CN)_6]^{3-}$. The driving force for oxidative quenching by this complex is –0.54 eV, the largest value for the series of oxidative quenchers examined.

It is difficult to reconcile the value of the bimolecular quenching constant determined for the oxidative quenching of photoexcited ruthenium-modified oligonucleotides by $[Ru(NH_3)_6]^{3+}$ and the low amount of oxidized product following quenching. These results suggest perhaps that a large percentage of the geminate pairs generated in the quenching reaction recombine to form the ground-state reactants. While

this assessment is preliminary, it may explain the observations. Very little Ru(III) product is generated in the presence of oxidative quenchers for samples containing **3**; even less is observed for the oligonucleotide samples. Perhaps the low yield is attributable to the nature of the $[Ru(bpy)_2(impy')]^{2+}$ complex. We can speculate that the negatively charge environment of the oligonucleotide may accelerate the geminate pair recombination. Based on the results described above, we can conclude that the $[Ru(bpy)_2(impy')]^{2+}$ complex is not suitable for use in the bimolecular quenching method.

References

(1) Chang, I.-J.; Winkler, J. R.; Gray, H. B. *J. Am. Chem. Soc.* **1991**, *113*, 7056-7057.

(2) Kelly, L. A.; Rodgers, M. A. J. *J. Phys. Chem.* **1994**, *98*, 6377-6385.

(3) Steenken, S.; Jovanovic, S. V. *J. Am. Chem. Soc.* **1997**, *119*, 617-618.

(4) Bock, C. R.; Meyer, T. J.; Whitten, D. G. *J. Am. Chem. Soc.* **1974**, *96*, 4710-4712.

(5) $\Delta G_q = -[E_{1/2}^{Q/Q-} - E_{1/2}^{Ru3+/Ru2+*}]$.

Appendix D:

Automated Synthesis of an Oligonucleotide Containing Ruthenium(II) Complexes at 3′ and 5′ Ends.

Summary

The preparation of a bis-metallated 11-mer oligonucleotide entirely by solid-phase methods was attempted. The reagents and oligonucleotide sequence used in the synthesis are shown in Figure D.1. The preparation of the ruthenium-containing solid support is described in Chapter 4. Synthesis and characterization of the phosphitylated $[Ru(acac)_2(T_{impy})]$ complex was performed by Dr. Natia L. Frank (T_{impy} = thymidine modified at the 5′ position with iminomethylpyridine) (N. L. Frank, unpublished results).

Oligonucleotide synthesis was initiated with the ruthenium-containing solid support (compound **5** in Chapter 4) using standard coupling procedures as dictated by the automated protocol for a 1 μmole scale. A 0.15 M solution of the ruthenium-containing phosphoramidite was delivered and allowed to couple for 30 minutes. The contents of the column were transferred to a test tube, and the crude oligonucleotide was manually cleaved in concentrated aqueous ammonia for 9 hours at room temperature. The resulting orange solution was filtered and evaporated to dryness using a SpeedVac.

Analytical samples of the crude oligonucleotide were analyzed by HPLC using ion-exchange methods (Figure D.2). The peaks labeled B, C, D in Figure D.2 were collected, desalted, and analyzed by ESI-MS techniques. The results are summarized below:

MS Sample	*Calculated*	*Found*	*Assignment*
Peak B, t = 9.5-9.85 min.	4117.9, $[M-H]^-$	4130.94, $[M-H]^-$	target plus 13
Peak C, t =10.15-10.3 min.	3425.5, $[M-H]^-$	3425.73, $[M-H]^-$	"n-1" oligonucleotide: 5′-CTCCTACACU$_{Ru(bpy)2}$
Peak D, t = 10.35-10.6 min.		4145.4, $[M-H]^-$	target plus 28

Figure D.1: Sequence of target 11-mer oligonucleotide prepared by solid-phase methods using the metal-containing monomers indicated. Abbreviations: acac = acetylacetonate, bpy = 2,2′-bipyridine.

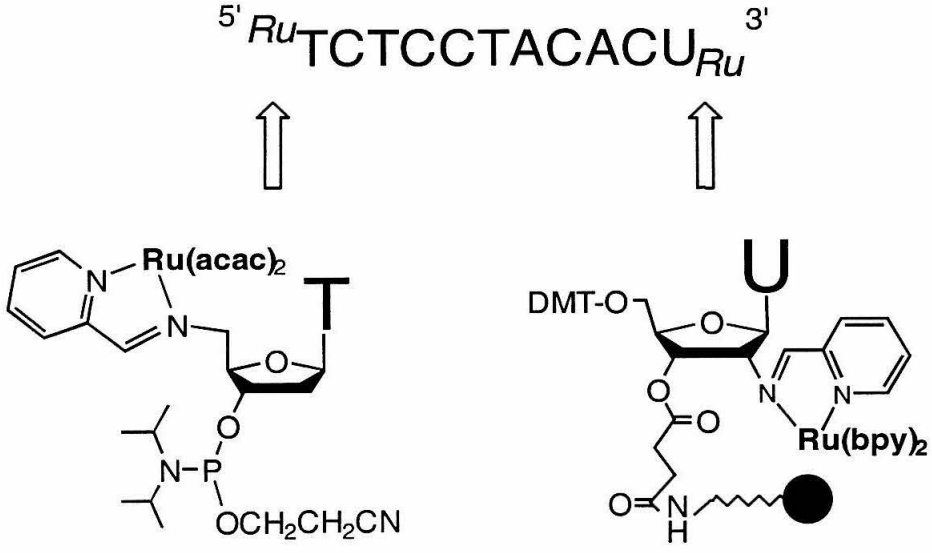
5' Ru TCTCCTACACU Ru 3'
Ru(acac)2
T
N
N
O
O
N–P
OCH2CH2CN
U
DMT-O
O
O
O
N
N
Ru(bpy)2
O
N
H

Figure D.2: HPLC trace of the crude mixture from the synthesis of 5′-^{Ru}TCTCCTACACU$_{Ru}$ achieved by solid-phase methods. Column type: Dionex NucleoPac 100. Gradient: 10-33% B over 1 minute, 33-44% B over 17 minutes (A = 10% acetonitrile; B = 10% acetonitrile, 1.5 M ammonium acetate). Flow rate: 1.0 mL/min; absorption monitored at 260 nm.

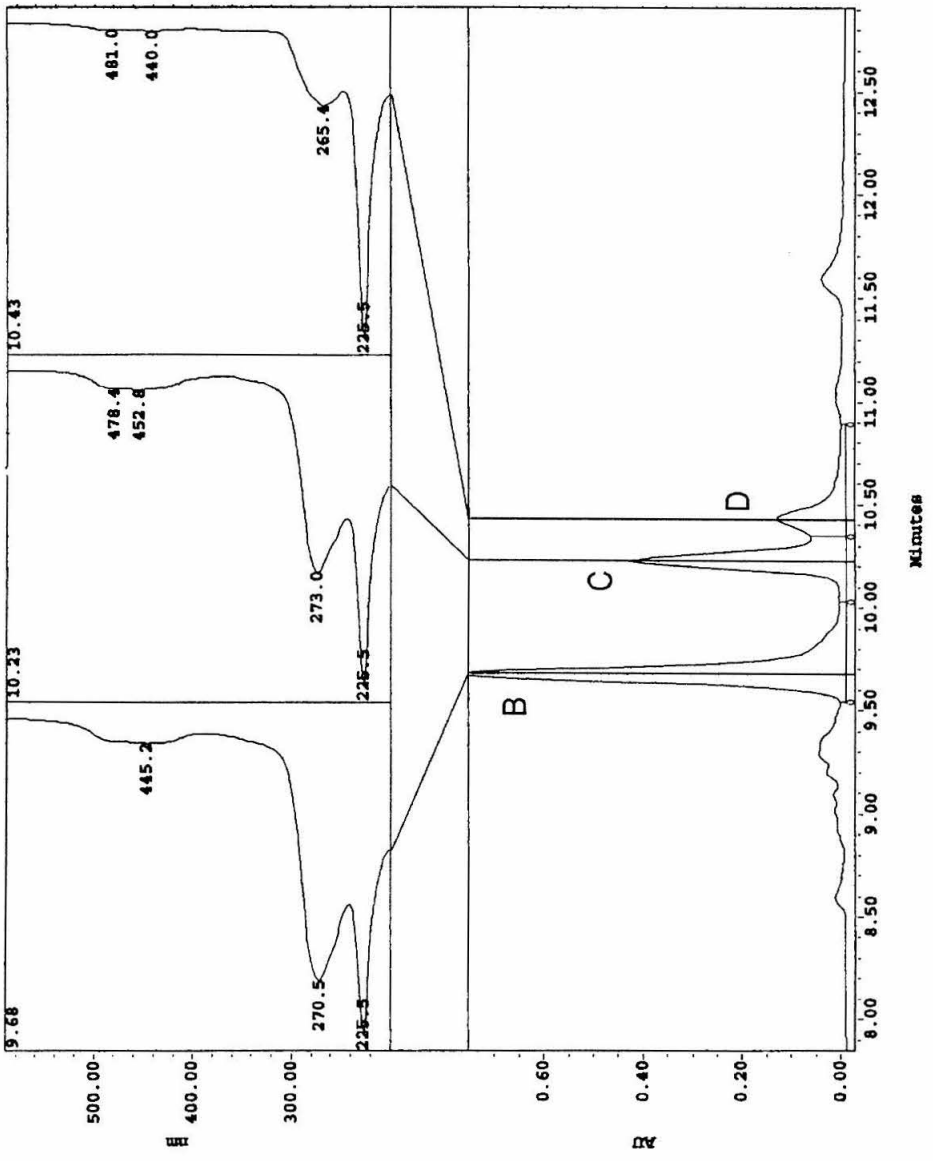
9.68
445.2
270.5
225.5
10.23
478.4
452.8
273.0
225.5
10.43
481.0
440.0
265.4
225.5
B
C
D
500.00
400.00
300.00
mAU
0.60
0.40
0.20
0.00
8.00
8.50
9.00
9.50
10.00
10.50
11.00
11.50
12.00
12.50
Minutes

The mass spectral results for Peak B strongly suggest the presence of the 11-mer oligonucleotide containing both ruthenium complexes. The fact that the target strand contains an additional 13-14 mass units is consistent with results obtained by Frank for oligonucleotides prepared from the phosphitylated [$Ru(acac)_2(T_{impy})$] complex. The putative species (M + 13 amu) is the product of the oxidation step that follows phosphoramidite coupling and subsequent cleavage in concentrated aqueous ammonia. The isolated oligonucleotides likely possess a ruthenium complex that has experienced further oxidation of the impy ligand to give a hydroxylated species:

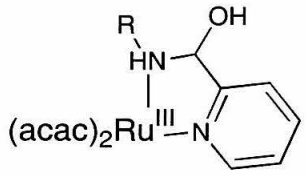

R = nucleoside

(Later experiments led to a revised workup procedure that involves reduction of $Ru(acac)_2$(impy)-modified oligonucleotides with dithionite prior to cleavage in ammonia. Mass spectral data of oligonucleotides thus treated were consistent with the calculated values for the intact ruthenium-containing oligonucleotides.)

The assignment of Peak C is based on the synthesis of the 10-mer oligonucleotide, 5′-CTCCTACACU$_{Ru(bpy)2}$ (Chapter 4). The mass spectral results support this assignment and confirm that Peak C in the chromatogram is the oligonucleotide resulting from inefficient coupling of the phosphitylated [$Ru(acac)_2(T_{impy})$] complex. The identity of Peak D is unclear. It may represent an oligonucleotide containing both metal complexes but that possesses impy nucleosides that have oxidized in the presence of concentrated

ammonia to give an OH addition product. Additional characterization by enzymatic digestion was not performed to confirm this suggestion.

Since the additional reduction step prior to cleavage in ammonia have been incorporated into the workup for $Ru(acac)_2(impy)$-modified oligonucleotides, attempts to prepare bis-metallated oligonucleotides completely by solid-phase methods can be resumed.

Appendix E:

HPLC Columns and Solvent Systems

HPLC Information

Reverse-Phase	A	B
Oligo R3 Perseptive Biosystems	100 mM ammonium acetate pH 8.5 or 10 2% acetonitrile	100% acetonitrile
C18 HS20154 Vydac	100 mM triethylammonium acetate, pH 7 2% acetonitrile	50 mM triethylammonium acetate, pH 7 50% acetonitrile
C18 HS20154 Vydac	100 mM triethylammonium acetate, pH 7 2% acetonitrile	100% acetonitrile
Prism C18 Keystone Scientific	100 mM triethylammonium acetate, pH 7 2% acetonitrile	100% acetonitrile
Ion-Exchange		
AX-100 SynChroPak	10% acetonitrile	10% acetonitrile 1.5 M ammonium acetate pH 6.0
Dionex NucleoPac 100	25 mM Tris, pH 8.0 0.5% acetonitrile	25 mM Tris, pH 8.0 0.5% acetonitrile 1.5 M ammonium chloride
Dionex NucleoPac 100	10% acetonitrile	10% acetonitrile 1.5 M ammonium acetate